

# **The Origin and Properties of Flint in the Upper Cretaceous Chalk**

Mohammed Musa Aliyu

Submitted in accordance with the requirements for the degree of  
Doctor of Philosophy

The University of Leeds

School of Earth & Environment

February, 2016

## **Declaration**

The candidate confirms that the work submitted is his own, except where work which has formed part of jointly authored publications has been included. The contribution of the candidate and the other authors to this work has been explicitly indicated below. The candidate confirms that appropriate credit has been given within the thesis where reference has been made to the work of others.

This copy has been supplied on the understanding that it is copyright material and that no quotation from the thesis may be published without proper acknowledgement.

The right of Mohammed Musa Aliyu to be identified as Author of this work has been asserted by him in accordance with the Copyright, Designs and Patents Act 1988.

## List of Publications

**Aliyu, M. M.**, Murphy, W., Collier, R. & Lawrence, J.A. (2015). Classification of flints for drill wear potential. In: Schubert, W., & Kluckner, A., (eds). Future Development of Rock Mechanics. *EUROCK 2015 and 64th Geomechanics Symposium. Austrian Society for Geomechanics*, 309 – 314. ISBN 978-3-9503898-1-4.

**Aliyu, M. M.**, Murphy, W., Lawrence, J.A. & Collier, R. (Under review). Engineering Geological Classification of flint. *Quarterly Journal of Engineering Geology and Hydrogeology*.

In the process of writing the above listed papers, the laboratory experiments, data analysis and the production of drafts of all the papers mentioned were carried out by the first author under the supervision of the co-authors. The co-authors contributed in reviewing and editing the papers prior to submission for publication. All the findings presented in these papers are directly drawn from this thesis and are reflected in various chapters of the thesis.

## Acknowledgements

I am profoundly grateful to Almighty God (Allah) for giving me the life, health and perseverance to see the end of this task. This thesis would have hit a brick wall without the intellectual, unflinching academic and moral support from my primary supervisor, Dr. William Murphy and my secondary supervisor Dr. Richard Collier. I have learnt much from the constructive criticism of my supervisors and became more enthusiastic from their motivation and guidance. I also owe my deepest gratitude to my former supervisor Dr. James Lawrence for introducing me to flints, sustaining his keen interest in this research and for his support for the overall project from the inception to completion. I would forever remain grateful for his help and confidence in me.

This thesis would not have seen the light of the day, without the generous financial support from the Petroleum Technology Development Funds (PTDF) Nigeria. I remain thankful for your generosity. I would also like to thank American Association of Petroleum Geologists (AAPG) for the 2013 Bernold M. "Bruno" Hanson Memorial Environmental Grant and the London Petrophysical Society (LPS) for the Hillier Academic Award. The financial support from the School of Earth and Environment of the University of Leeds and the student union is highly appreciated.

I would particularly like to thank Mr. Kirk Handley for his assistance in the engineering geology laboratory, his help in sampling flint at Lincolnshire and for timely stocking me with my laboratory supplies. I would also like to thank Dr. John Martin for his help in ultrasonic and tensile strength tests, and his useful discussions on most of my laboratory tests. My sincere appreciation goes to Dr Algy Kazlaucius, Mrs Lesley Neve, Dr. Golnaz, Dr. Carlos Grattoni, Dr. Samuel Allshorn, and Dr. Anthony Windross for their help and valuable discussions on various laboratory tests.

I am particularly grateful to Dr. Robert Fowell for the loan of tricone bit and a CD on cutting test of flints, Professor Finn Surlyk for his advice on Danish flints, and Dr. Jesper Milan for his assistance in sampling flints from the Sigerslev Quarry, Denmark. I am also deeply indebted to Mr Paul Hildreth for his help in sampling flints from the Ulceby Vale House Quarry, and for introducing me to the flint in the quarry. I would also like to thank Dr. Christopher Jeans for useful discussions on flints and his assistance during the fieldwork at Lincolnshire.

Lastly, a special gratitude to my parents for their prayers, my wife for her patience, my children Mustapha and Ibrahim for being the source of my happiness while writing this thesis, my sisters and brother for their moral support. I would like to thank my in-laws, brothers-in-law, Dr. Babagana Umara and Engineer Mohammed Umar for their good wishes, my friends for encouraging me and my colleagues in the University of Leeds for the fun we had.

## Abstract

One of the most critical geological/technical challenges affecting engineering projects in chalk with flints either for hydrocarbon/water exploration or infrastructural development is encountering flints, which mostly result in excessive wear or damage to cutting tools or drilling/tunnelling equipment. Overcoming this requires a regional understanding of the engineering properties of flints which are linked to various factors including the genesis/diagenesis of flints. To date, the genesis of flints remains debatable and the controls on engineering properties of flints on a regional basis have not been systematically investigated. This study sets to investigate: the genesis of flints, the engineering properties of flints across various geographical locations, the variations in these properties with colour, structures, origin, and morphology of flints, and the tectonic history of the host chalk. To achieve these objectives a series of physico-mechanical and petrophysical tests on flints and associated structures sampled from the Danish, English and French chalks have been carried out. A drillability test focusing on the grey and dark brownish grey flints using a standard tricone bit to reflect the rock mass characteristics of flint has been conducted. Petrographic studies comprising scanning electron microscopy, scanning electron microcopy-cathodoluminescence and X-ray diffraction have then been applied to analyse the genesis, diagenesis, microstructures, microtexture, and mineral phase/composition of flints. Results support the biogenic origin of flints through a calcite-silica replacement process and illustrate that engineering properties of flints correlate with colour, origin, and the diagenesis of flints, plus the properties and tectonic history of the host chalk. This study demonstrates that physico-mechanical properties of flints are controlled by their micro-structures/texture/fractures, structures, calcite inclusions and mineral compositions. The dark brownish grey flints with finer microtexture are the strongest, stiffest, densest, hardest, most abrasive and least porous materials with extremely high potentials to cause drill wear. By comparison, the grey flints located in a highly tectonized zone behave differently and are the weakest, less dense, less abrasive and the most porous flints with relatively lower potentials to cause drill wear. These findings offer new contributions to the understanding of the material properties of flints applicable to drillability prediction, tool wear evaluation and drilling/tunnelling system specifications in chalk with flints.

# Table of Contents

<b>Declaration .....</b>	<b>i</b>
<b>List of Publications .....</b>	<b>ii</b>
<b>Acknowledgements.....</b>	<b>iii</b>
<b>Abstract .....</b>	<b>iv</b>
<b>List of Tables.....</b>	<b>ix</b>
<b>List of Figures .....</b>	<b>ix</b>
<b>List of Abbreviations.....</b>	<b>xiii</b>
<b>Chapter 1 Introduction .....</b>	<b>1</b>
<b>1.1 Research Motivation and Background .....</b>	<b>1</b>
<b>1.2 Research Aim and Objectives.....</b>	<b>7</b>
<b>1.3 Thesis Structures .....</b>	<b>8</b>
<b>Chapter 2 Literature Review .....</b>	<b>9</b>
<b>2.1 Introduction .....</b>	<b>9</b>
<b>2.2 Scope and Objectives.....</b>	<b>10</b>
<b>2.3 Chalk: Distribution and Roles in Engineering.....</b>	<b>10</b>
2.2.1 Distribution of Chalk .....	10
2.2.2 Roles of Chalk in Engineering.....	11
<b>2.3 Engineering Properties of Chalk .....</b>	<b>11</b>
2.3.1 Petrophysical properties of Chalk.....	11
2.3.2 Porosity.....	11
2.3.3 Permeability .....	12
2.3.4 Density .....	12
2.3.5 Specific Surface Area .....	13
2.3.6 Pore Sizes .....	13
<b>2.4 Geological Settings of Chalk at the UK, French and Danish Study Sites.....</b>	<b>13</b>
<b>2.5 Northern Province Chalk (Yorkshire and Lincolnshire, UK).....</b>	<b>14</b>
<b>2.6 The Stratigraphic of the Northern Province Chalk.....</b>	<b>16</b>
2.6.1 Burnham Chalk Formation (Upper Turonian to Lower Santonian) .....	17
<b>2.7 Southern Province Chalk, UK.....</b>	<b>18</b>
2.7.1 Grey Chalk Sub-group.....	19
2.7.2 The White Chalk Sub-group.....	20
2.7.3 Lewes Nodular Chalk Formation (Middle Turonian to Middle Coniacian).....	21
2.7.4 Seaford Chalk Formation (Middle Coniacian to Middle Santonian) .....	21
<b>2.8 North Western France Chalk, Seaford and Lewes Chalk Formations Dieppe and Mesnil-Val respectively.....</b>	<b>22</b>
2.8.1 Seaford Chalk Formation, Haute-Normandy, France.....	23

2.8.2	Lewes nodular Chalk Formation, Picardy, France .....	23
<b>2.9</b>	<b>Maastrichtian Chalk Formations in Denmark.....</b>	<b>24</b>
2.9.1	Tor Chalk Formation at Stevns Klint, South East of Copenhagen, Denmark .....	25
2.9.2	Sigerslev member .....	26
2.9.3	Tor Chalk Formation at Møns Klint, Eastern Denmark.....	28
<b>2.10</b>	<b>Flints: Distribution and Formation .....</b>	<b>30</b>
2.10.1	Flint .....	30
2.10.2	Distribution.....	31
2.10.3	Formation .....	31
<b>2.11</b>	<b>The Structure/Physiques and Morphologies of Flints .....</b>	<b>32</b>
2.11.1	Flint Crust, Core and White Inclusions .....	32
2.11.2	Flint Morphology .....	33
2.11.3	Tabular Flint.....	33
2.11.4	Tubular Flint.....	34
2.11.5	Paramoudra Flint .....	34
2.11.6	Nodular Flint .....	34
2.11.7	Sheet Flint .....	35
<b>2.12</b>	<b>Problems Associated with Flints from Engineering Geological Perspectives .....</b>	<b>37</b>
<b>2.13</b>	<b>Previous Research on Engineering Characterisation of Flints .....</b>	<b>38</b>
2.13.1	Mechanical Properties of Flints .....	39
2.13.2	Microscopic Classifications of Flints.....	45
2.13.3	Physical properties of flint.....	47
2.13.4	Flint Colour .....	48
2.13.5	Grain Size and Porosity of Flints.....	51
	<i>Grain Size</i> .....	51
<b>2.14</b>	<b>Chapter Summary.....</b>	<b>52</b>
<b>Chapter 3</b>	<b>Field and Experimental Methodology.....</b>	<b>54</b>
<b>3.1</b>	<b>Introduction.....</b>	<b>54</b>
3.1.1	Chapter Outline.....	54
3.1.2	Scope and Objectives of the Chapter .....	55
<b>3.2</b>	<b>Fieldwork, Sampling Flint, Description, and Preparation .....</b>	<b>56</b>
3.2.1	Fieldwork and sampling of flints .....	56
3.2.2	Sample Description and Preparation.....	66
<b>3.3</b>	<b>Strength and Deformability Characterisation Tests.....</b>	<b>73</b>
3.3.1	Uniaxial Compressive Strength (UCS) Test and Static Elastic Parameters .....	73
3.3.2	Tensile Strength Test (Three-Point-Disc Method) .....	75
3.3.3	Point Load Strength Index Determination .....	79
<b>3.4</b>	<b>Petrographic Analysis.....</b>	<b>82</b>
3.4.1	X-Ray Diffraction (XRD) Analysis.....	83
3.4.2	Scanning Electron Microscopy (SEM) Analysis on Rough Flint Samples .....	83
3.4.3	Thin Section Microscopy.....	85
3.4.4	Scanning Electron Microscopy-Cathodoluminescence (SEM-CL) Analysis .....	86

<b>3.5</b>	<b>Wear Classification Tests on Flint Materials.....</b>	<b>87</b>
3.5.1	Determination of Cerchar Abrasivity Index (CAI).....	88
3.5.2	Estimation of Equivalent Quartz Content (EQC).....	90
3.5.3	Rock Abrasivity Index (RAI) Test.....	91
3.5.4	Vickers Hardness Number of Rock (VHNR).....	93
3.5.5	Shore Hardness (SH) Measurement .....	94
3.6.1	Estimation of Ultrasonic Velocities and Dynamic Elastic Data.....	96
3.6.2	Determination of Porosity image analysis (using ImageJ).....	99
3.6.3	Measurement of Porosity using He Porosimeter .....	101
<b>3.7</b>	<b>Particle Size and Shape Analysis using ImageJ.....</b>	<b>104</b>
<b>3.8</b>	<b>Determination of Micropetrographic Index of Flints.....</b>	<b>104</b>
<b>3.9</b>	<b>Experimental Procedures for Large Scale Drilling Test on Flint Blocks .....</b>	<b>107</b>
<b>3.10</b>	<b>Statistical Analysis to Compare between the Estimated Parameters.....</b>	<b>111</b>
<b>3.11</b>	<b>Chapter Conclusions.....</b>	<b>112</b>
<b>Chapter 4</b>	<b>Presentation and Analysis of Experimental Results .....</b>	<b>114</b>
<b>4.1</b>	<b>Introduction .....</b>	<b>114</b>
4.1.1	Chapter Layout.....	114
4.1.2	Scope and Objectives.....	114
<b>4.2</b>	<b>Strength Parameters .....</b>	<b>115</b>
4.2.1	Uniaxial Compressive Strength of Flints and Static Elastic Parameters.....	115
4.2.2	Tensile behaviour of Flints.....	123
4.2.3	Point Load Strength Index Data .....	124
<b>4.3</b>	<b>Geotechnical Wear and Drillability Parameters of flints .....</b>	<b>126</b>
4.3.1	Cerchar Abrasivity Indices of Flints at Different Loading Conditions.....	126
4.3.2	Equivalent Quartz Content of Various Structures and Colour of Flints.....	128
4.3.3	Rock Abrasivity Index of Grey and Dark Brownish Grey Flints.....	130
4.3.4	Vickers Hardness Number of Flint Data.....	132
4.3.5	Shore Hardness Parameters.....	134
<b>4.4</b>	<b>Petrophysical Properties of Flint Materials.....</b>	<b>136</b>
4.4.1	Ultrasonic Velocities and Low Strain Elastic Properties of Flint Materials .....	136
4.4.2	Image Analysis (IA) .....	140
4.4.3	Porosity Trends in Flints Materials using He Porosimeter .....	144
<b>4.5</b>	<b>Particle Size Distribution and Shape of Various Flint Colours and Structures .....</b>	<b>146</b>
<b>4.6</b>	<b>Large Scale Laboratory Drilling Test Results on Flints .....</b>	<b>150</b>
<b>4.7</b>	<b>Correlations of different Geotechnical Properties Investigated .....</b>	<b>152</b>
<b>4.8</b>	<b>Chapter Summary.....</b>	<b>155</b>
<b>Chapter 5</b>	<b>Microstructural and Mineralogical Characterisation of Flint Materials and the Surrounding Chalk.....</b>	<b>157</b>
<b>5.1</b>	<b>Introduction .....</b>	<b>157</b>
5.1.1	Chapter Layout.....	157



<b>5.2</b>	<b>Surface Micromorphology and Silica cementation in Flint Materials</b> .....	<b>158</b>
5.2.1	Scanning Electron Microscopy of Flints, White Crust and Surrounding Chalk.....	158
<b>5.3</b>	<b>Mineral Phase and Composition in Flint Materials</b> .....	<b>173</b>
5.3.1	Mineral Phase Identification/quantification of Flints and the Chalk Surrounding Flint .....	174
<b>5.4</b>	<b>Microstructure of Flint Components from Thin Section Microscopy</b> .....	<b>178</b>
<b>5.5</b>	<b>Scanning Electron Microscopy-Cathodoluminescence (SEM-CL) of Flint Materials</b> .....	<b>190</b>
<b>5.6</b>	<b>Micropetrographic Index (<math>I_{pr}</math>) and Engineering Properties of Flints</b> .....	<b>196</b>
<b>5.7</b>	<b>Chapter Summary</b> .....	<b>198</b>
<b>Chapter 6</b>	<b>Discussion of Research Results</b> .....	<b>201</b>
<b>6.1</b>	<b>Introduction</b> .....	<b>201</b>
6.1.1	Chapter Structure.....	201
<b>6.2</b>	<b>Material Mechanical Properties of Flints</b> .....	<b>201</b>
6.2.1	Strength, Density and Static Elastic Properties of Flints .....	201
<b>6.3</b>	<b>Geotechnical Wear Behaviour of Flint</b> .....	<b>205</b>
6.3.1	Abrasivity of Flint (CAI, EQC and VHNR).....	205
6.3.2	Rock Abrasivity Index (RAI) .....	207
6.3.3	Shore Hardness Properties of Flint.....	210
<b>6.4</b>	<b>Petrophysical Properties of Flints</b> .....	<b>211</b>
6.4.1	Ultrasonic Properties of Flints: Ultrasonic Velocities $V_p$ , $V_s$ and Dynamic Modulus Young's Modulus ( $E_d$ ) .....	211
6.4.2	Micropetrographic Index and Engineering Properties of Flints .....	213
6.4.3	What are the Porosity-Flint Colour/Structure and Grain Size-Flint Colour/Structure Trends? . .....	214
<b>6.5</b>	<b>How do Flints from Different Environments Correlate?</b> .....	<b>220</b>
<b>6.6</b>	<b>What is the Origin of Flints?</b> .....	<b>222</b>
6.6.1	The Formation of Flint .....	222
<b>6.7</b>	<b>What are Geological Controls on Material Properties of Flints?</b> .....	<b>224</b>
6.7.1	The roles of physical properties of chalk on physical properties of flints .....	224
<b>6.8</b>	<b>Engineering Properties of Flint</b> .....	<b>226</b>
6.8.1	Influence of Microtexture/Microstructures in Material Properties of Flint .....	226
6.8.2	Influence of Morphology .....	227
6.8.3	Effects of Macrostructures/Tectonic of the Host Chalk on the Properties of Flint .....	228
6.8.4	Influence of Mineral Composition .....	229
<b>6.9</b>	<b>Is there any Relationship between Drillability and Colour of Flints?</b> .....	<b>230</b>
<b>6.10</b>	<b>What are the Implications of the Study in Practical Concept?</b> .....	<b>231</b>
6.10.1	Implications for laboratory/large scale characterisation of flints .....	231
<b>6.11</b>	<b>Relationships between Some Mechanical Properties of Flints</b> .....	<b>233</b>
<b>6.12</b>	<b>Summary of the Chapter</b> .....	<b>234</b>
<b>Chapter 7</b>	<b>Conclusions and Recommendations</b> .....	<b>236</b>

7.1 Conclusions .....	236
7.2 Recommendations for Future Investigation .....	240
References .....	242
Appendices.....	263

## List of Tables

Table 2.1 : Technical challenges caused by hitting or encountering flints in chalk. ....	38
Table 2.2: Summary of Mechanical Properties of Flints.....	39
Table 3.1: Details of sampling sites.....	57
Table 3.2: Description of flint nomenclatures used for each study site derived .....	57
Table 3.3: Description of all the abbreviations used for flint types and colour.....	68
Table 3.4: Core bits specifications designed by the author for drilling flints .....	72
Table 3.5: Details of samples used for UCS test.....	74
Table 3.6: Details of flint samples used for tensile strength test.....	76
Table 3.7: Details of samples employed for the point load strength index test.....	81
Table 3.8: The guideline for the interpretation of abrasiveness (Cerchar, 1986) .....	90
Table 3.9: RAI classification (Plinninger, 2010).....	92
Table 4.1: Laboratory programmes for the data presented in this chapter.....	115
Table 4.2: Summary of dynamic elastic properties of flint materials.....	136
Table 5.1: Summary of mineral composition of chalk surrounding flint samples. ....	174
Table 5.2: Summary of mineral composition of the carbonate inclusions in flints .....	175
Table 5.3: Summary of mineral composition of white crust surrounding flints .....	176
Table 5.4: Summary of mineral composition of different flint categories.....	177
Table 5.5: Micropetrographic index of flints ( $I_{pf}$ , in red fonts).....	196
Table 6.1: Summary of mechanical properties of flints. ....	202
Table 6.2: Summary of CAI, VHNR and EQC of different classes of flints.....	206
Table 6.3: EQC and VHNR for chalk, the different flint types and structures. ....	207
Table 6.4: Summary of Rock abrasivity index (RAI) results for different flint types/classes .....	209
Table 6.5: Showing minimum, maximum and average $V_p$ , $V_s$ and $E_d$ of flints.....	212
Table 6.6: Statistical relationships between $I_{pf}$ and some engineering parameters.....	213
Table 6.7: Summary of porosity of flints measured using Helium porosimetry and image analysis.....	215
Table 6.8: Grain size of the different classes of flints .....	219

## List of Figures

Figure 2.1: Map depicting regional tectonic structures of Yorkshire (After Gale & Rutter, 2006).....	16
Figure 2.2: Lithostratigraphic divisions of Upper Cretaceous Chalk of Northern Province, UK and the Anglo-Paris Basin.....	20
Figure 2.3: Exposure of the Cretaceous to Danian succession at Stevns Klint, Denmark. ....	27
Figure 2.4: Lithostratigraphic subdivisions of Maastrichtian to Danian succession revealed at Stevns Klint .....	28
Figure 2.5: Detail views of Møns Klint succession, Denmark.....	30

Figure 2.6: A conceptual model showing different flint structures.....	33
Figure 2.7: Different flint morphologies (a) Tabular flint, Burnham Chalk, at North Landing, UK. (b) Tubular flint, Lewes Chalk Formation.....	36
Figure 2.8: Different flint samples described as Figure 2.8 above.....	49
Figure 2.9: (a) to (e) Flint samples from Burnham Chalk, North Landing (Ludborough Flint band). .....	50
Figure 3.1: Outline of research outlines employed in this study .....	55
Figure 3.2: Study locations indicated by the red circles (Note: north-west Europe chalk distribution was re-drawn from Mortimore (2012)).....	58
Figure 3.3: Stratigraphic columns of Burnham Chalk Formation showing flint bands from which flints were sampled at North Landing and Lincolnshire (Modified from Mortimore et al., 2001; Mortimore, 2014, Hildreth, 2013 for Ulceby Vale House Quarry. ....	59
Figure 3.4: Flint bands and nodules in the Burnham Chalk Formation, Northern Province, UK. ....	60
Figure 3.5: Stratigraphic column of Seaford Chalk Formation at East Sussex and Dieppe indicating the flint band from which flints were collected (Redrawn from Mortimore, 2014).....	61
Figure 3.6 Extensive bands of nodular flints .....	62
Figure 3.7: Stratigraphic Column of Lewes Chalk Formation at Mesnil-Val indicating the sampled flint band (Mortimore et al., 2001). .....	63
Figure 3.8: Flint bands and Nodules in Danish Chalk Cliffs. ....	64
Figure 3.9: Stratigraphic column of Tor Chalk Formation at Stevns Klint indicating the sampled flint band (Modified from Surly, 1979; Hart et al., 2004). ....	65
Figure 3.10: Flint samples showing fracture network and carbonate inclusions. ....	67
Figure 3.11: Flint samples exhibiting different colour and various degree of carbonate inclusion. ....	69
Figure 3.12: (a-d) Weathered and highly fractured Flint samples (Ludborough Flint band) from Burnham Chalk, north Landing. ....	70
Figure 3.13: Grey flint sampled from Ludborough Flint band, Burnham Chalk Formation at Ulceby Vale Quarry, Lincolnshire. ....	71
Figure 3.14: Sample preparation program. ....	72
Figure 3.15: UCS test setup and samples. ....	74
Figure 3.16: Uniaxial compressive strength test set-up (not to scale).....	75
Figure 3.17: (a) Tensile Strength system for Three-point test;.....	78
Figure 3.18: (a) Point load experimental equipment used for the test;.....	80
Figure 3.19: Illustration of Point load testing equipment and typical sample failure (not to scale). ....	81
Figure 3.20: XRD analysis samples and sample preparation.....	83
Figure 3.21: (a) Scanning Electron Microscopy (SEM) Set-up; .....	85
Figure 3.22: (a) Thin Section Microscopy apparatus; .....	86
Figure 3.23: SEM-Cathodoluminescence (SEM-CL) set-up used for this studies. ....	87
Figure 3.24: CAI test Set-up. ....	89
Figure 3.25: Cerchar abrasivity index test equipment highlighting how specimen were tested (not to scale). ....	89
Figure 3.26: Drill bit lifetime ( $\text{mbit}^{-1}$ ) prediction from EQC (%) (Plinninger, 2008).....	91
Figure 3.27: Drillbit lifetime ( $\text{mbit}^{-1}$ ) prediction from RAI (Plinninger, 2008).....	92
Figure 3.28: Drillbit lifetime ( $\text{mbit}^{-1}$ ) prediction from VHNR ( $\text{kgmm}^{-2}$ ) (Plinninger, 2008). ....	93
Figure 3.29: Shore hardness test setup.....	95
Figure 3.30: Schematic presentation of Shore hardness test equipment.....	95
Figure 3.31: (a) Ultrasonic pulse testing set-up;.....	97
Figure 3.32: Schematic diagram of Sonic velocities measuring apparatus (not to scale) .....	98

Figure 3.33: Flowchart showing the Porosity estimation and grain size analysis process.....	100
Figure 3.34 (a) Stereopycnometer used for He Porosimetry; (b) complete set-up for He porosimetry.....	101
Figure 3.35: He-porosimetry system showing the principle of operation (not to scale) .....	102
Figure 3.36: (a) BNLUK, (b) BLSUK, (c) TMKT, (d) TSKT, (e) SEUK, (f) SDFr, (g) LMFr. Red areas represent cemented portions, while white areas represent un-cemented portions. ....	106
Figure 3.37: (a) Dark brownish grey flint in the Seaford Chalk at Dieppe, France before testing. ....	107
Figure 3.38: Core bits for drilling test.....	108
Figure 3.39:(a) Designed bit holder and (b) Sample holder at the top and support box (next page).....	108
Figure 3.40: Drilling test set-up .....	110
Figure 4.1: Schematic presentation of how different classes of flints response to loading.....	117
Figure 4.2: Typical stress-strain curves for UCS tests on flint samples representing six study sites. ....	118
Figure 4.3: Estimated Uniaxial compressive strength (UCS) for flints derived from all the study sites.....	119
Figure 4.4: Static Young's modulus ( $E_s$ ) for flint samples .....	120
Figure 4.5: Static Poisson's ratio ( $\nu_s$ ) representing each study site. ....	121
Figure 4.6: Density of flint samples from the entire study locations. ....	123
Figure 4.7: Estimated tensile strength of flints by each study site. ....	124
Figure 4.8: Corrected Point load strength index ( $I_{s(50)}$ ) of flint samples from each study site. ....	125
Figure 4.9: Cerchar abrasivity index (CAI) for chalk surrounding flint, different flint colour and structures	127
Figure 4.10: Variation of Cerchar abrasivity index (CAI) with flint colour and geographical locations. ....	128
Figure 4.11: Equivalent quartz content (EQC) of chalk surrounding flints, flint structure and colour.....	129
Figure 4.12: Equivalent quartz content (EQC) for different chalk/flints samples representing each study site, .....	130
Figure 4.13: Rock abrasivity index for different flint samples drawn from all the study sites. ....	132
Figure 4.14: Change in Vickers hardness number of rocks (VNHR) for the surrounding chalk, different colour and structures of flints .....	133
Figure 4.15: Vickers hardness number of rock (VNHR) for flints (different colour) .....	134
Figure 4.16: Distribution of Shore hardness (SH) of flints with different flints samples categorised according to colour and study sites. ....	135
Figure 4.17: Measured compressional velocity ( $V_p$ ) of different flint samples .....	137
Figure 4.18: Estimated shear waves velocity ( $V_s$ ) as a function of flint colour/locations. The.....	138
Figure 4.19: Dynamic Young's modulus ( $E_d$ ) for different flint samples investigated. ....	139
Figure 4.20: Variation of dynamic Poisson's ratio by flint type/colour, and origin. ....	140
Figure 4.21: Processed SEM images for determination porosity of flints using ImageJ.....	142
Figure 4.22: Dark brownish grey flints from the Tor Chalk at Møns Klint, Denmark. ....	143
Figure 4.23: Porosity obtained from Image analysis as a function of flint origin/morphology and colour...	143
Figure 4.24: Variation of porosity with flint types, location, colour and morphology. ....	145
Figure 4.25: Comparison between porosity derived from Helium Porosimetry ( $\phi_{He}$ ) and ImageJ porosimetry ( $\phi_{im}$ ) as a function of flint types/geographical locations. ....	146
Figure 4.26: Processed SEM of dark brownish grey flints from the Tor Chalk at Møns Klint.....	147
Figure 4.27: Processed SEM images for grain size analysis of flints using ImageJ.....	148
Figure 4.28: Variation of grain size for samples of flints categorised according to colour and geographical locations. ....	149
Figure 4.29: Dark brownish grey and grey flints after drilling showing different drilling patterns and grits.	151
Figure 4.30: Worn drill bits after drilling through flints. ....	152
Figure 4.31: (a) Correlation between UCS and $I_{s(50)}$ . (b) UCS and $T_o$ .....	153
Figure 4.32: Correlation between $I_{pf}$ and (a) Point load strength index, (b) Tensile strength. ....	153

Figure 4.33: Correlation between $V_p$ and $V_s$ for flint samples from all the study sites.....	154
Figure 4.34: Correlation between porosity derived from Helium porosimetry ( $\phi_{He}$ ) and porosity measured using image analysis ( $\phi_{im}$ ). .....	155
Figure 5.1: SEM secondary images of chalk surrounding flints.....	159
Figure 5.2: SEM secondary images of carbonate inclusions in flints.....	160
Figure 5.3: SEM secondary images of White crust (WCr) surrounding flints.....	163
Figure 5.4: Same as 5.3 (b) but magnified version to show the fusing of silica .....	163
Figure 5.5: (a) Scanning Electron Image (SEI) of flint-crust boundary from the North Landing Flint.....	164
Figure 5.6: SEM secondary images of flints. (a) Light grey flint, BNLUK (larger image of (a) is shown as Figure 5.8).....	166
Figure 5.7: Light brownish grey flint from Tor Chalk at Møns Klint, Denmark.....	167
Figure 5.8: Same as Figure 5.6a.....	167
Figure 5.9: SEM secondary images of brownish grey flints.....	169
Figure 5.10: Enlarged version of Figure 5.9(a) depicting the intercrystalline microfractures (red arrows), quartz aggregates and intermittent silica cement (enclosed in red)in the sample.....	169
Figure 5.11: SEM secondary images of flints.....	171
Figure 5.12: Dark brownish grey flint from Tor Chalk at Møns Klint, Denmark.....	172
Figure 5.13: Dark brownish grey flint from Lewes Chalk at Mesnil-Val, France.....	172
Figure 5.14: Thin Section photomicrographs of crust-flint from samples collected at the North Landing, UK.....	180
Figure 5.15: (a) Thin Section photomicrographs of white crusts surrounding flints sampled from the North Landing transmitted in CPL.....	181
Figure 5.16: Thin Section photomicrographs of flints collected from the Burnham Chalk at North Landing, UK.....	182
Figure 5.17: Thin Section photomicrographs of flints collected from the Burnham Chalk at Lincolnshire, UK.....	183
Figure 5.18: Thin Section photomicrographs of flint from the Seaford Chalk at Dieppe, France.....	184
Figure 5.19: Thin Section photomicrographs of flint from the Seaford Chalk at East Sussex, UK.....	185
Figure 5.20: Thin Section photomicrographs of flint from the Seaford Chalk at Dieppe, France.....	186
Figure 5.21: Thin Section photomicrographs of flint from the Lewes Chalk at Mesnil-Val, France.....	187
Figure 5.22: Thin Section photomicrographs of flint from the Tor Chalk at Stevns Klint, Denmark.....	187
Figure 5.23: Thin Section photomicrographs of flint from the Tor Chalk at Stevns Klint, Denmark.....	188
Figure 5.24: Thin Section photomicrographs of different portions of flint from the Tor Chalk at Stevns Klint, Denmark. The figures also show the well preserved forams (red arrows) and Red Algae (black arrows) in the samples. (c) and (d) are illustrated in CPL.....	188
Figure 5.25: Thin Section photomicrographs of flint from the Tor Chalk at Stevns Klint, Denmark.....	189
Figure 5.26: Thin Section photomicrographs of flint from the Tor Chalk at Møns Klint, Denmark.....	190
Figure 5.27: a, c and d SEM-CL images of flints from the Burnham Chalk at North Landing, UK.....	191
Figure 5.28: a, c and e are SEM-CL of flints from the Burnham Chalk at Lincolnshire, UK.....	192
Figure 5.29: (a), (c) and (e) SEM-CL of flint samples from Seaford Chalk, East Sussex, UK.....	193
Figure 5.30: (a), (c) and (e) SEM-CL of flint samples from the Seaford Chalk, Dieppe, France.....	194
Figure 5.31: (a), (c) and (e) SEM-CL of flint samples from the Lewes Chalk, Mesnil-Val, France.....	195
Figure 5.32: (a), (c) and (e) SEM-CL of flint samples from the Tor Chalk, at Stevns Klint Denmark.....	195
Figure 5.33 : (a), (b) and (c) are SEM-CL photomicrographs of flint samples from the Tor Chalk, at Møns Klint, Denmark.....	196

Figure 5.34 : (a) UCS against $I_{pf}$ , (b) RAI against $I_{pf}$ (Note the on map decription of flint colours in 5.34 (a) applies to 5.34 (b)).	197
Figure 5.35 : (a) $I_{s(50)}$ against $I_{pf}$ , (b) To against $I_{pf}$ (Note the on map decription of flint.....	197
Figure 5.36: Conceptual Model that summerises the evolution of flint	200
Figure 6.1: Summary of RAI results for different classes of flints.	209
Figure 6.2: UCS versus $\phi_{He}$ . The grey flints in tectonically disturbed chalk is enclosed in red.	217
Figure 6.3: Conceptual Model illustrating variations in material properties among different flint categories (not to scale).	221
Figure 6.4: Conceptual Model of tectonically disturbed formation showing why other tests are not affected by fracturing.	229

## List of Abbreviations

ANOVA	Analysis of variance
ASTM	American Society for Testing and Materials
BG	Brownish grey Flint
BLSUK	Flint from the Burnham Chalk Formation at Lincolnshire, UK
BLSUK <sub>t</sub>	Tabular Flint from the Burnham Chalk Formation at Lincolnshire, UK
BLSUK <sub>n</sub>	Nodular Flint from the Burnham Chalk Formation at Lincolnshire, UK
BNLUK	Flint from the Burnham Chalk Formation at North Landing, UK
BSE	Back Scattered Electron
CAI	Cerchar Abrasivity Index
Ch	Chalk
CL	Cathodoluminescence
COV	Covariance
CPL	Crossed Polarised Light
DBG	Dark brownish grey flints
DSDP	Deep Sea Drilling Project
Ed	Dynamic Young's Modulus
EDX	Energy Dispersive X-Ray Spectroscopy
EDXRF	Energy Dispersive X-Ray Fluorescence
Eh	Redox Potential

EQC	Equivalent Quartz Content
Es	Static Elastic Young's Modulus
Fr	France
GF	Grey Flint
GPa	Giga Pascal
He	Helium
HRC	Rockwell Hardness
IDD	Intact Dry Density
I <sub>pf</sub>	Micropetrographic Index
LBG	Light Brownish grey Flint
LG	Light grey
LVDT	Linear Variable Displacement
K-Pg	Cretaceous-Paleogene
LG	Light grey
LMFr	Flint from the Lewes Chalk Formation at Mesnil-Val France
LS	Lincolnshire
MPa	Mega Pascal
n	Number of samples or specimens
NL	North Landing
PPL	Plane Polarised Light
RAI	Rock Abrasivity Index
SD	Standard Deviation
SDFr	Flint from the Seaford Chalk Formation, France
SEI	Secondary Electron Image
SEUK	Flint from the Seaford Chalk at East Sussex
SEM	Scanning Electron Microscope
SEM-CL	Scanning Electron Microscope-Cathodoluminescence
SGch	Spotted Grey Chalk

SH	Shore Hardness
SWI	Spotted White Inclusion
SSI	Silicified White Inclusion
TBM	Tunnel Boring Machine
TMKT	Flint from the Tor Formation Møns Klint
TSKT	Flint from the Tor Chalk Formation at Stevns Klint
VHN	Vickers Hardness Number
VHNR	Vickers Hardness Number of Rock
WCr	White Crust
WI	White Inclusion
XRD	X-Ray Diffraction



# Chapter 1 Introduction

## 1.1 Research Motivation and Background

Flint has received significant attention for several decades; initially as a vital Palaeolithic material for manufacturing tools and later as one of the most critical engineering geological threats to drilling or tunnelling in chalk-bearing flint. Flint is a siliceous, cryptocrystalline rock that forms in chalk and composed of mainly silica (about 70-99%), with few impurities dominated by calcite and occasional traces of clay minerals. Embedded in chalk, flint exists in different colours ranging from white, grey, light grey, light brownish grey to dark brownish grey flints and in various morphologies including nodular, Paramoudra, sheet, tabular, and tubular flints (see Chapter 2 and Bromley, 1967; Shepherd, 1972; Bromley et al., 1975; Nygaard, 1982; Clayton, 1984; 1986). In addition to different morphology, flint is identified with various structures which include white or red crust (this can be completely siliceous or have a significant quantity of calcite), white inclusions (this is rich in calcium carbonate) and the core (this is dominated with silica). Flint is widely distributed just as the host chalk and is mostly found in several countries in Europe, significant parts of Asia, few sections of Africa, America (Shepherd, 1972), Middle East and Australia (Mortimore, 2010).

In recent decades, the growing engineering significance of chalk as a hydrocarbon reservoir, aquifer or host to some infrastructures like a gas cavern, houses, tunnels, railways and piles for foundations have led to several engineering projects in chalk with flint. In petroleum engineering chalk is investigated for hydrocarbon exploration, because chalk serves as oil and gas reservoir in places like the North Sea and Texas. In hydrogeology, chalk is drilled for water exploration because chalk serves as one of the most important aquifers in the UK and Israel (see Mortimore, 2012). Similarly, in civil engineering chalk is tunnelled, excavated or drilled to support varieties of engineering projects mentioned above.

In the process of excavating or drilling chalk for the purposes mentioned above, several engineering geological/technical challenges are faced. Encountering flint constitutes one of the major geotechnical or engineering geological challenges in chalk-bearing flints. These challenges usually result in damages incurred from rapid destruction of drilling or tunnelling equipment in the form of drill bit wear, wearing of the picks, cutter arms, cutting face and crushing cones. In addition to these, the hardness of flint can also inhibit project progress due to rapid wear of drilling bits (Peterson, 1974) and deflecting of drill bits away from flint bands (Hahn-Pedersen, 1999).

Experiencing these challenges has enormous economic and technical consequences, which have previously resulted into a highly costly decision involving an extensive review of the project (Peterson, 1974), retrieval of the drill string, the total change in drilling well (Hahn-Pedersen, 1999), and change in drilling method (Varley, 1990). In some cases, the whole tunnel and tunnel boring machine had to be redesigned (Cumming, 1999; Mortimore, 2001), while in some projects both drill bit and the drill rig had to be replaced (Star Banner, 2001). In some instances, the teeth of Hydromills (Symes, 2012) and cutter (McDonald, 2012) have to be replaced. In most of these case studies, the consequences had resulted in longer rig times, loss of man-hours, leading to the overall delays in project completion with subsequent rise in the total project costs beyond the original contract costs.

In view of problems associated with working in chalk with flint, it is vital to define and understand the formation and properties of flint in the Upper Cretaceous Chalk for effective engineering projects in chalk with flint. Also important is the need to study the link between various properties of flint within the Upper Cretaceous Chalk which can be related to the genesis and diagenesis of flint, considering one; the distribution of chalk across the globe, two the roles of chalk in various aspects of human development and three the threats posed by the embedded flint to engineering projects in chalk with flint. Additionally, the need to dig or excavate through chalk with flint due to the growing demand for energy and infrastructural development in chalk with flint also point to the importance of understanding the evolution and properties of flint. Similarly, appreciating how the properties of flint vary with geographical locations or region/origin, colour, mineral composition and morphology of flint would help in identifying the capacity of the drilling or tunnelling machine that can suitably be deployed to the field and would help in selecting suitable drilling/tunnelling method for any site. Furthermore, defining the geomechanical properties of flints would also prevent the need to re-design the entire project/drilling programme or the need to replace the tunnel boring machine (TBM) or the drilling rig/method, which is usually expensive, and time-consuming.

Several researchers have studied and significantly contributed to the present understanding of several aspects of flint across various industries. Flint symposia from the 1970s onwards are typical examples (e.g. Sieveking & Hart, 1986). One of the aspects of flint research that have gained significant attention is in archaeology. Recent studies in this industry have mainly focused on provenance of some flints (Harding et al., 2004; Olofsson & Rodushkin, 2011; Olausson et al., 2012) and other investigations have concentrated on the genesis of various flint artefacts and flint nodules from various sources (see Bustillo et al., 2008; Huges et al., 2010; Graetsch & Grunberg, 2012; Högberg et al., 2012; Moroni & Perelli, 2012; Prudêncio et al., 2015)

using different chemical techniques. One of the gains of these studies is the successful identification of chemical compositions within various flint colours and structures.

Before 1984, there were ample researches on the genesis of flint and these studies have significantly contributed to the current understanding of the evolution and behaviour of flint. The work of Clayton (1984;1986) provided one of the most comprehensive geochemical evidence of flint formation, and since then more studies on the genesis of flint using various approaches have been springing up (e.g. Madsen & Stemmerik, 2010) but the origin of flint remains a subject of debate. Besides the formation of flint, recent advances in mineralogy of flint (Masen & Stemmerik, 2010; Lindgreen et al., 2011; Graetsch & Grunberg, 2012; Lindgreen & Jakobsen, 2012; Jakobsen et al., 2014) have improved the present understanding of the properties of flint. Most of these studies have demonstrated that flint is composed of  $\alpha$ -quartz with subordinating impurities (e.g. calcite, clay). However, there is the need for proper understanding of how the mineral composition of flint vary with colour, structures as well as the engineering properties of flint. Understanding this variation especially at regional scale would provide useful information for modelling flint for engineering projects.

One of the major areas in the chain of flint studies that has received significantly little attention despite being a key to understanding the abrasiveness and drillability of flint is the characterisation of mechanical properties of flints. For example, the hardness of flint derived using Vickers Hardness Number of Rock (VHNR) was only published in Pradel & Tourenq (1972). Similarly, the abrasiveness of flint studied using CAI method was only reported in Cumming, (1999) and Fowell & Abu Bakar (2007). The CAI was concluded to be unsuitable for the estimation of the abrasiveness of flint (Cumming, 1999). Similarly, information on porosity of flint is also limited, with significantly few reported investigations (e.g. Weymouth, 1951; Michelseen, 1966; Latridou et al., 1986; Jakobsen et al., 2014) while the ultrasonic properties of flint are possibly never investigated. Therefore, the scarcity of data on abrasivity, hardness, porosity and ultrasonic properties of flint points to the need for more investigations on these properties of flint. This is to understand the wear behaviour of flint and to detect how structural details of flint vary with type and conditions of flint.

Like the abrasiveness, hardness and porosity data of flint, published data on the strength properties of flint is limited (Latridou et al., 1986; Cumming, 1999; Smith et al., 2003; Mortimore et al., 2004). Iller (1963) pioneered the study of strength of flint and found a relationship between strength and the microtexture of different colours of flint. Pradel & Tourenq (1967) illustrated that Grand-Pressigny Flint has more durability than coarse sandstones and polished jasper Opal. Pradel & Tourenq (1972) illustrated the suitability of Grand-Pressigny Flint for tool making using fragility test. Varley (1990)

examined the strength of flint from Humberside and reported a strength value, which suggested the investigated flint is extremely strong. Fowell & Martin (1997) investigated the cutterbility of flint and assessed the strength properties of Paramoudra flint. These authors found that flint is extremely strong in compression and relatively weak in tension.

Cumming (1999) conducted one of the most comprehensive studies on strength characterisation of flint focusing on flint in the Southern Province Chalk of the UK. In that study, flint was shown to have variable strength, significantly affected by weathering and tectonic processes. The study also established that flint was extremely strong, but the strength of flint was lower in weathered, fractured, carious and pale flints. The study also informed the need for understanding the geology of the host chalk environment, the diagenesis of the host chalk, the formation, diagenesis and post-diagenetic processes of flint for the evaluation of material properties and evolution of flint. The study further mentioned that other factors such as temperature, depth of deposition, the chemical composition of silica, the rate at which flint is formed and post-depositional influence may have effects on strength properties of flints. Furthermore, the study suggested that the strength of flint may likely vary with geographical locations.

Domański & Webb (2000) explored the relationship between the microstructures of some Polish flint samples and the fracture toughness. These authors showed that the fracture toughness of flint varies with microstructures, microtexture and the extent of calcite inclusions in the flint samples. Smith et al. (2003) estimated the strength properties of flint sampled from Cray and Brighton and established that the strength of flint varies and is controlled by the presence of internal flaws. The observations of these researchers supported the work of Cumming (1999) on flint from the same geographical location. The study also mentioned the likely variation in strength properties of flint with geographical location.

Therefore, in view of the above reviewed studies and investigations by several engineering teams on characterising the sizes, frequency, strength and abrasivity of flints for tunnelling projects, a critical examination of these studies revealed the following facts:

- There is no complete characterisation of flints on a regional basis especially in relation to the drillability and cutterbility of flints and some aspects of origin of flint remains unresolved. Most existing studies of flints are either confined to a region or geographical location. Thus, understanding the regional trend in material properties of flint is necessary for wider applicability of experimental results and for proper modelling of flint especially where projects might pass through various regions.

- To date, there is no existing abrasiveness method that has been successfully applied or can be used to evaluate the abrasiveness of flints and data on abrasivity of flints is lacking. Hence, there is the need for the establishment or determination of a suitable, simple and cheap method for characterising wear behaviour of flints.
- The relationship between the mineral phases/composition of flint, the evolution, the diagenesis and the mechanical properties of flint has also not been investigated.
- The links between the geology of the host chalk, the tectonics of the host Chalk, the post-depositional processes experienced by the flints and the material properties of flints have not been examined.
- There is currently no detailed attempt to relate some of the most important mechanical properties of flint needed for the design of engineering projects and the relevant cutting tools/equipment with the variation in colour, mineral composition, morphology, microtexture and microstructures of flint.
- The variation in mineral composition of flints with structures and colour has not been explored. Therefore, exploring such variation could help in proper understanding of the causes of variability in the engineering properties of flints, since flints exist in different colours and structures (white crust, white inclusion and core).
- Despite the difficulties in sample preparation and high cost of testing flint, models that can be used to estimate the engineering properties of flint are still lacking. Developing or deriving these models, especially from simple and cheap non-destructive methods, would significantly reduce or eliminate the difficulties and costs associated with preparing and characterising flint samples.
- Besides the large scale cutterbility test conducted by Crab & Hignett (1980) and Fowell & Martin (1997), attempt to understand the cutterbility of flint at larger scale, which could help in modelling the actual field behaviour of flints, data on drillability of flint at this scale is lacking. Therefore large-scale drillability data are crucial for understanding the drillability of flints at rock mass scale and understanding this would assist in the prediction of tool/equipment performance, the selection and design of suitable excavation method in chalk with flints.

Therefore, in light of the problems posed by flints on the engineering projects in chalk with flint, and the significant roles of chalk to humanity, this study builds on the previous studies of flints by addressing the facts mentioned above on flint research. This study, will therefore, contribute to the understanding of the genesis, drillability, abrasiveness, and engineering properties of flint, and to the development or

identification of suitable methods for characterising flints. Investigating flints focusing on the above listed facts provides some keys for proper modelling of abrasivity and drillability of flints. Thus, in this study different structures (white crust, white inclusion and flint colour) and colours of flints were identified. Sampling was made by considering variation in colour, and morphology of flint. In an attempt to understand the influence of tectonic experience of the host chalk on properties of the embedded flint, sampling of flint was also based on the variability in tectonic history of the host chalks in the respective study sites. The strength of flint was investigated using the uniaxial compressive strength (UCS), point load strength index  $Is_{(50)}$  and the tensile strength ( $To$ ). The  $Is_{(50)}$  and  $To$  were also determined to understand the crushing and tensile strength of flints and to apply the two methods to develop model for the prediction of UCS from these simple tests. The density of different coloured flint was measured using the calliper method described in ISRM (2007). The static deformability (static Young's modulus and Poisson's ratio) of flint was determined using strain gauges.

The abrasivity of flint and associated structures were studied using Cerchar abrasivity (CAI), VHNR, Equivalent Quartz Content (EQC), and Rock Abrasivity Index (RAI). The Shore Hardness (SH) was applied to measure and understand the hardness of flints. He-Porosimetry was used to estimate the porosity of flints while ImageJ was used to measure the porosity of flint considering variation in colour and structures of flints. Particle size of flints was determined to identify textural variation within different colour of flints using image analysis (ImageJ). Ultrasonic pulse method was used to measure the ultrasonic pulse velocities and dynamic Young's modulus of flints so as to detect the influence of microfractures on different flints samples. The ultrasonic properties were also determined to establish any correlation with the destructive methods so that mechanical properties of flints can be determined from the ultrasonic method being a non-destructive method. The mineral phases and composition of flints were determined using X-ray diffraction to identify any link between degree of silica cementation, calcite silicification (all refer to microstructures, henceforth), mineral composition and mechanical behaviour of flints. The evolution of flints, the influence of diagenesis on properties of flints, the controls on properties of flints, and the link between mechanical properties of flint and mineral (silica) phases, microtexture (degree of cementation and silicification), and microstructures of flints were investigated using SEM, thin section microscopy and SEM-CL. The relationships between engineering properties of flints were investigated and a relationship between engineering properties of flints and micropetrographic index was developed.

## 1.2 Research Aim and Objectives

### Aims:

This study aims at investigating the genesis and properties of flints in relation to engineering projects in the Upper Cretaceous Chalk. The study has the following specific objectives and covers flints found in quarries and cliffs exposures along the coasts of the UK, Denmark and France.

### Objectives

The objectives of this study are summarised below:

- Investigation and characterisation of flints from different geographical locations.
- To investigate the physical/mechanical properties of different classes of flints
- Examination of wear properties of flints and identification of suitable method (s) of determining these properties for flints.
- Determination of petrophysical properties of flints and how these change with flint class.
- To employ petrographic approaches to identify the genesis, and diagenesis of flints and to understand the controls on material properties of flints by identifying:
  - (a) the link between geology/physical properties of chalk with diagenesis, and post-depositional processes experienced by flints from various sites.
  - (b) the variation in engineering properties of flints with microtexture or microstructures, macro/microfractures, colour, and morphology.
- Determination of relationship between colour, structures, material properties of flints with mineral composition.
- Identification of suitable method and development of models for characterisation of flints.
- Application of large scale laboratory drilling test to delineate the rock mass drillability of flints.
- Integration of research findings, testing the hypotheses and recommendations for best practice.

### 1.3 Thesis Structures

This thesis is composed of seven chapters. In **Chapter 2** the published literature on the Chalk is reviewed as the host rock to the subject of this thesis, which is flint. The distribution of chalk, the roles of chalk in engineering, the engineering properties of chalk, and the geological settings of chalk in the study sites are also reviewed in the first part of this chapter. The second part of this chapter is dedicated to the review of published literature on flint, the distribution, the formation, the structure, and morphologies of flint. Problems associated with flint from the engineering point of view and previous researches on the engineering classification of flint are also reviewed in this chapter.

In **Chapter 3** field and experimental approaches employed to answer the research questions are explained. This commences from the fieldwork, sampling of flint, description and preparation of flint samples. The chapter also discusses the strength, deformability, petrographic, wear and ultrasonic pulse experiments conducted in the thesis.

**Chapter 4** contains the results of strength, deformability, geotechnical wear, drillability, petrophysical, and correlations between different geotechnical parameters.

**Chapter 5** contains the data derived from the Scanning Electron Microscopy (SEM), quantitative and qualitative mineral, thin section microscopy and Scanning Electron Microscopy-Cathodoluminescence (SEM-CL) analyses of flint and associated structures. This chapter concludes with quantitative petrographic analysis (micropetrographic index).

**Chapter 6** discusses the mechanical, wear and petrophysical properties of flints. This chapter also discusses the correlation between flints from various environments, the genesis and geological controls on material properties of flints. The relationships between the engineering properties of flint and factors like microstructures, microtexture, colour and mineral composition of flint are then discussed in this chapter. In this chapter, the relationship between the drillability and colour of flint is discussed and this was followed by the discussion of the overall implications of the study.

**Chapter 7** draws together the conclusions reached in accordance with the set objectives and based on the findings from both the field and experimental observations. The chapter further presents suggestions for future research.



## Chapter 2 Literature Review

### 2.1 Introduction

In Chapter 1 the research aims were introduced. This chapter, therefore, focuses on reviewing the geology, features and engineering of the two major rock types that form the basis for this research. First the chalk and second the flint, which is the main subject of this research. There is an extensive literature covering most aspects of chalk (Scholle, 1974; Hancock, 1975; Wood & Smith, 1978; Mortimore, 1986; Bloomfield et al., 1995; Surlyk, 1997; Bell et al., 1999; Mortimore et al., 2001; Mortimore, 2014) including those related to engineering (e.g. Lord et al., 2002) and geochemistry. This review will only emphasise those aspects of chalk which are relevant to the investigation of the flints based on the objectives outlined in Chapter 1.

The chapter is broadly divided into two major parts. The first part summarises chalk by reviewing the definition and the distribution of chalk across the globe. The engineering properties of the host chalk and the geological settings of chalk deposits are also reviewed especially with regard to the study sites. This is to establish any link between local geology, the engineering behaviour of the host rock and the material properties of the embedded flints.

In the second part of the chapter flints are discussed. This section covers the definition, formation and distribution of flints. The formation of flints has received widespread attention in the past (Bromley et al., 1975; Knauth, 1979; Clayton 1984; Bennett et al., 1988; Maliva, 1988; 1991, Behl et al., 1992; Minguez et al., 1994; Umeda, 2003; Madsen et al., 2010; Lindgreen, 2012; Jakobsen et al., 2014), yet its origin remains uncertain.

The physical features of flints, comprising of a crust and a flint core are also covered in this part of the chapter, to give the reader a clear picture of what the features that flint entail, as they are referred to in the subsequent chapters. Towards the end of the chapter, different flint morphologies are reviewed and discussed to give an insight on their features as two morphologies comprising of tabular and nodular flints will be investigated (Chapter 3), their material properties compared (Chapters 4 and 5) and then further discussed in Chapter 6.

The challenges with flints arising from engineering projects which is a major focus of this study are reviewed and discussed. Existing studies on the engineering properties of flints are reviewed and critiqued to explore the existing research gap, and to pinpoint where the current study fits into the relevant existing research map. The chapter is then closed by a summary of the chapter highlighting some questions upon which the thesis was based upon and proposing goals for Chapter 3.

## **2.2 Scope and Objectives**

This chapter is divided into fourteen (14) sections. The scope and objectives of the chapter are given in Section 2.2; this is then followed by the definition, distribution and the roles of chalk (Section 2.3). While the engineering properties of chalk are reviewed in Section 2.4, the geological background of chalk in the study sites are also reviewed (Sections 2.5 to 2.9). The definition, distribution and formation of flints are discussed in Section 2.10, while the physical features of flints and flint morphology are discussed in Section 2.11. The chapter proceeds by reviewing geotechnical challenges associated with encountering flints within chalk (Section 2.12), and then proceeds by reviewing previous investigations of the materials properties of flints (Section 2.13). The chapter is then summarised in Section 2.14 and completed by raising some questions related to the research hypotheses.

## **2.3 Chalk: Distribution and Roles in Engineering**

Chalk definition: several researchers (Hancock, 1975; Bell et al., 1999; Mortimore et al., 2001; Harris, 2007) have already defined chalk. Chalk is a pure, white, grey, or red limestone comprising of more than 98% calcium carbonate mainly from coccoliths, and few microfossils like Bryozoa, Ostracod tests, and spines of Echinoids. Chalk is typically divided into a fine fraction (70-90%) with particle sizes in the range 0.5-4  $\mu\text{m}$ , and 5-25 % being a coarse fraction dominated by the size range of 10-100  $\mu\text{m}$  (Hancock, 1975).

### **2.2.1 Distribution of Chalk**

Chalk is found commonly in the north east and south of England and spreads out to the eastern England, across the North Sea, to the northern part of Germany, Denmark, Holland, and Poland (Rayner, 1981). Chalk forms landscapes that extend from the Southern Province Chalk hills through France and which continue to the hills of the Crimea, Kazakhstan and the Judean desert (Mortimore et al., 2001). Chalk deposits are also found in Egypt, Libya, Belgium, Northern Ireland, Iraq, Lebanon, Israel, Norway, and Sweden. Chalk is also found in Bulgaria, Turkey, Texas (Austin), Syria, Arkansas, Mississippi, Alabama and Australia. Thus, considering this wide distribution of chalk, the significance of studying the engineering behaviour of flint which is embedded in chalk cannot be underestimated.

## **2.2.2 Roles of Chalk in Engineering**

The roles of chalk in engineering cannot be overemphasised. Chalk has been significant since the early stage of human life with some of the earliest evidence of human activity in the UK making flint tools and ball pits to extract flints for knapping. More recently chalk has a variety of applications in various fields of life, ranging from engineering, hydrogeology to petroleum engineering. Chalk serves as an important Oil reservoir in America and Western Europe. In most of the countries where chalk is found, the materials are excavated for houses, tunnels, road networks, and rail lines or as caverns for storing gas. Chalk beds also serve as important aquifers in some countries such as the UK, Denmark, Jordan (Mortimore, 2012) and Israel. Significant portions of these chalk deposits bear flint bands, which are among the key features causing technical challenges when boring through chalk, either for engineering structures or for exploration (Oil or water). Therefore, studying the Upper Cretaceous flints is significant considering the distribution of chalk across the globe.

## **2.3 Engineering Properties of Chalk**

### **2.3.1 Petrophysical properties of Chalk**

This section of the thesis reviews the various studies on the petrophysical properties of Chalk. These properties have either direct or indirect impact on the strength of chalk, and may reflect the diagenesis of the embedded flint.

### **2.3.2 Porosity**

Chalk porosity is partly controlled by the effect of burial depth, being controlled by the degree of mechanical compaction, and by the initial composition of fossils. Early diagenesis and late cementation also have influence on the porosity of chalk. Factors such as intrafossil cements, particles size, hydrocarbon saturation, throat diameter, tectonic history, regional diagenetic processes, the degree of cementation, mineralogy, and stylolitisation (Hancock, 1975).

The porosity of chalk varies spatially and stratigraphically. Bell et al. (1999) for example, reported a porosity variation between southern and northern England Chalks. Most porosity values reported for the white chalk of southern England falls in the range of 35-47%, whilst porosities of about 40 % are typical for the Ekofisk Chalk (Hancock, 1963; Carter et al., 1974; Scholle, 1974; Bell et al., 1999) which is similar to porosity of

40-50% at the Stevns Klint Chalk (Frykman, 1994; Strand et al., 2006; Nnaemeka, 2009) and 40-44% for the Chalk at Møns Klint (Foged, 1994). The porosity of the harder chalks of Yorkshire average less than 25%, about 17-20% being reported by Scholle (1974).

Hancock (1975) showed the variation in porosity with depth, where the porosity of soft chalk was reported to reduce from an initial range of 38-48% to approximately 15-30 % at a depth range of 1500-2000 m, with a further reduction to 2-25% when depth increases to 2700-3300 m. Porosity variations also exist within the same region, chalk formation and between chalk formations. In the Anglo-Paris Basin for instance, porosity of chalk was shown to vary within a chalk formation, between chalk formations and across different lithology (see Mortimore & Pomerol, 1998). The porosity trends observed in different chalk beds and between different locations/formations could relate to the diagenetic experience of the embedded flint bands.

### **2.3.3 Permeability**

Permeability in chalk depends on porosity, specific surface area, the degree of cementation, diagenesis, grain size, pore size, pore connectivity, discontinuity patterns, the presence of secondary fractures, and burial depth. The chalk is considered to have dual permeability, the permeability of the material and the permeability of the fracture in chalk formations leading to higher permeability within the entire rock mass (Bell et al., 1999). Most high permeability values found in the chalk are because of the presence of secondary fractures in the rock, or due to the effect of secondary fissures caused by calcite dissolution. The typical permeability of chalk ranges from  $5.12 \times 10^{-5}$  to  $10^{-2}$   $\text{md}^{-1}$  (Ineson, 1962; Scholle, 1974; Price, 1985 and Bell et al., 1999).

### **2.3.4 Density**

The density of chalk is an important parameter which may relate to the hardness, and strength characteristics of the embedded flints. Clayton (1983) reported dry densities from 1.25 to 2.50  $\text{Mgm}^{-3}$ , while Mortimore et al. (1990) presented a range of 1.43 – 2.32  $\text{Mgm}^{-3}$  for the Chalk in the Southern England and 2.30  $\text{Mgm}^{-3}$  for the Middle Chalk of Yorkshire. These values, therefore, based on the hardness classification proposed by Mortimore et al. (1990) indicated that Yorkshire Chalk has very high density while the Southern England Chalk from Kent is low-density chalk. These authors attributed the variation in hardness of chalk to the formation of various sizes of rhombic crystals, silicification of coccoliths, plugging of pores by micro spar, variations in degree of interstitial secondary calcite (cited in Bell et al., 1999), and the presence of silica or apatite. As observed in the porosity variation (Section 2.4.1), the differences in density

between different chalk deposits could be linked to the overburden pressure and diagenesis.

### **2.3.5 Specific Surface Area**

The specific area of chalk relies on some factors like carbonate content and mineralogy of other non-carbonate fraction (Hjuler & Fabricius, 2007). This property determines the ease with which fluid flow within the Chalk. For the chalk materials the specific area ranges from 1-7 m<sup>2</sup>g<sup>-1</sup> (Røgen et al., 2002), while for some mineral constituents in chalk are 0.5-3.5 m<sup>2</sup>g<sup>-1</sup> for calcite (Røgen et al., 2002; Megawatti et al., 2013) and 5 m<sup>2</sup>g<sup>-1</sup>, 15 m<sup>2</sup>g<sup>-1</sup>, and 60 m<sup>2</sup>g<sup>-1</sup> for quartz, kaolinite, and smectite respectively (Røgen et al., 2002). Thus, these values show that calcite has the least value of specific area, which in turns means it is more permeable than the remaining mineral constituents.

### **2.3.6 Pore Sizes**

Pore sizes of chalk are important parameters in defining both the petrophysical and geomechanical properties of the rock. This feature varies according to the depth of burial, presence of marl, depositional environment, sediment transport process and the stratigraphic location of the Chalk. The greater the burial depth, the smaller the pore sizes as the Chalk grains are compressed due to overburden pressure. Patsoules & Cripps (1982) tested chalk samples from the North Sea and Yorkshire and found that majority of the pore sizes fall in the range of 0.01-3 mm. The test showed higher median pore diameters from the Upper to Lower Chalk of Yorkshire while the East Anglia and southern Chalks recorded median pore diameters of 0.65 and 0.39 mm respectively.

## **2.4 Geological Settings of Chalk at the UK, French and Danish Study Sites**

The rifting of the Mesozoic supercontinents and the subsequent rise in sea-levels, reaching their historic peak during the Cretaceous period resulted in the formation of thick beds of chalk sediments (Mortimore et al., 2001) covering significant parts of the world including northern Europe which encompasses the study areas of this research. These chalk deposits were originally the remains of calcitic fossils that accumulated on the seabed. Subsequent post-depositional and post-rift tectonic processes, erosion, uplift, and reactivation of existing faults resulted into the various forms, shapes,

thicknesses and deformity seen in various Chalk successions around the world. The depth of deposition of chalk varies from one location to another. The English Chalk for example was deposited 100 to 500 m water depth (Mortimore et al., 2001). Conversely, the chalk deposits in the North Sea Central Graben believed to have been deposited in deeper water (e.g. see Japsen, 1998).

## **2.5 Northern Province Chalk (Yorkshire and Lincolnshire, UK)**

The English Chalk forms outcrops in Yorkshire and continues from the north via Lincolnshire and East Anglia, to southern England (Mortimore, 1983). This includes a series of very fine-grained, pure limestones with a thickness ranging from 400-600 m (Shepherd, 1972; Rayner, 1981; Mortimore et al., 2001; Harris, 2007). The English Chalk groups are broadly divided into three main provinces, the Southern, Northern and Transitional Provinces (Mortimore, 1983). The Chalk of these Provinces varies in terms of lithology and hence density and hardness (Mortimore et al., 2001), as shall be explained in the following sub-sections.

The Northern Province Chalk outcrops over parts of north-west Europe was deposited in deeper water deposits than the Southern Province Chalk (Mortimore et al., 2001; Gale & Rutter, 2006) and is suggested to be deeper water deposits than the chalks at Stevns and Møns Klint. The Northern Province Chalk is more associated with the Boreal Realm while the Southern Province Chalk is more related to the Tethyan Realm (Mortimore et al., 2001) and is characterised by the presence of massively bedded tabular flints at some formations (e.g. Burnham Chalk Formation), while *Thalassinoides* burrow and continuous tabular or lenticular flints have also been observed in the Province (Mortimore & Wood, 1986). The total thickness of chalk bearing flints in this Province is believed to be about 185 m from the base of the flints in the Welton Chalk Formation (Figure 2.2) up to the upper flints at the high stack in the Burnham Chalk Formation (Mortimore et al., 2001). The colours of the flints observed in this Province vary considerably from white, and grey to pale grey. Other colours such as brownish grey and light brownish flints are also noticeable. Dark brownish grey flints dominate the Southern Province Chalk, the north western French chalk and the south eastern Danish Chalk. Samples of flints in this investigation were obtained from the Chalk of the Anglo-Dutch Basin; Anglo-Paris Basin and south east part of the Danish Basin comprising the three countries mentioned above. The chalk formations from which flint samples were collected are summarised in Chapter 3.

The Northern Province Chalk is overlain by Quaternary (Devensian) deposits of tills, sands and gravels. The thickness of these glacial deposits varies to a maximum of

more than 50 m in the southern part of the Holderness Plain (Gale & Rutter, 2006). The Northern Province chalks stretches over Yorkshire, Lincolnshire, Humberside and the North Norfolk chalks (Mortimore & Wood, 1986). Parts of these chalk successions continue to the east into to the North Sea, where more than 800 m of chalk was deposited (Woodland, 1975; Glennie, 1998). The chalk in this province is divided into two major subgroups of Grey and White Chalk. The Grey Chalk subgroup extends from the lowest part of the Glauconitic Marl and to the base of the Plenus Marl Member, while the White Chalk subgroup commences from the base of the Plenus Marls Member to the top of the chalk deposits (Mortimore et al., 2001).

The Chalk in Yorkshire was deposited as post-rift sediments covering boundary between two major regional structures, the Mesozoic Cleveland Basin and the Market Weighton block. The northern margin of the Market Weighton block is marked by the Howardian-Flamborough Fault Zone (Figure 2.1). This fault belt is characterised by numerous East-West trending faults cutting the Yorkshire Chalk, and forms one of the most faulted and fractured zones in the region. It is especially well expressed at North Landing.

Besides, the East-West trending faults, North-south trending faults are also commonly seen at the Flamborough Head area (Stammer, 1995). The Chalk succession here is highly fractured (c. 0.2-2 m spacing) and are characterised by a consistent orientation and fall in the regional fracture sets category (Welch et al., 2015). Fracturing and associated deformations in these chalk beds are due to the post-Cretaceous tectonic activity that resulted in the reactivation of faults beneath the Chalk beds and numerous events of disturbance in the chalk beds (Stammer, 1995; Gale & Rutter, 2006).

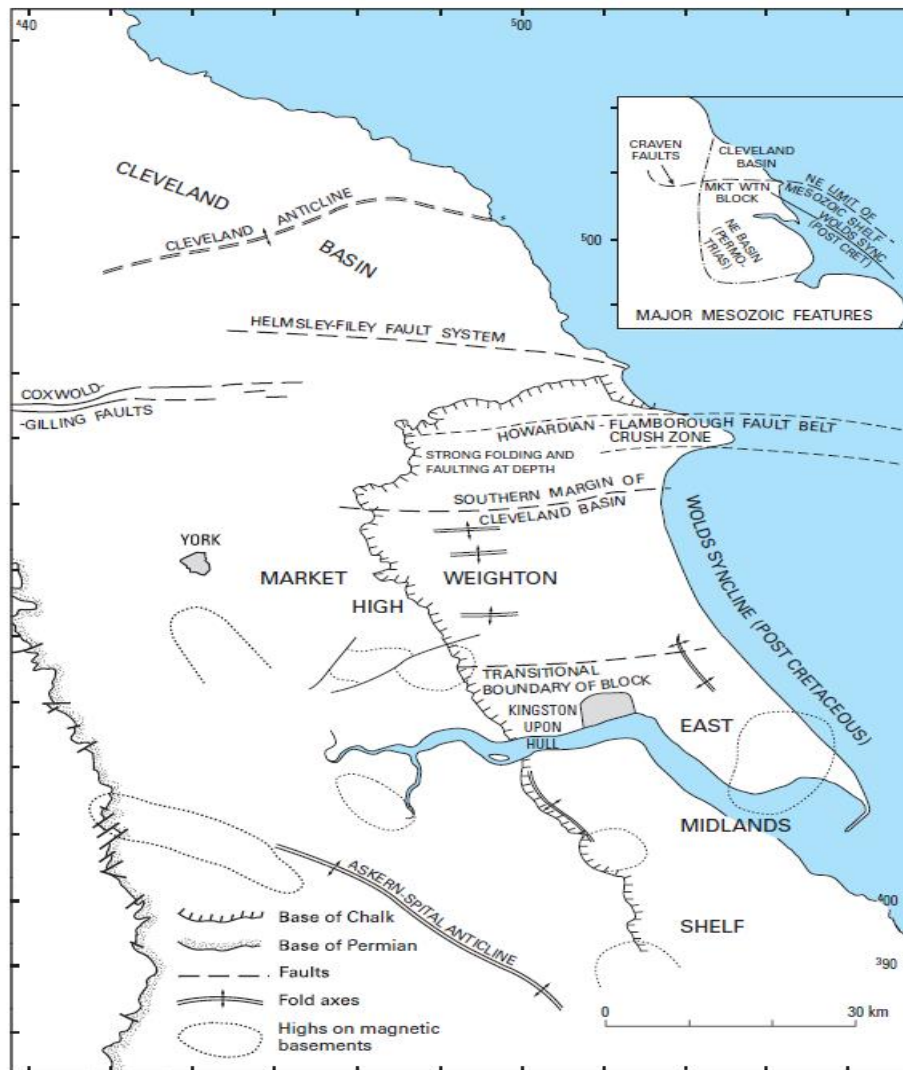


Figure 2.1: Map depicting regional tectonic structures of Yorkshire (After Gale & Rutter, 2006)

Therefore, having reviewed, and compared the Northern Province Chalk with the Southern Province Chalk, which was followed by a brief review of structural aspects of the Yorkshire Chalk, subsequent discussions will cover the lithostratigraphic of Chalk in the entire study sites. This will commence with the Northern Province Chalk.

## 2.6 The Stratigraphic of the Northern Province Chalk

The Northern Province Chalk is divided into six formations (Figure 2.3) comprising the Ferriby, Welton, Burnham, Flamborough, and Rowe Chalk Formations (Mortimore et al., 2001; Mortimore, 2014). Of these, the Ferriby and Rowe Chalk formations are flintless, while the Burnham Chalk Formation has mainly carious flints with tabular flints at the base of the formation and nodular flints found at some locations (e.g. Ulceby Vale House Quarry) while the Welton Chalk Formation possesses nodular flints (Wood



& Smith, 1978). Of recent, the presence of white flint in the Flamborough Chalk Formation has been reported in Mortimore (2014). In addition to the presence of flints, the basal part of the Chalk comprising the Ferriby Chalk Formation is rich with marls (dominated by clay minerals) and marly chinks (Gale & Rutter, 2006). While the upper part of the Chalk sequence is usually purer with a small amount of non-carbonate content (Gale & Rutter, 2006). The focus of this part of the thesis will be on Burnham Chalk Formation being the sampling unit for this study in the Northern Province. For detailed description of the remaining chalk formations in this province, refer to Wood & Smith (1978); Witham (1991); Mitchell (1995); Sumbler (1999); Mortimore, et al. (2001); Mortimore (2014).

### **2.6.1 Burnham Chalk Formation (Upper Turonian to Lower Santonian)**

The Burnham Chalk Formation overlies the Welton Chalk Formation (Figure 2.3), and is the formation from which flint samples were collected at North Landing and Lincolnshire for this study. The formation is flinty, thinly bedded and is about 130 to 150m thick (Wood & Smith, 1978; Pitman, 1986; Hopson, 2005), which reduces to about 85 to 100 m thick around the Market Weighton area (Gale & Rutter, 2006). Burnham Chalk Formation has interchanging features, where hard massively bedded Chalk, changes to thin, softer Chalk, interfused with marls (Wooton and North Ormsby Marls) of different sizes. The basal part of the formation starts from the Upper Turonian, through Coniacian, while its upper boundary terminates at Lower Santonian stage. The topmost boundary of this formation marks the horizon with the highest flints occurrence (Mortimore & Wood, 1986; Witham, 1991), while its base marks the entry of large tabular flints (Mortimore et al., 2001) identifiable over the entire Wolds (Mortimore, 2014).

The Burnham Chalk Formation houses the Ravendale Flint, the Triple Tabular Flint and the thick Ludborough flints (see Mortimore et al. 2001; Mortimore, 2014). The competency of flints (e.g. strength) changed toward the top of the formation, where the presence of carious flint is noticed (see Mortimore, 2014 for more details). The base of this formation contains harder chinks, which contain closely spaced grey tabular flints (Wood & Smith, 1978). Tabular flints reach about 0.3 m thick or higher (Wood & Smith, 1978; Gale & Smith, 2006). The thickness of these flints thins out towards the top of the formation, and becomes less obvious; less developed and randomly distributed (Mortimore et al., 2001).

At North Landing and Lincolnshire (at Ulceby Vale House Quarry) Paramoudra flints are also seen in this formation. This flint morphology are prominent in the chalk beds below the Ulceby Marl and above this marl the formation is characterised by the

presence of chalk layers with *Zoophycos* streaks (Mortimore, 2014). In addition to the Paramoudra Flint, semi-tabular and nodular flints are also common at Ulceby Vale House Quarry, Lincolnshire. Carious flint is reportedly noted above Wooten Marl in Mortimore (2014) this is also traceable at Ulceby Vale Quarry, Lincolnshire (Hildreth, 2013). The Burnham Chalk Formation is overlain by the Flamborough Chalk Formation.

## **2.7 Southern Province Chalk, UK**

It is not the intention of this study to provide the detailed geology and stratigraphy of the Southern Province Chalk in this section as this has been previously covered in details (e.g. Mortimore, 1986; Bristow et al., 1997; Mortimore, 2001; Mortimore et al., 2001; Mortimore, 2014). However, a brief description of each formation is discussed herewith with more focus on the Seaford and Lewes Chalk Formations being the formations from which flints are sampled in the Anglo-Paris Basin for this study. The aim of reviewing these formations is to provide the reader with the background on the stratigraphy of the Southern Province Chalk, so as to derive some geological clues on the geological features of chalks in each geographical location investigated, should a trend in properties of flints from these geographical locations be identified.

The Southern Province Chalk covers the Chalk formed in outcrops at the Chiltern Hills, North, and South Downs, as well the Chalk in coastal parts of Kent and Sussex (see Mortimore & Pomerol, 1998) (Figure 2.3). Unlike, the Northern Province Chalk, the Southern Province Chalk is softer and consists of massive chalk, which can occasionally be nodular. The weakness of the Chalk in this Province is attributed to the poor and lack of intergranular cementation. The porosity of the Chalk in this province also varies from that of the Northern Province as discussed previously (Section 2.4.1), with the porosity of the latter controlled by mechanical compaction, and crushing, while that of former is mainly affected by the presence of clay (Shepherd, 1972).

The Southern Province Chalk group is divided into two major subgroups; the Grey Chalk Subgroup and the White Chalk Subgroup. These subgroups are previously classified into three divisions, the Lower, Middle, and Upper Chalks. In total, these Chalk divisions comprise of nine chalk formations namely the Zig Zag and West Melbury Marly Chalk Formations which belong to the grey chalk subgroup. The remaining seven chalk formations comprising the Holywell, New Pit, Lewes, Seaford, Newhaven, Culver and Portsdown Chalk formations belong to the White Chalk subgroup (Figure 2.3). Most chalks in this province have flints. The colour of flints in these chalks are dark grey or black (Mortimore & Pomerol, 1998) but dark brownish grey flint is also prominent in this Province.

### **2.7.1 Grey Chalk Sub-group**

The Grey Chalk subgroup formerly categorised in the Lower Chalk division starts from the Glauconitic Marl Member up to the base of the Plenus Marls Member (Figure 2.2). This Chalk division consists of the West Melbury Marly and Zig Zag Chalk Formations. The presence of flints has not been reported in these chalk formations and are therefore not described in these thesis. Detailed descriptions of these formations can be found in Bristow et al. (1997); Aldiss et al. (2004); Woods (2006); Mortimore et al. (2001); Mortimore (2014).

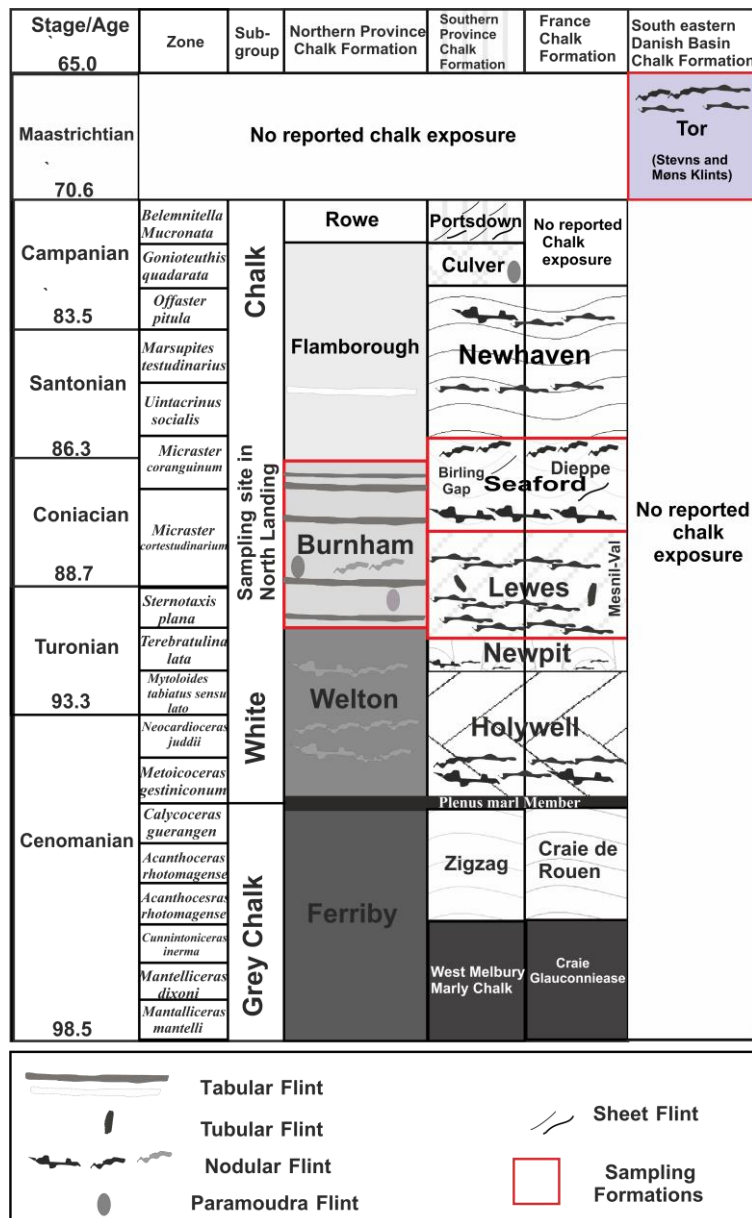


Figure 2.2: Lithostratigraphic divisions of Upper Cretaceous Chalk of Northern Province, UK and the Anglo-Paris Basin (Adapted from Mortimore, 1983; 1986; Bristow et al., 1997).

### 2.7.2 The White Chalk Sub- group

The White Chalk Subgroup comprises the former Middle and Upper chalks (consisting of seven chalk formations). All the chalk sequences in this subgroup covering the seven chalk formations contain flints. The White Chalk Subgroup is identified from the Plenus Marl and composed of pure, soft, white chawks. This subgroup is made up of seven chalk formations; the first two chalk formations comprise the Holywell Nodular Chalk and the New Pit Chalk formations (Figure 2.2) formerly of the Middle Chalk division. The remaining five chalk formations formerly represented the Upper Chalk

division and are earlier outlined in Section 2.7 (also see Figure 2.2 for these formations). Among the chalk formations in the White-Chalk Sub-group, the present review will concentrate on the Lewes Nodular and Seaford Chalk formations, which represent the sampling units in the Anglo-Paris Basin, while details of the remaining chalk formations in this Sub-group can be found in Mortimore (1986); Mortimore & Pomerol (1998); Bristow et al. (1997); Mortimore et al. (2001); Mortimore (2014).

### **2.7.3 Lewes Nodular Chalk Formation (Middle Turonian to Middle Coniacian)**

This formation marks the transition from the uniform, smooth chalk with the rare occurrence of flint to Nodular, non-uniform, coarser, and flinty chalk. The formation commences from the beginning of hard and nodular chalk bed (Mortimore et al., 2001). The top and the base of the formation are respectively defined by the presence of Shoreham Marl 2 and Glynde Marls. As the name implies, Lewes Nodular Chalk Formation comprises of hard to very hard nodular chalk with hardgrounds. The physical properties of chalk beds in this formation is irregular, the arrangement is such that hard chalk layer (with density from medium through high to very high density) is interlayered with low density, weaker, and more aggregated chalk (Mortimore, 2014). Towards the base of the formation, the first major flint bands, mostly dark brownish grey nodular flints are revealed. Lewes Chalk Formation is conspicuously divided into two by the presence of the bands of nodular flints and the Lewes Marl (Mortimore & Pomerol, 1994). The flint bands are mostly parallel to the bedding, laterally extensive and can be traced throughout the stratigraphy (Mortimore, 1986; 1997; Mortimore et al., 2001).

In addition to nodular flint, tubular and semi-tubular flints are also noticed at some locations in this formation. The formation is about 60 m thick in East Kent (Aldiss et al., 2004) while at the East Sussex the formation is 80 m thick (Mortimore et al., 2001). Clay-lined, steeply inclined fractures with curvilinear fracture surfaces are identified with this formation (Mortimore, 2014), but there is minimal or no evidence of impact or extension of these fractures on to the flint nodules as noticed with the North Landing Flints. This formation is overlain by the Seaford Formation.

### **2.7.4 Seaford Chalk Formation (Middle Coniacian to Middle Santonian)**

The Seaford Chalk Formation is one of the formations from which flint samples were collected for this study in the Anglo-Paris study sites. This formation is described in Mortimore (1986); Mortimore & Pomerol (1997); Bristow et al. (1997); Mortimore et al. (2001); Mortimore (2014). The type locality of this chalk formation is at Sussex. The formation comprises of smooth, soft-firm, fine-grained pure white chalk, embedded with

abundant dark brownish grey nodular flint. The formation is also identified by the presence of semi-continuous bands of massive nodular flints (Mortimore, 1986; Bristow et al., 1997), though sheet flints are also noticeable at the cliff exposures in the Seaford Head (Figure 2.2). Apart from the Seaford Head, flint samples can be found at Shoreham Cement Works as extensive semi-tabular flint with a thickness in the range of 200-400 mm (Cumming, 1999).

The Upper part of this formation is marked by the presence of Buckle Marl, while to the base, the formation marked by the Shoreham Marls (Mortimore, 1986). This basal part of the formation exhibits some nodularity, comprising of flint bands with marls seams (Shoreham and Belle Tout Marls) (Mortimore, 1986; Mortimore et al., 2001). The formation comprises of the Belle Tout Beds, Cuckmere Beds, and the Haven Brow Beds. The thickness of this formation falls between 45 to 61 m, with a thickness of about 52 m in East Kent (Aldiss et al., 2004). The formation also houses the Seven Sisters Flint (Mortimore, 1986) visible in the cliffs at Seaford Head as conspicuous marker Beds. These marker beds form the boundary between Belle Tout, and the Cuckmere Beds (Mortimore, 1986; Mortimore, 2001). The Cuckmere Bed is characterised by the presence of vertical joints, which is also seen in the overlying bed, called the Haven Brow Beds (Mortimore, 2014). The Haven Brow Beds contains bands of flints comprising of Bedwell's Columnar Flints. In addition to this flint, the formation also possessed varieties of flint bands (see Mortimore et al., 2001; Mortimore, 2014 for details). The Seaford Chalk Formation is overlain by the Newhaven Chalk Formation.

## **2.8 North Western France Chalk, Seaford and Lewes Chalk Formations Dieppe and Mesnil-Val respectively**

The cliffs in the Eastern part of English Channel spans 120 km from Le Tilleul to Ault. The chalk cliffs are vertical, and range from 20 to 100 m high (Duperret et al., 2005) but the average of 70 m have been reported (Costa et al., 2004). The chalk cliffs are intersected from SW-NE by two major faults namely; the Bray and Fécamp-Lillebonne faults. These faults contributed in shaping the structures of the Upper Cretaceous Chalk successions. The cliffs are also intersected by the dried and drained valleys traversing from the lands perpendicularly to the cliff edges at a right angle. The chalk cliff in this study location is overlain by the quaternary deposits. Mortimore (2001; 2011) described the chalk formations in these cliffs as Craie de Rouen, Holywell, and New pit, Lewes Nodular, Seaford and Newhaven Chalks (Figure 2.2).

Details of these formations are described elsewhere (Mortimore & Pomerol, 1987; Mortimore 2001; Duperret et al., 2004). At this point, it is important to note, that

only the chalk formations in the current study sites will be discussed below, since the same lithostratigraphic divisions described in Mortimore et al. (2001) and Mortimore (2014) for Southern Province can be applied to the French side of the English Channel. The Southern Province chalks on the English and the French coasts form part of the Anglo-Paris Basin (Mortimore, 1987). The chalk formations to be discussed in the French sites consist of the Seaford Chalk Formation at Dieppe and the Lewes Chalk Formation exposed at Mesnil-Val all in France.

### **2.8.1 Seaford Chalk Formation, Haute-Normandy, France**

In the first study site, the west of Dieppe, the Middle Coniacian to Middle Santonian Seaford forms the major chalk exposure in the cliff. Although, the formation is also exposed between Dieppe and Le Treport and is traceable at East Sussex, UK (See Mortimore, 1986; Mortimore & Pomerol, 1987; Pomerol et al., 1987; Mortimore, 2001). The formation is characterised by relatively homogenous, pure, white chalk rich in CaCO<sub>3</sub>. This pure chalk consists of a large number of continuous bands of nodular flints (Mortimore et al., 1990; Duperret et al., 2002; Costa et al., 2004). The flints are mostly extensive, dark brownish grey, regular and serve as conspicuous marker beds in almost the entire cliff section (Mortimore, 1986). In addition to the presence of nodular flints, sheet flints, marl seams, and nodular hardgrounds are also present in the formation (Duperret et al., 2012).

### **2.8.2 Lewes nodular Chalk Formation, Picardy, France**

In the second study site at Mesnil-Val-Plage in Picardy, France, the dominant chalk formation is the Lewes Nodular Chalk Formation of Turonian to Lower Coniacian Stage as described in Mortimore (2001). This chalk formation is described in Mortimore (1983; 1986; 1987); Mortimore & Pomerol (1987); Bristow et al. (1997). The formation is up to 50 m high, 20 m in the SW, and thickens to 80m at Le-Treport. The chalk formation has continuous cubic and sub-vertical fractures restricted to the beds and forms the topmost section of the *Terebratulina lata*, *Sternotaxis plata*, and *Micraster Cortestudinarium* (Mortimore, 1986; Bristow et al., 1998). The formation comprises of gritty, well bedded, and hard to very hard nodular chalk of the Upper Cretaceous with extensive nodular flint bands.

Flint bands comprising Bo Peep Flint, Lewes Nodular Flint, overlain by Criel Flint are exposed in the lower part of the cliff section (Senfaute et al., 2009) Upper Turonian stage. The upper part of the succession that falls in the Lower Coniacian stage and sits on the Navigation Marl signifies the end of Turonian stage (see

Mortimore, 1983; 1986; Mortimore et al., 2001). The upper part of the cliff is characterised by regular flint bands. These flint bands are parallel to the bedding, laterally extensive, and stratigraphically traceable (Senfaute et al., 2009).

Apart from the presence of nodular flints, tubular flints are also visible at some spots on the chalk cliffs, and the presence of several marl seams are also evidenced (Mortimore et al., 2001; Aldiss et al., 2012). Fracturing in this part of the chalk is restricted to beds, and fractures are mostly cubic and subvertical (Senfaute et al., 2009). In addition to this, vertical joints free from clay infilled are also common on this cliff (Senfaute et al., 2009).

## **2.9 Maastrichtian Chalk Formations in Denmark**

The Danish study sites are located in the south eastern part of the Danish Basin (Figure 3.2 for study sites). The Danish Basin is a WNW-ESE trending basin that is flanked to the south by the Ringkøbing-Fyn High and to the north-east by the Fennoscandian border zone (Nielsen, 2003; Anderskov et al., 2007). The Fennoscandian border zone forms a barrier between Danish Basin and the Precambrian Baltic shield (crystalline basement complex). The Danish Basin is an intercratonic Permian-Cenozoic basin that was created by the late Carboniferous-Early Permian crustal extension. The crustal extension was succeeded by subsidence led by thermal cooling and local rifting. The basin forms part of the extensive Epeiric Sea that inundated greater parts of northern Europe in the Late Triassic-Jurassic Periods (Surlyk, 1997; Nielsen, 2003). As the surging of the larger parts of the northern Europe by the Epeiric Sea continued, the gradual climatic change resulted in the hike in the sea level. This resulted to peak transgression exposing only traces of low-lying Islands in the north-western Europe during the late Campanian-Early Maastrichtian (Surlyk, 1997).

The rise in sea level following the gentle climate change during this period provided suitable environments (arid climate) for the massive production, growth and development of coccolithoid algae and other associated pelagic skeletal fragments. This later settle (following quiescent condition) on the sea floor, forming the thick, extensive basin-wide chalk beds seen in the Danish Basin (Stevns Klint and Møns Klint Successions inclusive) and the rest of the northern Europe.



### 2.9.1 Tor Chalk Formation at Stevns Klint, South East of Copenhagen, Denmark

Stevns Klint is one of the flint sampling sites for this study and is a geologically interesting site situated in the south eastern part of the Danish Basin about 45 km south of Copenhagen. The site reveals a cliff section spanning up to 15 km, and 41 m high, consisting of rock successions ranging from the Upper Cretaceous (Upper Maastrichtian) coccoliths-rich chalk to the Tertiary deposits. The Cretaceous (Upper Maastrichtian) Chalk at the Stevns Klint forms the oldest exposed rock units in the Stevns Klint succession, whereas the Lower Tertiary, Danian Limestone is the youngest rock unit (Figures 2.3 and 2.4). In between these two rock ages is the clearly defined Cretaceous-Paleogene boundary. The lithofacies in these two rock ages are conspicuously exposed at the Stevns Klint sections. These are comparable to the sections seen in the adjacent quarries especially the Sigerslev quarry which is about 4 km away from the Stevns Klint section (Højerup) and forms the sampling point for this research.

Structurally, Stevns Klint section is bound to the Northeast by the Ringkøbing High and to the Southeast by the Sorgenfrei-Tornquist zone (Hart et al., 2004; Hart et al., 2005; Anderskov et al., 2007). The Chalk deposits at Stevns Klint were not significantly disturbed or deformed by the glacier (Frykman, 2001; Hart et al. 2004) or by tectonics compared to the chalk deposits at Møns Klint, Denmark and at the North Landing, UK. This is evidenced by the absence of glaciotectionic structures, besides the slight sub-vertical and horizontal fracturing of the chalk reported by Frykman (2001). The subhorizontal fractures seen in the chalk units were interpreted to originate from the isostatic rebound (Rosenbom & Jakobsen, 2005).

The geology of the units forming the Stevns Klint successions and the adjoining quarries have been described in details (e.g. Christensen et al., 1973; Håkansson et al., 1974; Bromley, 1979; Surlyk, 1979; Toft, 1986; Surlyk, 1997; Frykman, 2001; Hart et al., 2004; 2005; Surlyk et al., 2006; Anderskov et al., 2007) and will therefore, be discussed briefly herein. The stratigraphy commences from the Upper Maastrichtian Chalk of the Tor Formation, which comprises of Sigerslev (White and grey chalks), and Højerup Members. This comprises of soft, fine-grained, pure white and grey coccoliths-rich chalk deposits to the early Palaeogene. These chalk deposits form part of the epicontinental chalk sea that engulfed larger part of the north-western Europe during the Late Cretaceous period (Damholt & Surlyk, 2012) and are revealed to the present level at Stevns Klint as a result of massive uplifts (Frykman, 2001; Knudsen & Looten, 2013). The chalk successions at Stevns Klint are considered as shallow water deposits (Surlyk, 1997), deposited at estimated depth range of 100-150 m (Bromley, 1979; Hart et al., 2004), which thickens to the north up to 450 m in a

deep well (Grøndal-1) (Frykman, 2001). The overall thickness of the Maastrichtian Chalk at Stevns Klint reaches about 40 m (Surlyk, 1997; Frykman, 2001).

The Maastrichtian Chalk at Stevns Klint is unconformably overlain by the Lower Danian Fiskeler (Fish Clay) Member of the Rødvig Formation (Figure 2.3 and 2.4). The Fiskeler Member represents the K-Pg boundary, which marked the end of the Cretaceous Period. This is overlain Cerithium Limestone Member of the Rødvig Formation, which is capped by the Quaternary tills. The glacial till span all of the Stevns cliff section at various thickness, with erosion surfaces seen randomly distributed over different sections.

### **2.9.2 Sigerslev member**

Of the above mentioned stratigraphic units, the Sigerslev Member of the Tor Formation (Figure 2.4) is the focus of this review because the unit forms the sampling member for this study, while more descriptions of the remaining rock units at Stevns Klint are provided in Toft (1986); Surlyk (1997); Frykman (2001); Hart et al. (2005); Damholt & Surlyk (2012). The Sigerslev Member is dominated by the Maastrichtian Chalk. This Maastrichtian Chalk at Stevns Klint comprises of three different categories of chalk: the benthos-rich mound bedded pure white chalk that grades up to the wavy to near horizontally bedded benthos-poor (Zoophycos-rich) white chalk. The third category that is directly overlying the Zoophycos-rich chalk unit is the bryozoan-rich grey chalk (Wakestone).

All the chalk units forming the Sigerslev Member have some bands of nodular flint, which are more developed, forming an extensive band of flint nodules in the Zoophycos-rich white chalk. These flint bands are extensive and visible in several sections of the cliff as consistent marker beds (Figure 2.3). The extensive bands of flints are 3-4 m below the K-Pg boundary (Frykman, 2001), and reduces to a meter the K-Pg boundary at the Sigerslev Quarry. The flint nodules identified with these chalk units have been suggested to originate from intense silicification of the *Thalassinoides* burrows and are mostly traceable over the stretch of the Stevns Klint section (Surlyk, 1997; Surlyk et al., 2006).

In addition to the well-developed flints, two closely spaced, bioturbated incipient hard grounds are also common in the Zoophycos white chalk unit. The flint band is sand-witched by these two closely spaced, phosphatised, intensively bioturbated incipient hardgrounds. The flint band is located at about 300-500 mm below the upper hardgrounds (Surlyk, 1997; Surlyk et al., 2006). The two hardgrounds enclosing this flint band are separated at about a distance of 100-250 mm apart, with the possibility of meeting at a point to form a unit of hardground (Surlyk et al., 2006).

Above the upper hardground, a slight change in lithology is revealed, where the white chalk grades up to the grey chalk (Wackestone).

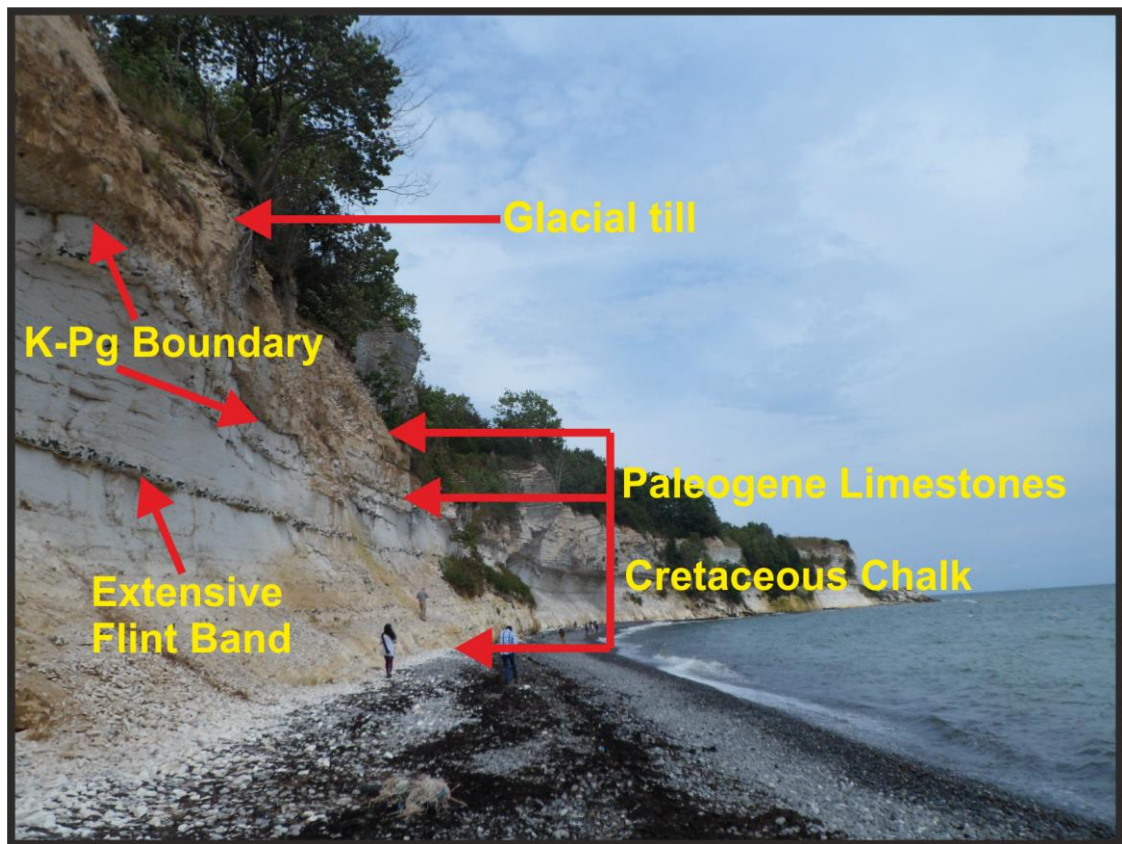


Figure 2.3: Exposure of the Cretaceous to Danian succession at Stevns Klint, Denmark. Note the extensive band of flint and the K-Pg boundary clearly demarcated on the cliff profile. These features are traceable in the Sigerslev Quarry where flint samples were collected for this study.

The combination of the oldest white chalk, the white chalk with poor benthic fossils, up to the hardgrounds are classified as Sigerslev Member forming part of the Tor Formation (Surlyk et al., 2006). The two hardgrounds in this unit indicate remarkable hiatus as a result of significant fall in sea level (Hart et al., 2005) with eventual cease or slow in sedimentation. The Upper hardground of the Sigerslev Member forms the lower boundary of the member, while the base of the Danian Fiskeler Member which commences from the grey chalk forms the upper boundary of the unit. The grey chalk is about 2.5-5m thick with high content of Bryozoans (Frykman, 2001; Surlyk et al., 2006) and is deposited in tiny irregular mounds traced out by bands of nodular flints (Surlyk, 1997). The presence of bands of nodular flints from the silicification of *Thalassinoides* burrows in this chalk unit signifies the period of low sedimentation (Surlyk et al., 2006).

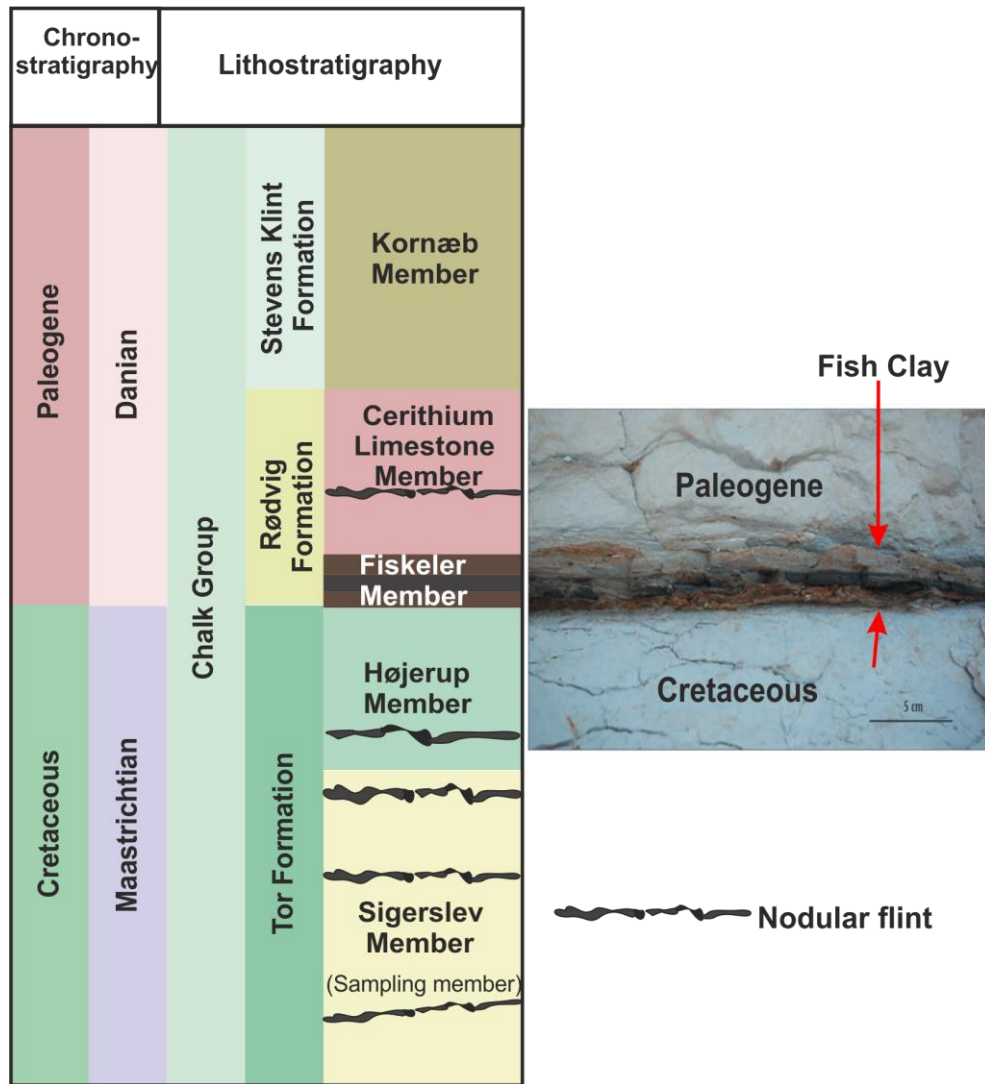


Figure 2.4: Lithostratigraphic subdivisions of Maastrichtian to Danian succession revealed at Stevns Klint (Modified from Surlyk et al., 2006; Damholt & Surlyk, 2012).

### 2.9.3 Tor Chalk Formation at Møns Klint, Eastern Denmark

On the Møns Island, an extensive N-S trending cliff comprising of the Upper Cretaceous to Quaternary deposits called Møns Klint (refer to Figure 3.2 for map of this site), which is the second flint sampling site for this research in Denmark is revealed. Situated in the south eastern part of Denmark, Møns Klint is located further south of Stevns Klint - the cliff is about 130 m high with a span of 6 km (Pedersen, 2000). The geology of Møns Klint succession is described elsewhere (Aber, 1979; Pedersen, 2000; Busby et al., 2004; Lawrence, 2007; Pedersen & Gravesen, 2009; Jelby et al., 2014). The first profile of Møns Klint sections was drawn by Puggard (1851) and his work still reflects the current profiles of the cliff seen presently at Møns Klint (Figure

2.5). The cliff revealed a conspicuous glaciotectionic thrust sheets of Upper Cretaceous Chalk of Lower Maastrichtian age overlain by the Quaternary unconformity.

The Lower Maastrichtian chalk at Møns Klint correlates with upper most part of the Tor Formation traceable in the North Sea (Surlyk et al., 2003) and comprises of fine-grained, pure, coccoliths-rich matrix with preserved microfossils, and macrofossils (invertebrates). The chalk is soft with porosity reported by Hutchinson (2002) in the range of 40-44 % and is of shallow water deposit (Surlyk & Birkelund, 1977) as indicated by the presence of benthos-rich chalk and omission surfaces in the cliff. The chalk is bioturbated, rich in flint, with rare incipient hardgrounds (Stemmerik et al., 2006). Bands of nodular flint and several *Thalassinoides* burrows are evident in the chalk as mentioned above and have outlined the bedding layouts of the chalk succession. Flint bands are also seen at Hvidskud (thickest succession in the cliff, 60 m) located in the southern section of the cliff (Jelby et al., 2014).

The architecture of the cliff appeared such that, the cliff successions consist of glacially steeply inclined layers of chalk interchanging with near parallel layers of glacial deposits as interbeds (Hutchinson, 2002). The arrangement is made such that, each thrust sheet is overlain by combine till and glaciogenic sediments that are superimposed by a thrust sheet with a similar set-up. Each alternating thrust sheet is then separated from the next sheet by thrust and fault (forming imbricate fan (Figure 2.5)). Towards the centre of the cliff this arrangement is interfered by an antiformal stack (stacked chalk beds) (Figure 2.5), while the northern section of the cliff revealed a complex deformation associated with glacial thrust from the Northeast.

Aber (1979) described three advances related to the glaciodynamic of the Møns Klint succession. The three advances comprise of the Old Baltic advance, the Northeast Advance, and Young Baltic Advance. The Young Baltic ice faulted the glaciotectionic complex at Møns Klint from the south, while from the east the northern part of the complex was superimposed by the readvancement of ice from southern Sweden between 17 000 and 15 000 years BP (Pedersen, 2000).

These Advances, therefore, resulted in various types of glaciotectionic processes revealed at Møns Klint. The typical glaciotectionic processes exposed consist of systems influencing the development of thrust mechanisms and proglacial glaciotectionic landforms, comprising of the hill hole pair, the mega blocks and the rafts (Lawrence, 2007). The Hill represents the Møns Cliffs which were thrust up and pushed forward to the hole in the form of thrust sheets about 5 km to the south of the Balkan Sea (Lawrence, 2007). Ductile, brittle and lower limit deformations are also seen at the Møns Klint (Lawrence, 2007).

The glaciotectionic complex of the Møns Klint is defined by the imbricate fan and the antiformal stack (Figure 2.5) seen in the cliffs. The imbricate fan comprising of

steeply dipping thrust sheets of Maastrichtian Chalk overlain by till and glaciogenic sediments characterised the southern section of the cliff (recent part of the deformation complex) (Pedersen, 2000). The antiformal stack formed the horizontal wedges of till that is traversing the chalk, the dipping thrust faults, and the bedding in both the central part of the cliff and the northern sector of Dronningestolen (Pedersen, 2000).

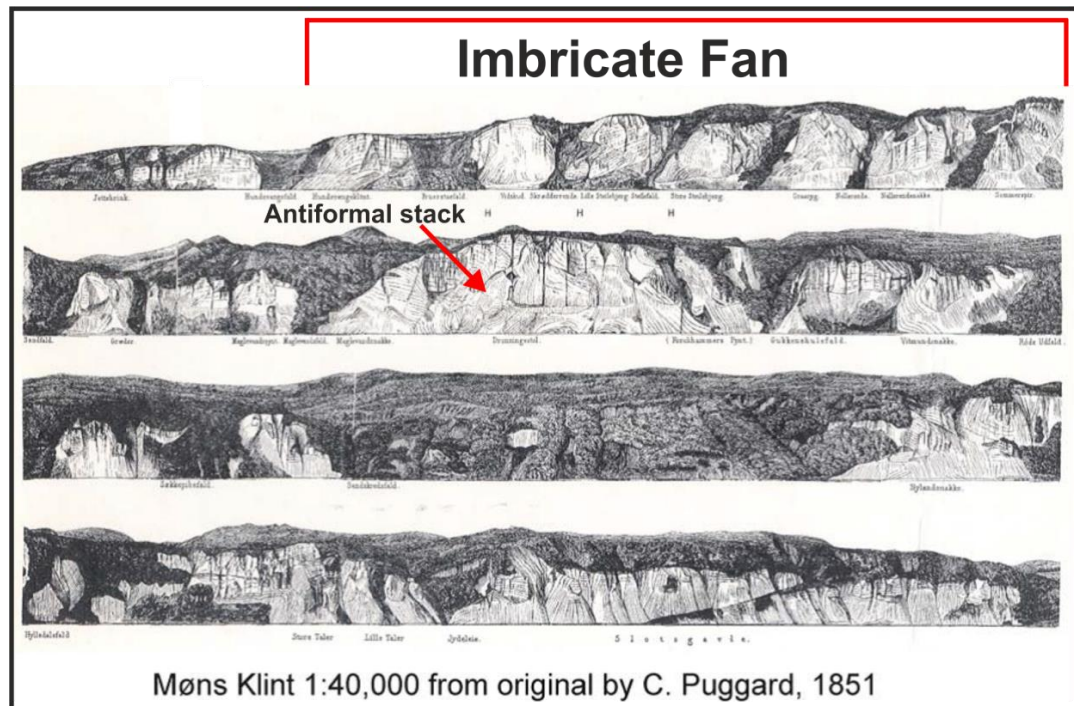


Figure 2.5: Detail views of Møns Klint succession, Denmark, clearly depicting glaciotectonic structures described in the text. The Imbricate fan and the Antiformal stack (red arrow) can be clearly seen in the drawings (Originally drawn by C. Puggard, 1851, but modified from Lawrence et al., 2004).

## 2.10 Flints: Distribution and Formation

This section introduces the main research subject. The section presents an overview of the definition of flint, the distribution and previous studies on the origin of flint. The structures, physical features and morphologies of flints are also presented in this section.

### 2.10.1 Flint

The definition of flint and the lists of various flint morphologies have been provided in Chapter 1, p. 1. The various flint morphologies are described below.

### **2.10.2 Distribution**

In Europe flint is found in Belgium, Denmark, France, Germany, Poland, Sweden, and UK. In the UK, flint is found over a significant span of the chalk deposits South east coast of England to Flamborough Head Yorkshire. Flint displays various morphologies: nodular burrow-form, tubular and sheet flints in the Southern Province and tabular as well as Paramoudra flints in the Northern Province. Mortimore & Wood (1986) identified contemporaneous Turonian flints maximum in these Provinces and is reportedly believed to be contemporaneous with the same stratigraphic framework of flint bands traceable through the English Channel to Northern France. This stratigraphic framework of flint bands equate with that of Luneburg Successions in Germany and Heligoland (Mortimore & Wood, 1986). Flints are also distributed in Chalk successions of North German plain, Lower Campanian of Lägerdorf and Lüneburg as well as in the Upper Maastrichtian Chalk at Hemmoor in Germany.

### **2.10.3 Formation**

Understanding the origin of flint is significant for the proper characterisation of the rock. Several efforts in the past two centuries have tried to propose an acceptable theory for the genesis of flints. Despite these efforts, the origin of the rock remains uncertain (Shepherd, 1972; Behl et al., 1992; Mortimore, 2010). Shepherd (1972) discussed various theories on flint formation from early 18th to late 19th centuries and divided the theories into syngenetic, penecontemporaneous, and epigenetic. Details of these categories of theories are provided in his classic book titled: *Flint: Its Origin, Properties and Uses*.

Some of the prominent propositions described, believed that flints were formed from flowing rivers carrying silica derived from their contacts with siliceous rocks (Tarr, 1917). Further research lead to the proposals that flint is formed as a result of the following: silica-calcite replacement (Van-Tuyl, 1918), filling of tests or parts of Sea Urchins and brachiopods by silica gel (Brydone, 1920), dissolution of chalk by CO<sub>2</sub> from volcanic eruption (Wroost, 1936), dissolution of calcite and precipitation of silica at redox boundary (Illies, 1949).

Research on the genesis of flint resulted in the suggestion that the origin of flint is due to: the precipitation of silica caused by the change in Eh and pH (Sass & Kolodny, 1972); mixing of silica-rich meteoric water, biogenic opal with marine waters (Knauth, 1979); or the actions of microbial products (H<sub>2</sub>S) as the precursor for the silica-calcite replacements (Håkansson et al., 1974; Bromley et al., 1975; Clayton,

1984). Maliva & Siever (1988) suggested that flint was formed because of the force of crystallisation-controlled mechanisms. The actions of organic acids was proposed to be the reason for flint formation (Bennett et al., 1988; 1991), while, by contrast, the effects of force of crystallisation and depression of solution were also proposed as the genesis for flint formation (Minguez et al., 1994).

Madsen & Stemmerik (2010) added void filling and phase transformation to the silica-calcite replacement theory as the pre-requisite for flint formation. Lindgreen & Jakobsen (2012) upheld Wroost, 1936 view on the action of CO<sub>2</sub> from volcanic eruptions as the means of providing the silica needed for flint formation.

The limitation of the majority of the work on flint formation is that they were mostly proposed based on investigating flint samples from a particular geographical location. It is difficult to extrapolate such observation because of diagenetic processes.

## **2.11 The Structure/Physiques and Morphologies of Flints**

### **2.11.1 Flint Crust, Core and White Inclusions**

Flint are often found to have carbonate rich crust surrounding the silica rich core which often appears white, red or dark depending on the mineral composition. The thickness of the crust also varies. The North Landing flint, for example, has thicker and weaker crust (Figure 2.6a) than the dark brownish grey flints of the southern England as well as the north western French flint (Figure 2.6b). Flint crust forms the external material that surrounds the flint core. The flint core is usually darker, harder and stronger than the crust. The core can be completely silicified while in some cases could have white inclusion sometimes called the flint meal. The white inclusion is usually white similar to the surrounding chalk. In some cases, this white inclusion is partially silicified and significantly controlled the material properties of flint.



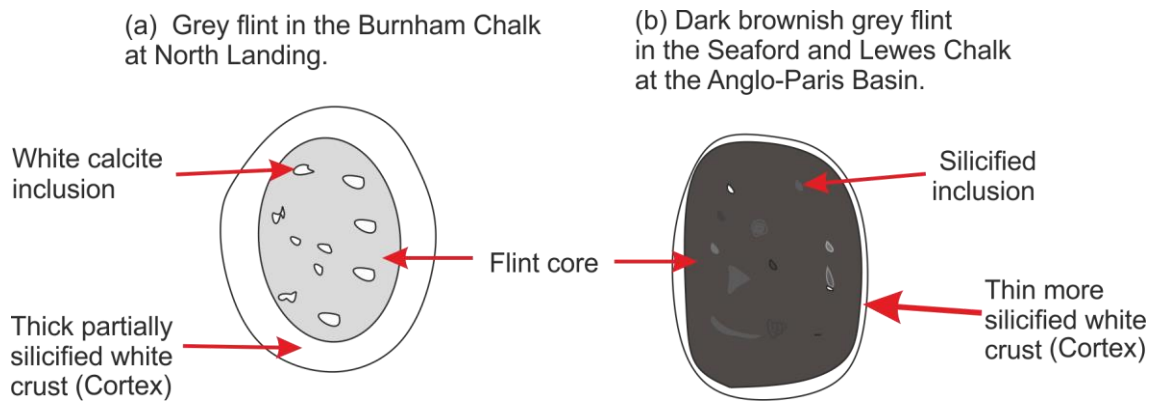


Figure 2.6: A conceptual model showing different flint structures comprising of white crust (with different thickness, the flint core and the white inclusions).

### 2.11.2 Flint Morphology

Flint morphology constitutes one of the important aspects of flint that has been investigated (e.g. Bromley & Ekdale, 1986). Flints occur in different morphologies, including: Paramoudra; sheet; nodular; tubular; and lenticular flints. Whether the geomechanical properties of flints, which have direct impact on its drillability, vary with flint morphology is unknown. Thus, this study will compare the mechanical properties of the two most predominant flint morphologies observed in the present study sites. These are the tabular and the nodular flints. However, in the interest of completeness flint morphologies, in general will be reviewed.

### 2.11.3 Tabular Flint

Several flint nodules can coalesce to form more or less continuous beds called tabular flints (Wood & Smith, 1978; Mortimore, 1986; Clayton, 1986) (Figure 2.7a). Tabular flint can be over 300 mm thick. Clayton (1984) described the formation of tabular flints as a result of series of processes undergone by sediment-laden solution in the sub surface. These processes involve various stages of diffusion and mixing of the solution in sediment fixed around the highly permeable chalk related to bioturbated structures (Clayton, 1984). Tabular flints are believed to form in chalk with well-developed bedding, with a uniform profile or where burrows are poorly defined (Clayton, 1986). Tabular flints are more prominent in the Northern Province chalks, where they form the boundary between Welton and Burnham Chalk Formations (Wood & Smith, 1978) than at any other seven study sites investigated.

#### **2.11.4 Tubular Flint**

Tubular flints typically form as the name implies, in the shape of a tube (Figure 2.7b). Tubular flints usually occur as a slender tube which could be 20 to 30 mm. The structure of the tube comprises of the central core, which could be empty or in some cases filled with chalk and other carbonaceous materials. The annulus of the tube consists of a completely silicified material which is mainly the flint. Tubular flint is described in Evans (1859); Mortimore (1983; 1986). This flint morphology can be found in the Lewes Chalk at Mesnil-Val, France and in the Chalk of the Southern England.

#### **2.11.5 Paramoudra Flint**

The name Paramoudra originated from the Northern Ireland (Shepherd, 1972) and are sometimes called sea Pears (Figure 2.7c). Paramoudra flints are barrel-shaped or ring-like flints characterised by the glauconitised or ferruginised burrow of a trace fossil called *Bathicnus paramoudrae* (Bromley & Ekdale, 1984). They usually appear as hollow cylindrical flints and form as vertically continuous flint structures. Paramoudra flints existed because of the reactions in the burrow (Clayton, 1984). Paramoudra flints can be a meter or more in diameter and several meters in length, with some of them measuring up to 9 m in length (Bromley & Ekdale, 1986). Such flints are found in Norfolk coast (Sidestrand), Yorkshire coast (e.g. at the Flamborough Head, North Landing), and in Northern Ireland. These flints are also formed in the Spetisbury Chalk member as Warren Farm Paramoudra flints (Mortimore & Pomerol, 1991; Mortimore, 2001) and the Southern England as Bedwell columnar flints (Rowe, 1900; Bromley et al., 1975).

#### **2.11.6 Nodular Flint**

Nodular flints are variably distributed within the host chalk. These flints reflect the outline or features of burrows or feeding patterns of some fossils that lived within the chalk seabed (Shepherd, 1972). Clayton (1986) associated the formation of Nodular flint to the variations in porosity and permeability of the host Chalk, which led to the non-uniform agitation of sulphide and O<sub>2</sub>. Nodular flints vary in sizes, some are only a few mm in size, while others can form blocks of more than 600 mm (Shepherd, 1972). Nodular flints vary in shape; in some places they exist as slender finger-like, or cylindrical in shape, which can both be in horizontal and vertical orientation (Figure 2.7d). The peculiar shapes of these flint morphologies were suggested to be as a result of silification *Thalassinoides* and their host environment (Bromley, 1967; Felder, 1971).

These finger-like nodules have been observed to form a network of nodules. More of these massive nodules may have burrows or contain projections (Bromley & Ekdale, 1986). Nodular flints are found in the chalk beds of the UK, France, Denmark, and Germany.

#### **2.11.7 Sheet Flint**

Sheet flints are specifically formed within the shear planes and fractures in the Chalk (Figure 2.7e). They are formed along the zones of fracture in Chalk (Bromley & Ekdale, 1986) during the early compaction of the chalk, simultaneous fracturing and fluid expulsion. They can be subhorizontal and occasionally subvertical. Clayton (1986) suggested the occurrence of Sheet flint at H<sub>2</sub>S-O<sub>2</sub> mixing zone created by early stage conjugate joint due to sediment dewatering. Sheet flint is usually few mm thick, but can be up 20 mm thick.

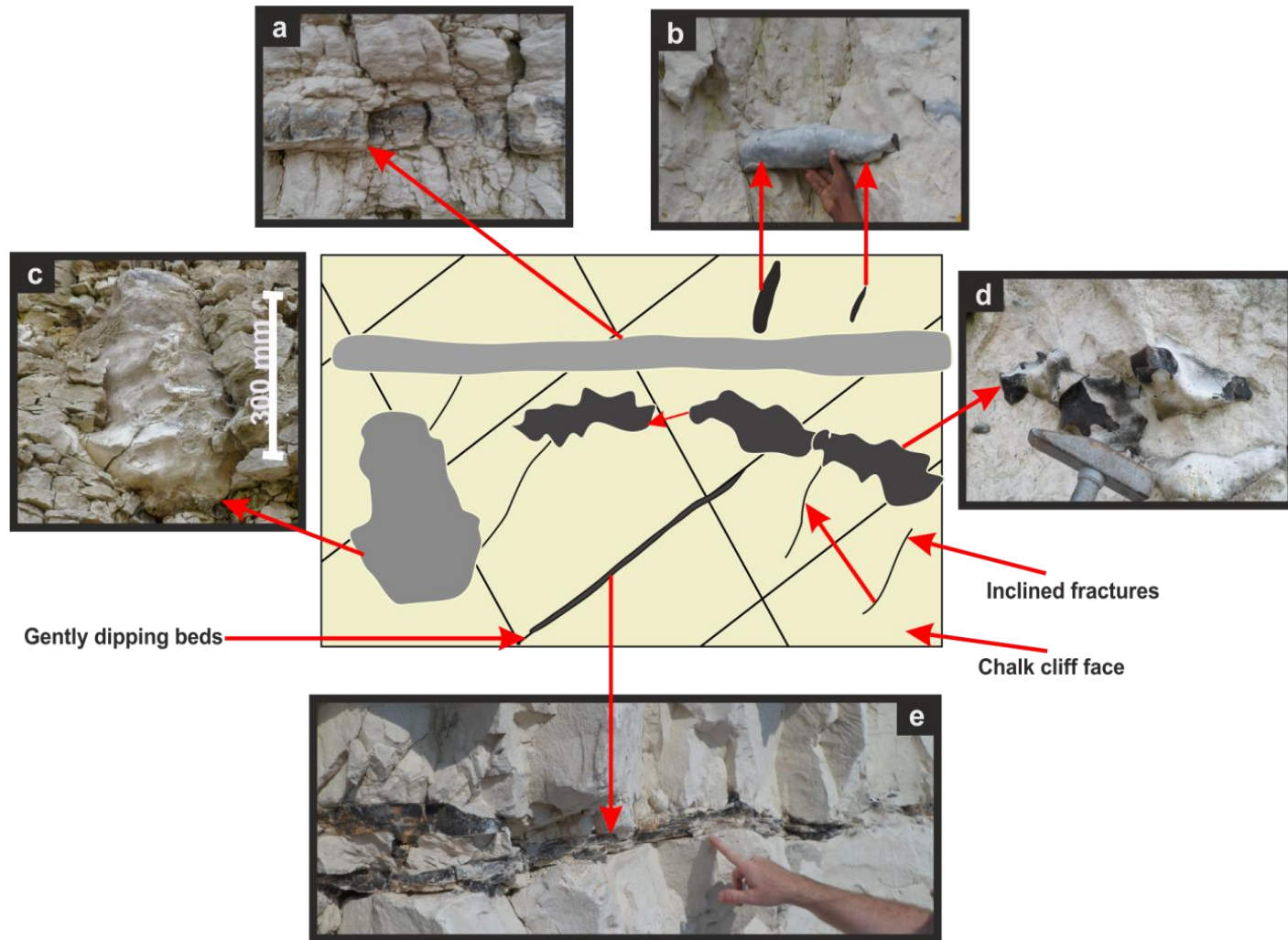


Figure 2.7: Different flint morphologies (a) Tabular flint, Burnham Chalk, at North Landing, UK. (b) Tubular flint, Lewes Chalk Formation at Mesnil- Val, France. (c) Paramoudra Flint, Burnham Chalk Formation at Ulceby Vale House Quarry, Lincolnshire, UK. (d) Nodular flint, Seaford Chalk Formation at Dieppe, France. (e) Sheet flint, Seaford Chalk at East Sussex, UK.

## **2.12 Problems Associated with Flints from Engineering Geological Perspectives**

This section of the thesis reviews some previously published case studies describing problems encountered while drilling or tunnelling through chalks bearing flints. Limited data on such are published in scientific/engineering literature. The Deep sea drilling project (DSDP) (Peterson, 1974) was among the pioneer projects that reported the magnitude and the effects of geotechnical problems caused by flints on drilling equipment. In the project, unanticipated, extremely hard flint bands were encountered resulting in damage to Tungsten Carbide drag bits, milled cutter bits, and diamond bits initially used. This resulted in extensive review of the project, the outcome of which, eventually led to the recommendation of the use of Tungsten Carbide Roller bits for the completion of the project.

Unexpected technical challenges were again reported by Mærsk Olie og Gas when the flexible drill bit that was used for horizontal drilling could not drill through bands of flint in the Dan Field Chalk oil reservoir (Hahn-Pedersen, 1999). The drill bit was found to be sliding over the flint beds and was deflected by the flint beds, with lack of progress and this led to the retrieval of the drill string, as a change to a drive drilling system to drill through the chalk bed (Mortimore, 2012). The consequences of these led to the overall redesign of the drilling program.

In the UK, an attempt to drill chalk with flints for a gas cavern at Killingholme was affected by encountering flint that damaged the rock header by destroying the pick and their boxes. This resulted in changing the entire excavation technique to blasting (Varley, 1990). Another project in the UK where both the tunnel and the tunnelling equipment was redesigned due to engineering geological challenges associated with flint is the Shoreham Harbour Tunnel, reported in Cumming (1999) and Mortimore (2001; 2012). According to these studies a TBM was damaged as a result of encountering flint that was stronger than the initially thought. This again resulted in a change to the tunnelling profile, and the TBM had to be taken back to Japan for re-enforcement to handle the stronger flint. This led to delay to the project completion with consequent increase in the project cost. Other notable similar examples are shown in Table 2.1.

Table 2.1 : Technical challenges caused by hitting or encountering flints in chalk.

Example	Problem	Consequences	Citation
\$ 52 Million project dev. of Munroe regional Hospital Ocala Florida, US.	Hitting a thick bed of flints in the process of smashing the flints.	24-inch drill bit damaged and drill rig worth several millions of Dollars destroyed. This led to cost extra of \$1 million with delay in the project.	(Star Banner, 2001)
New Metro line (Cityringen) Copenhagen, Denmark.	Hitting flint in chalk	500 teeth on Hydromills Destroyed and replaced.	(Symes, 2012)
Dock Yard Rail Way line extension to Woolwich, UK.	Cutting through chalk with flint	the entire cutter was replaced by more rugged cutter due to the abrasive wear experienced.	(McDonald, 2012)

### 2.13 Previous Research on Engineering Characterisation of Flints

Despite the issues identified in Section 2.12, the material properties of flints have gained little interest in the past five decades. The paucity of data on strength properties of flints has been previously acknowledged inter alia (Cumming, 1999; Smith et al., 2003; Mortimore et al., 2011; Mortimore, 2012). Table 2.2 summarises the previous works on mechanical properties of flints. The pioneering study on mechanical properties of flints was carried out by Iller (1963) who measured the bending strength of some English flints of 19.05 to 38.10 mm long flint bars. The test was conducted by applying a load on the centre of the bars until the sample failed. Bending strength was measured as failure load per area of the sample. The conclusion derived from that investigation was that flint has high strength related to the very fine grain structure of the rock. This study contributed significantly to our early understanding of the relationship between mechanical properties of flint and the microstructures of the rock. The narrow range of flint samples investigated in that study suggests the need for further study on mechanical properties of flints.

Table 2.2: Summary of Mechanical Properties of Flints (Modified from Cumming, 1999)

Author	Location/Flint type	Mean UCS MPa	Point load $I_{s(50)}$ MPa	Mean $\sigma_T$ MPa	CAI (0.1mm)	Shore Hardness
Iller (1963)	English flint	-	-	59-93	-	-
	Chalcedony	-	-	81-82	-	-
	Fused Silica	-	-	35-63	-	-
Pradel et al. (1967 and 1972)	Grey lustrous	409	-	57	-	-
	Grand Pressigny	391	-	68	-	-
	Fontmaure Jasper	57-178	-	8-38	-	-
	Grey'non' lustrous	244	-	35	-	-
Crabb et al. (1980)	Upper Chalk	250	-	-	-	-
Waite(1985)	Cromer	414	-	-	-	-
Varley (1990)	Killingholme	332	-	57	-	-
Smith et al.(1993)	Terrace Gravels	200	-	-	-	-
Ortiz et al. (1996)	Mexican	210-360	-	-	-	-
Wareing (1997)	Flint Gravels	-	-	-	-	-
Cumming et al. (1995)	Bermondsey, London	-	7.60	-	-	-
Fowell et al. (1997)	Portsmouth,	832	-	34.30	-	-
Cumming(1999)	Southern	777	-	-	4.03	-
Fowell & Abu Bakar (2007)	-	>300	-	-	4.50	-
Michie, 2010	North Landing	-	-	-	3.40,	75-100
Ihe (2011)	Selwicks Bay	-	-	-	2.60	69-105
	North Landing	-	1.30	-	3.30	319.30
	Thornwick Bay	-	12.80	-	3.80	329.30

### 2.13.1 Mechanical Properties of Flints

Cumming (1999) contributed a significant body of work on the mechanical properties of flints. The work investigated the strength properties of flint (UCS, tensile strength, and point load strength index) and abrasivity of flint (Cerchar Abrasivity Index and Equivalent Quartz Content) in relation to tunnelling and reached the following conclusions that:

- The greatest factor affecting the strength properties of flint is the post-diagenetic processes like weathering and tectonic events. The study provided the evidence of effects of weathering of flint on strength properties of flint when the UCS results of extremely weathered Thames Water Gravels (lower UCS) were compared to that of unweathered flint (higher UCS) samples tested in the

study. However, the evidence to correlate on the effect of tectonic activity on strength of flint was not investigated.

- It was suggested that there was a spatial variation in flint properties, not just a stratigraphic one.
- Silica chemistry (opal A, opal-CT, cristobalite, Chalcedony and  $\alpha$ -quartz) is among the factors expected to affect the strength properties of flint.

One of the main limitations of the work was that the study covered narrow range of flints from only the Southern Province Chalk. Therefore, the results might vary from the properties of flints elsewhere.

The need for investigating flint from other geographical locations has already been emphasised in Smith et al. (2003), the possible existence of variation in properties of flints was also suggested in Cumming (1999), and was tested by Domański & Webb (2000). The main differences between various flint colours were also questioned by Weymouth (1951).

Domański & Webb (2000) employed 15 mm diameter and 21.75 mm long flint samples to determine the fracture toughness of flint on different colours of Polish flints. These consisted of dark brown, banded and grey, white spotted flints to determine the suitability of these materials for flaking. The conclusion reached was that the fracture toughness of flint samples varies with flint colour, microstructure, presence of scattered calcite crystals and chalcedony inclusions.

One of the most recent published works on strength properties of flints was conducted by Smith et al. (2003) on flints sampled from Brighton and Cray. In that study, the UCS, Point load and the tensile strength of flint samples were investigated. The UCS test was conducted on both cuboidal samples and cores while the three-point disc was used for the tensile test. The general conclusion derived from that study was that flint materials possess a high and a wide range of strength, associated with fracturing within the samples. The study, therefore, suggested that, there is the possibility of reliance on variation in strength properties of flint with the origin of flint and that further investigations from other geographical locations or parts of chalk succession should be considered. These conclusions helped form some objectives of this study.

### *Uniaxial Compressive Strength (UCS) Test on Flints*

The examination of the UCS of flint has also received limited attention until the late 90s, when the demand for more engineering projects in chalk with flint was rising. Fowell & Martin (1997) conducted UCS tests on Paramoudra Flint collected from



Portsmouth using 20 mm cores to understand the cuttability of the flint. The conclusion derived from that study was that, Paramoudra Flint has a high intact strength, and the strength of the samples tested was strongly influenced by calcite inclusion and vugs. The results of strength tests on flint by Cumming (1999) supported the very high compressive strength of flint observed in Fowell & Martin, unpublished report (1997) and disproved low UCS values assigned for flint in previous studies. The study also observed that the UCS of flint is 2 – 3 times higher than previously believed (Fowell & Martin, 1997). The study further advised against relying on previously published data on the strength of flint for tunnelling designs.

Thus, conclusions derived from these studies might not be applicable to flint in the Northern Province or elsewhere or where the flint materials are highly tectonically disturbed, or where the chalk is probably formed as deeper water deposit. The conclusion reached in those studies, might also not also be applicable where the embedded flint is lighter or have a different mineral composition, and is less silicified than the samples investigated in the previous studies.

#### *Young's Modulus of Flint*

The only previous work on elastic properties of flint was carried out by Cumming (1999). The study used the linear variable differential transformer (LVDT) to measure the axial deformation of the flint sampled from the Chalk successions in the Southern Province, UK. Although, the study pioneered the characterisation of the deformability of flint materials, the use of LVDT to measure the axial deformation of flint materials likely limited the Young's Modulus (E) results because of deformation of the loading platens. As such the LVDT recorded the deformation of both the rock and the platens. Therefore, to minimise this effect, the deformation of the loading platens has to be accounted for while analysing the elastic parameters. This has not been factored out in the earlier study. Thus, to avoid this problem the present research used 5 mm strain gauges attached to the centre of the sample for the measurement of both axial and lateral deformation of flint samples investigated in this thesis, from which the static Young's Modulus and Poisson's ratio was determined. Additionally, the present study will use Ultrasonic pulse velocities to determine the dynamic elastic parameters of flints. These will be related to the static parameters for the development of models for estimating elastic parameters of flint by avoiding the static methods which requires expensive, difficult and time-consuming sample preparation.

### *Point Load Strength Index ( $I_{s(50)}$ )*

One of the major reasons for determining  $I_{s(50)}$  is for the prediction of UCS for machine or excavation design especially on rock samples that are difficult to prepare for direct UCS tests. Loutridou et al. (1986); Cumming (1999); Smith et al. (2003) identified that preparation of flint samples for UCS is very difficult expensive and time consuming (Smith et al., 2003). Therefore, in such a situation, Point load strength index ( $I_{s(50)}$ ) serves as one of the simplest and cheapest alternative means of estimating UCS for different intact rock materials.  $I_{s(50)}$  can be used as important criteria for quick estimation of intact rock strength for machine/tool or excavation design prior to or during the site investigation. Cumming et al. (1995); Cumming (1999); Smith et al. (2003) and Ihe (2011) conducted experimental investigations of  $I_{s(50)}$  for flint. These studies provided the first set of  $I_{s(50)}$  data characterising flint. The  $I_{s(50)}$  results showed a wide range of results as, considering the fact that the flint samples tested, were drawn from various locations. For example, Cumming (1999) and Smith et al. (2003) samples were from the Southern Province of the UK, while in the Ihe (2011) study flint samples were collected from part of North Landing, UK, with  $I_{s(50)}$  reportedly 50 % less than that reported in Cumming (1999). Thus, the variation observed in the  $I_{s(50)}$  highlighted the possible differences in  $I_{s(50)}$  with geology, geographical locations and colour of flints.

Previous efforts to derive the correlation between UCS and  $I_{s(50)}$  (Cumming, 1999 and Smith et al., 2003) mostly resulted in the conclusion that the correlation is not applicable for flint. Instead, the application of  $I_{s(50)}$  for machine/tool and tunnelling design was suggested in both studies. Whilst, Smith et al. (2003) advised on the anticipation of  $I_{s(50)}$  greater than 16 MPa in the absence of site specific data, Cumming (1999) derived Equation 2.1 for the estimation of UCS from  $I_{s(50)}$ . The use of  $I_{s(50)}$  greater than 16 MPa suggested by Smith et al. (2003) may not be suitable where flint samples are lighter, carious or formed in the tectonically disturbed chalk, since these might hardly yield high  $I_{s(50)}$  as previously anticipated, this might be confirmed in Chapter 4. Similarly, the application of equation 2.1 to predict UCS from  $I_{s(50)}$  for flint could lead to overestimation of UCS. Thus, the present study will test the validity of UCS- $I_{s(50)}$  relationship by considering flint samples drawn from various/wider regions and formations.

$$UCS = 33.18I_{s(50)} + 469.50 \quad \text{2.1 (Cumming, 1999)}$$

Where UCS is the Uniaxial Compressive Strength (UCS, MPa) and  $I_{s(50)}$  is the corrected Point strength index (MPa).

### *Tensile strength (To) test*

Two major tensile strength testing methods were previously employed to measure the tensile behaviour of flint. These are the Brazilian Disc and the three-point disc methods. Fowell & Martin (1997) and Smith et al. (2003) used the three-point disc method to investigate the tensile strength of flint sampled from the Southern Province Chalk, UK. Cumming (1999) acknowledged the similarity between the tensile strength results obtained from Brazilian disc method and the three-point disc method. These methods of tensile strength tests are employed, depending on the brittleness of the flint material encountered.

Fowell & Martin (1997) investigated the tensile strength of Paramoudra flint sampled from Portsmouth using the three-point disc method. Smith et al. (2003) used the same method to characterise the tensile strength of flint sampled from Cray, Southern Province, UK. The two studies showed the tensile strength of flint was low relative to the equivalent UCS of flint derived from the studies, but can be classified as high when compared with the To of other common rocks. The tensile strength results derived from these two investigations are within closer range and similar to the tensile result of Killingholme flint published in Varley (1990). The results also correlate with the tensile strength of Southern Province flint determined by Cumming (1999). Similarly, Cumming (1999) used the Brazilian disc test on flint samples from the Southern Province Chalk to characterise the tensile strength of the samples. The study concluded that flint has a high tensile strength, but suggested further tests, because of the limited sample size from which the conclusion was derived.

The present study, therefore, adopted the three-point disc method to determine the tensile strength of flint, because the method is easier, cheaper and faster than the Brazilian disc method. The method is faster as it requires less surface finishing than the Brazilian method and is found to correlate well with the Brazilian method for testing flint and the direct tensile pull test (Brook, 1993).

The present study examined the tensile strength of larger sample size collected from various geographical locations covering the entire study sites for the present research. The possible influence of local geology of the site or the variation of strength properties of flint with flint colour and fracturing will also be investigated.

Therefore, there is the requirement for examining flint considering the influence of local geology on the host rock and the relationship between the strength of flint with mineral composition and microstructure/microtexture of the rock to build a more complete regional and broader picture. By looking at these conditions, this thesis, therefore, investigates the effect of these factors on engineering properties of flint and will establish the relationships between the UCS and other strength tests.

## *Abrasivity Investigations on Flint*

Abrasivity of flint has been one of the major geotechnical challenges affecting drilling or tunnelling in chalk with flints, but previous investigations on the abrasivity of flints are very limited. The few investigations on the abrasivity of flints are presented by Cumming (1999); Fowell & Abu Bakar (2007); Michie (2010) and Ihe (2011). These studies estimated the abrasivity of flints using the Cerchar abrasivity method, while in addition to this method, Equivalent Quartz Content (EQC) was also used to characterise the abrasivity of flint by Cumming (1999). The results of Cerchar Abrasivity Index (CAI) of flint from these studies showed the CAI of flint varies and can be categorised between very to extremely abrasive material. Ihe (2011) suggested a relationship between CAI of flint and stratigraphy on the basis of limited data. Michie (2010) and Ihe (2011) also established a relationship between CAI and flint colour, while (Cumming, 1999) observed the relationship between CAI and flint weathering. However, most of these studies acknowledged the weakness of the CAI method in describing the actual abrasivity of flint observed in the field, partly due to poor interaction between the Cerchar pin and the flint sample on one side, and partly because fine-grained microtexture of flint on the other side.

EQC has been employed by various experts in various fields of manufacturing (tool), engineering and engineering geology for initial stage of site investigation before tool wear (Thuro, 1997). The method involves in estimating the abrasivity of rock material by using quartz content of the sample with relative hardness, in this case the Rosiwal hardness (Thuro, 1997). The method is fully described in Chapter three (3) of this thesis.

In the present study the standard Cerchar abrasivity is used to measure the abrasivity of different colour and structures of flint. The standard Cerchar method is modified by increasing the load on the Cerchar pin from 7 kg to 9 kg to test whether this can increase the impact of the abrasivity of the rock to Cerchar pin, so as to solve the previously highlighted problem of the method on testing flint. Similarly, the EQC will be used to test the abrasivity of different structures and colours of flint sampled from various geographical locations. In addition to these methods, Rock Abrasivity Index (RAI) introduced in Plinninger (2002) and described in Plinninger (2008; 2010) will be employed to examine the abrasivity of flint further. This method (described in detail in chapter 3) will be employed to determine the abrasivity flint to account for the strength (strength, UCS) of flint in addition to the mineral composition of the flint.

### *Hardness test on flint materials*

Hardness is also one of the important rock properties that contributes to the drillability and abrasivity of rock. The only identified published data on the hardness of flint was presented in Lautridou et al. (1986). The study presented the Vickers Hardness Number of rock (VHNR) for Le Grand-Pressigny flint, which can be interpreted as medium abrasiveness to high abrasiveness category. The number of samples tested and the method (experimental or as geotechnical wear index) used to arrive at the reported hardness of the Le Grand-Pressigny flint were not mentioned.

The experimental approach of determining the VNHR involves the use of Diamond pyramid indenter with a square base. The angle between the opposite sides is  $130^\circ$  and the indenter is pressed on a sample under load range from 100- 200 kg. The relationship between the applied load and the area of the squared permanent impression left on the sample by the loaded indenter provides the VHN of the rock. The VHNR can also be determined as the product of total mineral composition (%) of rock and the Vickers hardness number for each mineral in the sample provided in a standard table (see Chapter 3 for more detail of this method). This approach is easier and faster, and is tested for flint in this study. Michie (2010) used the Shore Scleroscope (SH) to characterise the hardness of some flint materials sampled from the Northern Province Chalk, UK and found a wide range of hardness values for different flint colours. Table 2.2 provided the summary of previously conducted mechanical tests on flints.

#### **2.13.2 Microscopic Classifications of Flints**

The microstructures/microtexture of flint has been shown to be a significant indicator of how strong or abrasive flints behave during drilling or tunnelling. Studying these properties can also help in explaining the possible causes of variability of material properties of flint with colour intensity and other criteria like grain size, grain shape, and the degree of silica cementation. One of the microstructural analyses employed for this purpose is the Scanning Electron Microscopy (SEM). The application of methods such as the SEM has been used to show details of flints which could relate to the engineering behaviour of the rock.

The investigation of the relationship between microstructure and engineering properties of flint using SEM has attracted very little attention. SEM studies have previously been applied to study the microstructure of flint (Jeans, 1978; Clayton, 1984; Madsen & Stemmerik, 2010; Ihe, 2011) but the analysis has not been employed to investigate how the microstructure of flint relates to the colour, structure and the

material properties of flints. Jeans (1978) described different structures, colour and types of flint (etched and un-etched) from English Chalk using the SEM. The study found  $\alpha$ -quartz as the primary silica phase in the flint samples, with some minor calcite. The study also reported the presence of opaline silica in some flint samples from Surrey. The presence of opal-CT, preserved coccoliths and  $\alpha$ -quartz was noted in the cortex of flint samples collected in Wiltshire. This observation was supported by Clayton (1984) and by Madsen & Stemmerik (2010) on some flint materials collected from the Danish North Sea Chalk.

The detailed study by Clayton (1986, unpublished thesis) on the growth sequence of flints in the Upper Cretaceous Chalk of the Western Europe has significantly improved our understanding on the microscopic features of flints and the surrounding crust. The recent review of flints using SEM by Madsen & Stemmerik (2010) has pointed out the variation in microstructure between dark flint and the light grey flint and indicated the presence of more massive quartz cement in the dark flint than in the light grey flint. Although, these authors have highlighted the possible microscopic features of flint, the work has not provided sufficient analysis to characterise flint microstructures with colour and does not cover many flint colours observed in the field.

Ihe (2011, unpublished dissertation) investigated the microscopic features of Thornwick Bay flints and identified an increase in the extent of crystallisation as well as the grain size of these flints from the white flint to the Cortex. The study also microscopically observed a reduction in porosity and percentage of amorphous silica from the white flint to the cortex.

These microscopic investigations on flints have, however, improved our understanding on the microstructures of flints and the surrounding structures, but, some of these studies are either sample limited or site/regionally restricted, which cannot be generalised or applied in a broader context or wider regions. This implies the need for more microstructural investigations of flint from different regions that will not only define the variation in flint microstructure with different colours or structures, but will also relate these to the mechanical properties of the rock. Additionally, the extent or intensity of silicification as well as preservation or dissolution of microfossils which are also vital indicators of the material behaviour of the flint will be investigated in the present study.

#### *X-Ray Diffraction Analysis on flint material*

The investigation of mineral composition of flint using XRD has been investigated by several authors (Lindgreen et al., 2011; Graetsch & Grunberg, 2012; Jakobsen et al.,

2014). All these studies identified  $\alpha$ -quartz as the main silica phase in flints and most of them acknowledged the presence of subordinate calcite in the flint materials. Pawlikowski et al. (2014) confirmed this using Energy dispersive X-ray spectroscopy (EDX) and Hughes et al., (2010) confirmed this using Energy dispersive X-ray fluorescence (EDXRF) analysis. Pawlikowski et al. (2014) compared the chemical composition of the red and the dark crust surrounding flint. It was shown that the red crust is dominated by Iron ( $\text{Fe}^{3+}$ ) while the dark crust is composed of Mn. Further variation in mineral composition between different flint colours was observed between grey and the white flints from the Tyra Field, North Sea Central Basin investigated by Jakobsen et al. (2014). The study indicated the presence of more quartz in the grey flint than in the white flint. Therefore, if variation in mineral composition was observed with different colours of flint crust, it then logically follows that different colours, structures and origin of flint could have different mineral composition. If a variation is observed in the mineral composition of flint with colour, then so could be with other material properties of flints such as strength, hardness, porosity and abrasivity of flint.

### **2.13.3 Physical properties of flint**

Physical properties of flints are among the important criteria behind the rationale for this study. The physical properties reviewed in this study are the translucency, structures (crust, core and inclusion, See Figures 2.8 – 2.9), colour, and texture. Shepherd (1972) described flint as a material that is very hard to be scraped with a steel knife, but it wears glass with ease. Details on the physical properties of flint such as reactions to frost, heating, and cooling with cold water, reactions with acid, and alkalis can be found in Shepherd, (1972).

Pettitt et al. (2012) reported that flints from Southern and Transitional Provinces, as well as some portions of Southern Lincolnshire, are mostly nodular, dark, and translucent. Further at Northern Province flints are opaque, tabular to massively bedded and medium to light grey indicating a geographical variation.

Additionally, some flints appear translucent while others appear opaque. The appearance of flint in some cases varies according to flints location, formation and diagenetic processes undergone by the rock. In some instances, even within a formation, location or the same flints sample, translucency does vary significantly. For instance, flints found in the Welton and Burnham Formations of the Northern Province, UK are respectively graded as poor and opaque (Henson, 1985).

#### 2.13.4 Flint Colour

The colours of flints may vary with location (Figures 2.8 – 2.9), for instance, Shepherd (1972) reported the presence of pinkish flint in Egypt. This author suggested that variation in colour of flints was the result of staining or re-partination of flint by chemical actions in their depositional environments, which often lead to the formation of colours such as white, pale violet, pale brown, dark blue, and yellow. Anon (2005) reported the presence of red flint with black or white cortex called Roter Feuerstein at Helgoland in the North Sea.

Flint colours exist in different forms depending on the diagenetic processes undergone by the rock; post deposition and the geochemistry of the environment (see Sections 6.7, pp. 223 - 224). The presence of hydrous silica is also said to be responsible for the dark colour of the flints core (Cumming, 1999, unpublished PhD thesis).

Derived flints also exist; these occur because of the effects of weathering on exposed flints, leading to the staining of flints, thereby appearing in different colours (Shepherd, 1972) mentioned above. Thus, since most of the colour differences seen in the flint are likely or not associated with diagenesis and change in mineral composition of flint, the relationship between flint colouring and material properties will be investigated in this study.

Figure 2.8: Examples of different flint class and structures. (a) and (b) Fractured, weathered Flint samples from the Burnham Chalk at North Landing (Ludborough Flint band) showing remarkable white inclusions and fracturing in the samples. (c) Grey flint, Burnham Chalk Formation Lincolnshire (Ludborough Flint band). Note the partially silicified white inclusions in this sample. (d) and (e) Highly silicified dark brownish grey flints (Seven Sisters Flint band) from the Seaford Chalk Formation East Sussex and Dieppe respectively. Inclusions in these samples are highly silicified and fracturing was not seen as observed in (a) and (b). (f) Similar to (d) and (e) but sampled from the Lewes Chalk Formation at Mesnil-Val (Lewes Nodular Flint band). (g) and (h) similar to (d) to (f) but collected from the Tor Formation at Stevns Klint and Møns Klint respectively (After Aliyu et al., 2015).



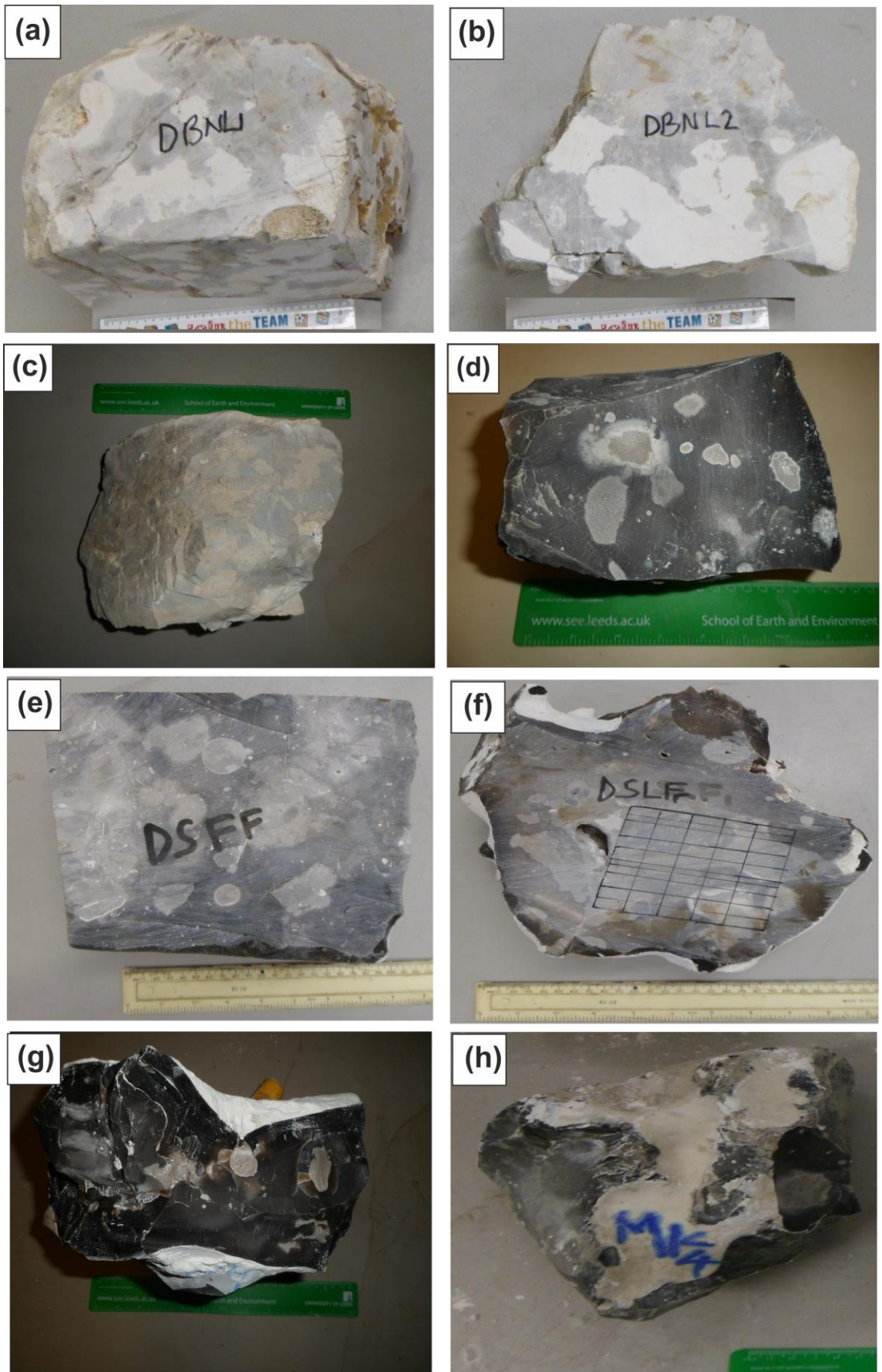


Figure 2.8: Different flint samples described as Figure 2.8 above.

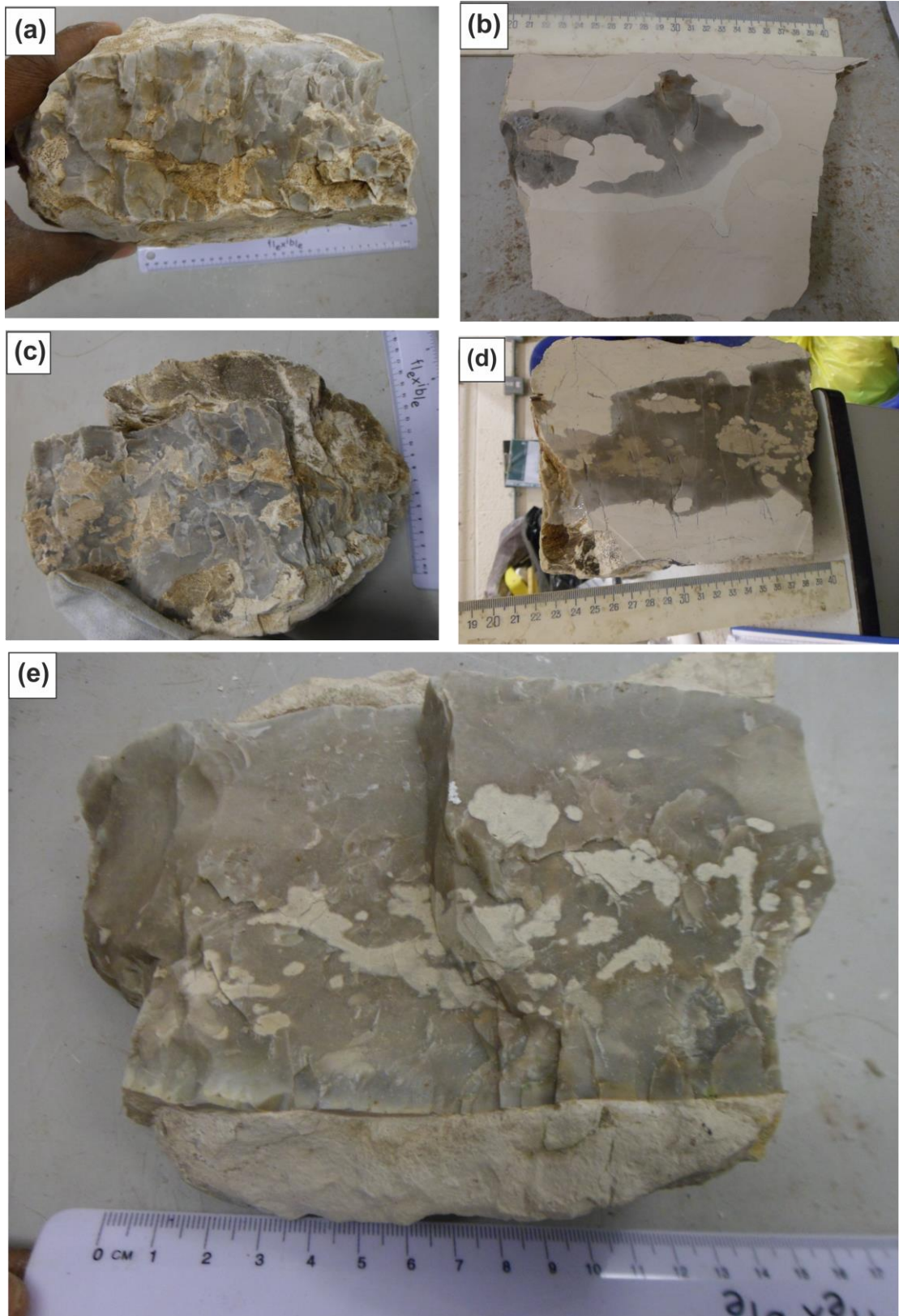


Figure 2.9: (a) to (e) Flint samples from Burnham Chalk, North Landing (Ludborough Flint band).

(a) Weathered and fractured sample with some inclusions. (b) Fractured sample of flint (core) surrounded by chalk and white crust (cortex). (c) Similar to (a). (d) Similar to (b) but more fractured and had more inclusions. (e) Brownish grey flint carbonate with remarkable white inclusions.

### 2.13.5 Grain Size and Porosity of Flints

#### *Grain Size*

Several important engineering properties of rock, including UCS, tensile strength, hardness, abrasivity, and elastic moduli can be affected by the grain size of the rock. The determination of grain size of flint is quite challenging because of fine nature of flints and this feature renders the applicability of the existing methods of grain size analysis to investigate flint is challenging. In a study of some English flints with optical microscopy on polished thin section, Iller (1963) showed that grain size of flint decreases with colour intensity, with the lighter opaque translucent areas reportedly having larger grain size (2-10  $\mu\text{m}$ ) than the dark translucent flint (<1  $\mu\text{m}$ ). Michelseen (1966) and Jeans (1978) reported similar grain size range for some English flints and dark flint from Stevns Klint respectively. These studies were recently supported by the work of Graetsch & Grunberg (2012); Jakobsen & Lindgreen (2012) on some Danish flints. Therefore based on these studies the mean grain size of flint is less than 1  $\mu\text{m}$  for dark flint. While for the white or lighter flints, larger grain sizes of up to 2  $\mu\text{m}$  or higher are obtainable. Madsen et al. (2010) reported about 2  $\mu\text{m}$  sizes for light grey flints of the Maastrichtian Chalk at Stevns Klint, Denmark. This study will investigate the grain size of categories of flints and relate this with material properties of flints.

#### *Porosity*

Few attempts have been made to measure the porosity of flints. In some cases the porosity of flint was estimated from the relationship between the density of the flint sample relative to the density of quartz (2.65  $\text{gcm}^{-3}$ ), without explaining the method used to estimate the density of the rock. For instance if a flint sample has a density of 2.54  $\text{gcm}^{-3}$ , then the porosity is estimated to be 4.15% regardless of whether the sample has very tight microfractures difficult for some methods of estimating density to detect. Examples of where this method was used to estimate the porosity of flint can be found elsewhere (Weymouth, 1951; Michelseen, 1966). A mercury porosimetry was used by Lautridou et al. (1986) at  $5 \times 10^7$  Pa on Tancarville and Goderville flints. However it was found that mercury did not penetrate pores within the samples and this prompted the use of automatic porosimetry at a higher pressure of  $1.7 \times 10^8$  Pa by the same author in an attempt to improve the result. This demonstrates the challenge at using the method on flint.

The difficulty associated with measuring the porosity of flint might be associated with the cryptocrystalline nature and the microstructure of the rock especially the

presence of tight joints and microfractures and the original porosity/pore throat diameter preserved in flint is not in the chalk. These features, therefore, call for the need for porosimetry method that uses a measuring medium with smaller molecular diameter than water and mercury. Presently, Helium (He) gas suit for this purpose given that He has a low molecular weight and an inert gas.

Jakobsen et al. (2014) applied He Porosimetry to measure the porosity of flint sampled in the Danish Chalk from the Tyra Field, North Sea. The He-Porosimetry method was employed for the structural characterisation of flint materials. It was observed that a significant porosity was associated with micropores from the structure of flint (usually comprising of Nano-size spheres). However this work involved somewhat limited sample size.

In addition to He-Porosimetry image analysis (using ImageJ software) will be used to measure the porosity of flint from the SEM micrographs. This will allow for comparison with the He-Porosimetry results. ImageJ would also be employed with a view to minimising the time and cost involved in sample preparation for He-Porosimetry of flint.

## **2.14 Chapter Summary**

The technical challenges associated with drilling through chalk with flints considering the economic importance of the Chalk and its distribution across the globe has been reviewed. The variation in physical properties of chalk such as porosity, density, and permeability with geographical locations has been outlined with a focus on formation in which flint is formed.

The general geology of the chalk deposits in all the study sites was also outlined. The review indicated that the chalk formations in the study sites have diverse and interesting depositional, tectonic and diagenetic histories. For example, the Chalk Formations at the North Landing and Møns Klint are harder, denser, and have been significantly affected by tectonic processes than any other chalk formations investigated in this study. Contrarily, the chalks at Lincolnshire, Anglo-Paris Basin, and the Stevns Klint experienced relatively milder tectonic disturbances.

In the chapter the lack of regional data on the mechanical properties of flints as has been identified. The strength, abrasivity, and hardness properties of flints have been reviewed.

The abrasive wear of cutting/drilling tools by flints is one of the major concerns in both the field and the machine/tools/equipment industries. However, specific studies to address this significant problem are limited and are normally site specific. The limited

understanding of abrasive behaviour of flint served as catalysts for the problem encountered in chalk with flint. Previous attempts to characterise the abrasiveness of flints concluded that CAI is not suitable for characterising the abrasivity of flints and suggested for further work on abrasiveness of flints. Since then there is minimal efforts towards exploring other means of establishing abrasivity.

Thus, the present investigation will address this lack of data by employing different approaches (RAI, EQC and VHNR) to characterise the abrasivity of flint. Additionally, different aspects of flints ranging from structures (crust, core and white inclusions) to the colour of flints sampled from different regions/locations would be investigated. The present study will also incorporate the roles of mineralogy and microtexture on abrasivity of flint to provide additional data on the wear behaviour of flint.

The questions arising from the literature review are: (1) are the properties of flints in the different sites similar enough to be treated the same? (2) What are the controls or causes of variation in properties of flint? (3) Can simple models for future investigations be developed from non-destructive tests since destructive means of testing are time consuming and expensive? (4) How do the microstructural and microtextural features of flints relate to the mechanical properties of the rock? (5) Are flints of different morphologies showing similar chemical/mechanical properties within morphological groupings? (6) Is there correlation between the mechanical properties of flint and the mineral composition of the rock? (7) Does the presence of opal-A, opal-CT, Chalcedony, cristobalite and  $\alpha$ -quartz affect the material properties of flints?

Before addressing questions 1-7, the techniques used to answer these questions will be outlined in Chapter 3. The methods used will be described as well as their limitations.

## **Chapter 3 Field and Experimental Methodology**

### **3.1 Introduction**

In Chapter 2, various aspects of chalk and flint have been reviewed, the research gaps have been identified and some questions that formed the basis for the present study have been raised. The present chapter therefore presents the field and experimental approaches employed to answer the research questions outlined in Chapter 1. The main research approaches involved sampling and investigating flints collected from the proposed study sites. The samples were drawn from some chalk cliff exposures and quarries in France, Denmark and the UK.

In this chapter the qualitative and quantitative methods applied to answer the research questions highlighted at the end of Chapter 2 will be described. The methods can be viewed from three different groups: geological fieldwork; sample description/preparation and laboratory tests. In the present chapter flint sampling, reasons for selecting sampling sites and different flint structures are described. The challenges experienced during the laboratory and quantitative approaches are discussed and testing programs are described. The procedures used to test the drillability of flint using the actual drill bits on large blocks are also described in this chapter. The chapter concludes with a description of the statistical method used to analyse the experimental results.

#### **3.1.1 Chapter Outline**

The chapter presents and discusses the approaches used to characterise flints for engineering project such as drilling, tunnelling and general excavation in Chalk. A chart that summarises the entire chapter is shown in Figure 3.1. Section 3.1 introduces and provides the scope of the chapter. The fieldwork, sampling collection process and sample preparation as well as the description of the samples are then discussed in Section 3.2. The experimental approach suitable for the understanding of the behaviour of flints in relation to the strength, abrasiveness, microtexture, ultrasonic properties, micropetrographic analysis and drillability are presented from Sections 3.3 to 3.9. The drillability of flint is measured in Section 3.9. The last part of the chapter describes the statistical techniques used for data analysis (Section 3.10) and the chapter is summarised in Section 3.11.

### 3.1.2 Scope and Objectives of the Chapter

This chapter covers the geological fieldwork conducted in all the study sites, the experimental methods set to achieve the set goals, and the statistical analysis used to analyse the engineering parameters.

The objectives of this chapter are:

- To present the stages used for field identification of flints, sampling of flints, classification of flint structures, colour and types.
- To describe the experimental techniques used to examine the trends and variability in the material properties of flints in relation to engineering.
- To identify why the experimental methods were used in this study and how the methods can assist in achieving the research objectives.

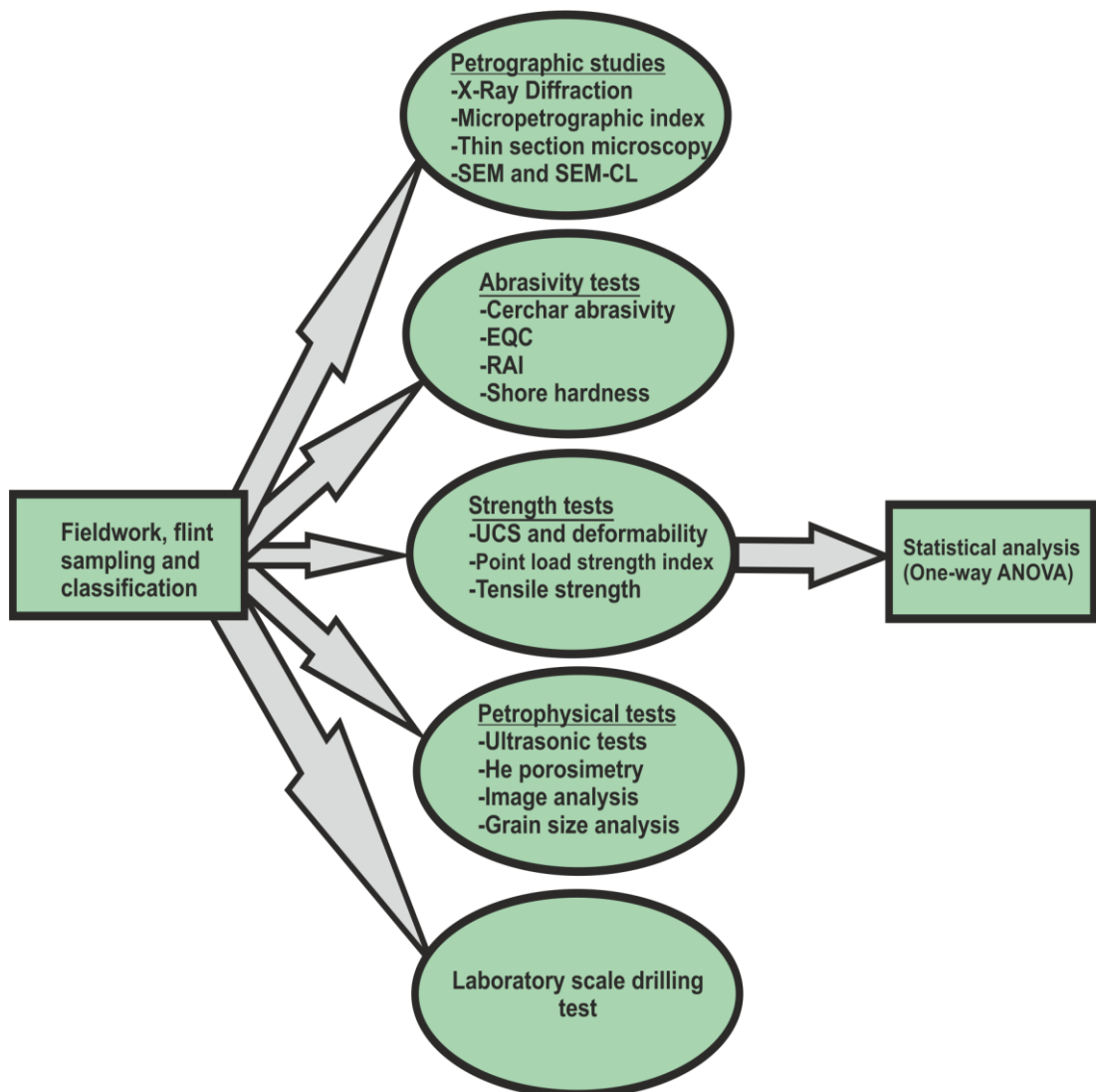


Figure 3.1: Outline of research outlines employed in this study

## 3.2 Fieldwork, Sampling Flint, Description, and Preparation

This section describes the sampling programme conducted in the field and explains how samples were obtained. The section also describes the various physical features of samples observed in the field and provides the breakdown of sample preparation. The challenges encountered while preparing the collected samples were also outlined.

### 3.2.1 Fieldwork and sampling of flints

Flint samples were collected from sites shown in Figure 3.2 for the identification, characterisation and sampling of various types of flints. Site visits were conducted in the Northern and Southern Provinces of the UK, the north western France, and the South Eastern Denmark (Table 3.1 sites location). Geological descriptions including lithostratigraphic positions of flints in each site were noted, and flint types/morphology was identified. This step was then succeeded by sampling flints for laboratory tests. Figures 3.3, 3.5, 3.5, 3.7 and 3.9 show the sampled flint bands in respective sites.

Among the existing flint morphologies, the tabular, nodular, Paramoudra, and sheet flints were identified in the study sites. The first three morphologies are more common in the Northern Province Chalk (Figures 3.4 a-e), while in the chalk formations at the Southern Province of the UK (Figure 3.6 a), the north-western France (Figures 3.6 b-c) and south eastern Denmark (Figures 3.8 a-d) nodular flint is dominant, though sheet flints are also conspicuous at some sites in the Southern UK. After identifying the different flint morphologies, flint samples were collected from various formations for laboratory tests.

Initially, samples were to be collected from the North Landing. However, because of the intense fracturing observed in the grey flints and chalk at North Landing raised a question of whether this intense fracturing was characteristics of the Northern Province chalk or just a local phenomenon which might significantly affect the material properties of flint. Such fracturing seems to impact on the engineering properties of the *in situ* flints and raised a research question as to whether the fracturing was associated with tectonics.

Therefore, to test this hypothesis sampling was undertaken away from the fault zones to provide a control. Chalk pits of: Pilmoor; Moor; Helperthorpe; and Woodhill Farms were visited (Yorkshire). However, the only suitable place for sampling was at Pilmoor farm, but all efforts by the author to reach the farm owner for sampling proved unproductive. So samples from the Ulceby Vale House Quarry at Lincolnshire (Figures 3.4 c & d) were used. Samples collected from this site comprised both Tabular and the nodular flints. The nomenclature of each sample type is provided in the Table 3.2.



At the North Landing (Figures 3.4 a-b) both Paramoudra and tabular flints were seen, but only the tabular flints were sufficient for collection. Unlike in the North Landing, nodular flints were collected from the southern Province of the UK, the north western France and the south eastern Denmark. In Denmark, flint samples were collected from the relatively less disturbed chalk in the Sigerslev Quarry at Stevns Klint (Figures 3.8 a-b) and from the glacially disturbed chalk at Møns Klint (Figures 3.8 c-d). At Stevns Klint, the flints samples were collected about 1m below the Cretaceous-Paleogene (Pg) boundary (see Figures 3.8 a-b) while at Møns Klint flint samples were collected in order to test the previously mentioned hypothesis. Sampling flint bands for all the study sites are shown in Figures 3.3, 3.5, 3.7 and 3.9 accordingly.

Table 3.1: Details of sampling sites

S/N	Sites/locations	Coordinates
1	Northern Province, North Landing, UK	[TA 243 706]
2	Northern Province, Ulcerby Vale House Quarry, Lincolnshire, UK	[TA 106 134]
3	Southern Province, East Sussex, UK	[TA 675 510]
4	Haute Normandie (Dieppe), France	[TW 196 769]
5	Picardy (Mesnil-Val Plage), France	[TW 539 265]
6	Sigerslev Quarry (Stevns Klint), Denmark	[55°19' 05" N, 12°26' 34" E]
7	Møns Klint, Denmark	[54°55' 22"N, 12°32' 37" E]

Table 3.2: Description of flint nomenclatures used for each study site derived from the formation and location of the respective samples. Atleast five flint blocks were collected from each site.

Sample Codes	Description	Flint Bands
BNLUK	Flint from the <u>B</u> urnham Chalk Formation at <u>N</u> orth <u>L</u> anding, <u>U</u> K	Ludborough Flint
BLSUK	Flint from the <u>B</u> urnham Chalk Formation at <u>L</u> incolnshire, <u>U</u> K	Ludborough and Nodular flint bands
SEUK	Flint from the <u>S</u> eafood Chalk Formation at <u>E</u> ast <u>S</u> ussex, <u>U</u> K	Seven Sisters Flint
SDFr	Flint from the <u>S</u> eafood Chalk Formation at <u>D</u> ieppe, <u>F</u> rance	Seven Sisters Flint
LMFr	Flint from the <u>L</u> ewes Chalk Formation at <u>M</u> esnil-Val Plage, <u>F</u> rance	Lewes Nodular Flint
TSKT	Flint from the <u>T</u> or Chalk Formation at <u>S</u> tevns <u>K</u> lint, <u>D</u> enmark	Prominent Flint band
TMKT	Flint from the <u>T</u> or Chalk Formation at <u>M</u> øns <u>K</u> lint, <u>D</u> enmark	-

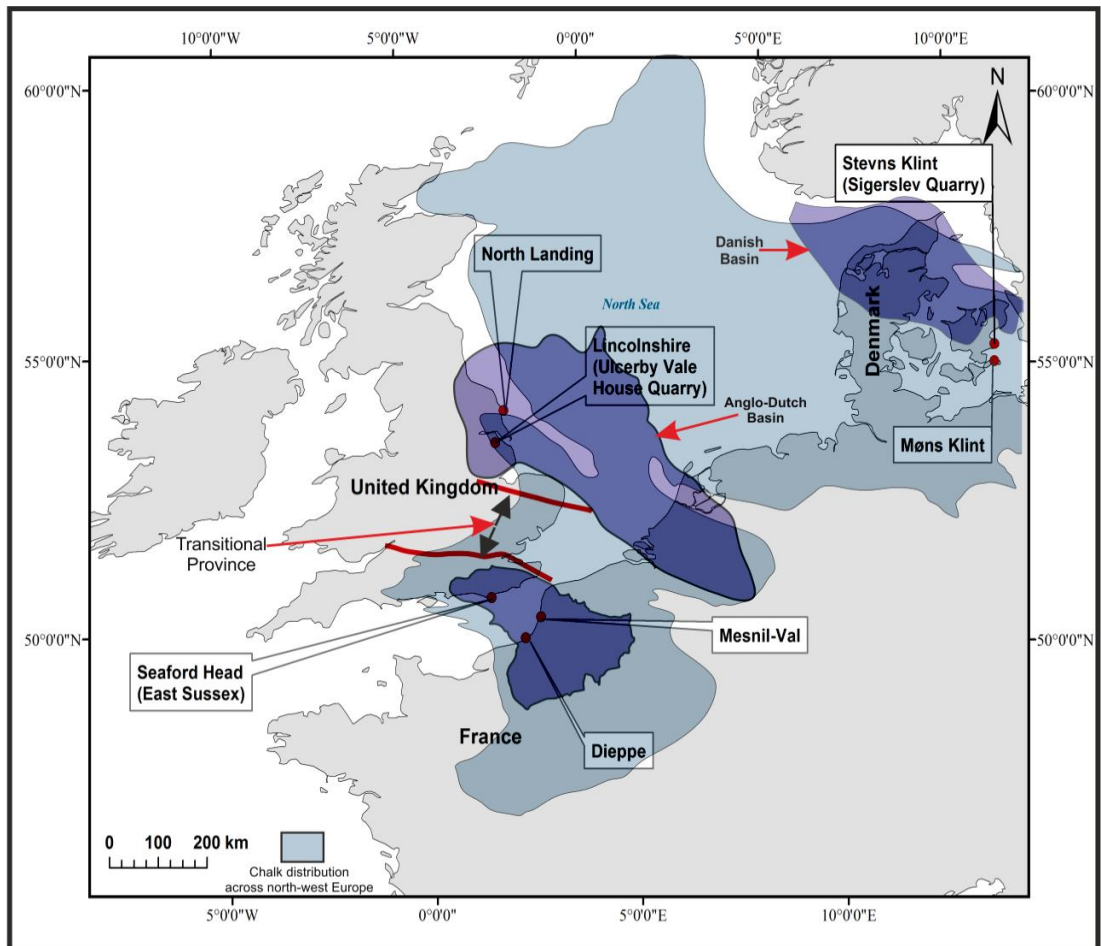


Figure 3.2: Study locations indicated by the red circles (Note: north-west Europe chalk distribution was re-drawn from Motimore (2012)).

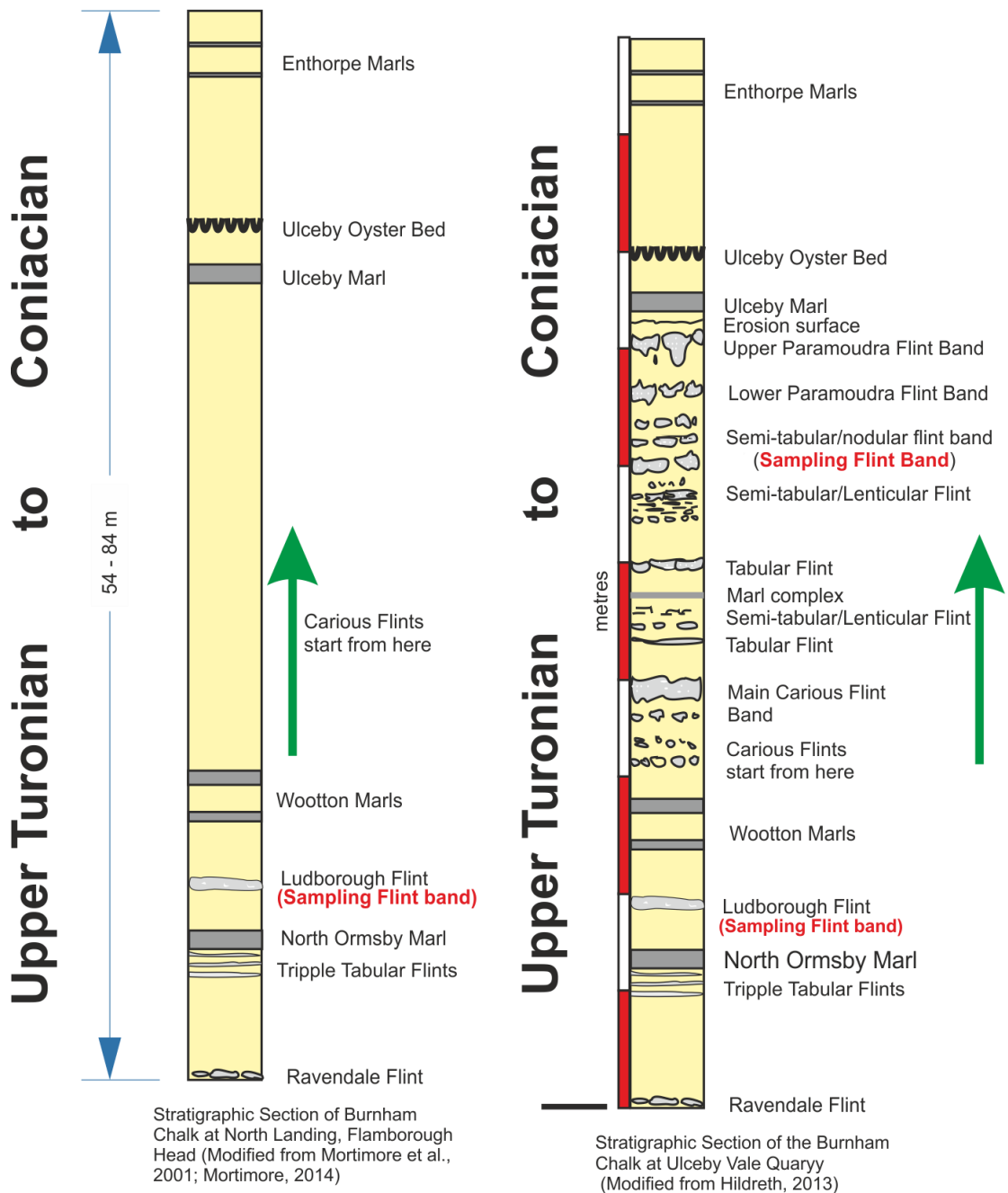


Figure 3.3: Stratigraphic columns of Burnham Chalk Formation showing flint bands from which flints were sampled at North Landing and Lincolnshire (Modified from Mortimore et al., 2001; Mortimore, 2014, Hildreth, 2013 for Ulceby Vale House Quarry).

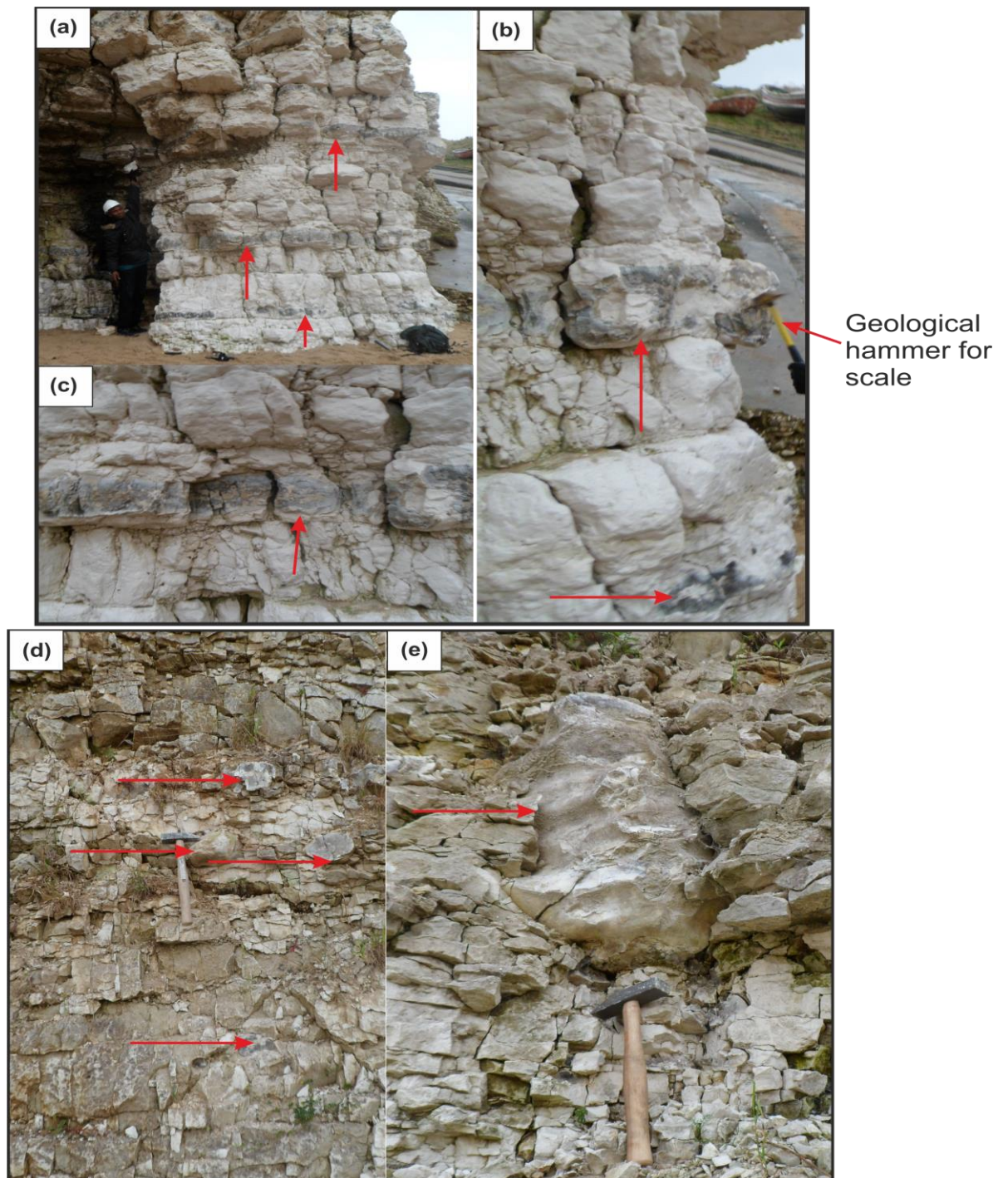


Figure 3.4: Flint bands and nodules in the Burnham Chalk Formation, Northern Province, UK. Note: red arrows show different flints mostly carious flints. (a) Highly fractured tabular flint bands at North Landing. (b & c) Larger views of (a) showing fractures in both chalk and flints with remarkable carbonate inclusions in flint samples. (d) Nodular flints in the Burnham Chalk at Ulceby Vale House, Lincolnshire, UK. (e) Paramoudra Flint at Ulceby Vale House Quarry, Lincolnshire, UK.

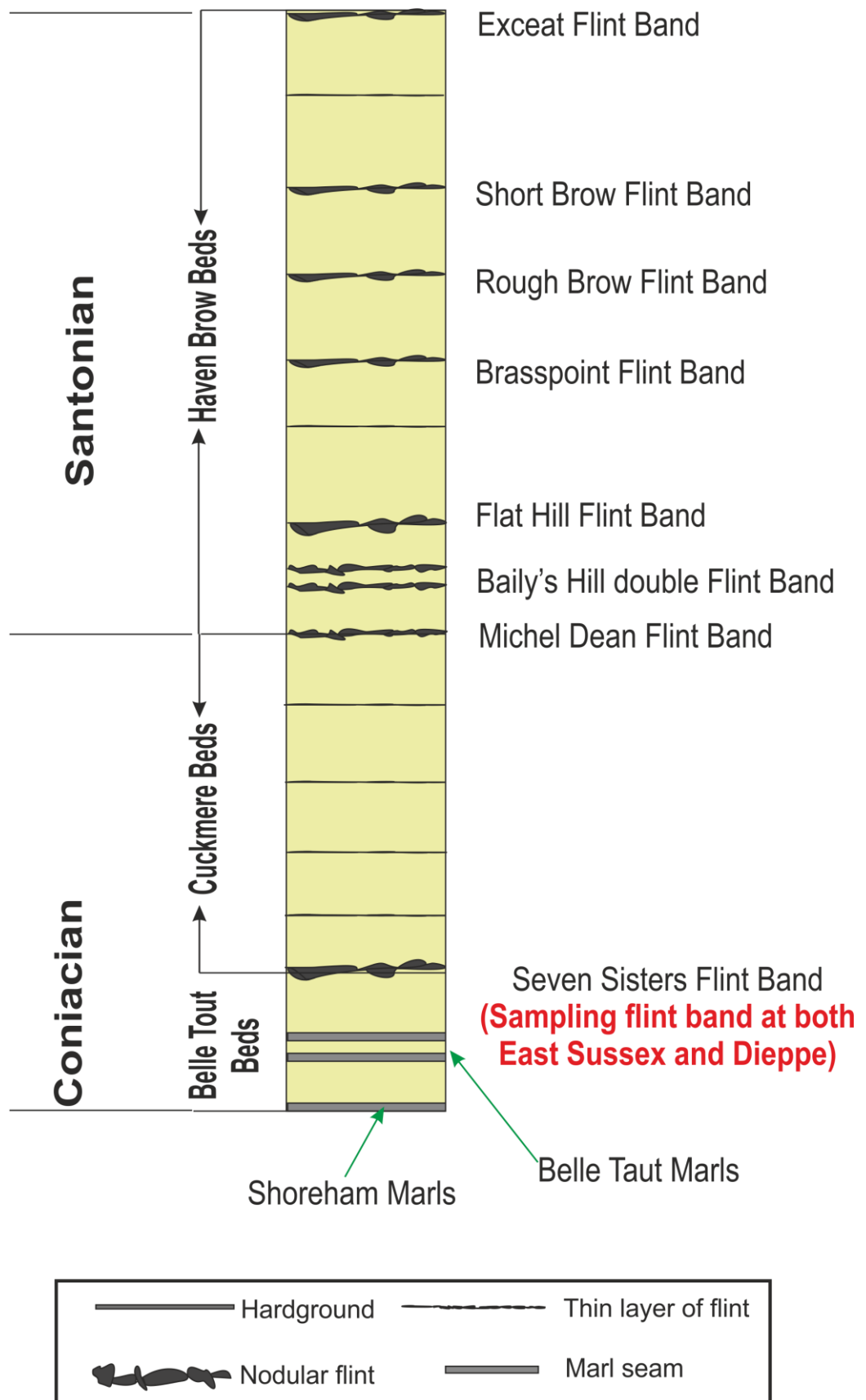


Figure 3.5: Stratigraphic column of Seaford Chalk Formation at East Sussex and Dieppe indicating the flint band from which flints were collected (Redrawn from Mortimore, 2014).

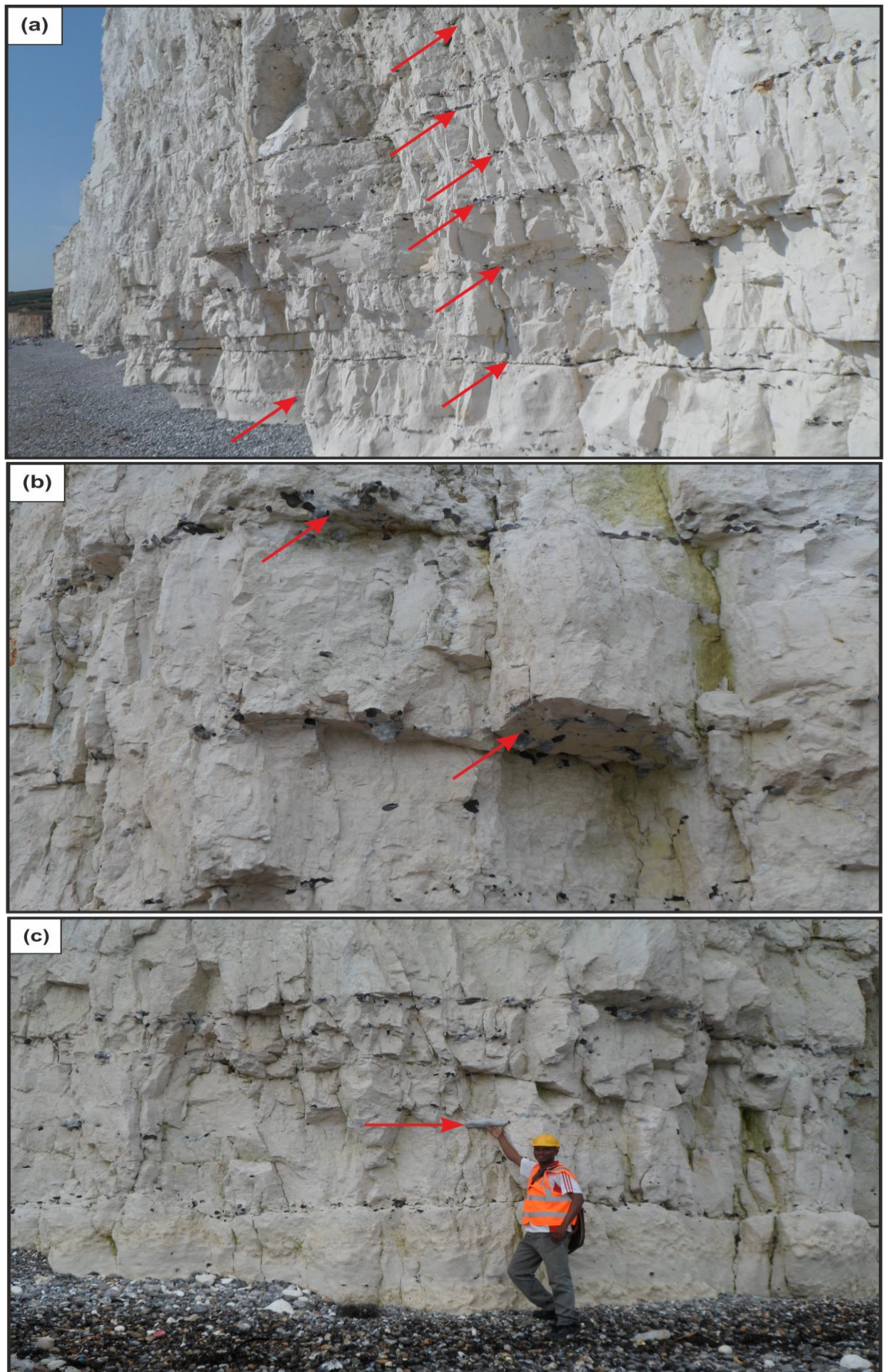


Figure 3.6 Extensive bands of nodular flints in (a) Seaford Chalk, East Sussex, UK, (b) Seaford Chalk, Dieppe, France and (c) Lewes Chalk formations, Mesnil-Val, France.

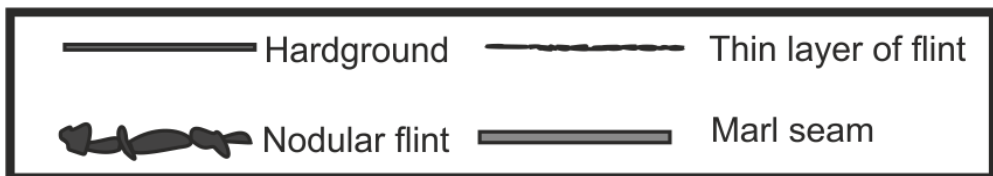
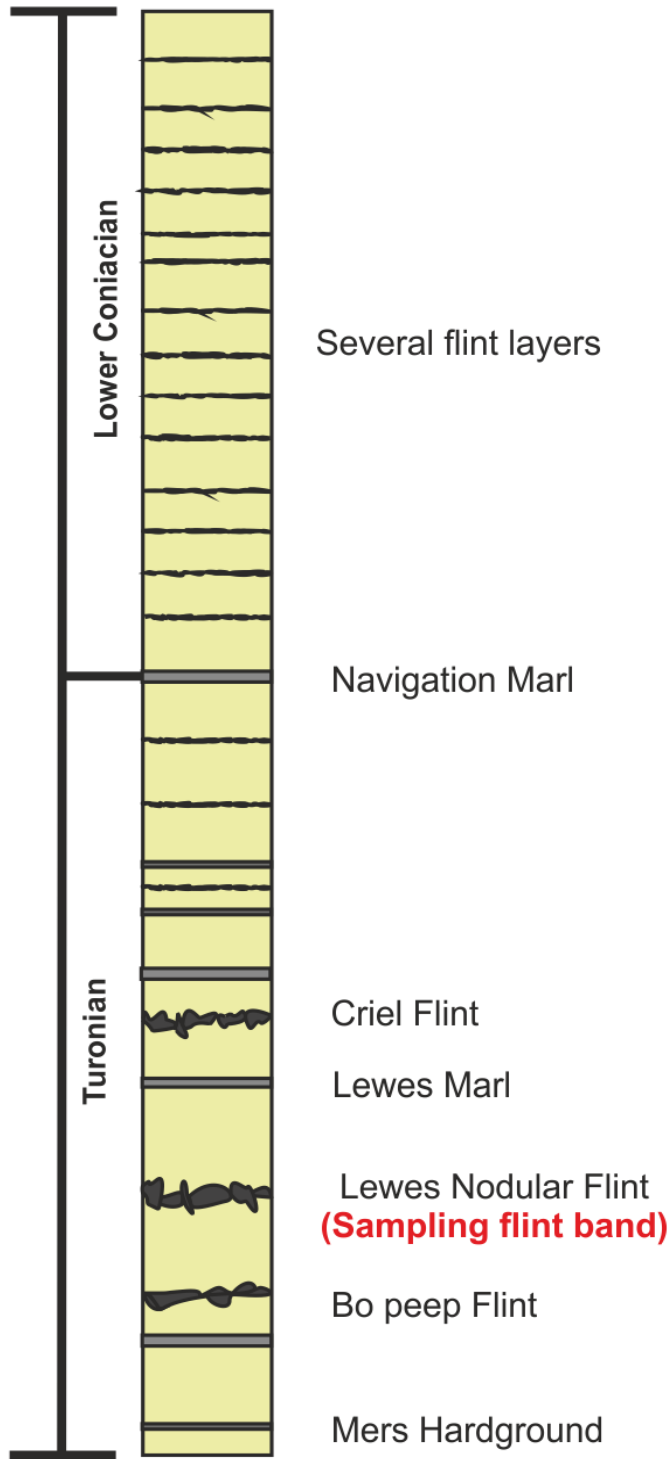


Figure 3.7: Stratigraphic Column of Lewes Chalk Formation at Mesnil-Val indicating the sampled flint band (Mortimore et al., 2001).

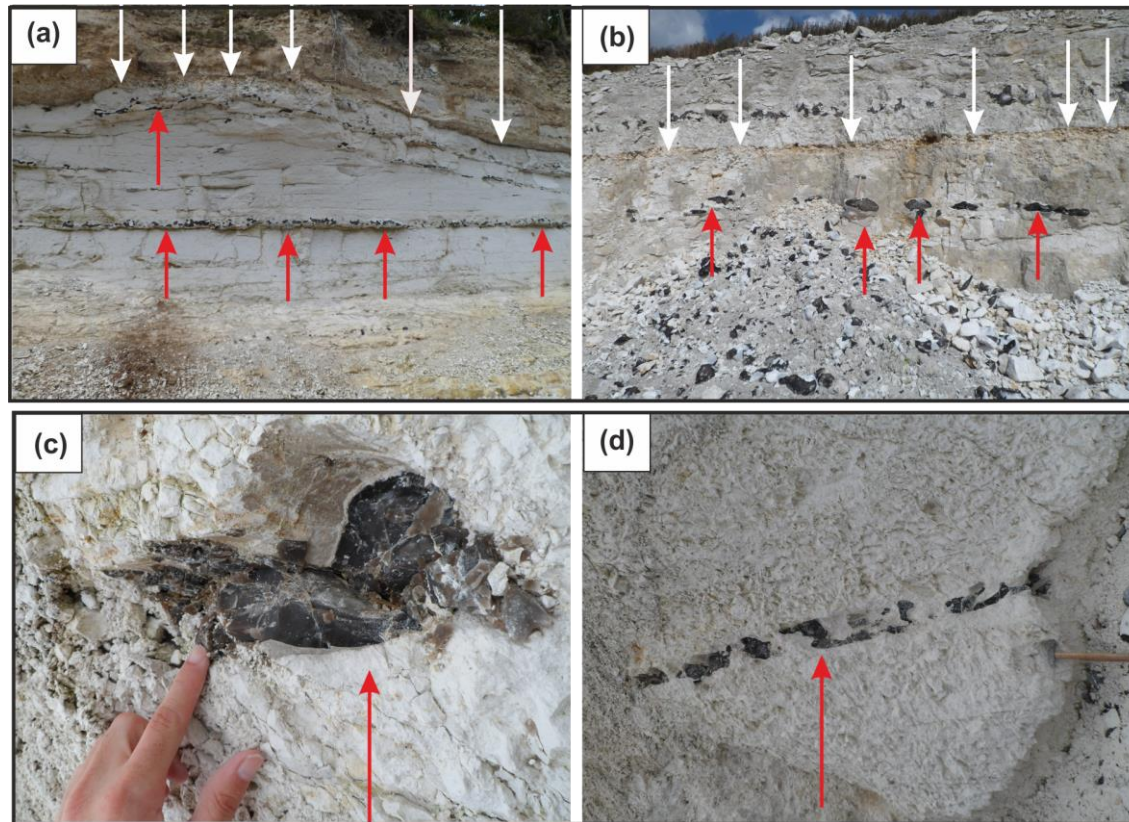


Figure 3.8: Flint bands and Nodules in Danish Chalk Cliffs. (a) Chalk cliff showing nodular flint bands at Stevns Klint, Denmark. (b) Chalk cliff exposure showing nodular flint bands at Sigerslev Quarry, Denmark. Note: In both Figures 3.5 (a) and (b) white arrows are indicating K-Pg boundary and red arrows are showing bands of flint nodules sampled for this study. (c & d) Disturbed flint nodules in glaciotectonically deformed chalk at Møns Klint, Denmark.



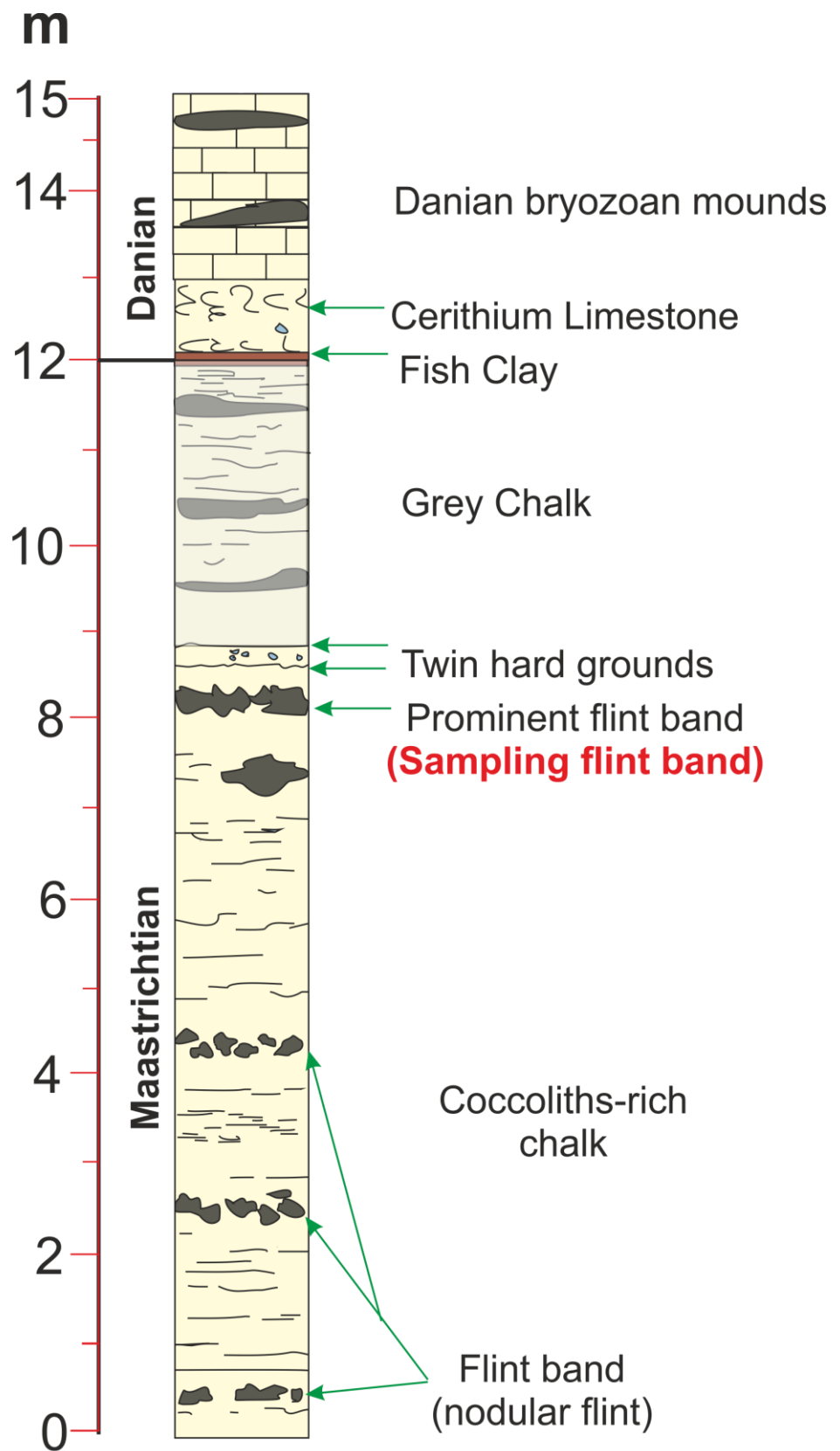


Figure 3.9: Stratigraphic column of Tor Chalk Formation at Stevns Klint indicating the sampled flint band (Modified from Surly, 1979; Hart et al., 2004).

### 3.2.2 Sample Description and Preparation

The morphologies, diagenetic features, and colour of flints are described. The colour was described using Munsell colour chart while the presence of fractures and white inclusions were noted based on physical observations (Figure 3.10). Table 3.3 explains the abbreviations used throughout this thesis to describe flint samples collected from the study sites. The different flint colour and types/structures of flints identified can be seen in Figures 3.11, 3.12, 3.13 and Table 3.3. In Table 3.3 the first letters of the sample codes represent the formation, for instance for BNLUK, B refers to Burnham Chalk Formation. The next two letters NL (BNLUK) and LS (BLSUK) respectively mean the locations i.e. North Landing and Lincolnshire. Meanwhile for the SEUK, SDFr and LMFr the next second letters E, D and M represent the respective locations of East Sussex, Dieppe and Mesnil-Val. The last two letters refer to country of sampling, where UK refers to the United Kingdom and Fr means France. In the TSKT and TMKT, the SKT and MKT represent Stevns Klint and Møns Klint.

The flint samples collected from the North Landing, UK are occasionally weathered, carious, and tabular, mostly grey (Figures 3.10a, b, c, d, e & 3.12 a-d) and highly fractured (both macro/microfractures). Fractures in these flints persist from the host chalk through the flint core and mimicked the vertically oriented and closely spaced fractures generally seen on the chalk cliff (Figure 3.4 a-c) with about 10 -12 fractures per 200 mm of flint block. The patterns of these fractures are likely influenced by the larger Flamborough Head Faults and likely attributed to the proximity of the North Landing Chalk to the Flamborough Head faults.

The North Landing Flint possessed white crust (Figure 2.9b) which can be up to 20 mm thick or higher, harder than the surrounding chalk, but softer than the enclosed flint core. These flint samples have remarkable quantity of calcite inclusions (Figures 2.9 and 3.12), which sometimes constitutes about 40-50% of the bulk sample. Most North Landing flint samples are up to 300 mm thick and in some cases most parts of the sample are dominated by light grey flint. Brownish grey flints are also found in the North Landing Chalk with significant quantity of calcite inclusion (Figure 2.9e).

In contrast with the grey flint from the North Landing Chalk, the dark brownish grey flints (Figures 2.8 d-h, 3.11, 3.13b-d) have very few highly/completely silicified inclusions. These highly silicified inclusions mostly appear as lighter spots on various parts of the samples. The dark brownish grey flints appeared more competent than the grey flints due to the absence of fractures similar to that seen in the grey flints. The white crust surrounding the dark brownish grey flints are thinner and harder when compared with the White crust surrounding the grey flints.

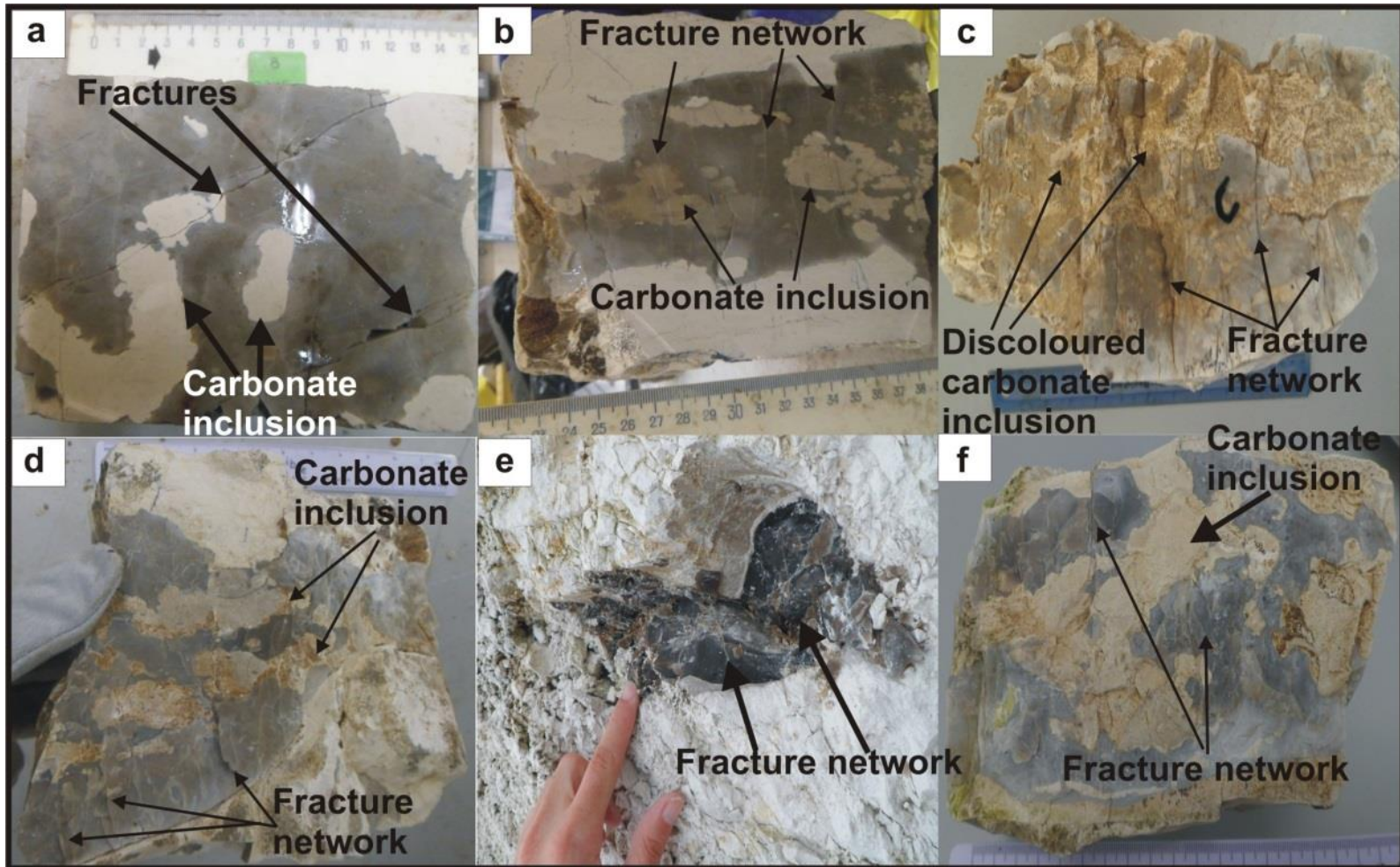


Figure 3.10: Flint samples showing fracture network and carbonate inclusions. (a-d and f) were samples from the Burnham Chalk Formation at North Landing, UK and formed parts of carious flints. (e) In-situ Flint sample from the Tor Formation at Møns Klint, Denmark.

Table 3.3: Description of all the abbreviations used for flint types and colour

Flint Colour/types	Description
Ch	Chalk
SGch	Spotted Grey Chalk
WCr	White Crust
WI	White Inclusion
SWI	Spotted White Inclusion
LG	Light Grey flint (N7)
GF	Grey flint (N5)
LBG	Light Brownish Grey flint (5YR 6/1)
BG	Brownish Grey (5G 2/1)
DBG	Dark Brownish Grey flint (5YR 2/1)

Note: The numbers and letters in bracket represent the colour codes presented using the Munsell colour chart.

Flint samples for UCS testing were drilled into cores using the Richmond S.R.2 radial drill at a speed of  $1500 \text{ Revmin}^{-1}$  (Figure 3.14a). This speed was used after trying various speeds, and this was found to be more efficient for drilling flint. Coring was successfully done in all the flint samples drilled, except the carious North Landing flints (BNLUK) which could not be drilled into cores. Moreover, all attempts to produce cores resulted in a broken piece of rock (Figure 3.14b and d). This difficulty in coring the BNLUK was attributed to the presence of a network of fractures and a significant proportion of white carbonate inclusions in the flint samples.

Therefore, to avoid the problem of coring the BNLUK for UCS test, cuboidal samples were prepared. The ends of both the cuboidal and core samples for the UCS test were flattened using surface planner and Tungsten carbide powder. Though, the Tungsten Carbide powder was reduced or made finer after few grinding of flints, and this made the smoothing process longer.

Besides, the problem of producing core from the BNLUK, another challenge encountered while preparing flint samples was the rapid wear of the coring bits. Initially, most of the core bits used were completely worn after coring only one or two flint samples of 25 mm (diameter) by 60 mm (length). Bespoke core bits with specifications shown in Table 3.4 were ordered to improve performance. Similarly, some blocks of flint samples comprising regular and irregular blocks were also cut for the remaining laboratory tests. Cutting was done using CM501 Honda rock/masonry sawing machine (Figure 3.14c). In both cutting and drilling water was used as both coolant and lubricant. The prepared samples were then used for laboratory tests.

Darkness and silicification of carbonate inclusion increase, while percentage of this inclusion decreases

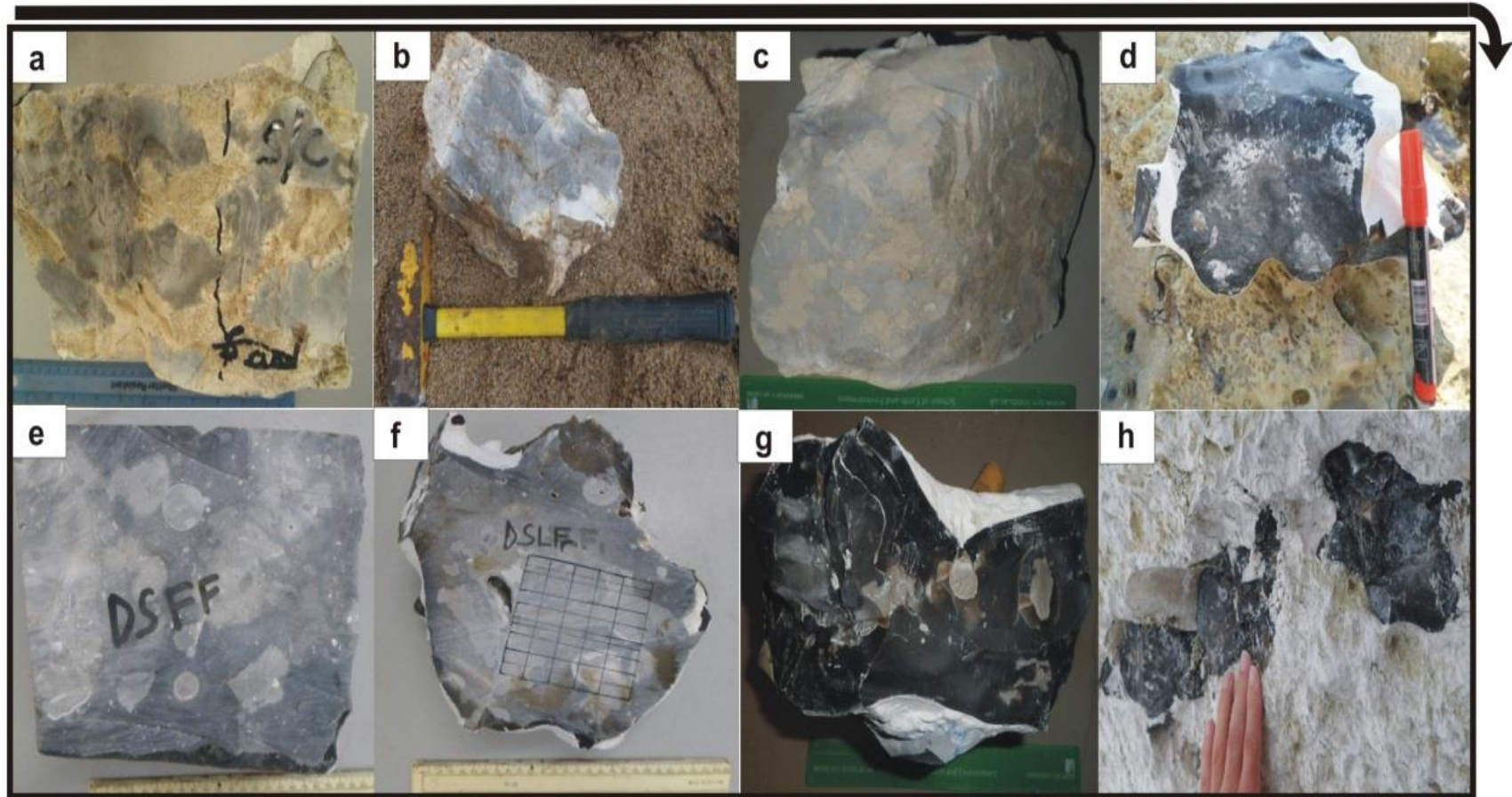


Figure 3.11: Flint samples exhibiting different colour and various degree of carbonate inclusion. (a and b) are BNLUK, (c) is BLSUK, (d) is SEUK, (e) is SDFr, (f) is LMFr, (g) is TSKT and (h) is TMKT sample.

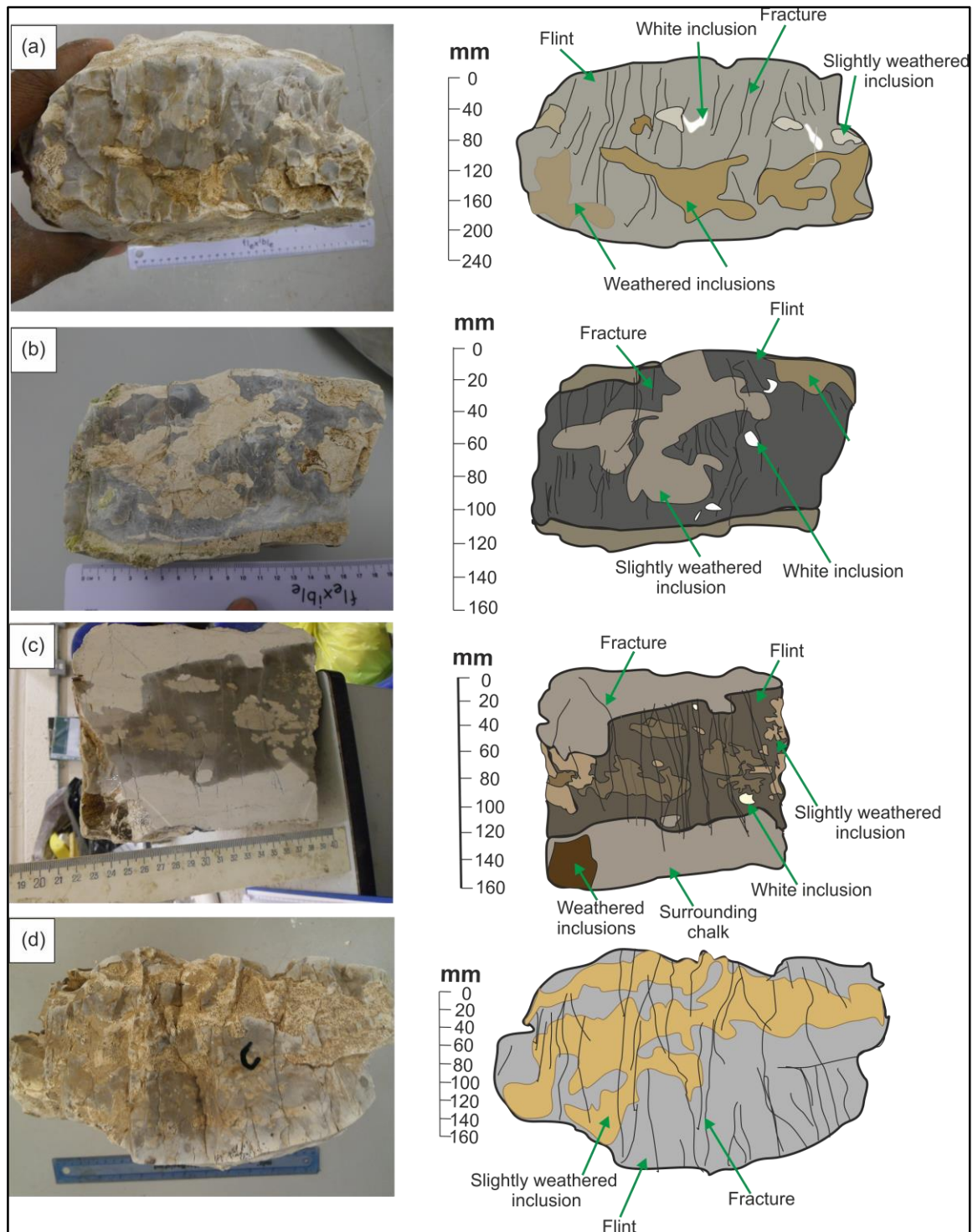


Figure 3.12: (a-d) Weathered and highly fractured Flint samples (Ludborough Flint band) from Burnham Chalk, north Landing.

Note the presence of inclusions (carbonate) and fractures in the samples. Most fractures in these samples are perpendicular to bedding and reflect the closely spaced, vertical tectonically induced fractures that characterised the site. Most of these fractures are persist through both flint and the host chalk. An average of about 10 -12 fractures can be counted in 200 mm long block of these samples.

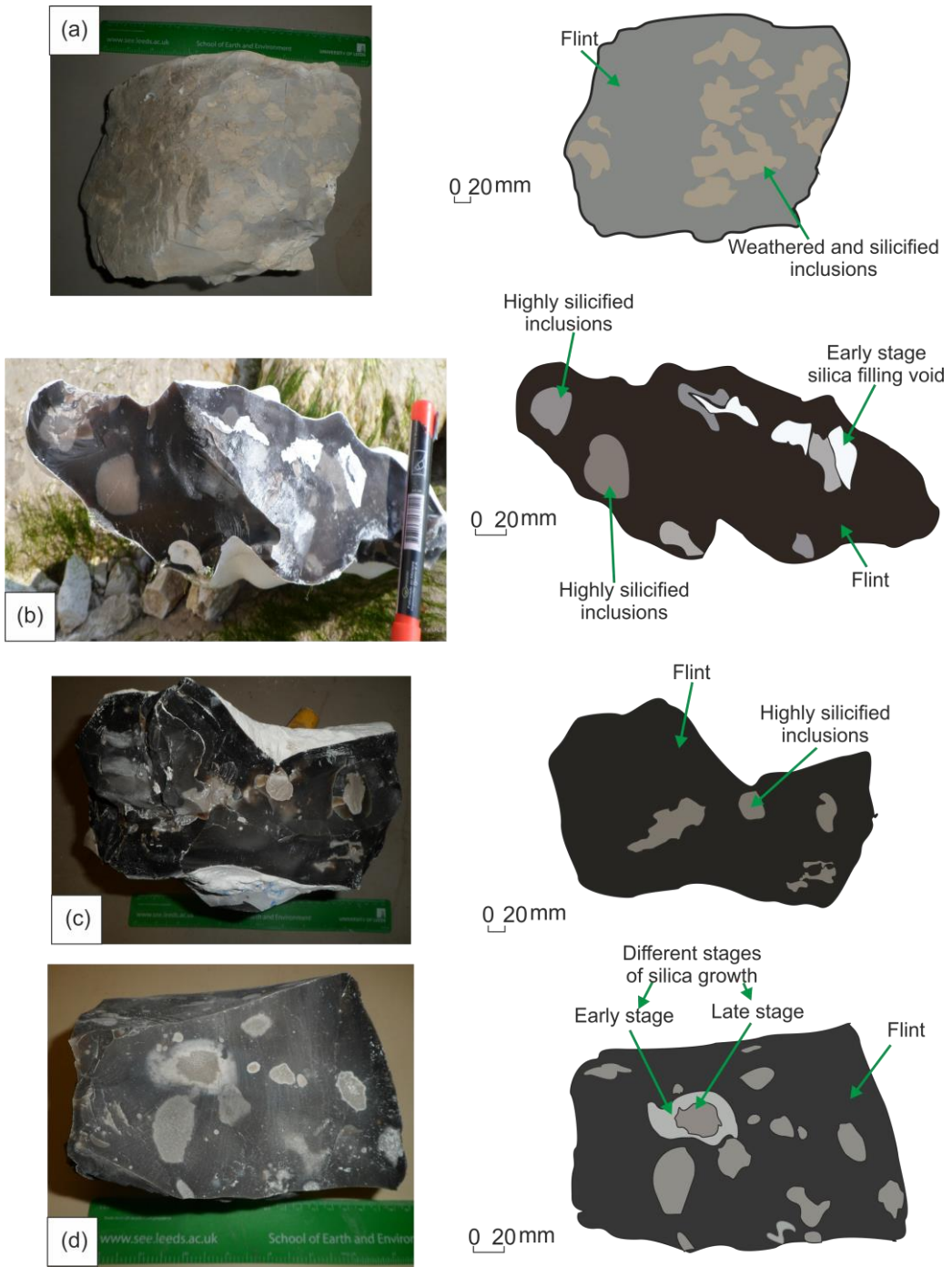


Figure 3.13: Grey flint sampled from Ludborough Flint band, Burnham Chalk Formation at Ulceby Vale Quarry, Lincolnshire.

Note the partially silicified inclusions and more competent flint core devoid of fractures seen in Figures 3.12. (b) Dark brownish grey flints from: (a) the Seaford Chalk East Sussex; (c) the Seaford Chalk Formation at Dieppe and (d) Lewes Chalk Formation, Mesnil-Val. Note the highly silicified inclusions and absence of fractures in the dark brownish grey flints. All the dark brownish grey flints have similar physical appearance.



Figure 3.14: Sample preparation program. (a) Coring flint samples for UCS, ultrasonic and He Porosity tests. (b) BNLUK flint sample which could not be drilled into suitable core because it is a carious flint, note the presence of inclusion in the sample, and the fractures forming the failure planes. (c) Cutting beams, irregular and regular blocks for mechanical tests. (d) Block from which (b) was cored.

Table 3.4: Core bits specifications designed by the author for drilling flints

Description	Specifications
Core barrel internal diameter	25 mm
Internal length	100 mm
Rock type being drilled	Flint
Drill coupling	1/2" BSP male end fitting
Drilled sample description	An extremely strong cryptocrystalline flint with mean UCS c.500 MPa
Matrix hardness	Soft matrix suitable for drilling extremely hard fine-grained materials (e.g. Series 10) and HRC 20, Crown height = 12 mm
Bit crown shape	Serrated V-ring/stepped profile
Kerf	Thin kerf
Stone/carat or Diamond concentration	90/100 or 60/80
Diamond size	1.07 mm



### **3.3 Strength and Deformability Characterisation Tests**

To define the geomechanical properties of flints in relation to drilling, tunnelling and other engineering geological purposes three laboratory strength tests for intact rock samples were employed in accordance with the ISRM (2007) standards. A summary of the procedures is provided with emphasis on the suggested method. The strength tests conducted are the uniaxial compressive strength (UCS), point load strength index, and tensile strength (three-point beam method, Brook, 1993) tests as discussed below.

#### **3.3.1 Uniaxial Compressive Strength (UCS) Test and Static Elastic Parameters**

The uniaxial compressive strength test was conducted on both cylindrical and cuboidal flint specimens in accordance with ASTM D2845 (1995); ISRM (2007); ASTM D7012-07 (2010) suggestions. The sample sizes, specimen geometry and respective sampling locations can be seen in Table 3.5. The choice of these sizes was dictated by the repeated failure of attempts to produce cylindrical core samples of NX (54 mm). The test was carried out using Denison machine with a capacity of 2000 kN operated at a stress rate of  $0.5 \text{ MPas}^{-1}$ . The device was calibrated and has an accuracy of 0.05 kN.

The static elastic parameters are derived from the responses of 5 mm axial and circumferential strain gauges fixed at the middle of the specimens to avoid the impact of end effects. The 5 mm strain gauges were used because the cryptocrystalline nature of the flint specimens meant very little strain was expected. Figure 3.15 shows the set-up and some samples used for the test. Figure 3.16 shows the schematic diagram of the UCS test set-up. Readings were recorded via the windmill logging system from where the associated static Young's moduli ( $E_s$ ) are determined from the average slopes of the straight line on the stress-strain graphs. The static Poisson's ratios ( $\nu_s$ ) are evaluated from the relationship between the gradient of the axial and diametrical stress-strain curves (Equations 3.1 and 3.2) as described in ISRM (2007); ASTM D7012-07 (2010).

Table 3.5: Details of samples used for UCS test

Flint Class	No. of samples	Flint Samples	Shape	Dia./breadth (mm)	l (mm)	l:d
1	11	BNLUK	Cuboid	18-32	63-67	2.0-3.5
2	10	BLSUK <sub>T</sub>	Cylindrical	24-26	60-65	2.5
3	10	BLSUK <sub>N</sub>	Cylindrical	24-26	57-65	2.4-2.5
4	20	SEUK	Cylindrical	23-26	54-62	2.3-2.4
5	20	SDFr	Cylindrical	23-37	53-77	2.1-2.3
6	20	LMFr	Cylindrical	23-25	48-60	2.1-2.5
7	15	TSKT	Cylindrical	24-25	61-66	2.5-2.6
8	5	TMKT	Cylindrical	24-25	61-64	2.5-2.6

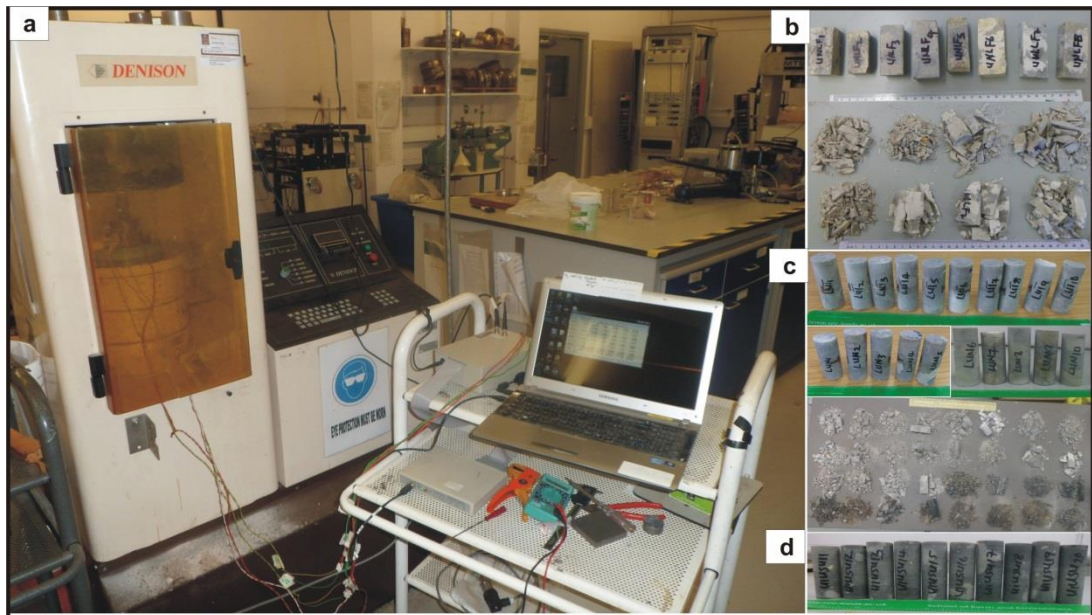


Figure 3.15: UCS test setup and samples. (a) Uniaxial Compressive Strength (UCS) test set-up; (b) BNLUK; (c) BLSUK and (d) SEUK samples before and after tests.

$$E_s = \frac{\Delta \text{ Axial stress}}{\Delta \text{ Axial strain}} \text{----- Equation 3.1}$$

$$\vartheta_s = \frac{\text{Slope of axial curve}}{\text{Slope diametral curve}} = \frac{E_s}{\text{Slope of diametral curve}} \text{----- Equation 3.2}$$

Where:  $E_s$  is the static Young's modulus (GPa),  $\Delta$  Axial stress is the change in axial stress from the stress-strain curve (MPa),  $\Delta$  Axial strain is the change in axial strain

derived from the stress-strain curve,  $\nu_s$  is the static Poisson's ratio. The results of these tests are presented in Chapter 4, Section 4.2.

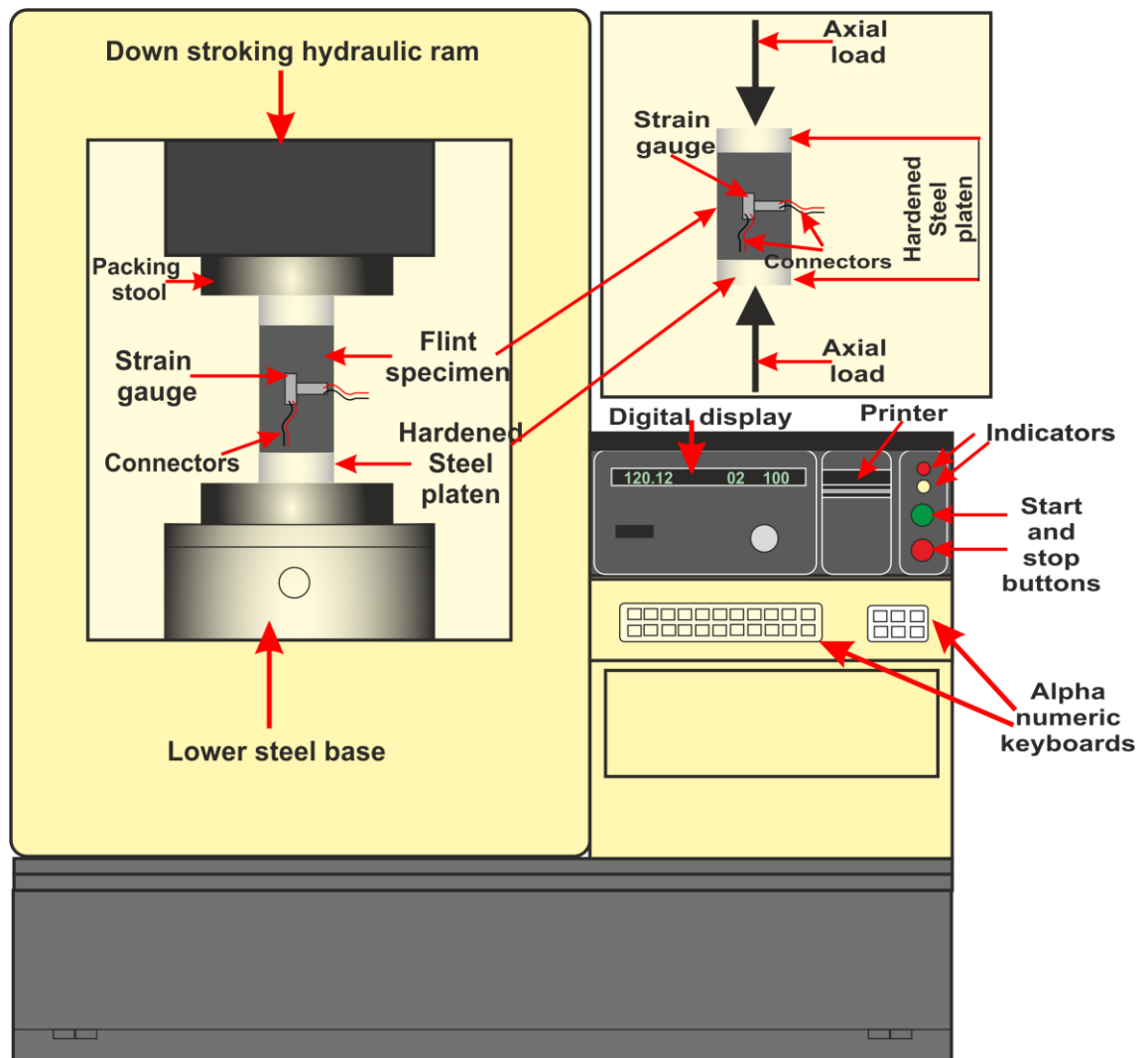


Figure 3.16: Uniaxial compressive strength test set-up (not to scale).

### 3.3.2 Tensile Strength Test (Three-Point-Disc Method)

Beams of flint samples with dimensions and sampling details shown in Table 3.6 were prepared. The prepared samples were tested using the Three-point-disc method as described in Brook (1993). The test was conducted using the MAND universal compression testing machine with a loading capacity of 250 kN, with an accuracy of 0.1 kN, operating at a scale of 0-10 kN for greater sensitivity. The Three-point-disc method was used because the test is simple, quick and does not require surface polishing. The test was also considered over other tensile strength tests due to the challenges encountered while trying to prepare cylindrical flint samples suitable for the Brazilian

test. In addition to the suitability of the testing method from the sample preparations perspective, the method had a good relationship with the direct pull test (Brook, 1993). The test also provided a good estimate of tensile strength when used on Paramoudra Flint (Fowell & Martin, 1997).

The Three-point test was carried out by placing each sample on two ball bearings separated at various spans (*l*) depending on the respective dimensions of the samples (Figure, 3.17). The samples were then tested by applying concentrated load at the centre of the sample until the sample fail in tension. The failure loads were recorded, and the tensile strength was evaluated using Equations 3.3 and 3.4 after rejecting the samples whose length (*l*) to thickness (*d*) ratio was less than 3. The tensile strength test results obtained from this test are provided in Chapter 4, Sub-section 4.2.2.

$$T_0 = \frac{P}{G} \text{ Equation 3.3}$$

$$G = \frac{4bd^2}{3l} \text{ Equation 3.4}$$

Where:

*T*<sub>0</sub> is the tensile strength (MPa), *P* is the failure load (kN), *G* is the geometry factor, *b* is the breadth of the sample (mm), *d* is the thickness of the sample (mm), *l* is the span between the ball bearings Figure 3.17.

Table 3.6: Details of flint samples used for tensile strength test

Number of sites	Flint Samples	Number of samples	d (mm)	b (mm)	l (mm)
1	BNLUK	8	9-19	18-27	40-48
2	BLSUK	15	10-20	10-30	48-64
3	SEUK	54	7-20	13-50	48-72
4	SDFr	20	10-15	18-33	48-64
5	LMFr	20	10-16	13-31	48-64
6	TSKT	17	10-15	18-33	48-64
7	TMKT	14	10-11	10-30	56-64

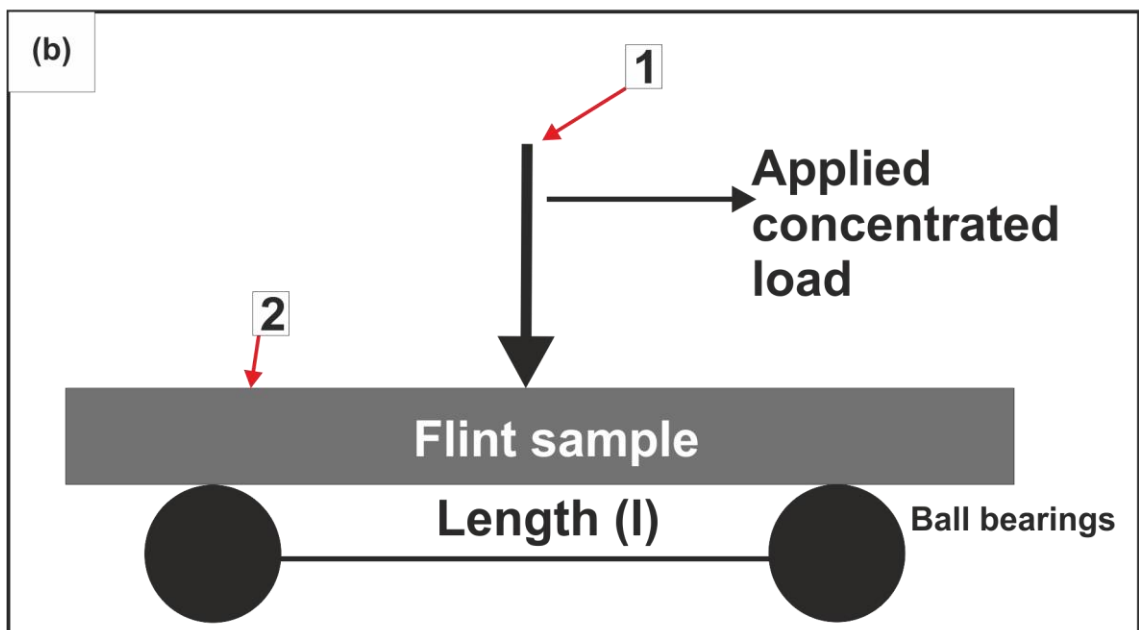
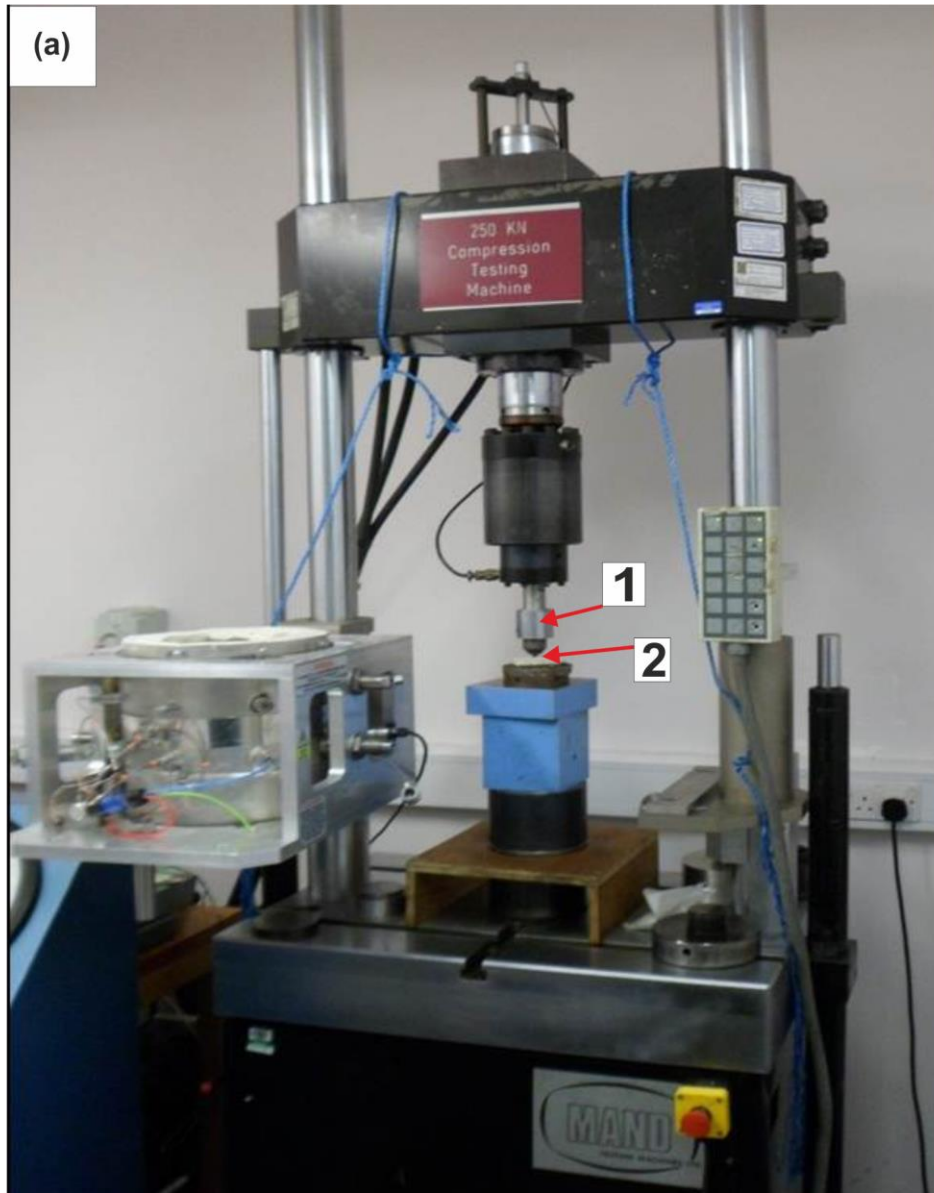




Figure 3.17: (a) Tensile Strength system for Three-point test; (b) Schematic diagram of the testing procedure (not to scale). (c) and (d) Flint samples before and after test.

### 3.3.3 Point Load Strength Index Determination

The Point load strength index test was conducted using the ELE point load tester (Figure 3.18). Figure 3.19 illustrates the schematic diagram of the testing system. The testing machine has the loading capacity of 56 kN with an accuracy of 0.05 N. The test is carried out on blocks and irregular lumps of flints in accordance with the ISRM (2007) suggestions. The description of the samples used for this analysis is presented in Table 3.7. The Point load strength index for each sample is obtained by subjecting the samples to steady load until the samples (Figure 3.18 b-e) fail within 10-60 sec. Then the failure loads are noted and recorded from which the point load strength index for each sample was calculated using Equations 3.5 to 3.10 (ISRM, 2007).



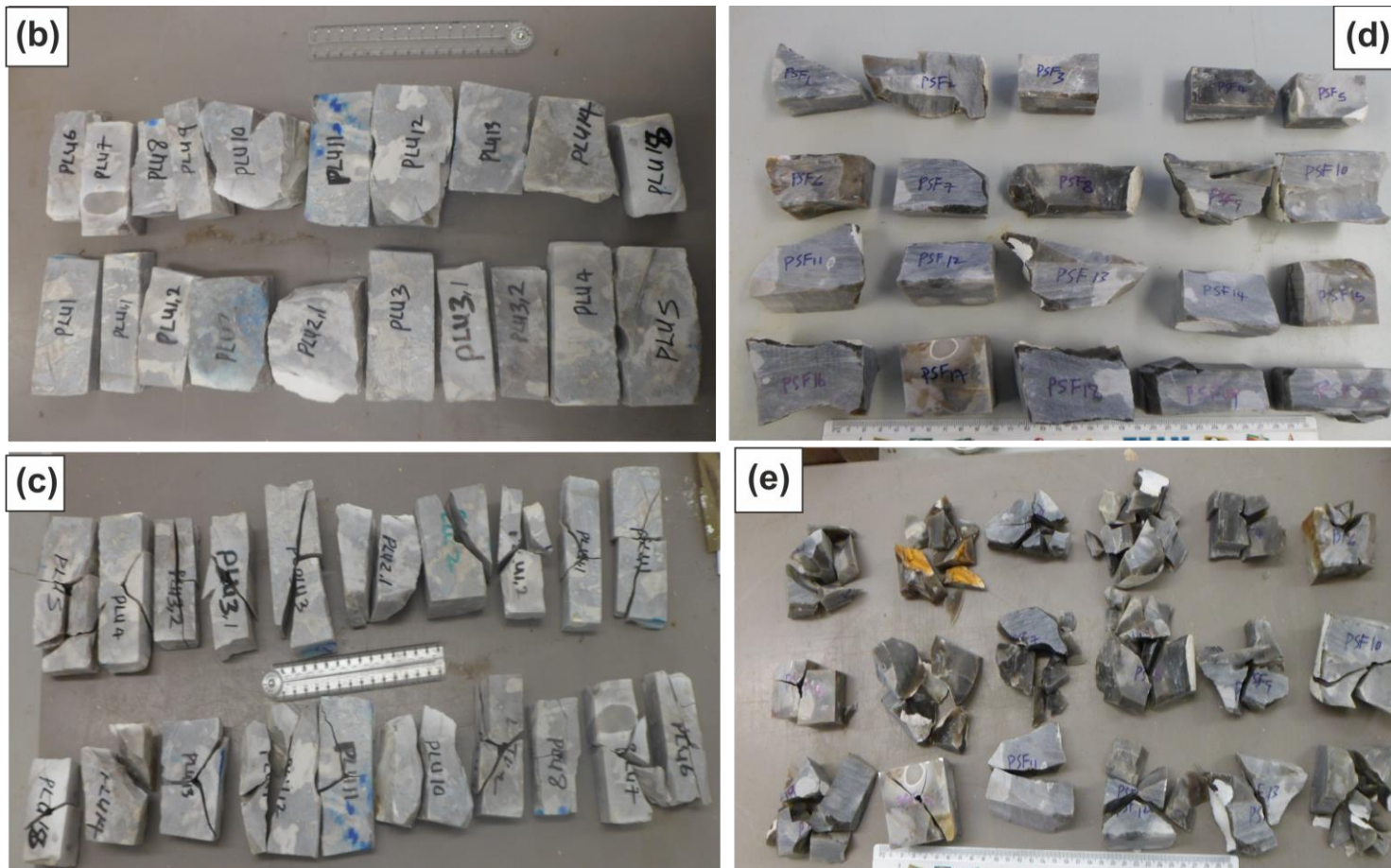


Figure 3.18: (a) Point load experimental equipment used for the test; (b and d) flint samples before test; (c and e) flint samples after tests (failed samples).



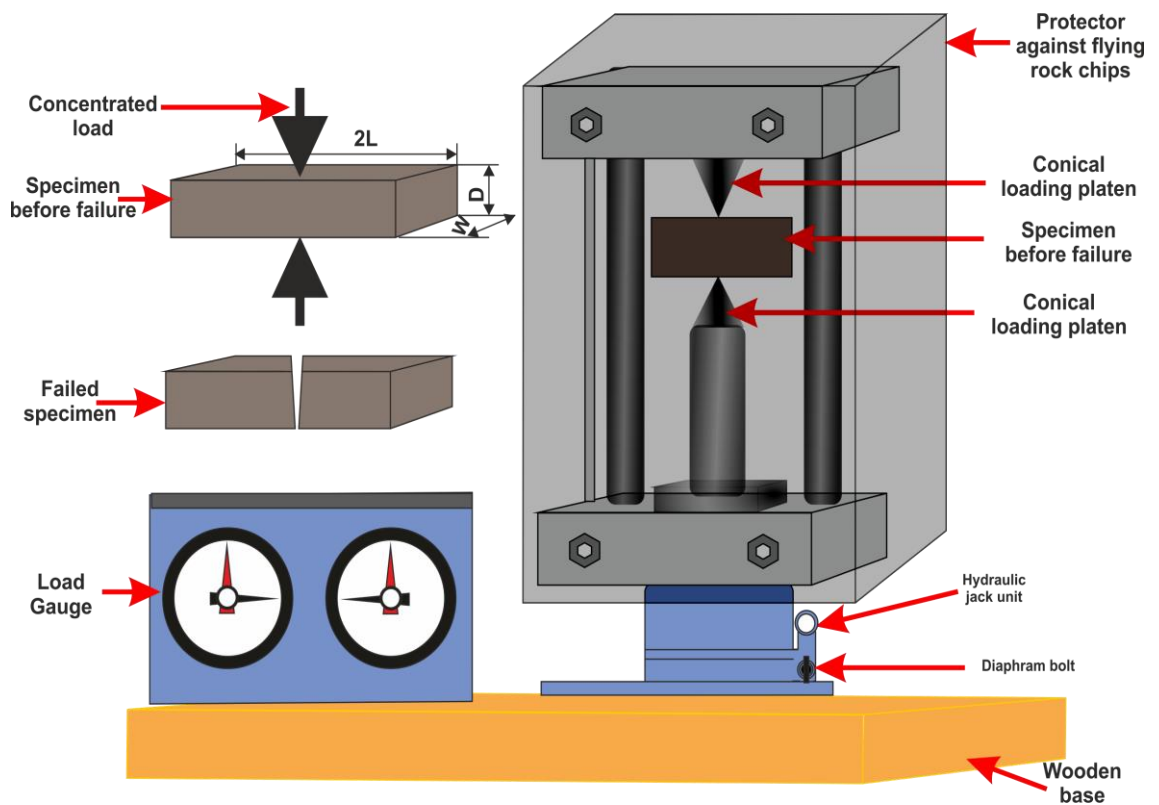


Figure 3.19: Illustration of Point load testing equipment and typical sample failure (not to scale).

Table 3.7: Details of samples employed for the point load strength index test

Flint Samples	Number of samples	l (mm)	w (mm)	d (mm)
BNLUK	49	9-79	12-48	10-45
BLSUK	20	63-107	29-61	14-36
SEUK	82	15-90	19-50	15-44
SDFr	20	50-72	30-42	20-32
LMFr	20	48-75	22-85	17-30
TSKT	16	60-102	30-55	17-33
TMKT	9	68-88	23-43	21-33

$$A = W \times D \text{ _____ Equation 3.5}$$

$$De^2 = \frac{4A}{\pi} \text{ _____ Equation 3.6}$$

$$De = \sqrt{De^2} \text{ _____ Equation 3.7}$$

$$I_s = \frac{(P \times 1000)}{De^2} \text{ Equation 3.8}$$

$$F = \left(\frac{De}{50}\right)^{0.45} \text{ Equation 3.9}$$

$$I_{s50} = F \times I_s \text{ Equation 3.10}$$

Where:  $A$  is the minimum cross sectional area of the point of contact for the loading platens on the sample ( $\text{mm}^2$ ),  $De$  is the equivalent sample diameter (mm),  $F$  is the Size correction factor,  $I_s$  is the uncorrected point load strength index (MPa), and  $I_{s(50)}$  is the corrected point load strength index (MPa).

### 3.4 Petrographic Analysis

In order to understand the external morphology, characterise, and quantify the mineral phases in the flint samples, analytical techniques comprising Scanning Electron Microscope SEM, SEM-CL, thin section microscopy and X-ray Powder Diffraction (XRD) were used. The former was considered to reveal the external morphology, mainly grain shape, grain orientation and degree of cementation because these features are keys to explaining the physical and mechanical behaviour of the rock. The latter was employed to define the mineral composition and silica phases present in the flint specimens. Examining the mineral compositions and silica phases in flint from different regions is vital for understanding the geological controls on the abrasivity and drillability of flint as well as explaining the genesis of flint, which can be linked to the material properties of flint.

The components of flints considered for these analyses were the white crust and the flint core. Various flint colour and types listed in Table 3.3 were also considered. These features were considered to be good enough to understand the variation in material properties of flints with structures and class of flint. Since understanding the strength properties of flints would aid in explaining the extent of variability observed in the strength of flint at the microscopic level.

Samples for Scanning Electron Microscopy were carefully chipped out from blocks of flint with various structures (white crust, inclusions) and classes (different colours). Samples for XRD analysis were also obtained by preparing fine powder from

each sample. The fine powder from each flint type/colours were packed into sample holder for laboratory analysis as shall be explained in Section 3.4.1.

### 3.4.1 X-Ray Diffraction (XRD) Analysis

A D8 diffractometer was employed for XRD powder diffraction on flint powder, ground white crust and the surrounding chalk to identify and quantify the mineral phases in these samples. The D8 diffractometer was equipped with a Cu  $\alpha$  tube, a primary Ge monochromator and uses a Lynx eye detector for the analysis of patterns.

The flint samples were manually ground into fine powder using agate pestle and mortar (Figure 3.20). The resulting powder was further sieved using 53  $\mu$ m sieve and then ground again to obtain as finer powder as possible. The prepared powder of all the samples investigated were scanned at an angular range of 2-90° 2 $\theta$  with scanning step of 0.01° using Cu  $\alpha$  radiation source. The Bruker EVA search match software was used for the identification of mineral phase. The identified mineral phases were then quantified using Bruker TOPAS profile and structure analysis software. The X-Ray trace patterns expressing the peaks for each mineral phase quantified are presented in Appendices 1-7 in the form of diffractographs, while the quantitative description of the samples are given in the form of tables in Chapter 5 (pp. 173-177).



Figure 3.20: XRD analysis samples and sample preparation. Some flint samples showing different colour for XRD analysis and to the right shows the grinding process.

### 3.4.2 Scanning Electron Microscopy (SEM) Analysis on Rough Flint Samples

Scanning electron microscopy (SEM) was conducted to examine the microtexture (degree of silica cementation) and external morphology (grain shape, sizes and orientation) of the flints, white crust and the surrounding chalk. The analysis was executed on both rough and polished flint and chalk samples (Figure 3.21) with sizes of

about 10x10x5 mm. The samples were drawn from all the study sites and were analysed based on colour differences and types identified in Section 3.2.2.

The samples were then coated with gold in a BIO-RAD-SC500 Sputter coater for 4-5 minutes to prevent the concentration of electrical charges on the surface of the samples. The coated samples were analysed using JEOL-JSM-6610LV SEM equipped with an Oxford Instruments energy dispersive X-Ray (EDX) detection analyser, to delineate and quantify mineral phases in the samples. SEM Images were acquired at an accelerating voltage of 15 keV.

The samples were prepared with the size range of 10x15x15 mm by considering their variations in colours and types. This sample preparation was achieved using 6" Bushler trimming saw in the thin section laboratory of the School of Earth and Environment, University of Leeds. The prepared, polished samples were used to quantitatively investigate the minerals present in the samples.

The sections of the cut samples were trimmed and ground to a smooth surface finish to prevent any possible electron interference. The ground samples were encapsulated in a 30 mm mould with a mixture of resin (70 g) and hardener (27.3 g) to preserve the original microstructure of the samples. The encapsulated samples were allowed to harden for about 2 1/2 hours, and the hardening process was supported by placing the mould bearing samples on the hot plate of the Gallen Kamp.

The hardened samples were polished on Buehler-Ecomet 250 polishing machine using 0.3 µm thick Alumina ( $\text{AlO}_3$ ) at a speed of 100 rpm for the head and 50 rpm for the base. The polished samples were then coated with 14.2 nm carbon film using the Quorum Q150T E carbon coating system (Figure 3.21d) in order to make the surface of the samples conducive to electron during the analysis. SEM analysis was conducted on the coated samples using Quanta FEG650 (Figure 3.21) from which the secondary electron, backscatter electron and EDS images were acquired.



Figure 3.21: (a) Scanning Electron Microscopy (SEM) Set-up; (b) flint samples used for rough SEM analysis; (c) polished flint samples used for SEM analysis (d) coated rough samples being coated with gold.

### 3.4.3 Thin Section Microscopy

Thin sections (Figure 3.22a) of flint samples were investigated using both plane and crossed polarised light. The flint core, and the white crust-core boundary were investigated to analyse the different quartz phases. This also allowed an understanding of variability among the flint samples in terms of microfractures, fossils conservation/dissolution, calcite-silica replacement, and recrystallisation and deformation phenomena to be obtained.

Thin sections were prepared in the School of Earth and Environment with a target thickness of 30  $\mu\text{m}$ . Difficulty associated with cutting flints as attempts to produce sections resulted in broken sections necessitated the use of these sizes. The other analysis was done using Leica DM750P polarising microscope (Figure 3.22b). The optical microscope was equipped with Leica DFC290 HD digital camera to capture the high-resolution micrographs, and the micrographs were processed using Leica application software suite at 500  $\mu\text{m}$ . The results of this test are given in Chapter 5.

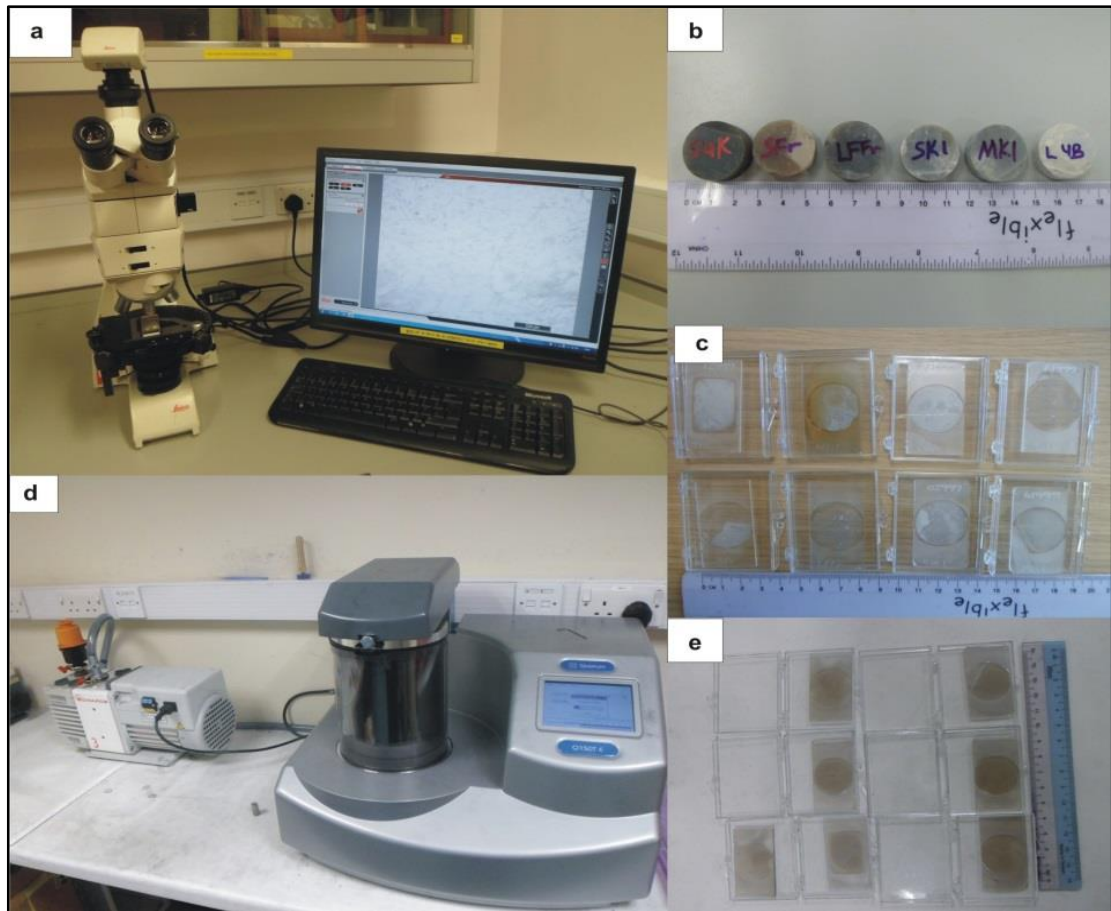


Figure 3.22: (a) Thin Section Microscopy apparatus; (b) Some samples used for the optical thin section microscopy; (c) are prepared thin sections of flint samples; (d) coating apparatus; (e) prepared flint thin section coated with carbon.

#### 3.4.4 Scanning Electron Microscopy-Cathodoluminescence (SEM-CL) Analysis

Flint samples from each of the present study sites are examined by Scanning Electron Microscopy-Cathodoluminescence (SEM-CL) analysis using FEI Quanta 650 FEG SEM equipment (Figure 3.23). The SEM system is coupled with KE Centaurus Cathodoluminescence (CL) detector for CL examination. The equipment is operated at accelerating voltage of 20 kV, and the analysis was conducted on uncovered polished thin sections of white crust and flint core. The thin sections were coated with carbon using Quorum Q150T E carbon coater to hinder any accretion of electrical charge during the CL analysis. The high-resolution cathodoluminescent micrographs are then acquired. For each CL micrograph obtained, a corresponding backscattered electron (BSE) image of that sample was also captured, and these were simultaneously used for further interpretations.



Figure 3.23: SEM-Cathodoluminescence (SEM-CL) set-up used for this studies.

### 3.5 Wear Classification Tests on Flint Materials

Five geotechnical wear indices were employed to characterise flint on the basis of colour, proximity of the host rock to geological structures and geographical locations. These criteria were considered to control the variability of the properties of flint material.

The Cerchar Abrasivity Index (CAI) was used to measure abrasiveness of flints by scratching the rock, while the Shore hardness was used to define abrasiveness based on hardness and elastic properties of flints. However, since the abrasiveness of rock also relies on the abrasive minerals in the rock, the Equivalent quartz content (EQC) and the Vickers hardness number of rock (VHNR) were used. But these methods, only relied on abrasive minerals, and ignored the role of rock strength (Plinninger, 2010). Therefore, to account for this, the Rock abrasivity index which in addition to abrasive minerals uses the strength parameter to explain the wear behaviour of the rock was used. The detail description of these wear indices are explained in the subsequent sub-sections.

### 3.5.1 Determination of Cerchar Abrasivity Index (CAI)

Cerchar abrasivity was published in France, by the Centre d'Etudes et Recherches des Charbonages (CERCHAR) de France in 1986. The test was introduced for testing the abrasiveness of rocks. Since the introduction of Cerchar test the test has been widely applied in laboratories for the estimation of TBM performances (Suana et al., 1982; Plinninger, 2004; Fowell & Abu Bakar, 2007; Kasling et al., 2010). The test was also used for the evaluation of tool wear rate and for the investigation of abrasivity of hard rocks (Plinninger, 2004). The detail outlines of the test are described in Sauna et al. (1982); Cerchar (1986); Kasling et al. (2010); Labas et al. (2012).

The Cerchar test uses the wear of a standardised steel cone of 90° to measure the abrasivity index of the rock sample. The Cerchar abrasivity index (CAI) is then determined as the diameter of the wear flat measured in 0.1 mm after scratching the rock surface over a span of 10 mm in a second.

The Cerchar abrasivity test was performed on lumps of flint samples as described in Cerchar (1986) on lumps of flint samples (Figure 3.24) of about 120x40x40 mm to measure the abrasiveness, cutterbility and drillability of flints. The test was conducted on smooth sawn cut surfaces for all the tested samples, using the standard the schematic diagram of Cerchar apparatus (Figure 3.24) with hard steel stylus of HRC 54-56. The stylus was then subjected to the static load of 70 N (see Figure 3.25) and readings were taken from the worn pin under a microscope following a scratch of 10 mm (length of scratch) on the samples. The CAI was defined as the average wear flat measurements expressed as 0.1 mm and was interpreted using Table 3.8.

This procedure was repeated for different colour and classes of flints categorised based on the diagenetic features of the flint samples such as white crust (WCr), spotted white inclusion (SWI) and white inclusion (WI). The test was then replicated at least four times on each feature using fresh unused stylus per test. The results of these tests can be seen in Chapter 4, Sub-section 4.3.1.



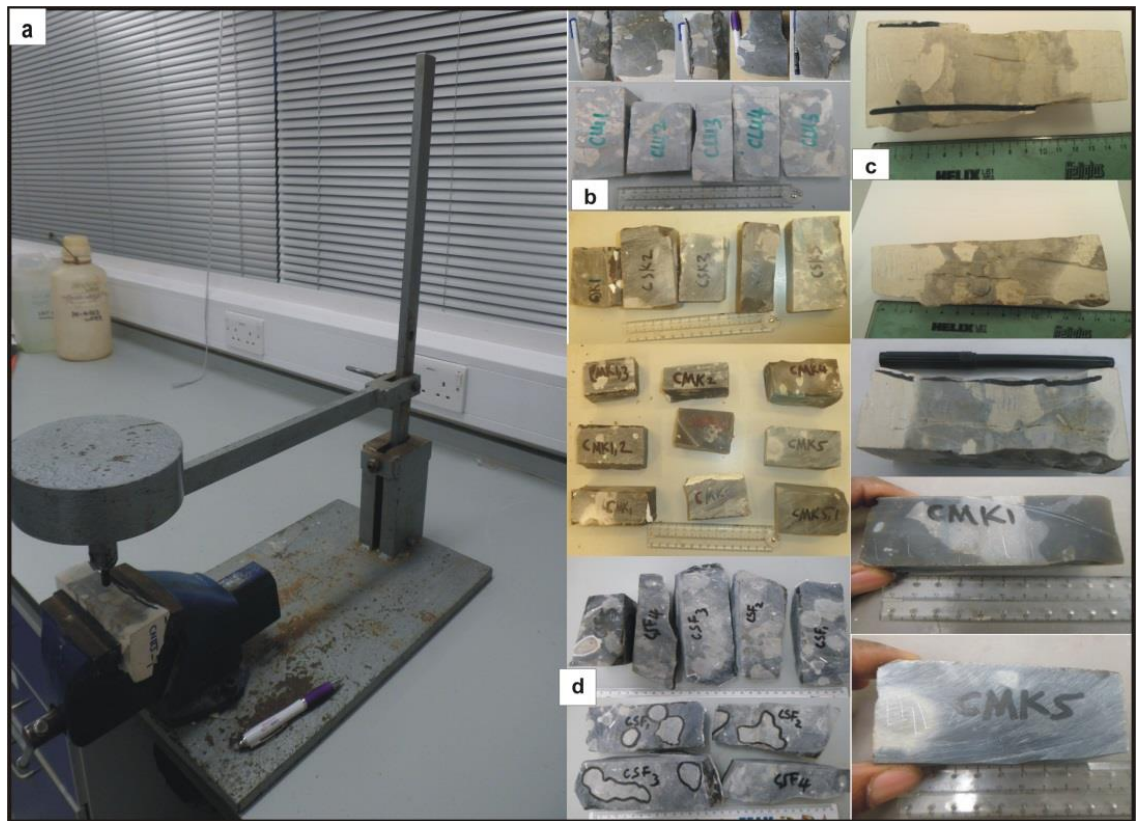


Figure 3.24: CAI test Set-up. (a) Cerchar abrasivity index (CAI) test equipment used; (b) flint samples used for the test; (c) flint samples after test light scratch marks on the samples; (d) flint samples showing how different colour of the flints was marked and tested.

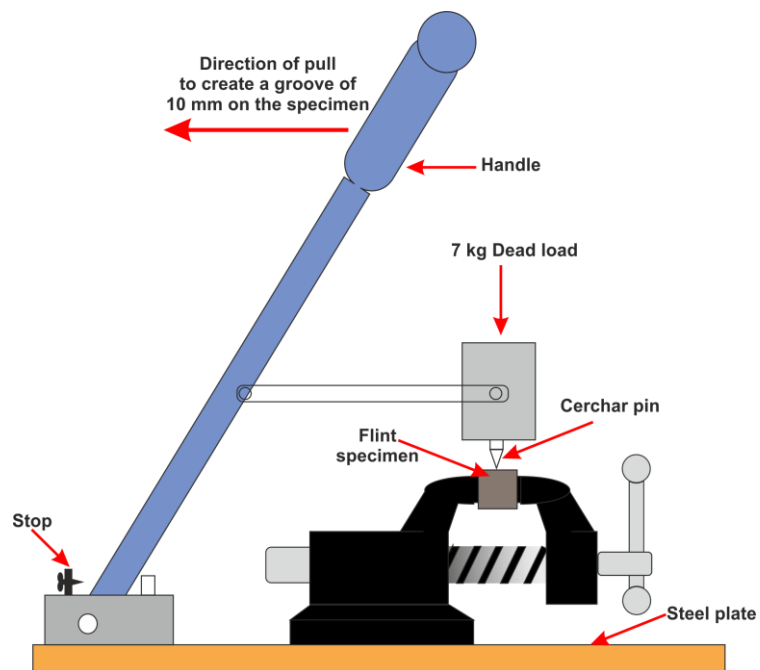


Figure 3.25: Cerchar abrasivity index test equipment highlighting how specimen were tested (not to scale).

Given the hardness of flint, a modification of Cerchar test was tried, by testing the samples using a static load of 9 kg instead of the recommended 7 kg. This decision was taken due to the lack of penetration from the 7 kg load on the wear flat of the test pin as it slid over the hard, smooth surface of the flint samples. Thus, the same number of tests described above was carried out and the summary of the results for the entire samples are provided in Chapter 4 and discussed in Chapter 6.

Table 3.8: The guideline for the interpretation of abrasiveness (Cerchar, 1986)

CAI (0.1mm)	Classification
0.3 – 0.5	not very abrasive
0.5 – 1.0	slightly abrasive
1.0 – 2.0	medium abrasiveness to abrasive
2.0 – 4.0	very abrasive
4.0 – 6.0	extremely abrasive
6.0 – 7.0	Quarzitic

### 3.5.2 Estimation of Equivalent Quartz Content (EQC)

Equivalent Quartz Content (EQC) was described in Thuro (1997). The test was developed to predict tool wear rate by appreciating the roles of all the abrasive minerals in the rock (Figure 3.26). This geotechnical wear index has gained prominence and has been extensively used for the prediction of primary wear in the TBM, tool and drilling industries. Thus, evaluating the EQC of flints could help in predicting the drillability of the rock prior to site investigation.

The EQC of flints of various colours/types: white crust and the immediate surrounding Chalk was evaluated using Equations 3.11 and 3.12. The EQC was evaluated by multiplying the relative Rosiwal grinding hardness for each mineral in the samples with the respective mineral content (Equation 3.11 and 3.12). The mineral compositions were determined using XRD instead of thin sections because of the fine-grained nature of the flint. The results obtained from this evaluation are presented in Chapter 4.

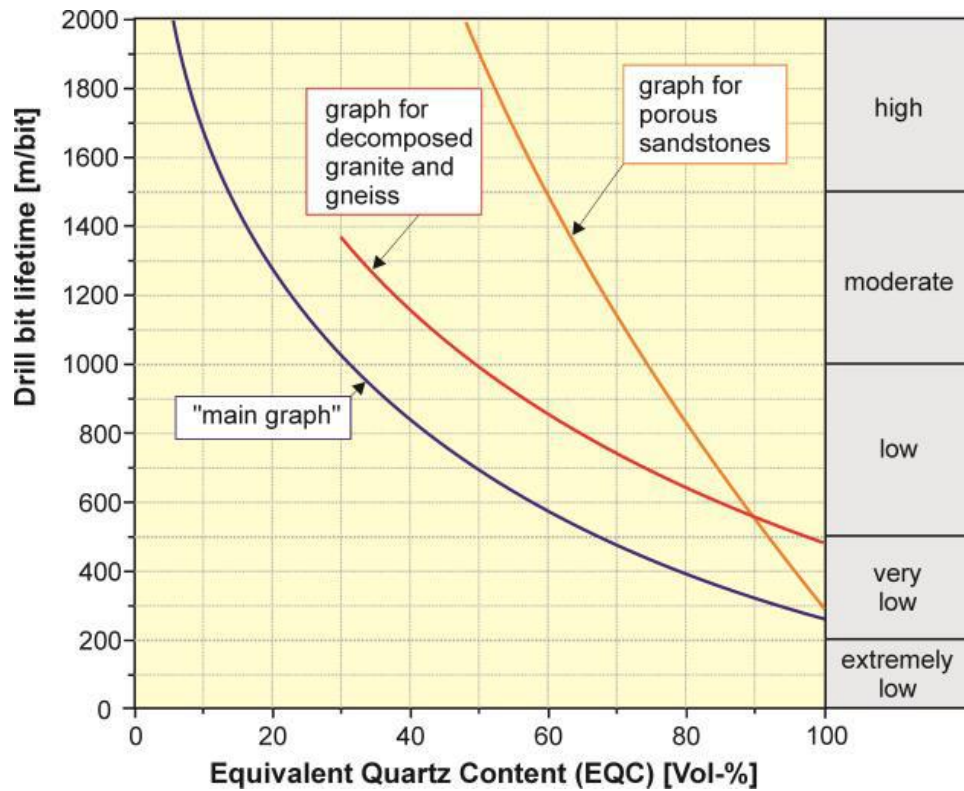


Figure 3.26: Drill bit lifetime (mbit<sup>-1</sup>) prediction from EQC (%) (Plinninger, 2008)

$$R_i = e^{\frac{\text{Mohs' hardness} - 2.12}{1.05}} \quad \text{Equation 3.11}$$

$$EQC = \sum_{i=1}^n A_i R_i \quad \text{Equation 3.12}$$

(Where:  $A_i$  is the amount of mineral volume (%) and  $R_i$  is the Rosiwal Grinding Hardness (%) estimated using Equation 3.11.)

### 3.5.3 Rock Abrasivity Index (RAI) Test

The Rock Abrasivity index (RAI) was developed due to the limitation of EQC test. The RAI approach was introduced by Plinninger (2002) and the practical concepts of the test were described in Plinninger (2008; 2010). Since its first emergence, the test has gained both national and international appeal in terms of applicability for wear prediction in several tunnelling works (Plinninger, 2010). RAI has a good correlation with drill bit life time (Plinninger, 2008; also see Figure 3.27) and the test has been found to be appropriate for characterising the abrasivity of hard rock (Plinninger, 2010). RAI was applied to characterise the abrasiveness of flint. The RAI of flints was

determined in accordance with Plinninger (2002) method. The index was estimated by multiplying the UCS of flint samples with the respective EQC (Equation 3.13), and the results were interpreted using Table 3.9 and Figure 3.27.

$$RAI = \sum_{i=1}^n A_i \times S_i \times UCS \quad \text{Equation 3.13 (Plinninger, 2002)}$$

Where: RAI=Rock abrasivity index; UCS=Unconfined compressive strength of rock (MPa);  $A_i$ =specific amount of mineral (%);  $S_i$ =Rosinval grinding hardness referred to quartz=100; and n=number of all minerals.

Table 3.9: RAI classification (Plinninger, 2010)

RAI	Classification
<10	Not abrasive
30-60	Slightly abrasive
10-30	Abrasive
60-120	Very abrasive
>120	Extremely abrasive

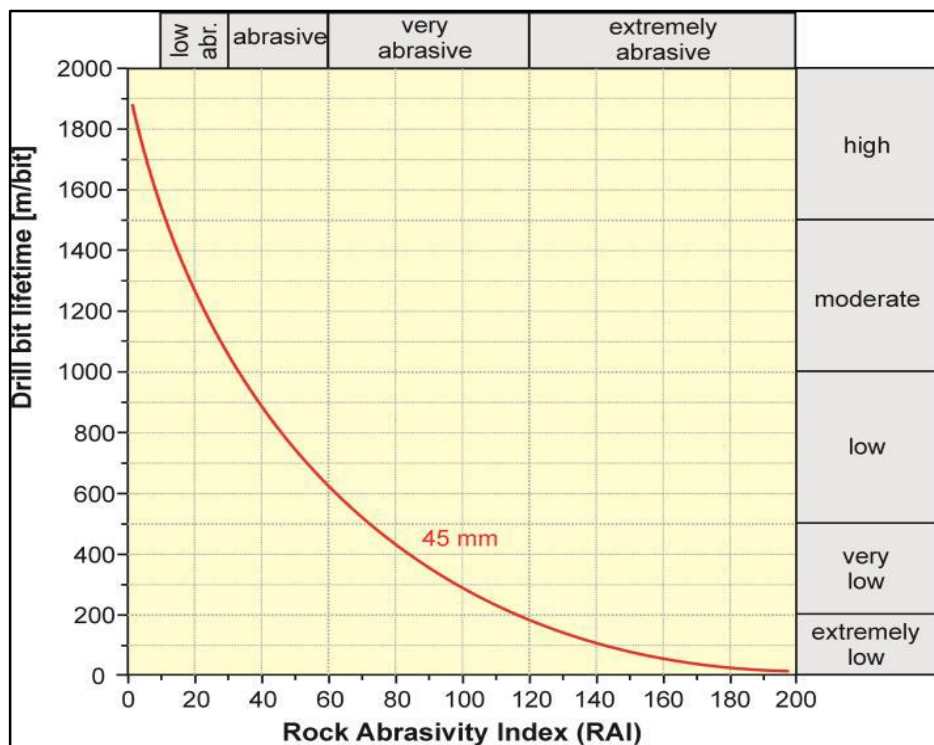


Figure 3.27: Drillbit lifetime (mbit<sup>-1</sup>) prediction from RAI (Plinninger, 2008).

### 3.5.4 Vickers Hardness Number of Rock (VHNR)

Vickers Hardness Number of the Rock (VHNR) was one of the most significant geotechnical wear indices used in practice for the prediction of cutting tools performance (see Figure 3.28). The index was developed to provide the aggregate hardness of rock considering the contribution of each mineral in the sample. The VHNR was used to evaluate and classify flints and the surrounding chalk samples according to the procedures described in Thuro (1997); Heiniö (1999); Plinninger (2008: 2010).

The VHNR was obtained by multiplying the Vickers Hardness Number (VHN) of each mineral in the samples by the respective proportion individual mineral in the samples (Equation 3.14). The VHN of each mineral in the samples were obtained from the standard VHN table of minerals (see Gokhale, 2011 for the Table), while the mineral compositions of all the investigated samples were determined using XRD analysis.

The measured hardness values of all the minerals in each sample were added together to give VHNR of the sample. This step was repeated for all the tested samples, and the results are presented in Chapter 4, Sub-section 4.3.4. The study was carried out on different flint colour, the white crust and the Chalk surrounding flints. The different colour of flints was considered to establish how variation in mineral composition among different colour and classes of flints affects the hardness of the rock in terms of drillability.

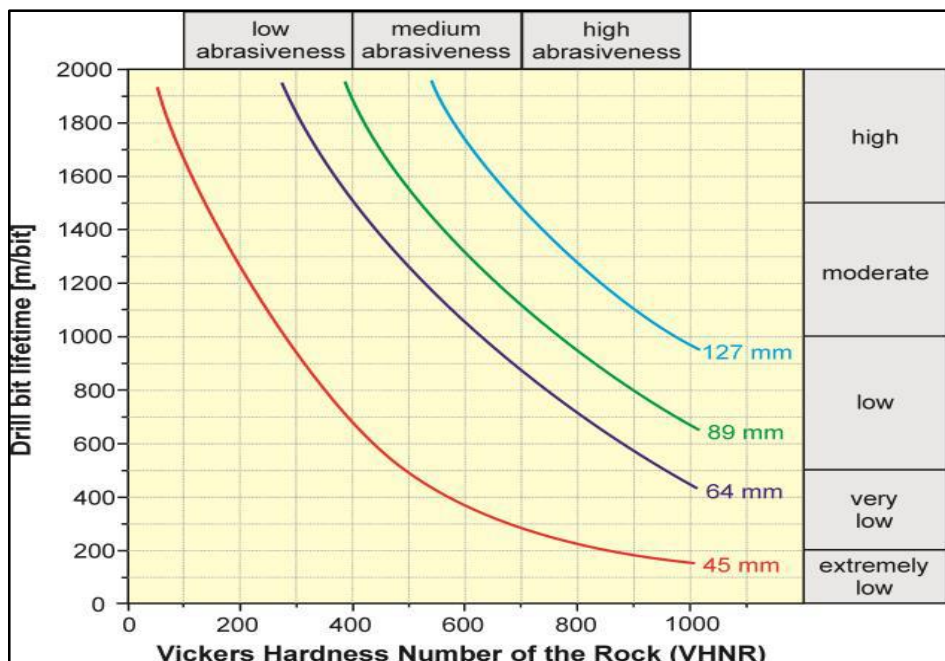


Figure 3.28: Drillbit lifetime (mbit<sup>-1</sup>) prediction from VHNR (kgmm<sup>-2</sup>) (Plinninger, 2008).

$$VHNR = \sum_{i=1}^n VHN_i \times A_i$$
 Equation 3.14

Where:  $VHNR$  is the Vickers Hardness Number of Rock ( $\text{kg/mm}^2$ ),  $VHN_i$  is the Vickers Hardness number of each mineral in the sample ( $\text{kg/mm}^2$ ), and  $A_i$  is the Amount of mineral, and  $n$  is the numbers of minerals.

### 3.5.5 Shore Hardness (SH) Measurement

Shore Scleroscope hardness (SH) was developed to measure the hardness of rock as a function of mineral composition, elasticity and matrix cementation of the rock. The SH has been widely applied in various engineering models and was used for the evaluation of the performances of roadheaders and drilling tools. In this study the SH test was conducted on flint samples in accordance with ISRM (2007) suggestions. For each flint sample (Figure 3.29a) emphasis was given to the different colour observed on the sample, and each colour was tested separately to identify any variation in the hardness of flints with colour. The surfaces of the samples were smoothed and divided into several square checks at 5 mm interval signifying points of indentation.

The test was carried out using the C-2 type Shore hardness testing machine (Figure 3.29b). This equipment comprises of a diamond-tipped hammer incorporated within a tube (see Figure 3.30), which has a calibrated measuring scale of 0-140. The equipment also has a base upon which the sample was placed and set horizontally by the use of a tilting level. A 2.44 g diamond-tipped hammer was allowed to drop freely on the sample, and the rebound height was noted and recorded from the incorporated measuring scale. This procedure was repeated fifty times on each specimen and readings were taken, while five highest as well lowest readings were discarded from the analysis. The average of the rebound heights from the remaining readings was taken as the shore hardness of the sample. The entire results from this analysis are presented in Chapter 4, Section 4.3.5, pp. 134-135.

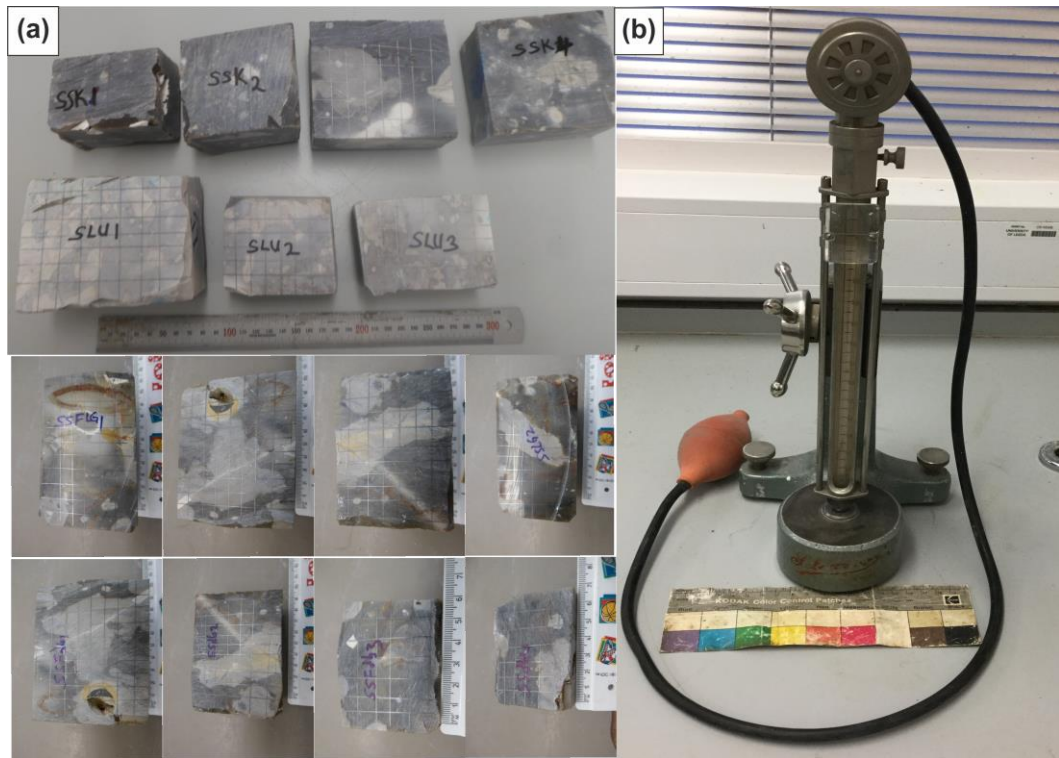


Figure 3.29: Shore hardness test setup. (a) Flint samples used for Shore hardness (SH) test; (b) Shore hardness test equipment used for the test.

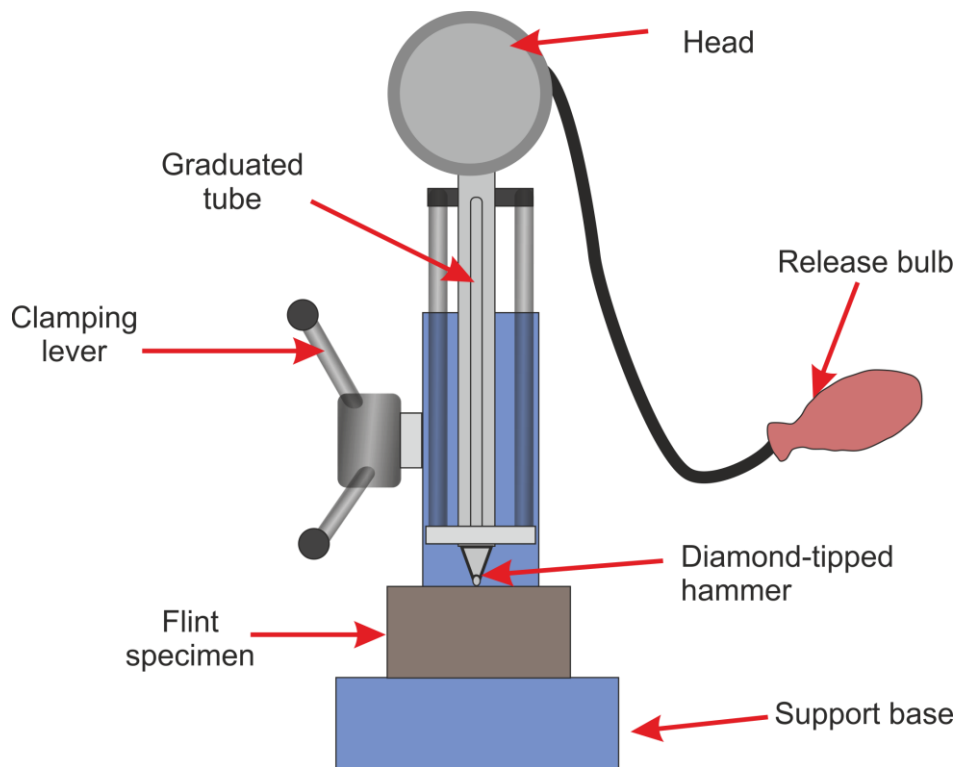


Figure 3.30: Schematic presentation of Shore hardness test equipment.

### **3.6 Determination of Flint Variability Based on Petrophysical Parameters**

Flint samples were investigated for the determination of ultrasonic pulse parameters, He Porosimetry, Porosimetry (by image analysis) and grain size analysis using image analysis. These examinations were conducted to identify the petrophysical properties of flints and relate these with the strength, abrasivity, drillability and textural variations of the flint materials.

He porosimetry was used to measure porosity of relatively larger samples incorporating fracturing seen in the sample.

Similarly, the grain size analysis was also employed to characterise flints using image analysis (ImageJ). This method was used because it is cheap, simple, and the mechanical damage of grain particles associated with other methods of grain size analysis is not a problem using this method. Thus, these petrophysical approaches used to characterise flints in this research are described in the subsequent chapter.

#### **3.6.1 Estimation of Ultrasonic Velocities and Dynamic Elastic Data**

The ultrasonic pulse velocities comprising of compressional wave velocity ( $V_p$ ) and shear wave velocity ( $V_s$ ) of flint were determined in accordance with ISRM (2007) suggested method for determining sound velocity. The test was conducted on all the flint samples later used for UCS testing. An Ergo Tech transducer pulse generator 1-10, with PC oscilloscope data logger, compressional wave transducer with frequency of 1 MHz, shear wave transducer with frequency of 500 kHz was used.

Flint specimens were placed between the two transducers (transmitter and receiver, see Figures 3.31, 3.32) under contact load of 0.2 kN. This load was achieved using the same testing machine described in Section 2.2.1. The transmitter was placed on top, while the receiver was at the bottom with the specimen (Figure 3.31 and 3.32). Acoustic coupling between the specimens and the transducers was achieved using honey, and a 0.1mm thick lead foil was used to prevent any entrapped air bubbles.

The effect of the lead foil was accounted for by initially measuring the transit times for the propagation of the compressional wave P-wave ( $t_{p0}$ ) and shear waves S-waves ( $t_{s10}$  and  $t_{s20}$ ) with the transducers in direct contact with each other before commencing the test. These initial transit times were then subtracted from the corresponding transit times measured with flint samples placed between the transducers (Equation 3.15 to 3.17) for both P-wave ( $t_p$ ) and S-waves ( $t_{s1}$  and  $t_{s2}$ ). The measured length of the sample and the measured transit time were used to estimate the ultrasonic pulse ( $V_s$  and  $V_p$ ).



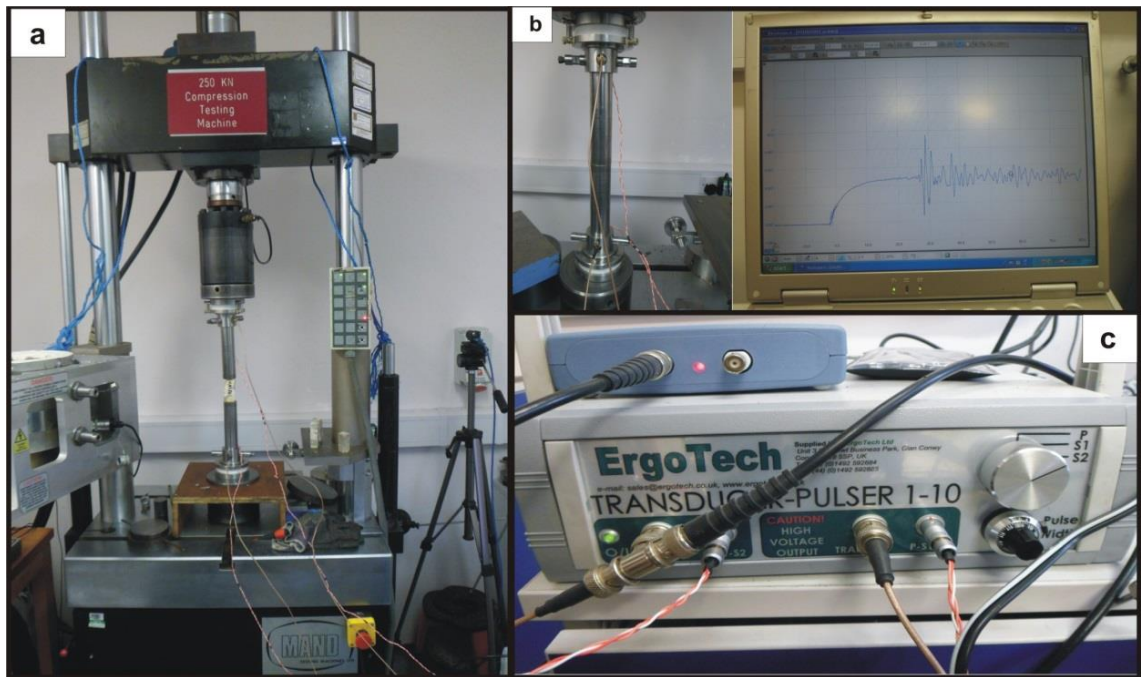


Figure 3.31: (a) Ultrasonic pulse testing set-up; (b) two transducers in direct contact with each other for initial calibration. To the right shows waves signal from the which the transit time was measured. To the bottom are the Oscilloscope data logger and Ergo Tech transducers pulse generator 1-10.

In order to evaluate the dynamic elastic constants; the velocities so obtained as well as the densities of all the specimens used for this test were used in the usual elastic equations (Equations 3.15 to 3.22) to determine the dynamic Young's modulus  $E_d$ , and dynamic Poisson's ratio  $\nu_d$ . The densities were determined in accordance with (ISRM, 2007) suggested method for determining the density of rock material using calliper method to obtain the volume of the specimens. The results of all the ultrasonic pulse velocities, the densities, and the dynamic elastic parameters are provided in Chapter 4, Section 4.4.1, pp. 135-140.

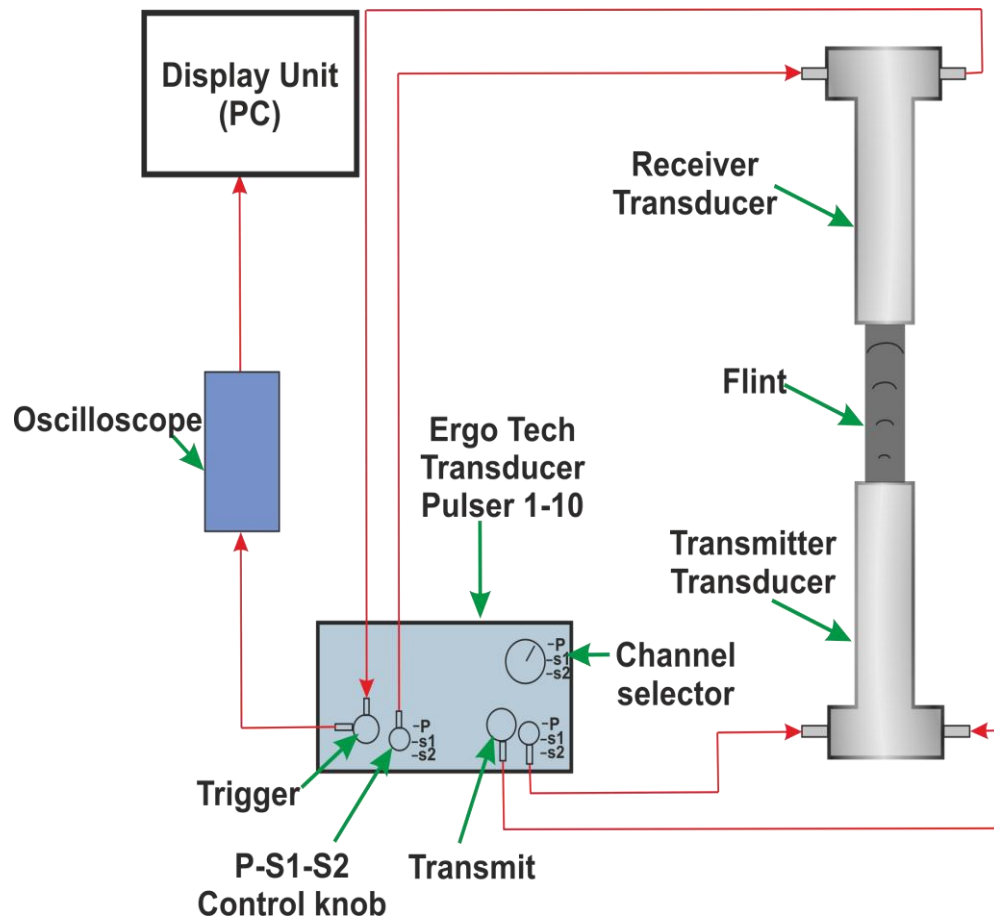


Figure 3.32: Schematic diagram of Sonic velocities measuring apparatus (not to scale)

$$\Delta_{tp} = (t_p - t_{p0}) \times 10^{-6} \text{ Equation 3.15}$$

$$\Delta_{ts1} = (t_{s1} - t_{s10}) \times 10^{-6} \text{ Equation 3.16}$$

$$\Delta_{ts2} = (t_{s2} - t_{s20}) \times 10^{-6} \text{ Equation 3.17}$$

$$\text{Average } \Delta_{ts} = \frac{\Delta_{ts1} + \Delta_{ts2}}{2} \text{ Equation 3.18}$$

$$V_p = \frac{(L \times 10^{-3})}{\Delta_{tp}} \text{ Equation 3.19}$$

$$V_s = \frac{(L \times 10^{-3})}{\text{Ave. } \Delta_{ts}} \text{ Equation 3.20}$$

$$v_d = \frac{(V_p^2 - 2V_s^2)}{(2V_p^2 - V_s^2)} \text{----- Equation 3.21}$$

$$E_d = 2\rho \left[ \left( \frac{V_p}{1000} \right)^2 \times (1 - \nu_d) \right] \text{----- Equation 3.22}$$

Where:  $t_p$  is the transit time of the compressional wave ( $\mu\text{s}$ ) with the sample between the transducers,  $t_{po}$  is the initial transit time ( $\mu\text{s}$ ) for compressional wave with the transducers in direct contact (without sample),  $\Delta_{tp}$  (s) is the difference between  $t_p$  and  $t_{po}$ ,  $t_{s1}$  and  $t_{s2}$  are the transit times of the orthogonal S-waves ( $\mu\text{s}$ ),  $t_{s1o}$  and  $t_{s2o}$  are the initial transit times of the orthogonal S-waves with only the transducers (i.e. without the sample),  $\Delta_{ts1}$  (s) is the difference between  $t_{s1}$  and  $t_{s1o}$ ,  $\Delta_{ts2}$  (s) is the difference between  $t_{s2}$  and  $t_{s2o}$ , *Ave.*  $\Delta_{ts}$  (s) is the average of  $\Delta_{ts1}$  and  $\Delta_{ts2}$ ,  $L$  is the length (mm),  $V_p$  is the P-wave velocity ( $\text{ms}^{-1}$ ),  $V_s$  is the S-wave velocity ( $\text{ms}^{-1}$ ),  $\nu_d$  is the dynamic Poisson's ratio,  $\rho$  is density of the sample ( $\text{gcm}^{-3}$ ), and  $E_d$  is the dynamic Young's modulus of the sample (GPa).

### 3.6.2 Determination of Porosity image analysis (using ImageJ)

The porosity of flints, white crust and surrounding chalk was evaluated by analysing Scanning Electron Microscopy (SEM) images of these samples using ImageJ. ImageJ is public-domain image analysis software written in Java by Ferreira & Rasband (2011). The software was developed by Rasband of the National Institute of Mental Health, Maryland in the USA and is described in Ferreira & Rasband (2011). The software allows the user to measure the size, shape, area, perimeter, porosity/pore classification and amount of particles or objects from SEM, TEM or thin section micrographs.

ImageJ has been widely applied in various fields and has been found useful in accurately characterising structures from images (Tuan et al., 2014). ImageJ has also been employed in industries and in several studies for the evaluation of sizes of nanostructures or particles (Hutchison et al., 2006). The software was also used to study the: particle distribution of materials (Kumara et al. (2011; 2012)); properties of particles in steel (Sujaya, 2014, unpublished dissertation) and used for the estimation of porosity of reservoir rocks (Krassakopoulos, 2013; Medina, 2013; Sujaya, 2014).

The evaluation of porosity of flint using Image analysis was achieved through the following steps:

- (a) Images from the SEM were uploaded on to the software;
- (b) The scale of the images was spatially calibrated by picking the straight line tool to draw a line that conforms to the original scale bar on the image. This was then followed

by entering 10  $\mu\text{m}$  in the known distance box, and 'um' (referring to  $\mu\text{m}$  in ImageJ) into unit of length portion of the Set scale dialog accessible via Analyze>Set scale. This step was to ensure that the subsequent length or measurements on the image were automatically transformed into the calibrated unit of  $\mu\text{m}$ .

(c) The calibrated images were then segmented to transform the images into binary images. This involved thresholding the images such that the interested features (pores or interparticle fractures) were made clearer and were separated from the background (particles or the flakes) using two different colours. The thresholding was achieved via Image>Adjust>Threshold. The slide bars from the fly out were adjusted to capture the required features, in this case, the pores.

(d) Lastly measurements were set to select the parameter required for analysis. In this case, the area ratio and circularity were selected.

(e) Finally the pore area was collected. The display results and summarise dialogs were checked on the fly out following the analysis step. These were checked to generate the results and summary of the results on the Excel sheet. From these data the area fraction which is the porosity was recorded. These steps were replicated up to five times for each of the investigated values. The replicated porosity measurements and the results were then recorded, the average of which, is the porosity of the sample.

The above-described procedures are presented in Figure 3.33.

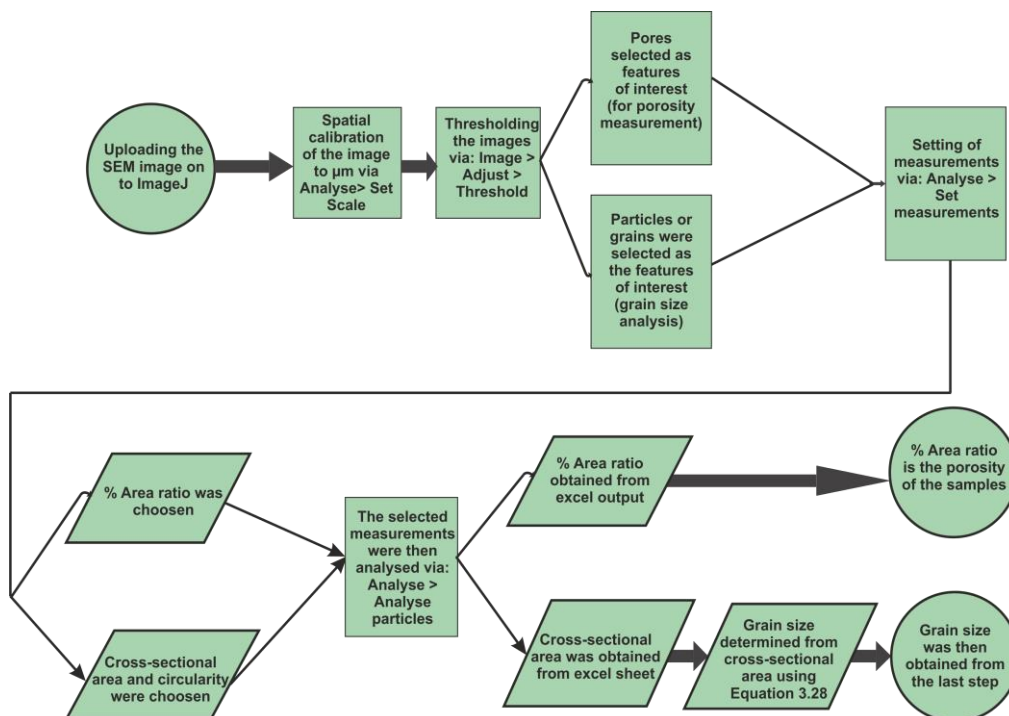


Figure 3.33: Flowchart showing the Porosity estimation and grain size analysis process.

### 3.6.3 Measurement of Porosity using He Porosimeter

Subsequently, the determination of porosity using image analysis (ImageJ) as described in Section 3.6.2 the idea of He porosimetry was used because the porosity determined through image analysis may not accurately measure the actual porosity of the rock material. This is due to small sample size for image analysis which may not include the influence of microstructures in the flint material.

He porosimetry was conducted on cylindrical cores and cuboid flint samples that were meant for UCS test described in Section 3.3.1. The test was conducted using Stereopycnometer constructed by Quantachrome Corporation (Figure 3.34). The equipment has two cells, the sample cell and the reference cell with known volume (Figures 3.34 and 3.35). The detailed procedure of He porosimeter is described in API (1998) and (Stereopycnometer user manual).

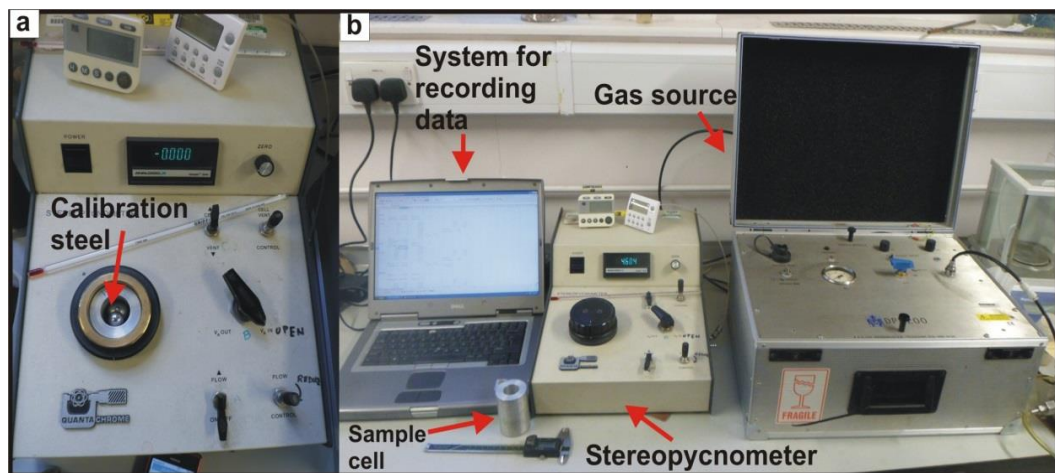


Figure 3.34 (a) Stereopycnometer used for He Porosimetry; (b) complete set-up for He porosimetry showing sample cell, gas source and data recording system.

He porosimeter is one of the fast and the most extensively used techniques for measuring rock porosity (Andersen, 2013). The method provides accurate and repeatable rock porosity measurements with high precision (API, 1998; Kazimierz et al., 2004). The method is based on the principle of Boyle's law and measures the porosity of rocks by estimating the grain volume of samples from the expansion of He gas.

He Gas expansion porosimeter was carried out on flint samples (core plugs) to measure the porosity of flints. The bulk volume  $V_b$  was determined by measuring the dimensions of the flint samples using callipers method following the ISRM (2007) procedure. The callipers method was used to obtain the  $V_b$  of flints because; the samples used for the test were prepared as core plugs.

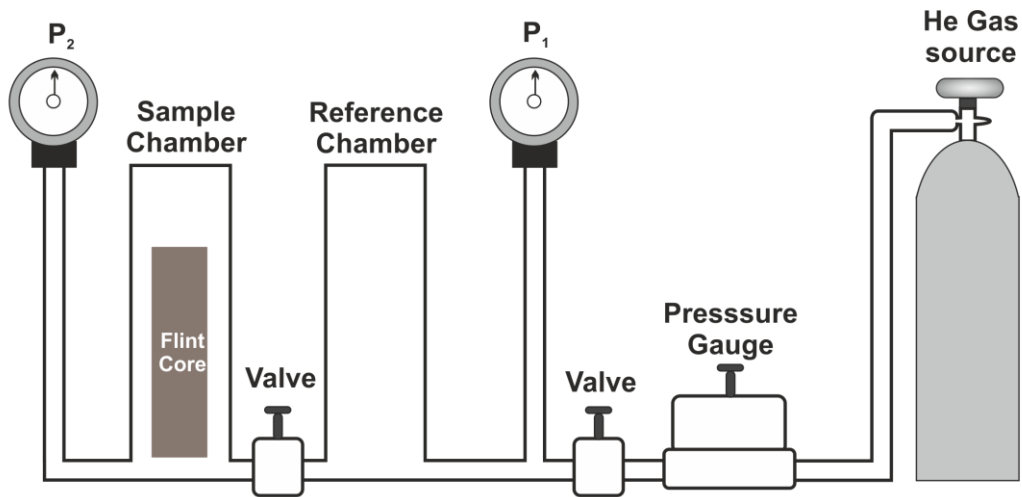


Figure 3.35: He-porosimetry system showing the principle of operation (not to scale)

The grain volume ( $V_g$ ) is determined by obtaining the calibrated sample cell volume ( $V_c$ ) as one of the required inputs. The following steps were carried out to determine the Porosity of flints:

(a) The main application of He porosimetry was to determine the porosity of flints by first obtaining the sample grain or matrix volume ( $V_g$ ). The  $V_g$  is determined by first calibrating the Porosimeter. The calibration was done by pressurising the reference cell with He gas to about  $1.10 \times 10^5$  Pa ( $P_1$ ) with the empty sample cell placed in the sample cell holder. The pressurised gas was then isothermally expanded into the sample cell for about six minutes. This led to the reduction in pressure, which equilibrates and the resultant equilibrium pressure ( $P_2$ ) was recorded from the digital display on the Stereopycnometer. This procedure was repeated six times to test for the repeatability of the procedure.

(b) The system was then vented out, and the calibration stainless steel cylinder or spheres with known volume ( $V_{cyl}$ ) were placed into the sample chamber. The initial pressure ( $P_3$ ) of about  $1.10 \times 10^5$  Pa was then admitted into the reference chamber and this was allowed to expand to equilibrium pressure ( $P_4$ ). These pressures were recorded and were then used to estimate the expansion volume  $V_{exp}$  (Equation 3.23) and the average value of  $V_{exp}$  was recorded for use as input for the evaluation of the required calibrated cell volume ( $V_c$ ). The ( $V_c$ ) was then calculated using Equation 3.24, and the mean value was recorded. Both  $V_{exp}$  and  $V_c$  were required to compute  $V_g$ .

(c) To estimate the  $V_g$  step (a) was repeated, but, in this case, the calibration cylinder or sphere in the sample cell was replaced with flint samples. The initial pressure ( $P_5$ ) and the expansion pressure ( $P_6$ ) at equilibrium were recorded after allowing the He gas to diffuse into the sample cell for six minutes. This expansion time was to allow the gas

to diffuse into any available pores within the samples. This expansion time was decided because of the fine nature of flint particles and was determined after several trials.

(d) Step (c) was repeated six times and  $V_g$  was then estimated using Equation 3.25 for each measurement of ( $P_5$ ) and ( $P_6$ ). The mean, SD and COV of  $V_g$  were the calculated and recorded.

(e) The sample pore volume ( $V_p$ ) was then determined using the mean  $V_g$  (Equation 3.26) and the Porosity was subsequently predicted (Equation 3.27) from the mean  $V_{exp}$  and  $V_c$ .

$$V_{ex} = \frac{V_{cyl}}{\frac{1}{\left(\frac{P_1}{P_2} - 1\right)} - \frac{1}{\left(\frac{P_3}{P_4} - 1\right)}} \quad \text{Equation 3.23}$$

$$V_c = \frac{V_{ex}}{\left(\frac{P_1}{P_2}\right) - 1} \quad \text{Equation 3.24}$$

$$V_g = \frac{V_c + V_{exp}}{1 - \frac{P_5}{P_6}} \quad \text{Equation 3.25}$$

$$V_p = V_b - V_g \quad \text{Equation 3.26}$$

$$\emptyset = \frac{V_p}{V_b} \times 100 \quad \text{Equation 3.27}$$

Where:  $V_{ex}$  is the volume of expansion cell,  $V_{cyl}$  is the volume of stainless steel cylinder or sphere used for the calibration,  $V_c$  is the calibrated volume of the sample cell,  $V_g$  is the grain volume of the samples,  $V_p$  is the pore volume of the sample,  $V_b$  is the bulk volume of the samples,  $P_1$  is the Initial pressure of the empty cell,  $P_2$  is the equilibrium pressure of the empty cell,  $P_3$  is the initial pressure of the sample cell filled with steel cylinder,  $P_4$  is the equilibrium pressure of the sample cell filled with steel cylinder,  $P_5$  is the initial pressure of the sample cell filled with rock sample,  $P_6$  is the equilibrium pressure of the sample cell filled with rock sample and  $\emptyset$  is the evaluated

porosity of the samples expressed in percentage. The units of volume and pressure are mm<sup>3</sup> and Pa respectively.

### 3.7 Particle Size and Shape Analysis using ImageJ

Particle size analysis of flints and the white crust was performed using ImageJ as described in Anon (2011) standard operating protocol. The steps taken to accomplish this follow the same steps from steps (a) to (c) described in Section 3.6.2. However, at the thresholding stage, the features of interest were the grain particles instead of the pores considered in Section 3.6.2 above.

The particles were segregated from the background and steps (d) and (e) of Section 3.6.2 were then applied, but in this case, the measurements were set to capture the area and the circularity of the samples. From these, the average area of the particles in the samples was determined, and the average diameter of the particles in each sample was calculated using Equation 3.28.

Equation 3.28 was used because circularity test indicated the particles in the sample are approximately circular. This is because the circularity scale in ImageJ categorised straight line as 0 to 1 as ellipse, indicating a perfect sample and most of the particles analysed are in the range of 0.8 – 1. This circularity range was the reason for using Equation 3.28 to evaluate the diameter taking the particles as spherical. These procedures were repeated for all the samples investigated, and the results are presented in Chapter 4, Section 4.5, pp.145-148.

$$d = 2 \sqrt{\frac{A}{\pi}} \text{ Equation 3.28}$$

Where  $d$  = particle diameter ( $\mu\text{m}$ ),  $A$  = Cross-sectional area ( $\mu\text{m}^2$ ) and  $\pi = 3.142$ .

### 3.8 Determination of Micropetrographic Index of Flints

The mineral composition of flint samples used for XRD and SEM analysis described in Sections 3.4.1 and 3.4.2 respectively were used to determine the micropetrographic index ( $I_{pt}$ ) of flints. The aims were firstly to identify the influence of cementation, mineral composition and microfractures on engineering properties affecting the drillability and cuttability of flints. Secondly to develop some models that can be applied to estimate the mechanical properties of flints from quantitative petrographic approaches. The



proposed  $I_{pf}$  is a modification of micropetrographic index ( $I_{pf}$ ) reported in Irfan & Dearman (1978).

Unlike earlier studies, the present study determined  $I_{pf}$  of flints using Equation (3.29). The sound parameters in this study comprises of the silica cement (%) and quartz content (%). The unsound parameters consist of voids (%), non-cement portions of samples (%) and secondary mineral constituent (calcite (%)). These parameters are expected to be the major controls on the physical/mechanical behaviour of flints. The mineral composition was determined from XRD analysis described in Section 3.4.1, p. 83 and the proportion of cement (red parts in Figures 3.36 a-g) and non-cemented portions of samples were determined from SEM images using Image analysis (Figures 3.36a-g).

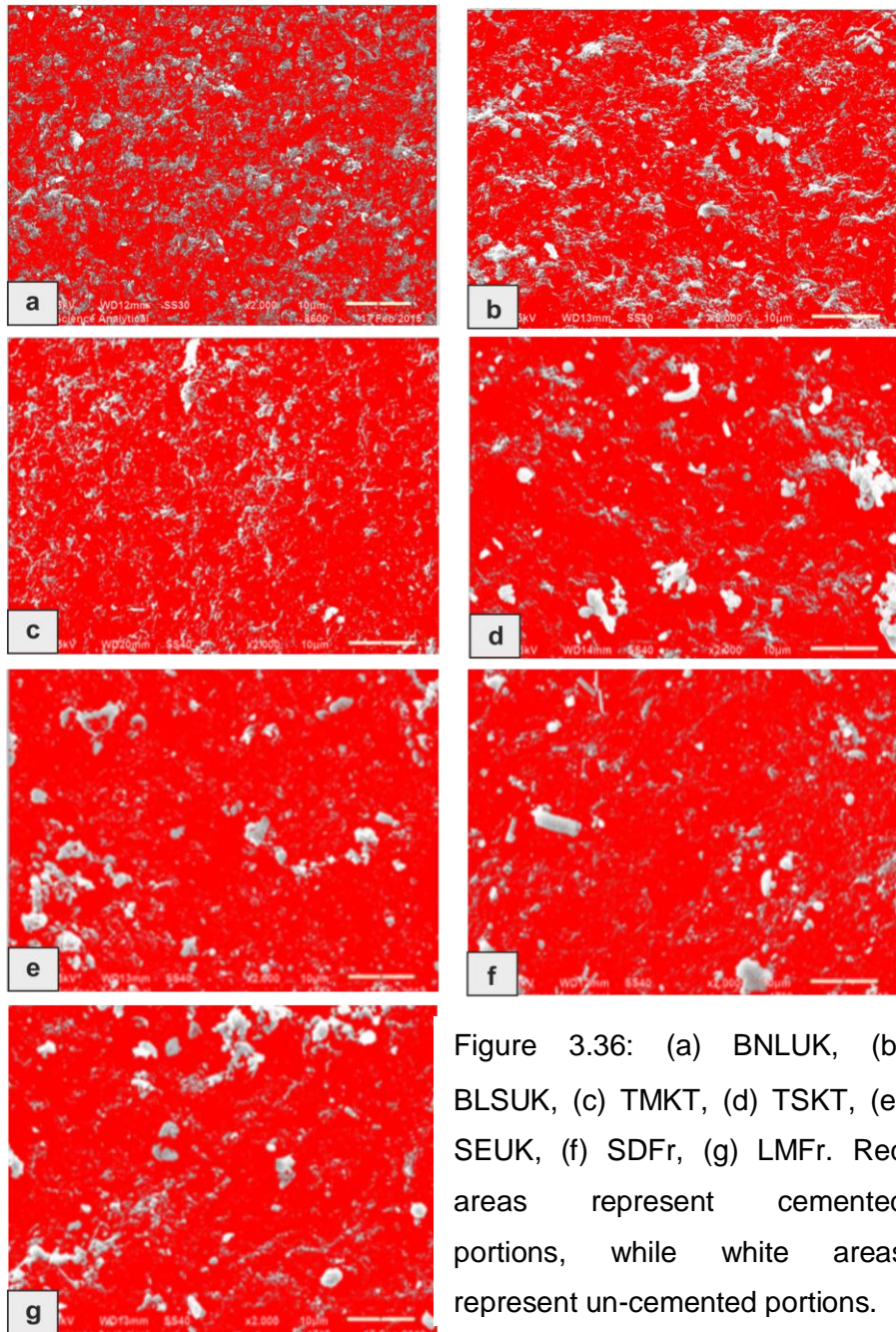


Figure 3.36: (a) BNLUK, (b) BLSUK, (c) TMKT, (d) TSKT, (e) SEUK, (f) SDFr, (g) LMFr. Red areas represent cemented portions, while white areas represent un-cemented portions.

The porosity was determined using Image analysis as described earlier. The determined  $I_{pf}$  was correlated with strength parameters (UCS,  $I_{s(50)}$  and  $T_o$ ) obtained as described in Sections 3.3.1 -3.3.3 and wear properties derived from RAI (Section 3.5.3) using regression analysis with confidence limit of 95%. The results of this study are presented in Chapter 5, Section 5.6, pp. 195-196.

$$I_{pf} = \frac{\% \text{Cement} + \text{Quartz content} (\%)}{\text{Non - cement} (\%) + \text{Calcite content} (\%) + \text{Voids} (\%)} \dots \dots \dots (\text{Equation 3.29})$$

### 3.9 Experimental Procedures for Large Scale Drilling Test on Flint Blocks

One area where flints caused some technical challenges is in the drilling industry. The only large scale cutting tests on flints reported in the literature was conducted by Fowell & Martin (1997).

Therefore, in this study flint samples (Figure 3.37) with sizes of 200 x 130 x 160 mm comprising grey flints (Figure 3.37a) sampled from disturbed Burnham Chalk of North Landing, UK and the dark brownish grey flint (Figure 3.37b) with sizes of 220 x 160 x 90 mm from the Seaford Chalk Formation at Dieppe, France were investigated. Technical challenges involving failure of the drill to progress and rapid wear of the drill bits restricted this investigation to two blocks of flints mentioned above.

A full scale laboratory drilling test was conducted using tricone (2 7/8", see Figure 3.38 a, b & d), and tungsten carbide coring bits (40 mm, Figure 3.38c). The main objective was to examine the variations seen in the mechanical, petrographic, petrophysical and abrasiveness tests on the drillability of blocks of flints categorised based on colour differences and geographical locations. To achieve this, a bit holder was designed to fit in the drill bits (Figure 3.39). A mild steel sample holder (Figure 3.39a) and a support box (Figure 3.39b) were designed to hold the sample that was cast in concrete and to permit for suitable adjustment to allow for proper alignment with the thrust bearing.

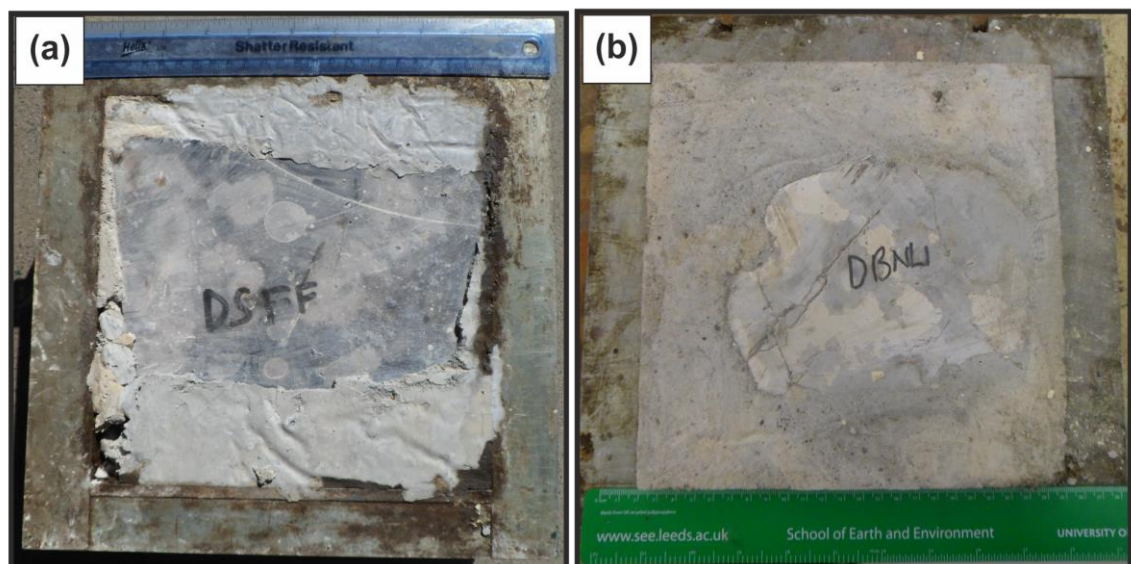


Figure 3.37: (a) Dark brownish grey flint in the Seaford Chalk at Dieppe, France before testing. (b) Grey flint in the Burnham Chalk at North Landing, UK.

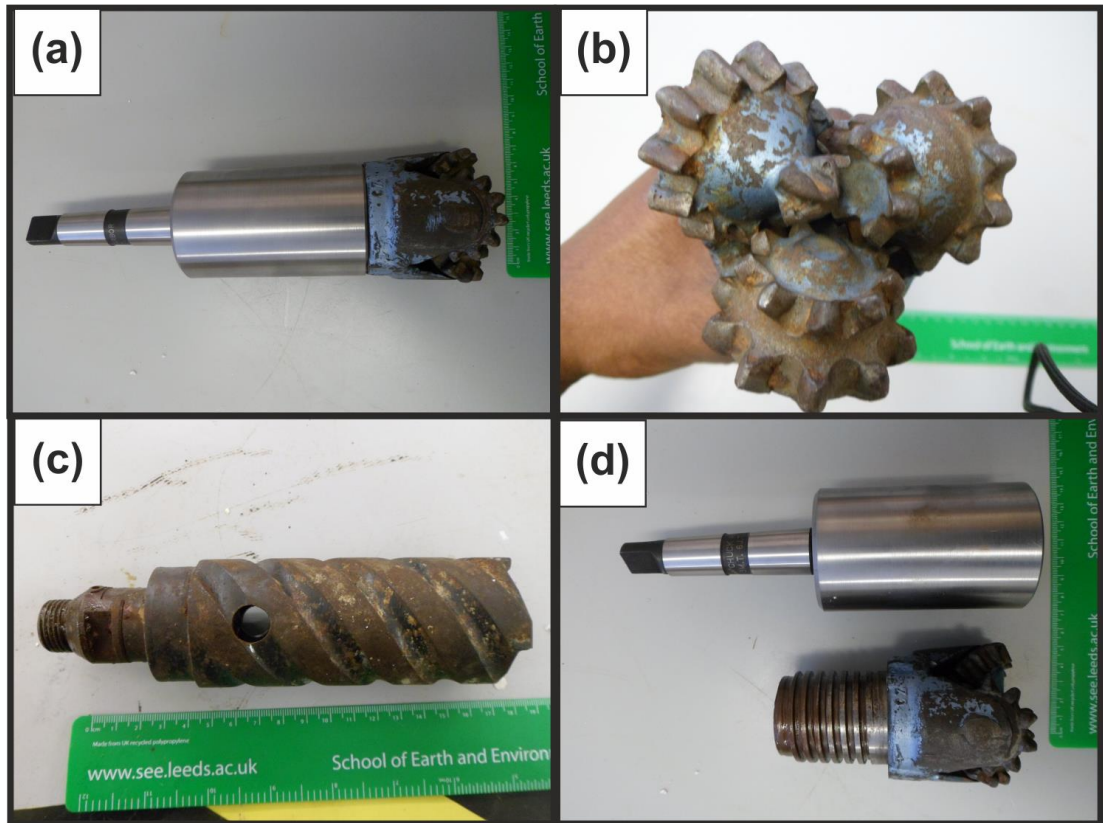


Figure 3.38: Core bits for drilling test. (a) Tricone bit fit to the holder. (b) Tricone prior to drilling. (c) Core bit with Tungsten Carbide insert. (d) Bit holder and Tricone bit.

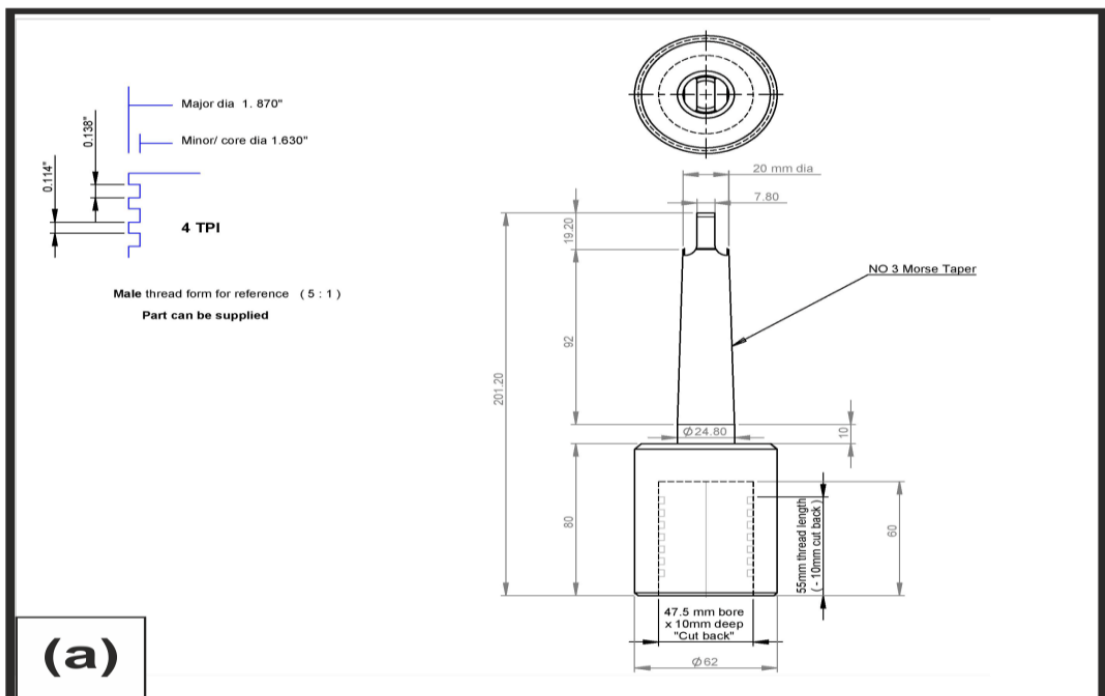


Figure 3.39:(a) Designed bit holder and (b) Sample holder at the top and support box (next page).

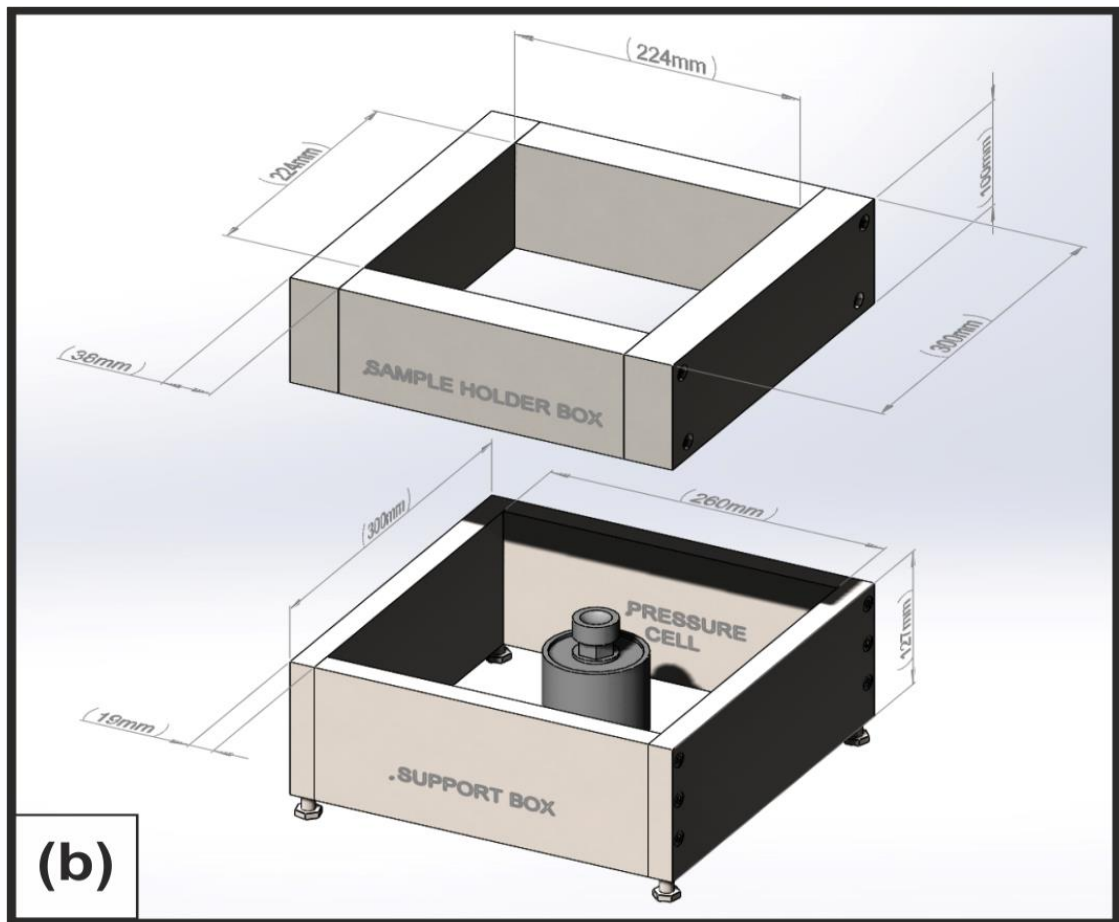


Figure 3.39 (b) Sample holder at the top and support box.

The tests were conducted using an S.R. 2. Radial Drill (Figure 3.40) with maximum rotary speed of 1500 rpm for drilling flints under atmospheric pressure. The drill has a capacity of up to 2 kN and standard field scale tricone, and tungsten carbide coring bits were used to drill the flint samples. The flint samples were cast into a shear box of sizes 300 x 300 x 200 mm using a concrete mix. The concrete mix was prepared with respective water: cement: aggregate proportion of 400 ml: 1 kg: 0.4 kg. The prepared samples set in concrete were allowed to set for two weeks.

Following the setting period, the prepared flint sample was mounted in the steel box and the entire assembly was clamped to drilling table. The steel box was constructed specifically for this test and comprises of the upper and the lower section. The upper section was designed in such a way that the pre-cast sample can fit in perfectly. The lower box was designed with four bolts that can be screwed in or out to allow for the adjustment of the assembly to suit the height of the thrust bearing and this can be adjusted. The arrangement allows the thrust bearing to respond to the slightest axial load applied on the bit.

The axial loading was achieved manually, by inserting the drill bit into the spindle, and lowering the whole system on the sample. Axial load was recorded on the computer from the response of the water resistance pressure cell on which the sample rested throughout the test. The pressure cell was set beneath the sample within the specifically designed mild steel support box. Cooling was achieved using tap water flowing through the flexible tube attached to the system. Penetration in mm was measured using the LVDT attached to the drill anvil and readings automatically logged by the computer. Both the LVDT and the pressure cell were set to initial reading before the commencement of reading.

Several efforts to record penetration rate and increase in loading rate using logger resulted in unreliable data due to problems in manual application of loads. The observed bottom hole pattern and the drilling chips from this test were reported. The downhole pattern was observed on two blocks of flint samples with different colour, micro/macrostructures and microstructures.

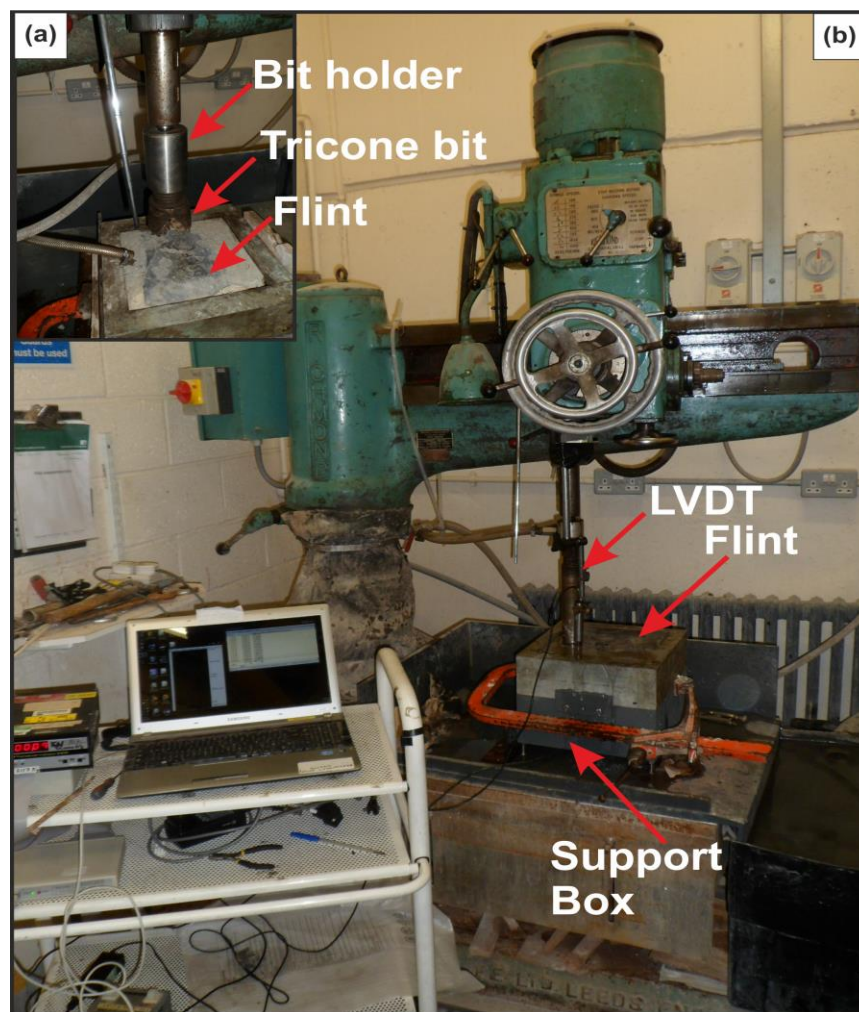


Figure 3.40: Drilling test set-up

### **3.10 Statistical Analysis to Compare between the Estimated Parameters**

The material properties of flints determined in the laboratory were analysed using One-way Analysis of Variance (ANOVA). The analysis was used to test the hypothesis that engineering properties of flints were the same regardless of the geographical locations/origin of the rock, because if different, different approaches will be required in designing drilling/excavation programs in flint of different origin. One-way ANOVA was preferred instead of the t-test, because for each factor (flint material property) to be tested there were more than two levels (precisely seven groups of flint samples from different geographical locations). The analysis was accomplished using the statistical software, Origin 9.1.

To commence the statistical examination the validity of applying the One-Way ANOVA has to be checked. This validity was examined by checking the assumptions upon which One-way ANOVA was based. These examinations were necessary to justify the suitability of the data for One-way ANOVA. The relevant assumptions checked comprise: the independence of the data; normality of the data; the presence of outliers in the data and the homogeneity of variances of the data.

The normality of the data was tested by investigating the histograms of all the tested data while the existence of outliers was checked by determining the skewness statistics of the data. Where the skewness values fall outside,  $\pm 1$  suggest the presence of outliers (Schumaker & Lomax, 1996). The uniformity of variances was tested using the Levene's test. These validity checks were succeeded by analysing the data by setting the Alpha ( $\alpha$ ) level to 0.05. Subsequent to this analysis, the difference in means between samples was found to be significant.

Following the detection of significant differences among the means of the statistically analysed samples, post hoc test using Tukey's honestly significant difference (HSD) method was conducted. The method was applied on the basis of the previously established assumptions that justify the use of One-way ANOVA for this study. The Tukey's method was employed to reveal which specific flint types/locations differ in terms of the measured material properties. The method was used because, it is the best choice for comparing pairs of means and can be used to analyse samples of both equal and unequal sample sizes (Stevens, 1999).

### 3.11 Chapter Conclusions

To determine the physical, mechanical and petrographic properties of flints a range of techniques were investigated. These included:

Mechanical strength tests

1. UCS
2. Point load strength index
3. Tensile strength ( $T_o$ )
4. Elastic properties

Mechanical wear tests

1. CAI
2. EQC
3. VNHR
4. Shore hardness
5. RAI

Petrophysical techniques

1. Porosity using both He and Image analysis (ImageJ)
2. Grain size derived using Image analysis (ImageJ)
3. Ultrasonic velocities
4. Dynamic elastic properties

Petrographic techniques

1. SEM
2. SEM-CL
3. Thin Section Microscopy
4. XRD

Large scale laboratory drilling test on flints.

The UCS,  $I_{s(50)}$  and  $T_o$  (determined using the three-point disc method) were used to examine the strength of different types of flint from various regions. The wear properties of flint/structures were investigated using mechanical approaches (CAI, SH) and geotechnical wear indices consisting of the EQC, VHNR and the RAI. Petrophysical properties of flint comprising of: porosity derived using He-Porosimetry and image analysis (ImageJ); grain size measured using ImageJ and the ultrasonic pulse velocities, the dynamic deformability estimated using ultrasonic pulse techniques were investigated. Variations were observed between flint types and regions in terms of these measured properties. The causes of these variations were studied by examining the microtexture, microstructures, mineral compositions and phases of flint and related structures (white crust, white inclusions) using petrographic techniques. The



petrographic methods employed for these tasks comprised of the SEM, SEM-CL, thin section microscopy and the XRD analysis. These methods were also used to investigate the link between the formation/diagenesis of flint and the material properties of flint. The results of all these investigations are presented in Chapter 4, with the exception of petrographic results, which are covered in Chapter 5.

## **Chapter 4 Presentation and Analysis of Experimental Results**

### **4.1 Introduction**

This chapter forms the first of two results chapters in this thesis. In Chapter 3, field and empirical approaches used to characterise the material properties of flints for engineering projects were presented and explained. This chapter presents, analyses and describes the experimental results (strength and abrasivity) obtained following the successful applications of the research methods described in Chapter 3. The second part of the results covering all the petrographic approaches used to explain the trend in the strength; abrasivity and drillability of flints are presented in Chapter 5.

#### **4.1.1 Chapter Layout**

The chapter is divided into 8 sections, with each section addressing a particular question. The first section introduces the chapter, outlines the extent, and the objectives of the chapter. Section 4.2 presents experimental results obtained from the three laboratory strength tests conducted. This is then followed by geotechnical wear and drillability characterisations of flints (Section 4.3). Petrophysical characterisation of flint materials is presented in Section 4.4 while Section 4.5 presents data from particle size analysis using ImageJ. The outcomes of the laboratory scale drilling tests on flints are presented in Section 4.6. The chapter is then concluded by developing simple models for the prediction of various engineering properties of flints from correlation analysis (Section 4.7) with subsequent presentation of the chapter summary (Section 4.8).

#### **4.1.2 Scope and Objectives**

This chapter has the following objectives:

- to analyse and present the experimental data based on the research questions presented in chapter 1, and establishing the trends in the results.
- to compare the material properties of flints and identify any variation in the engineering geological characteristics between the types, colour, structures and geographical distributions of flints.
- to develop some empirical models that can be used to predict the engineering properties of flints from simple, cheap, fast and non-destructive techniques.

The laboratory programmes and the respected sample sizes used for each test are shown in Table 4.1.

Table 4.1: Laboratory programmes for the data presented in this chapter

Lab Method	No. of sub-sample specimens	Output	Sample shape/type
UCS	124	UCS (MPa) , static Young's modulus, $E_s$ (GPa) static Poisson's ratio, $\nu_s$	Cores and cuboid
To (MPa)	148	Tensile strength	beams
$I_{S(50)}$ (MPa)	216	Corrected point load strength index	Block and irregular
CAI (0.1mm)	95	Cerchar abrasivity index	Blocks
EQC (%)	40	Equivalent quartz content	Flint powder
RAI	121	Rock abrasivity index	Cores and cuboid
VHNR ( $\text{kgmm}^{-2}$ )	40	Vickers's hardness number of rock	-
Shore Hardness	27	Hardness	Cube
Ultrasonic properties	121	Ultrasonic pulse velocities, $V_p$ ( $\text{ms}^{-1}$ ) and $V_s$ ( $\text{ms}^{-1}$ ), dynamic Young's modulus, $E_d$ (GPa) and Poisson's ratio, $\nu_d$	Cores and cuboid
Helium Porosimetry (%)	81	Porosity	Cores and cuboid
ImageJ Porosimetry	23	Porosity	Rough flint samples
Grain size analysis ( $\mu\text{m}$ )	23	Particle size	Rough flint samples

## 4.2 Strength Parameters

### 4.2.1 Uniaxial Compressive Strength of Flints and Static Elastic Parameters

The uniaxial compressive strength of flint samples was measured at a stress rate of  $0.5 \text{ MPas}^{-1}$  using core and cuboidal samples. The cuboidal samples were prepared from the BNLUK samples because of the fracturing and several inclusions in the samples that made it difficult to prepare cylindrical samples. The cores were prepared from both grey BLSUK and all the DBG flints. The prepared samples were subjected to loading until failure during which the stress and strain (lateral and axial) parameters were recorded. The deformation parameters were measured using the strain gauges and readings were taken from the windmill logger.

Physical observations show that failure in flints commences from reactivating pre-existing fractures or development of fresh fractures (Figure 4.1). This is followed by tensile or axial splitting of samples into sharp, thin slabs, with catastrophic failure (explosive). Similar observations for UCS tests on Southern Province flints were reported in Cumming (1999). The degree of shattering depends on the presence of inclusions in the samples (Figure 4.1). Failed samples with carbonate inclusions or partially silicified inclusions usually had larger shards or slabs, and this could be due to the adhesion between the siliceous and carbonates matrices. The explosive failure of flints indicates the necessity for wearing eye goggles whenever flint is to be tested.

Figure 4.2 presents the stress-strain curves representing flints from each study site, except the BNLUK. In Figure 4.2, it can be seen that all the flint samples exhibited a typical linear deformation (brittle failure) and failure occurred abruptly, unexpectedly, without any evidence of a post failure record. The static deformation parameters for BNLUK samples were not obtainable, because all attempts to measure the strain parameters for BNLUK samples proved impossible, because the strain gauges detached from the samples at early stages of loading due structural defects (fracturing in the samples, see Figures 3.4, p.60, 3.10, p.67, 3.12, p.70) associated with the samples (carius flints). In such cases, deformation readings from these samples were not recorded and this also applies to some samples from the BLSUK and DBG flints, which experienced early detachment of the strain gauges at the initial loading stage.

The UCS of flints is summarised in Figure 4.3. Figure 4.3 compares the UCS of flints collected from different geographical locations, with different colour and geological history. A wide range of UCS is observed within each site, ranging from as low as 25.2 MPa to as high as 943.2 MPa. The wide range in UCS of flints has been previously noticed to be due to fracturing in some samples (Cumming, 1999), presence of calcite vugs (Smith et al., 2003), and possible variation in microtexture and mineral contents. As can be noticed in Figure 4.3, the grey flints are the weakest samples studied. Among the grey flints, the BNLUK is the weakest material with a mean UCS of  $112.2 \pm 71.0$  MPa. By contrast, the BLSUK<sub>t</sub> (tabular) and BLSUK<sub>n</sub> (nodular) have relatively higher mean UCS when compared with the BNLUK samples despite being of the same colour.

The mean UCS of the dark brownish grey flints (DBG) are remarkably higher than the average UCS observed in the grey flints, and are consistent, with the exception of the average UCS of TMKT (Ave.  $395.8 \pm 173.1$  MPa) which is lower. The LMFr presents the highest mean UCS among the DBG flints category, with average mean UCS of  $560.3 \pm 178.4$  MPa.

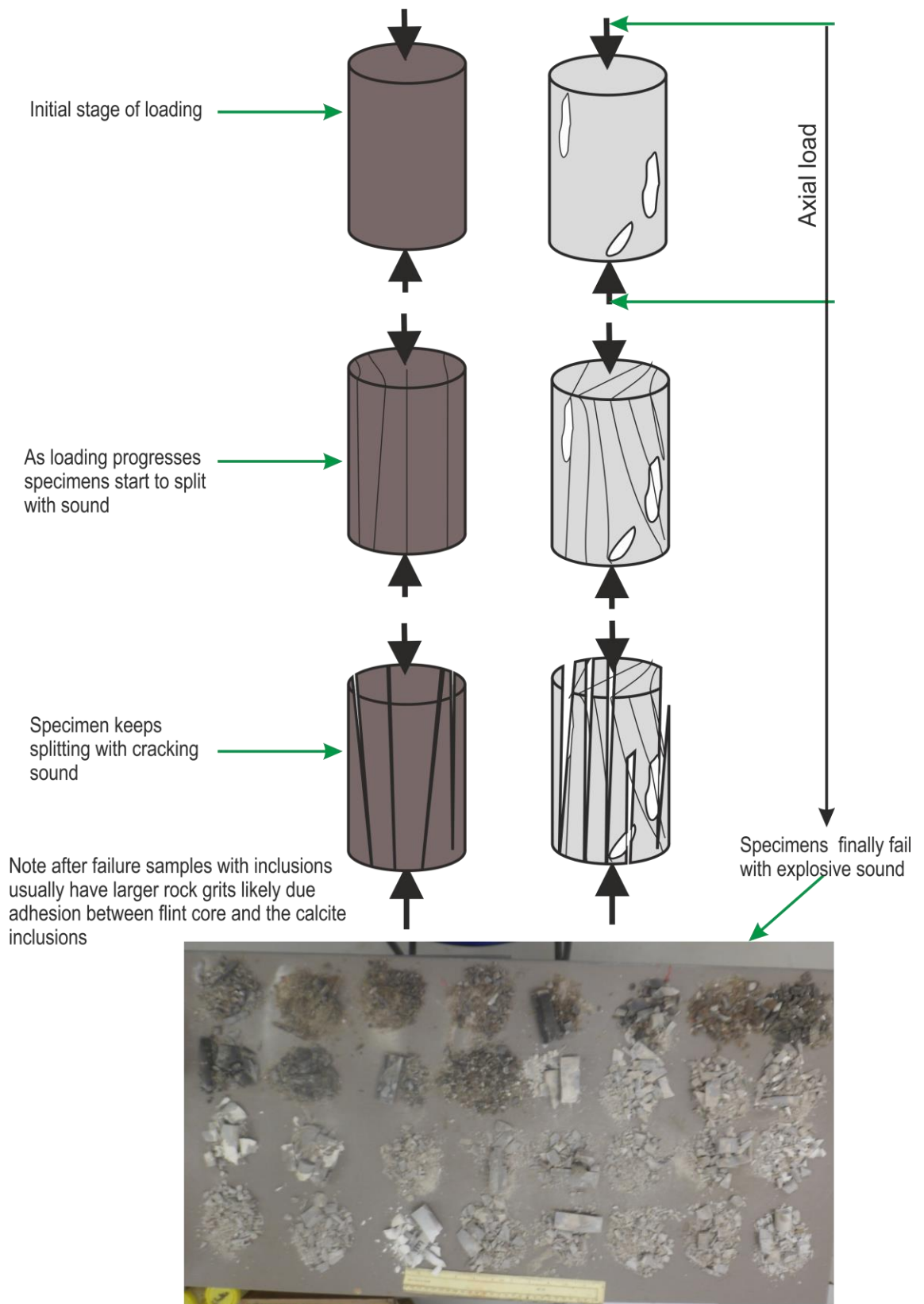


Figure 4.1: Schematic presentation of how different classes of flints respond to loading

The UCS results were subjected to a One-Way ANOVA to determine the statistical significance of the differences observed in the different flint samples tested. At the 95 percentile, the values of mean UCS for flints from all the study sites are significantly different [ $F(7, 97) = 10.5, p = 9.4 \times 10^{-10}$ ]. Post hoc comparison based on Tukey's HSD test showed that the average UCS for the BNLUK was significantly different from any other examined flint samples. This analysis implies that the BNLUK samples have the lowest compressive strength when compared with flint samples from other study sites. The results of this analysis re-enforced the primary observation of the results.

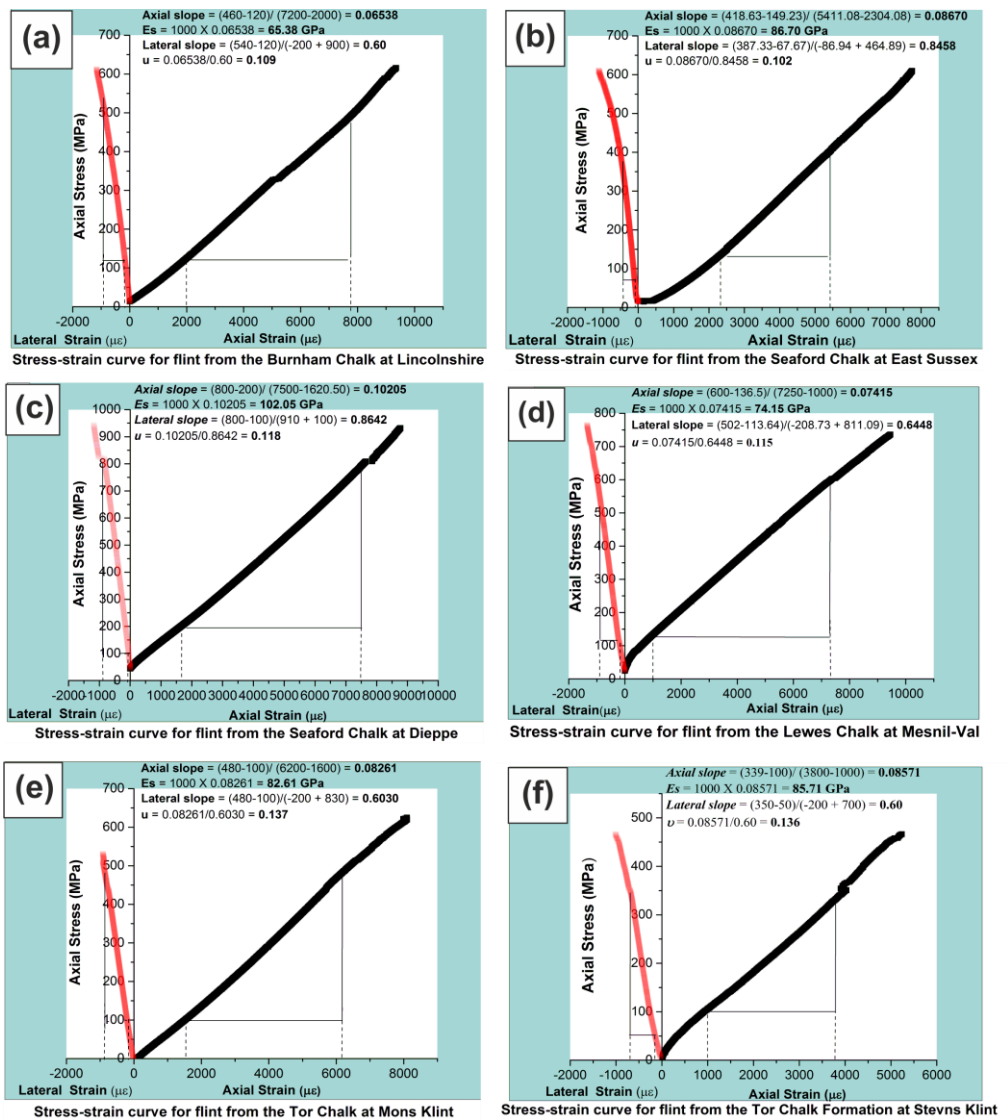


Figure 4.2: Typical stress-strain curves for UCS tests on flint samples representing six study sites. (a) Flint sample from Burnham Chalk at Lincolnshire, UK. (b) Flint sample from Seaford Chalk at East Sussex, UK. (c) Flint sample from Seaford Chalk at Dieppe, France. (d) Flint sample from Lewes Chalk at Mesnil-Val, France. (e) Flint sample from Tor Chalk at Stevns Klint, Denmark. (f) Flint sample from Tor Chalk at Møns Klint, Denmark. Note all samples show typical linear elastic deformation (brittle failure).

The lowest mean UCS recorded in the grey BNLUK samples could be ascribed to the fracturing (Figures 3.4, p.59, 3.10 (b & c), p.66, 3.12 (a-d), p.69 and heterogeneity observed in the samples (carious flints), rather than mineralogy alone, as against the stronger samples seen in Figures 3.11 (c-g), p.68 & 3.13 (a-d), p.70. This trend is also manifested among the DBG flints, where the TMKT exhibited the lowest UCS when compared with the remaining DBG samples. The general trend in the UCS results could be attributed to the pre-existing fractures/joints, and micro textural variations likely caused by diagenetic processes.

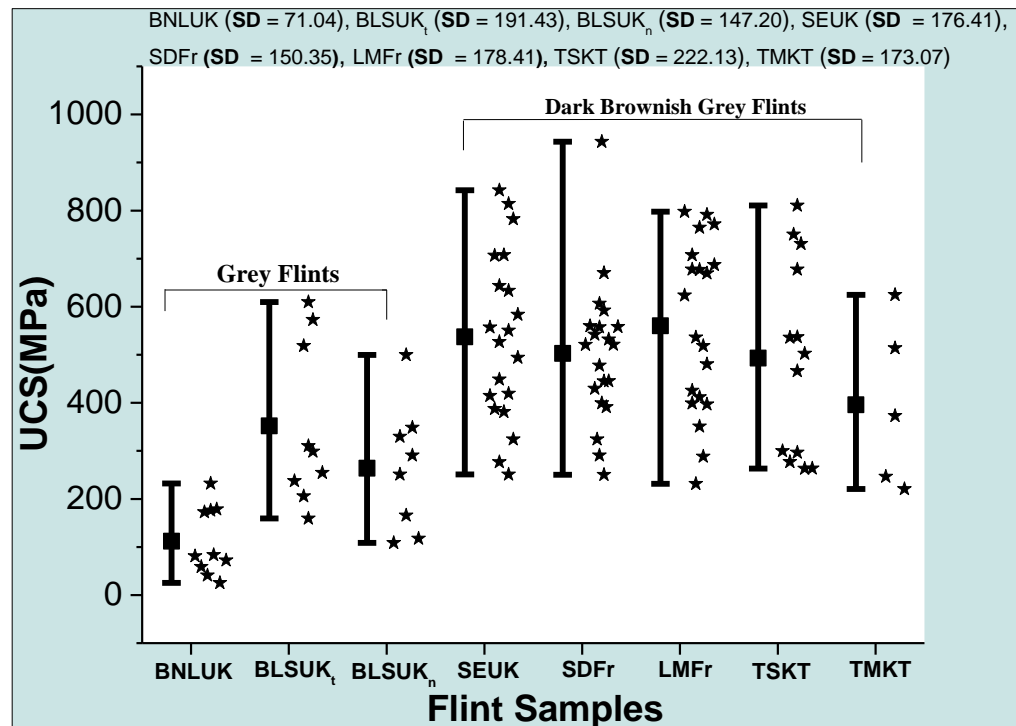


Figure 4.3: Estimated Uniaxial compressive strength (UCS) for flints derived from all the study sites. The samples are grouped into two, representing the grey and dark brownish grey (DBG) flints. A trend in the UCS can be seen between these flint colours. Not the grey flints from the highly disturbed flints at North Landing has the least UCS and the DBG flints from the glacially disturbed flints at Møns Klint has the lowest strength among the DBG flints.

### Static Young's Modulus ( $E_s$ )

The average static Young's modulus ( $E_s$ ) of the flint samples under study as a function of different study sites are illustrated in Figure 4.4. Figure 4.4 indicates the BNLUK<sub>t</sub> samples have lower stiffness than the BLSUK<sub>n</sub> and DBG flints. Perhaps, unexpectedly, the grey BLSUK<sub>n</sub> samples have high average  $E_s$  of  $83.8 \pm 12.1$  GPa, comparable with the  $E_s$  recorded by the DBG flints. This higher  $E_s$  exhibited by the BLSUK<sub>n</sub> could result

from the effects of sampling size because only the deformation parameters of four specimens of the BLSUK<sub>n</sub> samples were successfully recorded. As expected, the DBG flints maintained consistently higher and similar E<sub>s</sub> across the respective sites, apart from the TSKT and TMKT samples that have similar and relatively lower mean E<sub>s</sub> of 78.0±27.19 GPa and 78.3±21.1 GPa respectively.

The average static Young's moduli for all the study sites were subjected to a One-way ANOVA to understand the degree of variation in stiffness between the flint types. The results of this analysis showed the average E<sub>s</sub> for flints from all the study sites are significantly different and have an F ratio of [F(6, 79) = 2.7, p=0.02]. Tukey's HSD comparisons showed a significant difference between the means of E<sub>s</sub> for BLSUK<sub>t</sub> (Ave. 59.4±8.9 GPa) and LMFr (Ave. 85.4±13.3 GPa), SDFr (80.5±13.3 GPa), but there was no significance difference between the means of E<sub>s</sub> for flints from the remaining sites.

Although, limited data have been highlighted as one of the causes of the higher mean E<sub>s</sub> observed in the BLSUK<sub>n</sub> samples, a general trend of the results shows higher stiffness in the DBG samples than in the grey flints.

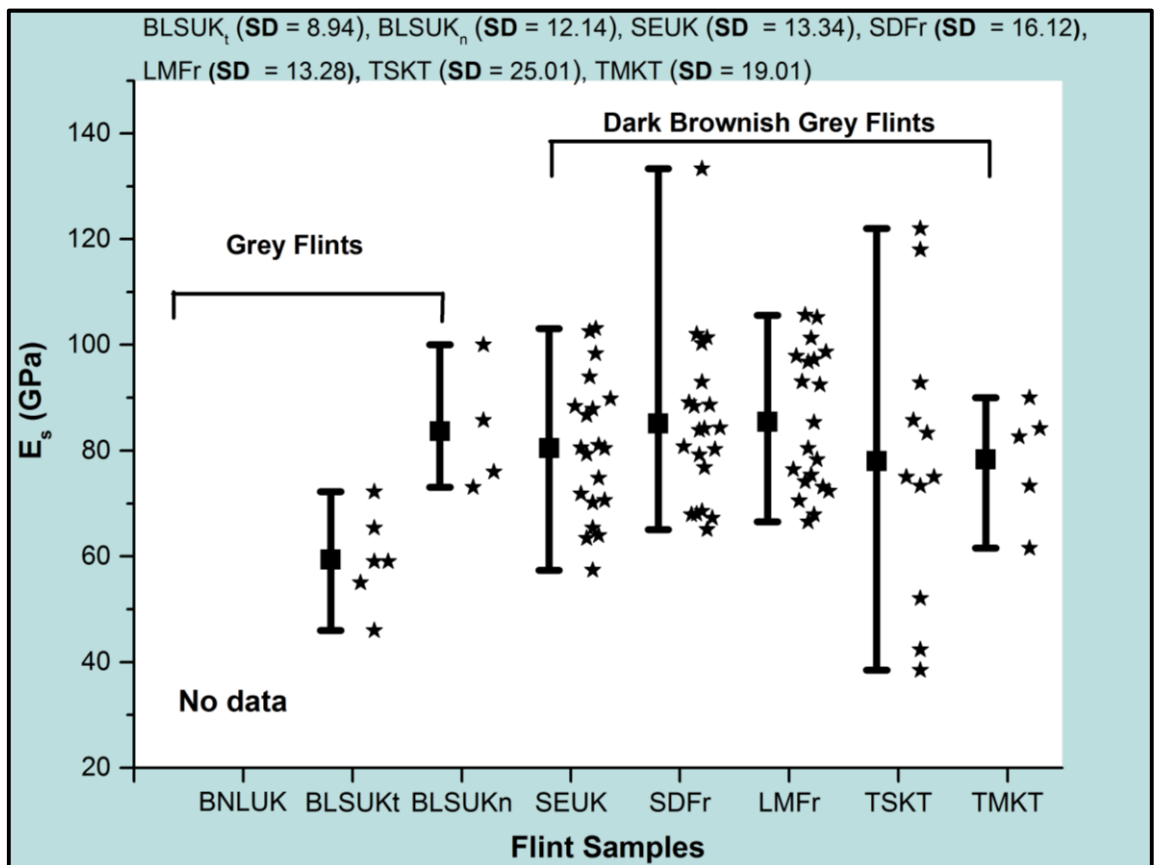


Figure 4.4: Static Young's modulus (E<sub>s</sub>) for flint samples against each study sites/flint types.



*Static Poisson's Ratio ( $v_s$ )*

The static Poisson's ratios ( $v_s$ ) of flint samples determined using the average method is shown in Figure 4.5. As observed in the previous results, the  $v_s$  of the investigated flint samples is widely distributed within each of the study sites. The wide range of  $v_s$  observed conforms to the presence of fractures, carbonate inclusions, and possible variation in the mineral contents in the flints. A general observation of  $v_s$  for the overall flint samples indicates the mean  $v_s$  varies from 0.048 to 0.231. The results also show the samples with higher UCS in both grey and DBG flints have high lateral stiffness. The mean  $v_s$  for the DBG flints varies from  $0.120 \pm 0.029$  for TMKT to  $0.137 \pm 0.049$  for TSKT. The disparity observed between the DBG flints is narrow when compared with that seen between grey flints, BLSUK<sub>t</sub> (Ave.  $0.128 \pm 0.027$ ) and BLSUK<sub>n</sub> (Ave.  $0.137 \pm 0.017$ ). An analysis of the means of  $v_s$  for all the tested samples using One-way ANOVA indicates the difference between the means  $v_s$  for all tested samples was not statistically significant [  $F(6, 79) = 1.95, p = 0.08, ns$  ].

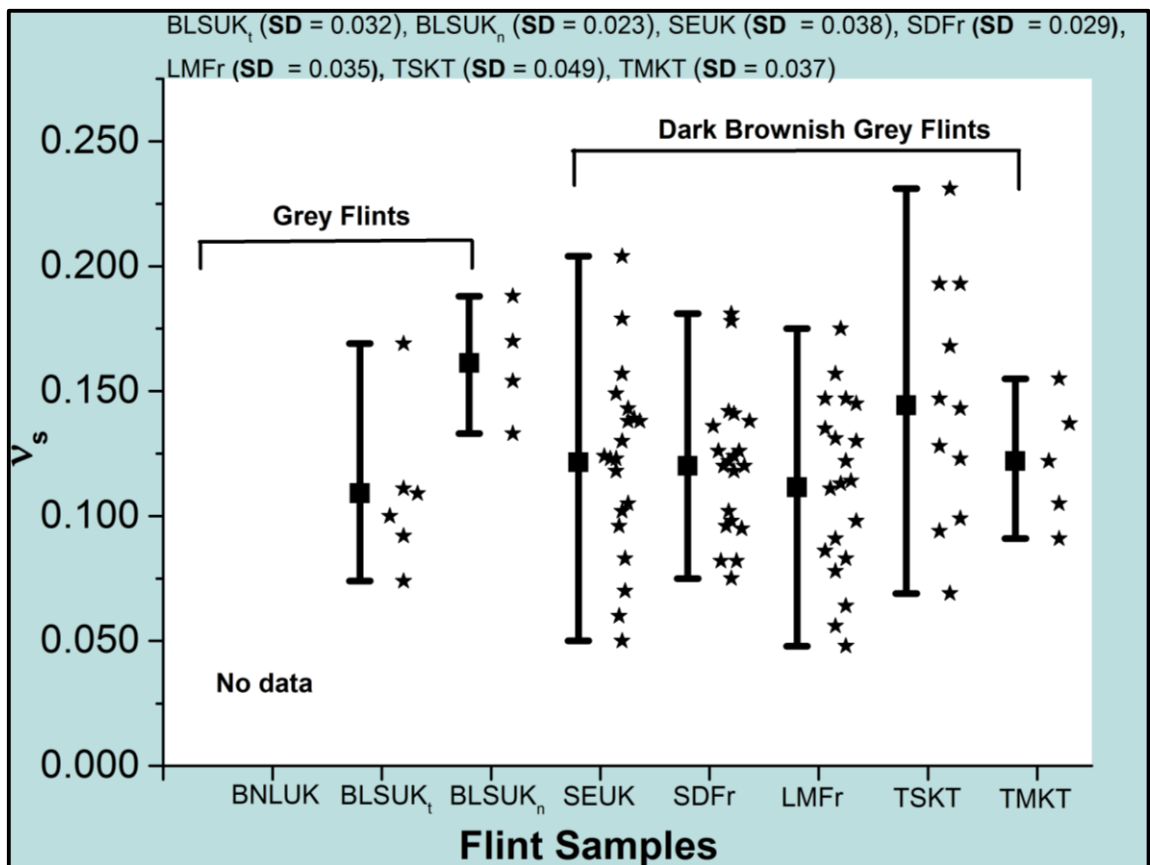


Figure 4.5: Static Poisson's ratio ( $v_s$ ) representing each study site.

### *Density of Flint ( $\rho$ )*

A relationship of density ( $\rho$ ) of flints as a function geographical locations, colour, morphology, microtexture and geology was investigated (Figure 4.6). The  $\rho$  of flints was determined from both cores and cuboid samples using the calliper method (ISRM, 2007). The results can best be explained by categorising the samples into three groups. The first group comprises the grey flints (BNLUK, BLSUK<sub>t</sub> and BLSUK<sub>n</sub>). This group has a lower mean density than any other samples with average  $\rho$  ranging from  $2.43\pm 0.12 \text{ Mgm}^{-3}$  to  $2.50\pm 0.05 \text{ Mgm}^{-3}$ , with the BNLUK samples being at the lower end of the spectrum.

The DBG flints consisting of the SEUK, SDFr, and LMFr form the second group. This group of flint materials are denser than any of the three groups and have a mean density ranging from  $2.66\pm 0.12 \text{ Mgm}^{-3}$  to  $2.69\pm 0.10 \text{ Mgm}^{-3}$ . In this group, the LMFr has the lowest mean density while the SEUK has the highest mean density. As noticed in the grey flints group, the average densities between the DBG flints are similar, with very narrow variation.

The TSKT and TMKT samples form the third group. These samples are slightly less dense than the second group of same colour (DBG flints) but denser than the grey flints. The average density of flint materials from this group is  $2.55\pm 0.013 \text{ Mgm}^{-3}$  for TSKT and  $2.58\pm 0.012 \text{ Mgm}^{-3}$  for TMKT samples. The differences observed in these three flint groups are to be expected due to the presence of internal flaws (such as pores whose presence simply translates to reduction in bulk mass of the sample ); and isolated carbonate inclusions in some of the samples, noticeable after sample failure. Variation in mineral composition and microtexture could also account for the identified differences.

To test how the mean  $\rho$  varies between the different flint types, One-way ANOVA was used and the analysis shows a significant different between the means [ $F(7, 101) = 13.22, p = 5.43 \times 10^{-12}$ ]. Further Post hoc test showed the difference in means  $\rho$  of the grey flints BNLUK, BLSUK<sub>t</sub>, and BLSUK<sub>n</sub> significantly differ from the average  $\rho$  for flints from any other study sites. The difference between the average  $\rho$  of TSKT and LMFr, SDFr, SEUK is also statistically significant.

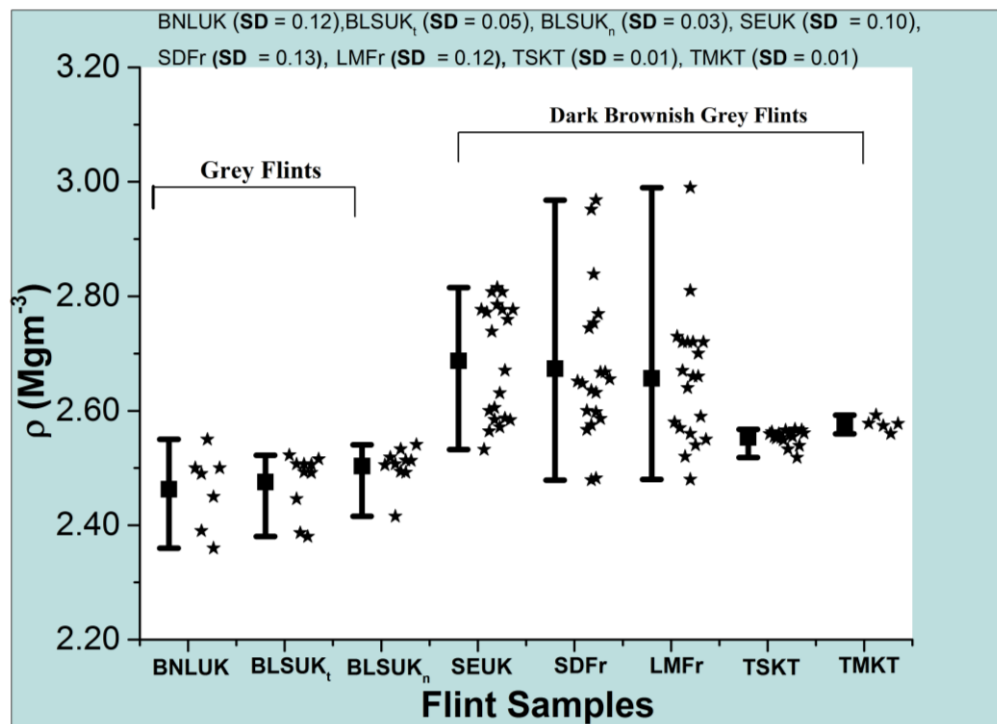


Figure 4.6: Density of flint samples from the entire study locations. Note the slight variation between the GF and DBG brownish flints. The trend follows the observation made in the UCS test, although, in this case, the difference between BNLUK and BLSUK samples is not significant.

#### 4.2.2 Tensile behaviour of Flints

Unlike the pattern of results obtained from the density test, where the difference between grey flints was narrow, the tensile strength of flints assumed similar patterns with the UCS results reported in this study. Figure 4.7 illustrates the tensile strength ( $T_o$ ) of flints from the seven study sites investigated using the Three-point disc test technique. The figure clearly shows the BNLUK (Ave.  $10.85 \pm 2.63$  MPa) has minimum  $T_o$  than both the BLSUK, and all the DBG flints. Pre-existing microfractures, microtexture, mineral content and inclusions of partially silicified carbonates (related to the carious nature of BNLUK) could account for this variation.

As expected, the DBG flints are much stronger than grey flints, with highest average  $T_o$  of  $43.01 \pm 20.61$  MPa observed in the SEUK sample. The high standard deviation observed in this sample demonstrates how widely distributed the  $T_o$  values for SEUK are, and this is a function of microstructural defects seen in some flint samples from this site. This wide range of  $T_o$  is also noticeable in the SDFr, LMFr, and TMKT. However, the BLSUK despite being grey, has an average  $T_o$  which is more comparable to the DBG flints, than the grey BNLUK. The high tensile strength observed in the BLSUK (Ave.  $\rho = 2.50 \text{ gcm}^{-3}$ ) samples is unsurprising because these

samples had more competent, more silicified carbonate inclusions and slightly denser matrix than the BNLUK (Ave.  $\rho = 2.43 \text{ gcm}^{-3}$ ) samples.

To explore which flint material or location significantly differs from others, One-way ANOVA was used. The results indicated a statistically significant difference in the mean  $T_o$  for the flint samples representing the seven study sites [ $F(6, 123) = 6.63$ ,  $p = 5.28 \times 10^{-6}$ ]. To understand how the flint samples differ from each other, a Post hoc test was employed. The test results showed the mean  $T_o$  for BNLUK (Ave.  $10.85 \pm 2.63$  MPa) was significantly different from the average  $T_o$  of any of the investigated samples.

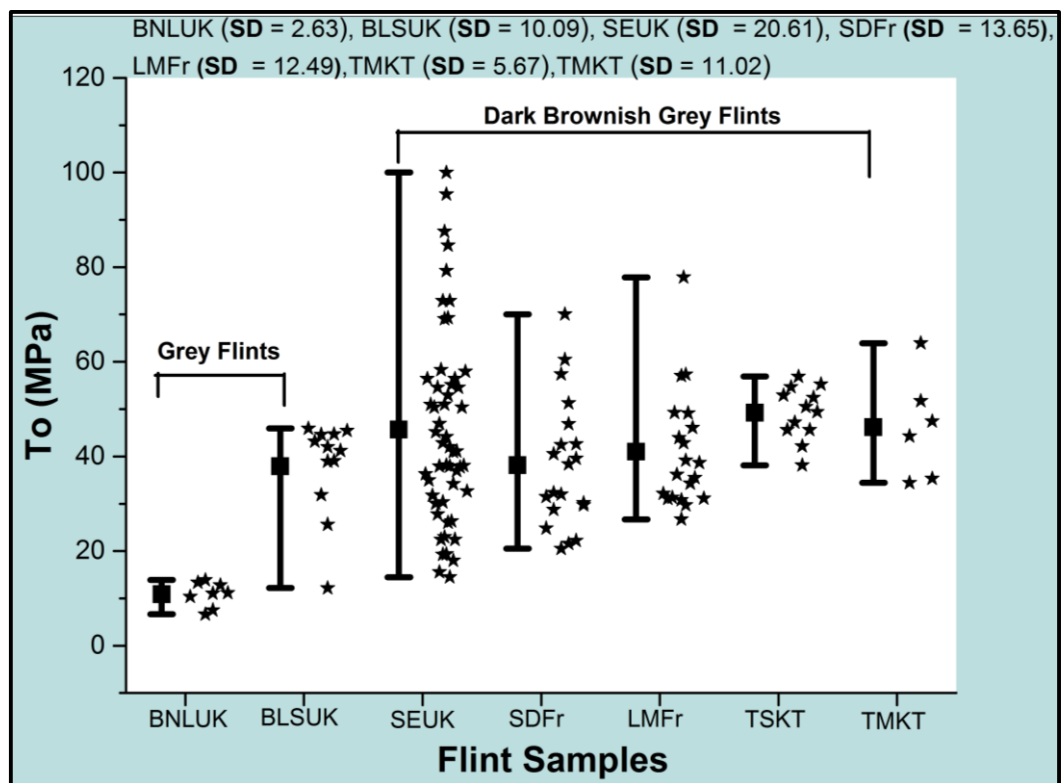


Figure 4.7: Estimated tensile strength of flints by each study site. As for the UCS, there is noticeable variation in the tensile strength of flint with calcite content and geology of the site. The apparent reduction in the mean tensile strength for the grey BNLUK (highly disturbed) and BLSUK samples explains this observation.

#### 4.2.3 Point Load Strength Index Data

The corrected Point-load strength index  $I_{S(50)}$  test results representing flint samples from the study locations are summarised in Figure 4.8. Figure 4.8 shows the  $I_{S(50)}$  values range from  $6.8 \pm 3.9$  to  $29.1 \pm 11.9$  MPa. Grey flints are weaker than the DBG

flints as observed in the UCS and To tests. The BNLUK (Ave.  $6.8 \pm 3.9$  MPa) consistently remains the weakest flint materials and this is likely due to fracturing and carbonate inclusions associated with the samples. In contrast to the BNLUK, the BLSUK has relatively higher  $I_{S(50)}$  (Ave.  $15.2 \pm 4.9$  MPa), than the BNLUK and this could be ascribed to the significantly fewer discontinuities observed in the samples.

From Figure 4.8, it can be seen that there is little difference between the DBG flints in terms of  $I_{S(50)}$ , with the SEUK (Ave.  $29.1 \pm 11.9$  MPa) being the strongest, while the TSKT (Ave.  $24.6 \pm 9.2$  MPa) has the least  $I_{S(50)}$  values among the DBG flints. In all the flint samples examined, a scatter in the overall  $I_{S(50)}$  was observed at each site, especially, in the SEUK where the range is wide, as demonstrated by the larger standard deviation.

A One-Way ANOVA depicted that the means  $I_{S(50)}$  for all the flint samples differed significantly [  $F(6, 205) = 39.4, p=0$  ]. Follow-up Post hoc HSD test revealed the mean  $I_{S(50)}$  for BNLUK greatly differ from all other tested samples. The same analysis also showed the BLSUK significantly varies from the means  $I_{S(50)}$  for LMFr, SDFr, SEUK, and BNLUK. The variation in the  $I_{S(50)}$  of these flint materials could be due to the variability in structural/textural defects associated with some samples, and this also contribute to shaping of the flint properties.

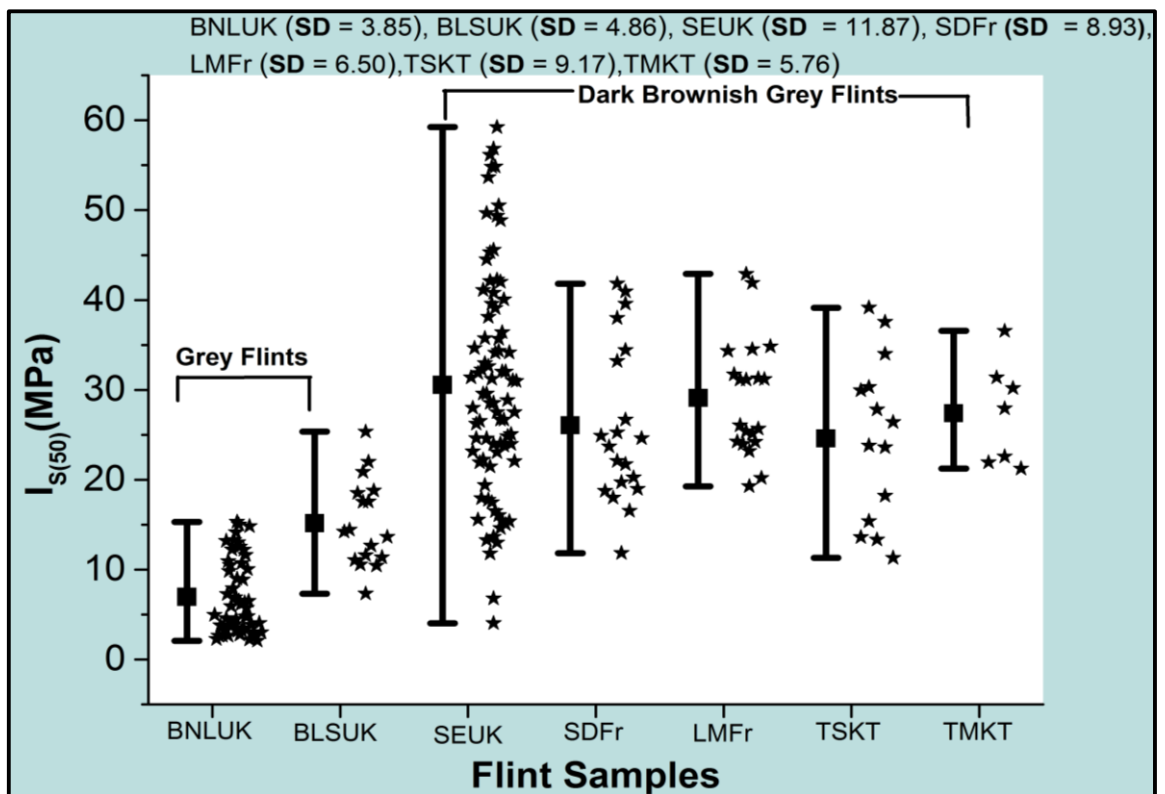


Figure 4.8: Corrected Point load strength index ( $I_{S(50)}$ ) of flint samples from each study site. Note the differences in the  $I_{S(50)}$  between the grey flints and the dark brownish grey flints.

### 4.3 Geotechnical Wear and Drillability Parameters of flints

#### 4.3.1 Cerchar Abrasivity Indices of Flints at Different Loading Conditions

The Cerchar abrasivity indices (CAI) for different structures of flints from the North Landing Chalk determined using both 9 kg and 7 kg static loads are illustrated in Figure 4.9. As can be observed from Figure 4.9, the CAI values for the chalk surrounding the flint (Ch,  $1.37 \pm 0.36$  (0.1 mm)), the white crust (WCr,  $1.76 \pm 0.49$  (0.1mm)), and the white inclusion (WI,  $1.69 \pm 0.28$  (0.1mm)) having the least silica content were significantly lower than for flints (presented based on colour as LBG, LG, BG) .

The relatively higher CAI results (for LBG, GF, and LG) observed in Figure 4.9 represent the flints, and the mean CAI values for these samples are more than a twofold increase when compared with the above-mentioned less abrasive materials. Though, slight variations in abrasivity was noticed between the flint materials, with the light grey/light brownish grey flints being less abrasive while the grey/dark brownish grey flints being most abrasive.

The silicified inclusion (SSI) formed the intermediate between the two different materials (less and most abrasive samples) in terms of CAI, and had a slightly lower average CAI when compared with flints, but recorded a slightly higher CAI of up to 2.87 (0.1mm) than the CAI range of 1.37-1.74 (0.1mm) for the chalk, white crust, and white inclusion. Thus, indicating possible effects of variation in mineral composition on abrasivity of flint materials, which would be investigated in the subsequent chapters.

The trend in CAI values observed among the different structures of flints from the BNLUK samples showed how variable the abrasivity of flints can be, even within samples of the same origin. The increase in the CAI values from chalk to the flints (Figure) indicates the role of mineral composition on the abrasivity of flints. However, a general comparison of the mean CAI for the examined flint structures using both 7 kg and 9 kg static loads do not yield any appreciable improvement on the measured CAI as expected (Figure 4.9).

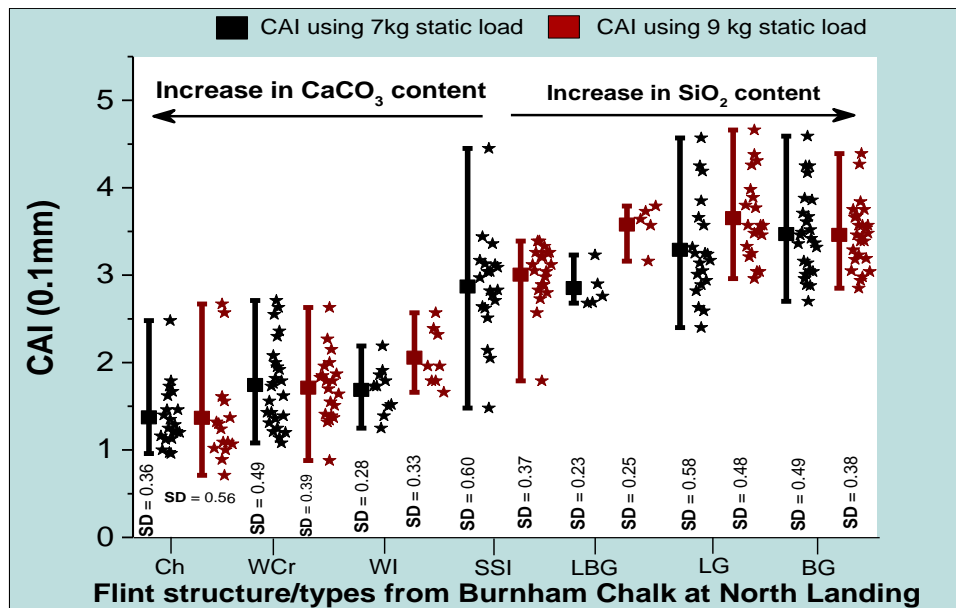


Figure 4.9: Cerchar abrasivity index (CAI) for chalk surrounding flint, different flint colour and structures (white inclusion, white crust, and silicified inclusion). As can be noticed there is no significant difference between CAI measured using the 9 kg and 7kg static loads. Note a clear difference between silica-rich and carbonate-rich samples.

To compare the abrasivity between flints collected from all the seven study sites, CAI were determined (Figure 4.10) by considering the dominant flint colour in each study location. As previously mentioned, the grey (GF) and light grey (LG) flints are dominant at the BNLUK, and BLSUK samples. While the dark brownish grey (DBG) and light brownish grey flints (LBG) are dominant among the SEUK, SDFr, LMF<sub>r</sub>, TSKT, and TMKT samples. The GFs were compared with equivalent LG flints (within the same material) as well as with the DBG flints from other locations. So also, the CAI values for DBG flints were compared with equivalent CAI for LBG flints from the same materials. The data obtained from these comparisons are summarised in Figure 4.10. As can be seen from Figure 4.10, the BNLUK ( $3.47 \pm 0.49$  (0.1 mm)) and the TMKT ( $3.46 \pm 0.21$  (0.1 mm)) samples recorded the lowest mean CAI, while the LMF<sub>r</sub> ( $4.23 \pm 0.47$  (0.1 mm)) had the highest average CAI value. The mean CAI values for the LG/LBG flints (in red) were slightly lower than the average CAI for the GF/DBG flints (in dark). Although, a slight variation in CAI was observed between these flint types/colour, but, for practical purposes the CAI values for most of these samples fall in the very abrasive category (Cerchar, 1986), with the exception of the CAI for the LMF<sub>r</sub>, which falls in the extremely abrasive material category.

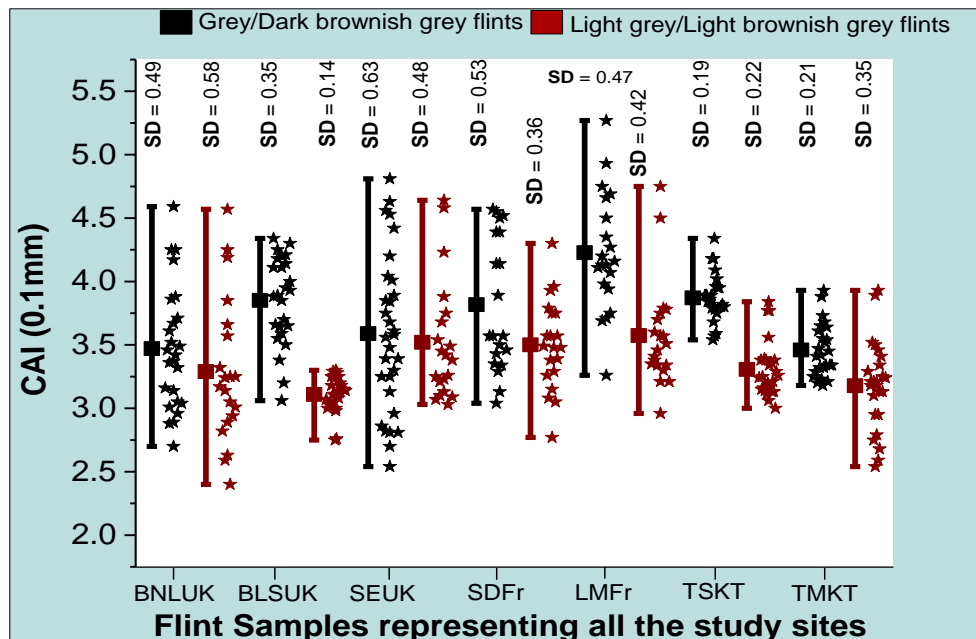


Figure 4.10: Variation of Cerchar abrasivity index (CAI) with flint colour and geographical locations. The differences in CAI between the grey/dark brownish grey flints and the light grey/light brownish grey flints are evidenced. There is no significant difference in CAI between the grey and the dark brownish grey flints.

#### 4.3.2 Equivalent Quartz Content of Various Structures and Colour of Flints

Following the inability of CAI to adequately characterise the drillability and abrasiveness of flints, despite distinct variation in mineral composition observed between the different flint types, structures, and colour, the equivalent quartz content (EQC) was used as described in Chapter 3, Section 3.5.2, and p.90. The procedure provides the technical parameters that can be employed to predict the drill bit life span by considering the role of each mineral in the rock sample and the respective Rosiwal grinding hardness. The product of these two variables express as a percentage gives the EQC of the rock.

Figure 4.11 shows the EQC of different structures/colour of flints and the surrounding chalk for BNLUK. The EQC was observed to vary with flint colour, structure and with possibly, the percentage of silica/carbonate in the samples. The calcite-rich samples exhibited significantly lower EQC (2.55-15.60%) than the silica-rich samples (76.50-98.13%). Just as in the CAI, the EQC for the silicified inclusions (with moderate silica content) was found to fall in between the siliceous and the carbonate samples.



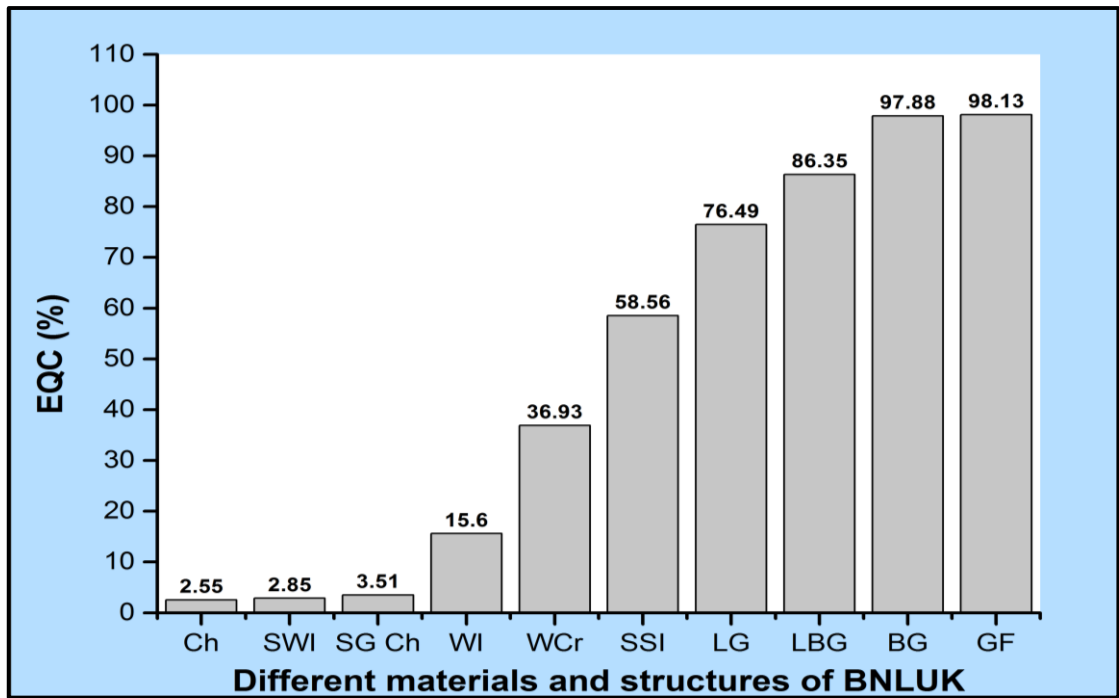


Figure 4.11: Equivalent quartz content (EQC) of chalk surrounding flints, flint structure and colour collected from the Burnham Chalk at the North Landing. As observed in the CAI, there is a general trend where EQC increases with flint colour/structure.

Figure 4.12 compares the evaluated EQC of flint structures/colour/surrounding chalk with geographical locations. It can be observed that, for the chalk material, the measured EQC from all the investigated sites were similar and noticeably lower (less than 3%). While there was considerable variation in EQC between LG and GF flints, a comparison between GF and DBG, as well as between LBG, and DBG flints show minor differences among the different flint category. Interestingly, the white crust or cortex (WCr) from the grey flint (BNLUK) was surprisingly less abrasive than equivalent material from the Seaford Chalk Formation (SEUK and SDFr), and the variation was sharp. The abrasiveness of the WCr surrounding the Seaford Chalk Formation was more or less related to the flint while that of the WCr surrounding the Burnham Chalk Formation was closer to the chalk. This, therefore, could be explained by the variation in the mineral composition between these materials. The inability of this method to detect significant differences in EQC between the grey flints and the DBG flints, despite the differences observed between the samples in terms of microfracturing, and strength raised a significant concern over the use of the method.

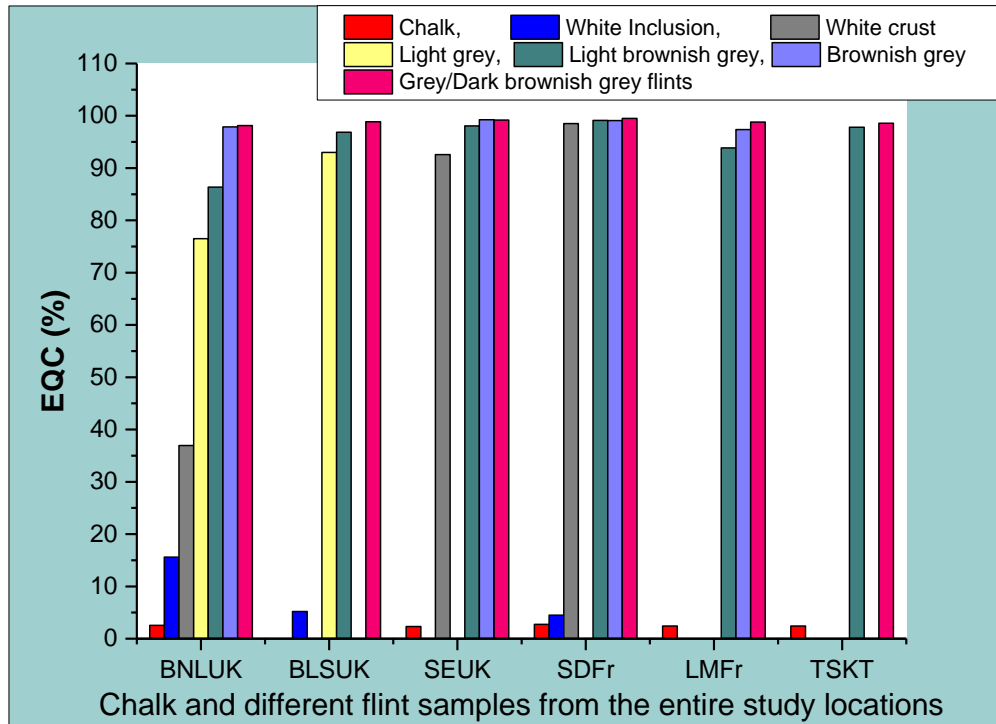


Figure 4.12: Equivalent quartz content (EQC) for different chalk/flints samples representing each study site, and some variations with respect to colour/geographical locations. The EQC is seen to depend on carbonate content and by extension on colour intensity.

### 4.3.3 Rock Abrasivity Index of Grey and Dark Brownish Grey Flints

Since the reliance of EQC on abrasive minerals as the major contributing factor affecting the drillability, and abrasiveness of flint, rock abrasivity index (RAI) was used to examine the abrasiveness of flints. The RAI was considered because as mentioned in Chapter 3, Section 3.5.3 in addition to mineral contents, the RAI accounts for rock strength (Plinninger, 2010) as a contributing factor to the abrasiveness of rock. The RAI of flints was determined using the UCS results obtained in Section 4.2 and the EQC determined in Section 4.3.2 above. The derived RAI for flints as a function of flint study sites and colour are illustrated in Figure 4.13. The RAI data was broadly categorised into grey and dark brownish grey flints, which are the dominant flint colours in the study sites. The data for each group was analysed and comparisons were made between and within groups.

Based on this analysis and comparisons, a wide range of RAI across the samples was seen to vary from 24.7 to 938.6. Figure 4.13 also shows the grey flints (BNLUK and BLSUK) are remarkably less abrasive, relative to the dark brownish grey flints from the remaining study areas. However, a comparison between the grey flints

shows the average RAI of the highly tectonically disturbed BNLUK was lower than the mean RAI for the BLSUK and was the lowest among all the investigated flints. The RAI values of BNLUK correspond to the very abrasive material (Table 3.6) with drill bit lifetime of  $290 \text{ mbit}^{-1}$  (Figure 3.15, p.74). Meanwhile, very similar results were noted when the mean RAI for tabular flint ( $\text{BLSUK}_t$ ) and nodular flint ( $\text{BLSUK}_n$ ) were compared. It can also be observed that among the dark flints, the TSKT and TMKT were the least abrasive materials with RAI averages of  $418.4 \pm 219$  and  $390.6 \pm 170.8$  respectively. While the DBG flints from the Chalk of the Anglo-Paris Basin ( $\text{SEUK}$ ,  $\text{SDFr}$ , and  $\text{LMFr}$ ) have similar and the highest average RAI values.

To test the statistical relationships between mean RAI values for the different flint samples evaluated, One-way ANOVA was applied. The analysis indicates a significance difference among the average RAI values for the measured samples [ $F(7, 100) = 9.98$ ,  $p = 2.12 \times 10^{-9}$ ]. Post hoc tests of pair-wise mean differences in RAI among the flint samples studied were determined using Tukey's HSD. The analysis showed that BNLUK significantly differ from all the flint samples with the exception of BLSUK and the TMKT samples. The BLSUK also varied significantly from SEUK, SDFr and LMFr samples.

Nevertheless, the data derived using RAI to predict abrasiveness of flints provides more reliable information on abrasivity of flints than the traditional EQC, and Cerchar methods. This observation was based on the response of the RAI method to some geological controls affecting the abrasive wear behaviour of the various flint materials examined on the basis of colour, morphology and geographical locations.

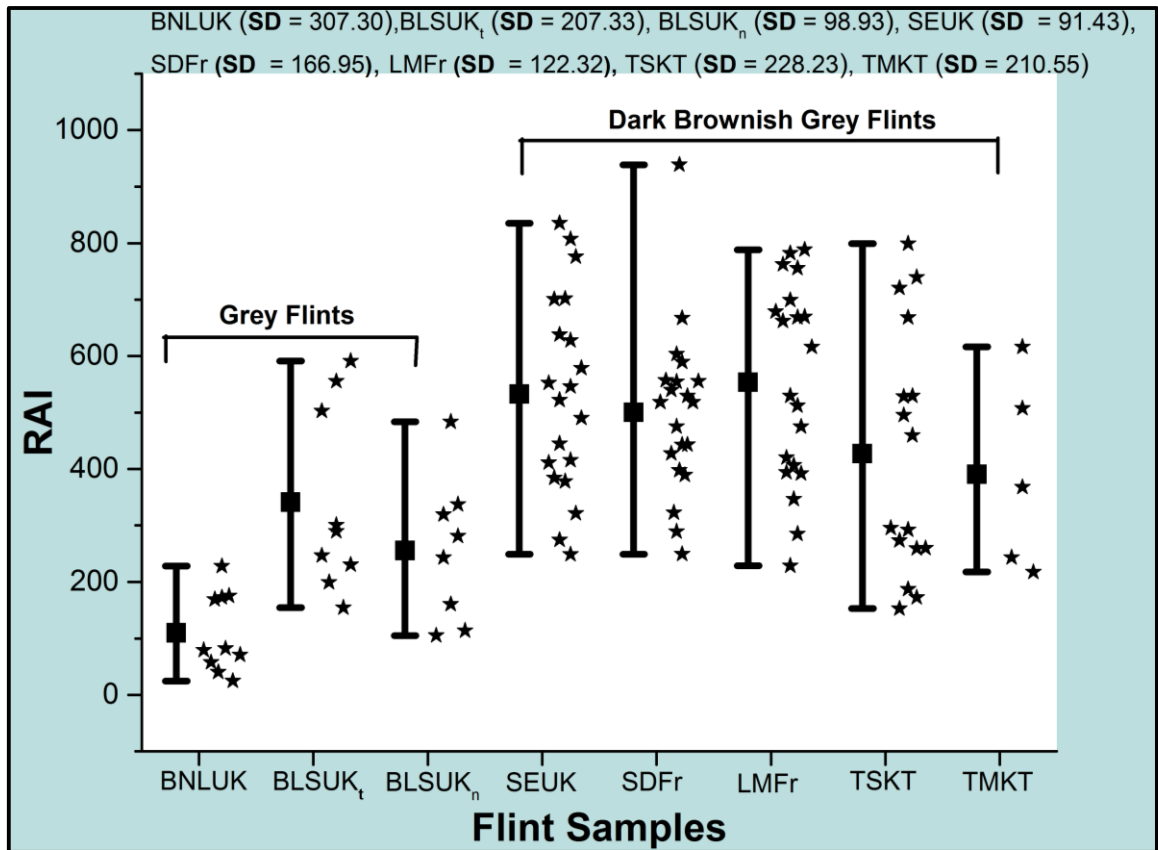


Figure 4.13: Rock abrasivity index for different flint samples drawn from all the study sites. An increase in the mean RAI values from the grey flints to the dark brownish grey flints is observed.

#### 4.3.4 Vickers Hardness Number of Flint Data

Vickers hardness number of rock (VHNR) for various flint types/colour/structures and chalk surrounding flints was determined as described in Section 3.5.4, using equation 3.14. The VHNR for these materials were determined for two reasons: firstly, to understand the wear properties of flints considering the roles of the hardness of each mineral in flints/surrounding chalk. Secondly, to identify the control and variation of these properties between different flint types, colour, and surrounding chalk sampled from the different study sites investigated. The VHNR was used in this study because the samples are variable and could possess more than one mineral (comprising quartz and calcite) with clearly different crystals or grain hardness. Therefore, with this method the contribution of the individual mineral can be established and could be used to estimate the hardness and abrasiveness of the flint materials.

The mineral compositions (basically calcite and quartz) and identification for each sample was achieved using XRD analysis, while the corresponding Vickers hardness number (VHN) of the identified minerals were derived from the Table of VHN (Gokhale, 2011) as described in Chapter 3. The VHNR for each sample was evaluated

as the aggregate of the products of mineral contents and VHN of all the minerals in the sample. The VHNR for different flint structures/colour and the surrounding chalk for the BNLUK are presented in Figure 4.14, It is evident from Figure 4.14 that, there was a clear increase in the VHNR values from the carbonate-rich samples (Chalk = 162 kgmm<sup>-2</sup>) to the silica-rich samples (flints) with VHNR ranging from 920 to 1141 kgmm<sup>-2</sup>. The VHNR for the LG flints is the lowest among the flint samples. Closest to the flint, in terms of VHNR was the silicified inclusions (SSI), whose silica content was an intermediate between flinty and chalky samples, as against the white inclusions (WI), which had VHNR, that were more closely related to the chalk.

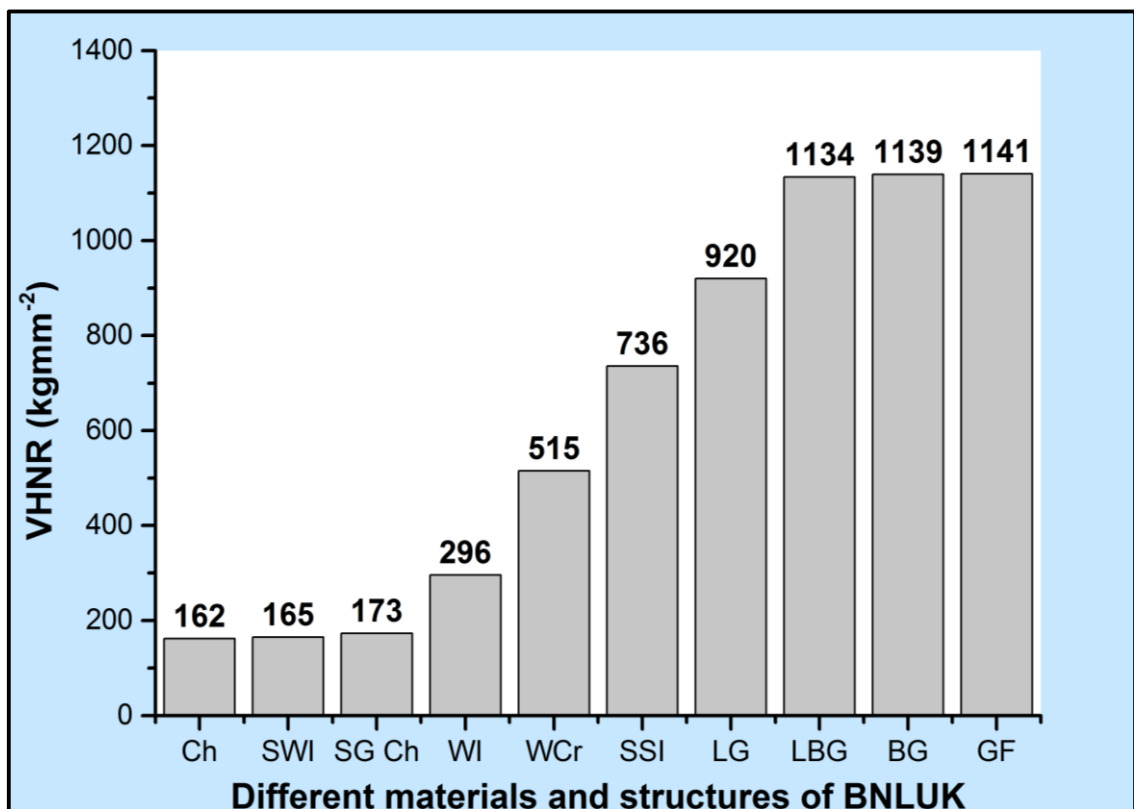


Figure 4.14: Change in Vickers hardness number of rocks (VHNR) for the surrounding chalk, different colour and structures of flints sampled from the North Landing. Note, the trend in the VHNR values increasing from chalk to flints.

The VHNR for flints, WCr and surrounding chalk from the seven study sites were compared (Figure 4.15) to establish the variation in hardness and abrasiveness of these materials with geology, locations and colour. The results indicate remarkable differences between flints, and all the carbonate-rich samples (chalk, white inclusion (WI), and white crust (WCr)) across all the study sites, with the exception of the WCr from the Seaford Formation which differed only slightly from the flint samples. The VHNR values for WCr from the Seaford formations (SEUK and SDFr) were observed to

be a twofold increase of the VHNR for the less silicified WCr surrounding the BNLUK. The chalk in all the study sites exhibited similar VHNR, while the VHNR for the entire flint samples regardless of colour and emplacement were curiously consistent, with little or no significant difference.

A general view of the VHNR data for flints regardless of locations and colour suggests that variations in abrasiveness based on VHNR exist between flint structures. These variations were not significantly evidenced between flint types.

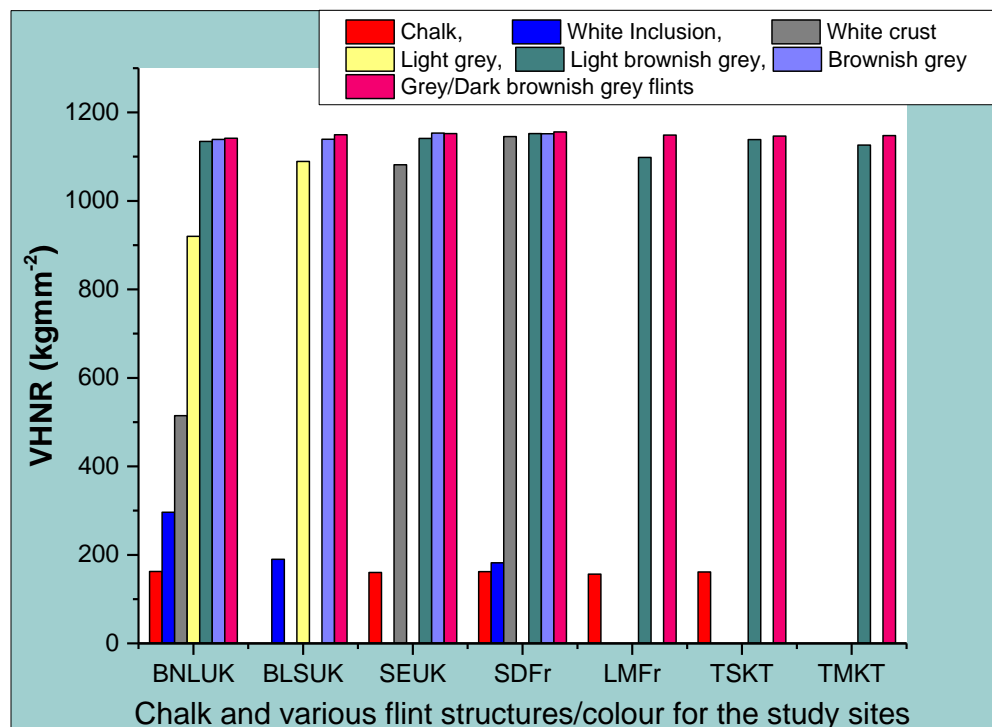


Figure 4.15: Vickers hardness number of rock (VNHR) for flints (different colour) representing all the study sites and the surrounding chalk. There are significantly clear differences between the flints and calcite-rich samples. However, the difference in VHNR for flints between the study sites is not significant.

#### 4.3.5 Shore Hardness Parameters

Shore hardness test (SH) was conducted in accordance with the ISRM (2007) suggested methods to examine the hardness of flints and investigate how this property varies with the flint colour, geology and geographical distribution. For this test, four major flint colours were identified and tested. The flint colours tested were: the GF (BNLUK, n=1; BLSUK, n=3), LG (BLSUK, n=3), DBG and BG flints (SEUK, n=6 for DBG, and n= 3 for LBG; SDFr, n=4; LMFr, n=2 and TSKT, n=5), where n simply refers to the respective sample size tested for each study site. Each of the flint samples was

tested as described in Chapter 3, Section 3.5.5, and SH was recorded as the average of the fifty (50) replicated rebound values after discarding the five highest and the least readings (ISRM, 2007). Figure 4.16 presents the SH data from the study sites comparing different flints on the basis of colour, locations and mineral composition.

From the results, the range of SH values obtained from the examined samples was from 80 to 117. The DBG flints consistently show higher average SH values, than the LG/LBG flint, while the GF (BNLUK) represents the weakest sample. The grey flints, BLSUK and BNLUK, when compared, show a noticeably different SH values, with the BLSUK being harder, despite possessing the same colour. This suggests, besides the variation in colour which has been reported to be associated with mineral composition (Aliyu et al., 2015), additional factors could be controlling the hardness of flints.

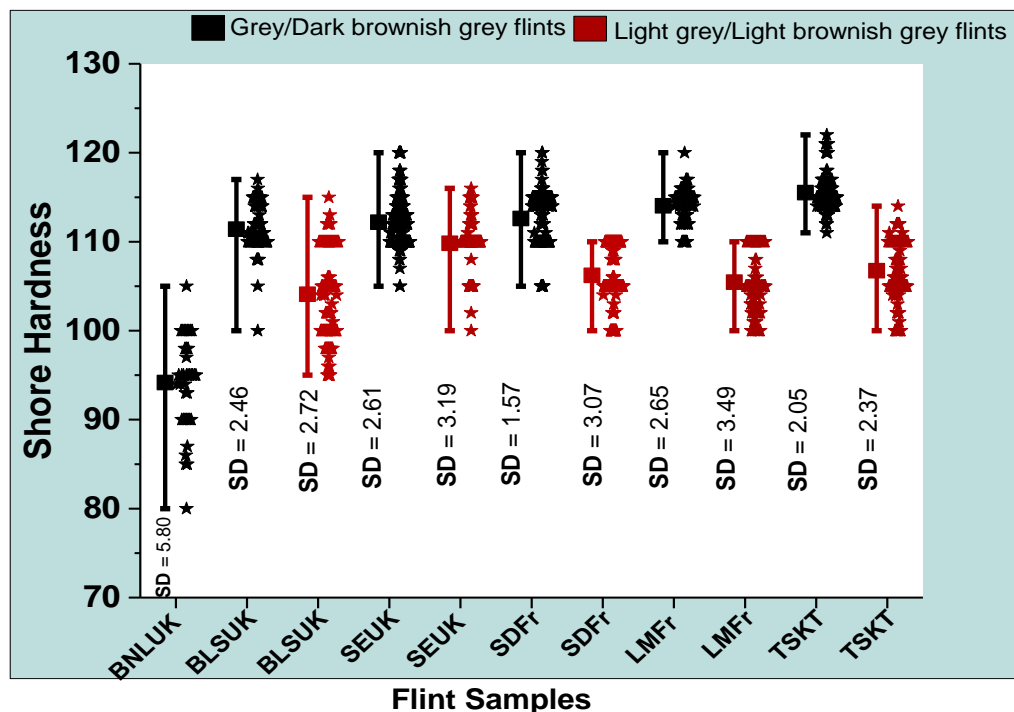


Figure 4.16: Distribution of Shore hardness (SH) of flints with different flints samples categorised according to colour and study sites. The difference in SH values between the two dominant colours within each site can be seen, with the light grey/light brownish grey sample being less hard than the grey/dark brownish grey flints.

## 4.4 Petrophysical Properties of Flint Materials

The section presents the data obtained from the Petrophysical studies.

### 4.4.1 Ultrasonic Velocities and Low Strain Elastic Properties of Flint Materials

The ultrasonic pulse velocities comprising of compressional ( $V_p$ ) and shear ( $V_s$ ) wave velocities were measured by the ratio of acoustic travel times data to the respective length of each flint sample. The measurements were conducted on all the flint samples used for the UCS tests, prior to testing. The measured velocities and the bulk density of each flint sample were used to evaluate the dynamic elastic constants (Young's modulus ( $E_d$ ) and Poisson's ratio ( $\nu_d$ )) using the standard elastic formulae described in Chapter 3. The measured  $V_p$  (Figure 4.17),  $V_s$  (Figure 4.18),  $E_d$  (Figure 4.19) and the  $\nu_d$  (Figure 4.20) were plotted against flint samples representing different geographical locations. The graphical plots were designed to understand the ultrasonic properties of flint materials, and to identify variations in these properties with colour, microtexture, microstructure and mineral content of flints.

In Figure 4.17 the  $V_p$  for all the flint samples showed a broad range of values within each study location, and this is a function of factors like the presence of carbonate inclusions, microfractures, joints and the geological variability (tectonic settings of the flint). A comparison of the mean  $V_p$  between flints shows the BNLUK (grey flints) have the lowest mean  $V_p$  (also see Table 4.2 for the summary results) and is followed by the TMKT (DBG). The TSKT shows the highest mean  $V_p$  and this is closely followed by the SEUK, BLSUK<sub>t</sub>, LMFr, SDFr and BLSUK<sub>n</sub> respectively. The differences in the mean  $V_p$  values between these flint samples with higher values are very slight, regardless of whether the samples are grey or dark brownish grey flints.

Table 4.2: Summary of dynamic elastic properties of flint materials

Parameters	Grey flints			Dark brownish grey flints			
	BNLUK	BLSUK	SEUK	SDFr	LMFr	TSKT	TMKT
$V_p$ ( $\text{ms}^{-1}$ )	5029.8	5431.5	5494.0	5465.2	5479.1	5539.9	5333.5
$V_s$ ( $\text{ms}^{-1}$ )	3191.7	3392.2	3523.2	3540.1	3540.3	3546.9	3476.1
$E_d$ (GPa)	103.8	127.3	137.9	137.9	137.4	134.1	128.0
$\nu_d$	0.161	0.135	0.150	0.136	0.138	0.143	0.129



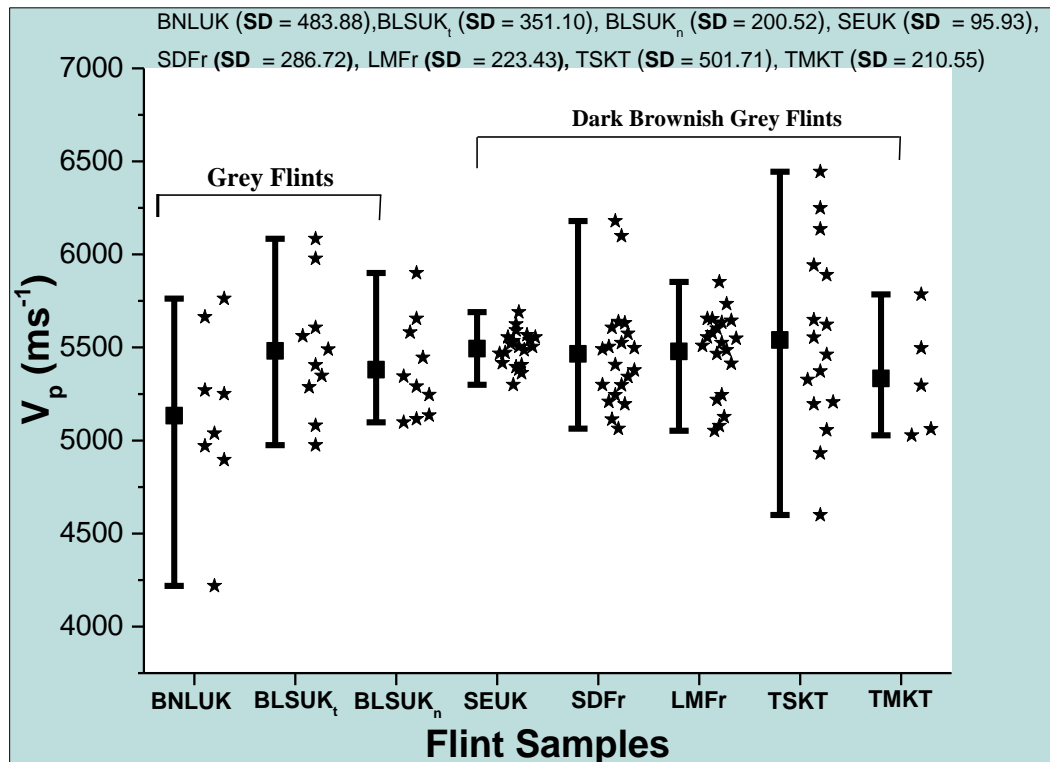


Figure 4.17: Measured compressional velocity ( $V_p$ ) of different flint samples collected from all the study sites.

The statistical relationships between mean  $V_p$  among all the investigated flint samples were studied using One-way ANOVA. The results of this test show the difference in mean scores for all the flint samples from the seven studied sites are statistically significant [ $F(7, 101) = 2.44, p = 0.02$ ]. Post hoc tests using Tukey's method illustrate that the mean  $V_p$  for BNLUK samples was significantly different (least) from the mean  $V_p$  for SEUK, SDFr, LMFr, TSKT, LMFr, but is not significantly different from that of TMKT.

The trend observed in  $V_p$  results was also reflected in the mean  $V_s$  (Figure 4.18 and Table 4.2) values for the same flint samples tested. The  $V_s$  values for the overall flint samples range between 2649.1 and 4166.5  $\text{ms}^{-1}$ . The BNLUK still retains the lowest mean  $V_s$  of  $3191.7 \pm 307.3 \text{ ms}^{-1}$ , while the average  $V_s$  of the remaining samples are similar regardless of differences in colour. The similarities observed in the mean velocities between the two flint samples of different colour among the samples with highest velocities, suggest the parameters that control flint mechanical properties of flint materials do not have significant influence on elastic wave velocities in flints. The lowest velocities values observed in the BNLUK and TMKT samples reflect the level of

fracturing identified with the samples, especially, the BNLUK samples, which in addition to structural defects have significant carbonate inclusions.

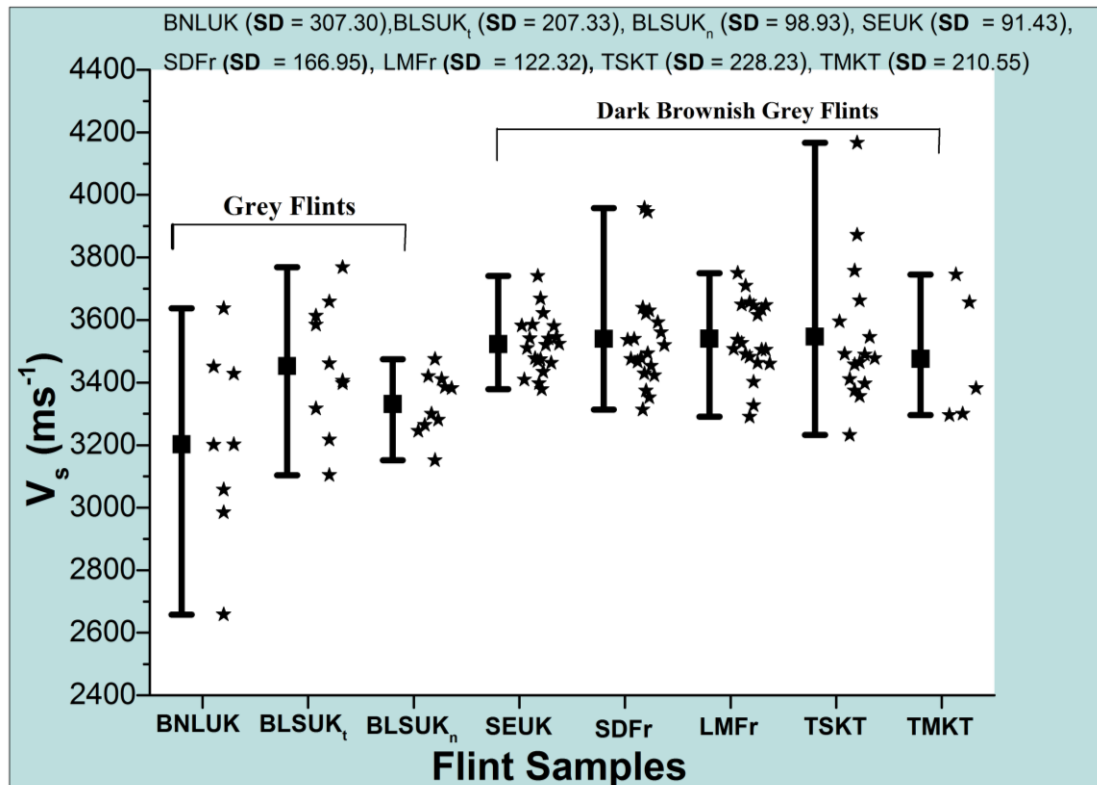


Figure 4.18: Estimated shear waves velocity ( $V_s$ ) as a function of flint colour/locations. The influence of fractures on the  $V_s$  for flint is clearly manifested in the BNLUK samples as suggested by the least average  $V_s$  observed in the sample.

The values of low strain Young's moduli ( $E_d$ ), represented in Figure 4.19, show the stiffness of flints from each study site. Figure 4.19 presents the results of  $E_d$  derived from ultrasonic pulse tests. The results indicate the stiffness of flint samples is characteristically controlled by the level of fracturing and carbonate inclusions in the samples. This observation was derived by categorising the investigated flint samples into two groups of grey and the dark brownish grey flints. The DBG samples comprising the SKT, SEUK, SDFr and LMFr showed the highest to lowest mean  $E_d$  respectively. This, however, contradicts with the lowest  $E_d$  results recorded from the BNLUK, which has pre-existing micro/macro fractures and has a greater proportion of calcite vugs. The roles of microfractures and inclusions is best explained by comparing the mean  $E_d$  for the grey BLSUK samples (BLSUK<sub>t</sub> and BLSUK<sub>n</sub>) which are not as disturbed as the BNLUK samples (which in addition to the massive fracturing have more carbonate inclusions). This comparison shows the average  $E_d$  of  $105.76 \pm 21.04$  for BNLUK is less by 18.85% for BLSUK<sub>t</sub> and 17.56% for BLSUK<sub>n</sub> samples.

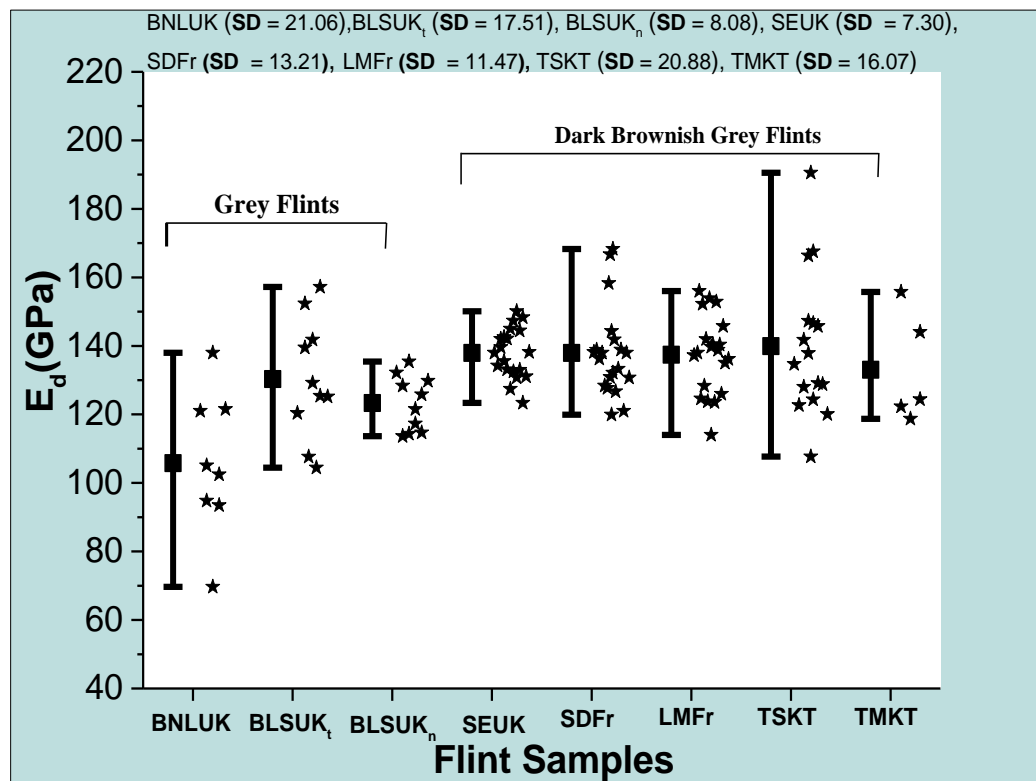


Figure 4.19: Dynamic Young's modulus ( $E_d$ ) for different flint samples investigated. The average  $E_d$  for the BNLUK samples was significantly different from the  $E_d$  of any other samples.

A One-way ANOVA was used to determine how the mean  $E_d$  for all the seven samples investigated vary. The analysis depicts a statistically significant difference between the means of the samples tested [ $F(7, 101) = 6.67, p = 1.71 \times 10^{-6}$ ]. As observed in the sonic velocities, Post hoc tests confirmed the BNLUK samples have the lowest mean  $E_d$  when compared with the mean  $E_d$  for flints from the remaining six study sites. The results of the dynamic Poisson's ratio ( $\nu_d$ ) relationships with different flint types are summarised in Figure 4.20. Figure 4.20 indicates the  $\nu_d$  of most DBG flint materials are very similar, with average  $\nu_d$  between  $0.100 \pm 0.033$  and  $0.111 \pm 0.022$ , except the TMKT, which has lower  $\nu_d$   $0.094 \pm 0.037$ . The deviation of the  $\nu_d$  for the TMKT samples from other similar materials could be due to the sampling size effects; because only five specimens were tested in the TMKT samples as against minimum of 15 specimens tested in the remaining DBG samples. By contrast, the BNLUK have the highest mean  $\nu_d$  of  $0.180 \pm 0.032$ , indicating that these particular samples will be less rigid than the DBG materials. For the BLSUK<sub>t</sub> and BLSUK<sub>n</sub>, the average  $\nu_d$  values between the two flint morphologies differ by up to 10.50% and are closer to the DBG flints than the BNLUK samples.

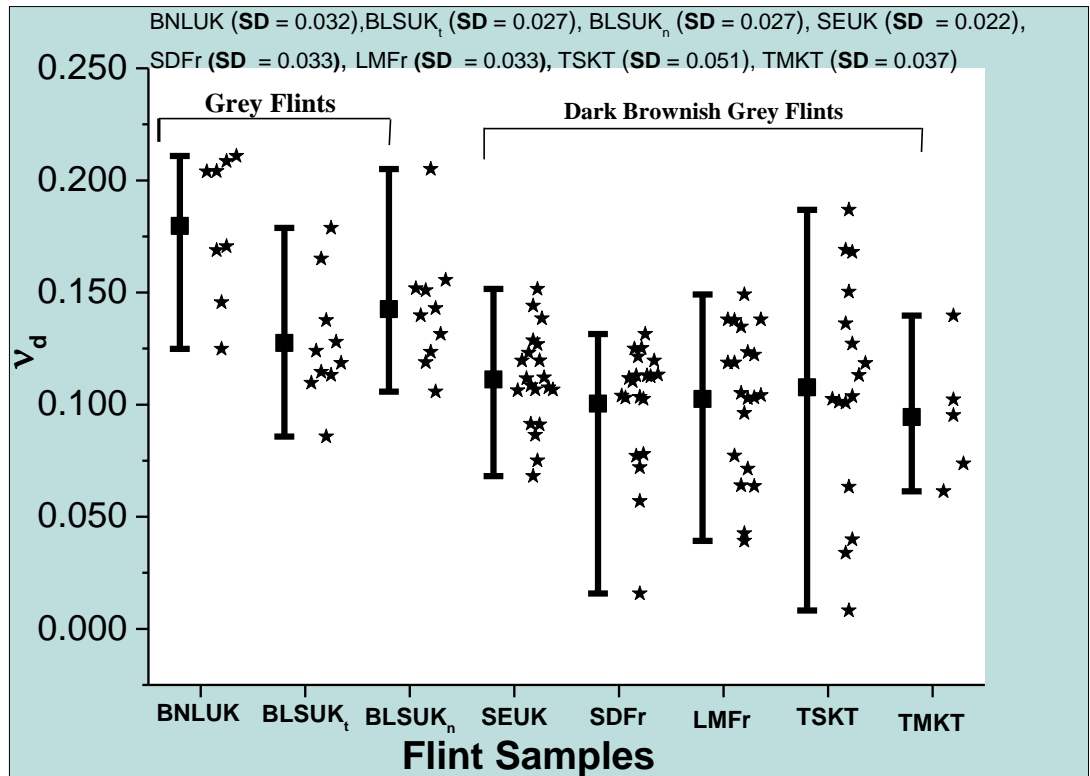


Figure 4.20: Variation of dynamic Poisson's ratio by flint type/colour, and origin. Slightly lower dynamic Poisson's ratio is observed in the dark brownish grey flints.

The differences in average  $\nu_d$  for all the samples from the study locations were analysed using One-way ANOVA and the results indicated there was no significant difference among the means  $\nu_d$  of the investigated samples [ $F(7, 101) = 0.72, p = 0.65, ns$ ]. Despite indicating no significance difference, there were slight variations in mean  $\nu_d$  between some samples. The differences in the average  $\nu_d$  shown by the different materials exist because of fracturing, probably due to the greater percentage of partially silicified rock matrices and the presence of carbonate inclusions in some samples.

#### 4.4.2 Image Analysis (IA)

The porosity ( $\phi_{im}$ ) of different flint types/colour was investigated using Image analysis (using ImageJ) on SEM images of flint samples. The ImageJ software was used to enable spot determination of the contribution of microtexture, microstructures and mineral composition (related to colour) on porosity of flints. The purpose of this is to explain the observations made in the previous mechanical tests conducted on flints. The  $\phi_{im}$  was determined by segregating the SEM images with a view to converting the

images into binary images. At this stage, it is significant to properly separate the pores/fractures from any background/noise, this is to avoid including some noise as pores. The images were then analysed and the percentage area ratio for each sample was obtained as the  $\phi_{im}$  of the sample.

Figures 4.21 and 4.22 present SEM images processed for porosity analysis using ImageJ. Figures 4.21 and 4.22 show the distribution and concentration of segregated pores (dark spots or dark lines for joints/fractures) against the backgrounds (rock particles or cement matrix in white), note the higher proportion of pores in the grey BNLUK flints than the dark brownish grey flints. This observation translates to the variation in porosity between the different colours of flints examined.

One of the advantages of using ImageJ is the ability to measure the porosity of various parts of a sample on the basis of microstructural variation. Therefore, given this advantage, different colour of flints comprising the DBG, LG and LBG were investigated. The measured porosity of these materials is illustrated in Figure 4.23. Figure 4.23 shows a broad range of  $\phi_{im}$  between flint colour/locations, with a mean porosity of flints ranging from  $0.47\pm 0.09$  % to  $4.54\pm 0.34$  % depending on colour, microtexture and geology of the flint materials. The grey BNLUK samples are the most porous flint materials when compared with any other investigated flint (Figure 4.21a). While the dark brownish grey flints are the least porous materials (Figures 4.21c-f & 4.22), and the  $\phi_{im}$  distribution within this colour is relatively uniform. The BLSUK samples have somewhat intermediate mean  $\phi_{im}$  between the BNLUK (Figures 4.21b) and the DBG flints.

It should be noted that the LBG flints have the highest mean  $\phi_{im}$  in each of the study sites. Looking at the BNLUK, it is clear the LG flints (Ave.  $4.39\pm 0.24$  %) closely succeed the LBG while the BG flints have the least mean  $\phi_{im}$ . A comparison between grey flints, BNLUK and BLSUK shows the latter (Ave.  $0.84\pm 0.08$  %) is clearly less porous than the former (Ave.  $3.53\pm 0.29$  %). This is due to the competent samples observed in the BLSUK samples as against the fractured samples of the BNLUK. The DBG flints are normally intact, stronger samples and have the lowest mean  $\phi_{im}$ , with averages ranging from  $0.47\pm 0.06$  to  $1.10\pm 0.07$  %. Most DBG flints have mean  $\phi_{im}$  below 1 %, except the SEUK, with mean  $\phi_{im}$  of 1.10 %. The relatively high mean  $\phi_{im}$  observed in the SEUK when compared with other DBG flints is attributed to the presence of samples having preserved inclusions.

In all the measured  $\phi_{im}$  for different flint types/ colour assessed, the results show the evidence of variation in porosity with colour, fracturing and to some extent locations. In most cases, the patterns in the results reflect the previous observations made from the mechanical and ultrasonic observation.

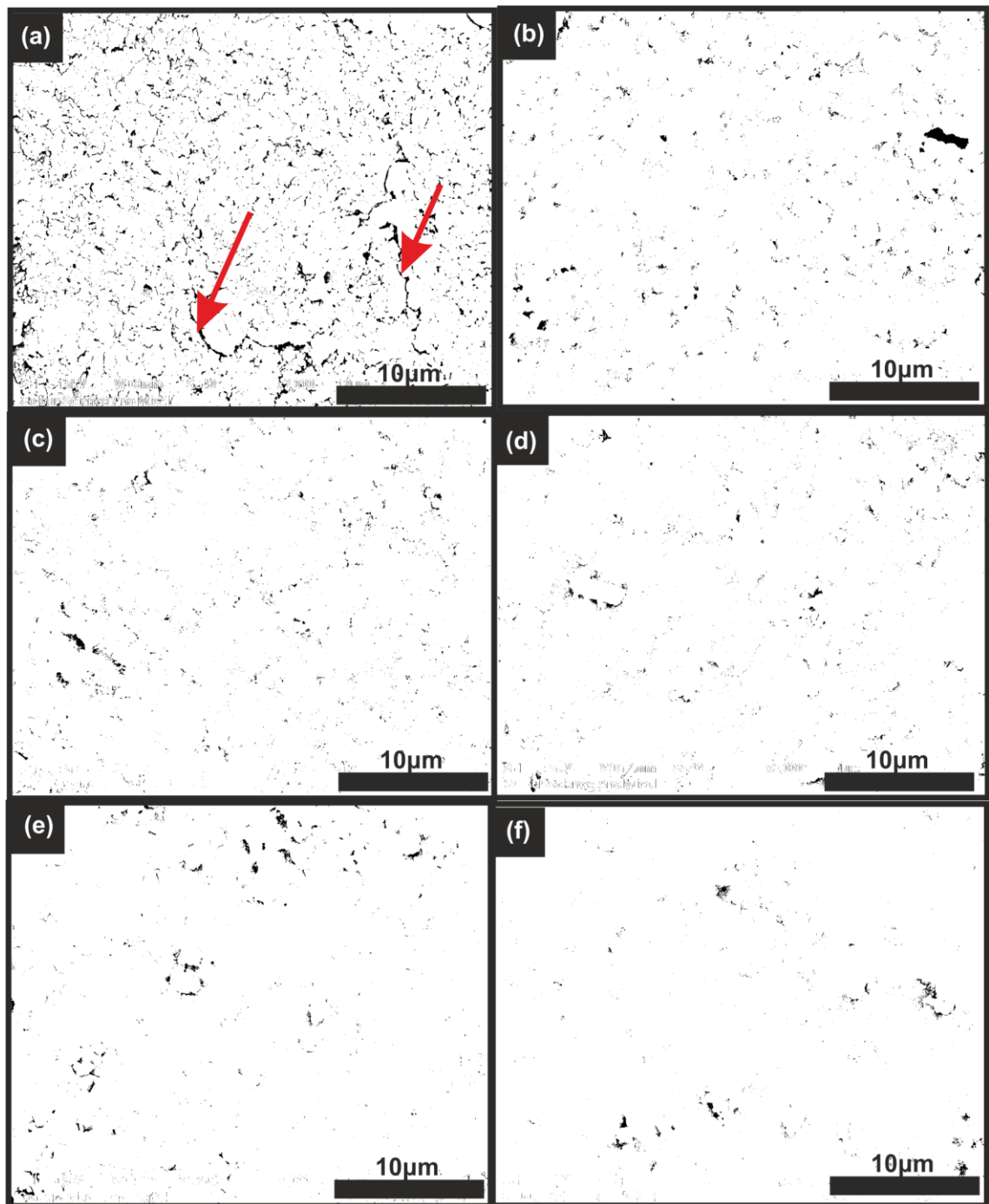


Figure 4.21: Processed SEM images for determination porosity of flints using ImageJ. (a) Highly fractured, grey flint from Burnham Chalk at North Landing, UK. (b) Grey flints from the Burnham Chalk at Lincolnshire, UK. (c) Dark brownish grey flints from the Seaford Chalk at East Sussex, UK. (d) Dark brownish grey flints from the Seaford Chalk at Dieppe, France. (e) Dark brownish grey flints from the Lewes Chalk at Mesnil-Val, France. (f) Dark brownish grey flints from the Tor Chalk at Stevns Klint, Denmark. Note red arrows indicate microfractures. Dark patches are pores while white portions are the cemented matrix.

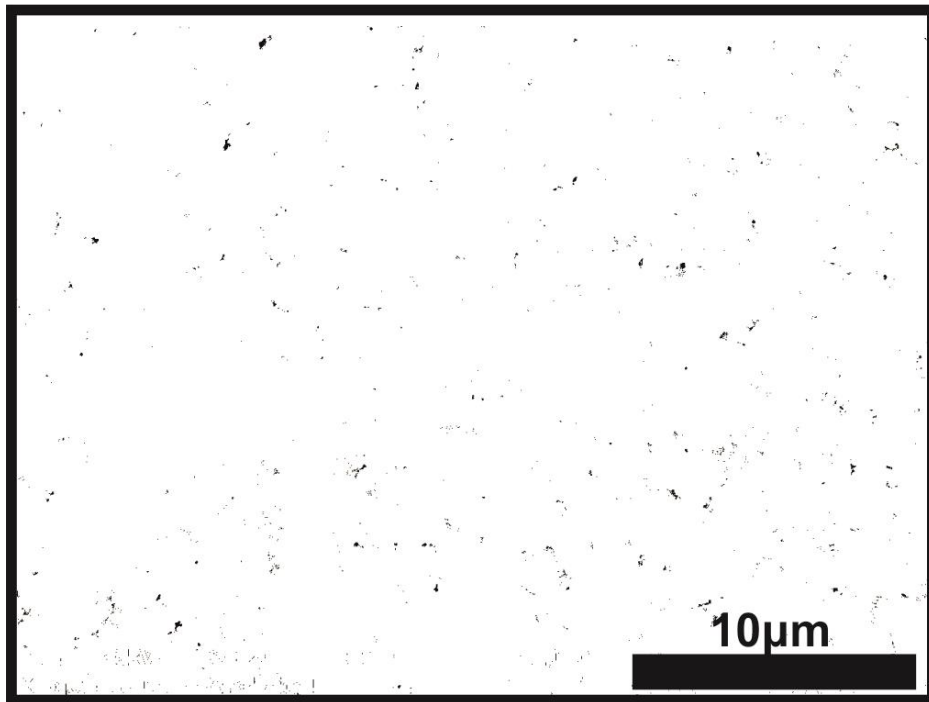


Figure 4.22: Dark brownish grey flints from the Tor Chalk at Møns Klint, Denmark. Dark patches are pores while white portions are the cemented matrix.

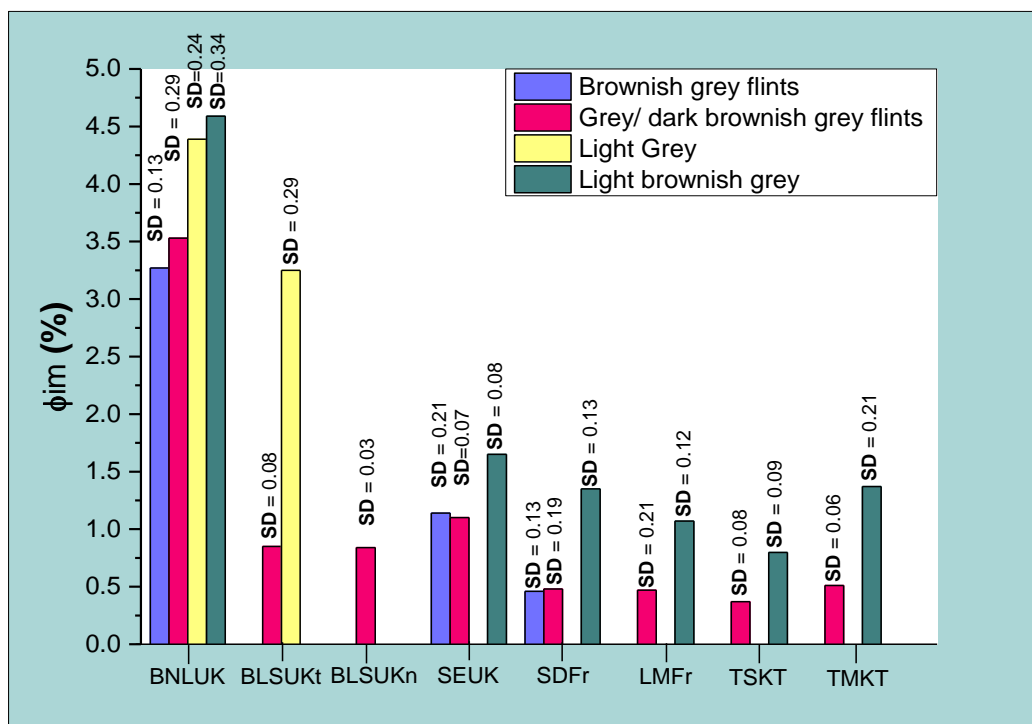


Figure 4.23: Porosity obtained from Image analysis as a function of flint origin/morphology and colour. There is clear variation in porosity of flint with colour and geology, although, higher porosity is observed in the North Landing flints.

#### 4.4.3 Porosity Trends in Flints Materials using He Porosimeter

The He porosimeter was used to determine the porosity ( $\phi_{He}$ ) of flints on the basis of colour and regional distribution. The He porosimetry was used to compliment for the sample size limitation associated with porosimetry using ImageJ. In the He porosimetry, larger flint samples meant for UCS tests were used, to improve understanding of how microstructures, microtexture, and geology affect the engineering properties of flints.

Figure 4.24 summarised the  $\phi_{He}$  derived from various flint samples and illustrates the measured  $\phi_{He}$  of flints studied varies from 0.07 to 9.19 %. The average  $\phi_{He}$  of relatively weaker, fractured BNLUK samples characterised with more granular particles is  $7.03 \pm 4.95$  %. The  $\phi_{He}$  results for the BNLUK samples (Figure 4.24), show that the  $\phi_{He}$  is influenced by an outlier with  $\phi_{He}$  of up to 17.77 %. This outlier is a flint sample dominated by several carbonate inclusions, suggesting the  $\phi_{He}$  measured on this sample was influenced by the carbonates, instead of the flints matrix or associated microfractures/joints. Excluding this outlier from the statistics yielded a value of  $\phi_{He}$  for the sample to  $5.50 \pm 2.57$  %. These samples are the most porous of all the flints investigated.

The mean  $\phi_{He}$  values for the grey, tabular (BLSUK<sub>t</sub>,  $\phi_{He} = 1.76$  %) and nodular (BLSUK<sub>n</sub>,  $\phi_{He} = 1.70$  %) flints collected from Burnham Chalk Formation at Lincolnshire is consistent and slightly higher than average  $\phi_{He}$  observed in the DBG flints (0.80 – 1.63 %). The DBG flints, however, have comparable mean  $\phi_{He}$ , with a low range of only 0.83 % between the least and the most porous of the DBG flints.

A One-way ANOVA between the means  $\phi_{He}$  for all the investigated samples showed significant differences between the flint samples [ $F(7, 53) = 6.18$ ,  $p = 2.64 \times 10^{-5}$ ]. Post hoc tests showed the BNLUK had significantly lower mean  $\phi_{He}$  than other flint materials from the remaining study sites at the 0.05 level of significance.

Thus, a general observation of Figure 4.24 shows the examined  $\phi_{He}$  of flint materials decreases from the highly fractured grey flints to the stronger more intact DBG flints. The variation observed in the investigated flint samples in terms of fracturing, and colour, corresponds with the magnitude of  $\phi_{He}$  observed between the flint colours. Nevertheless, the influence of microtexture and mineral composition might also play a role, and these will be investigated in Chapter 5 (pp. 159-195).



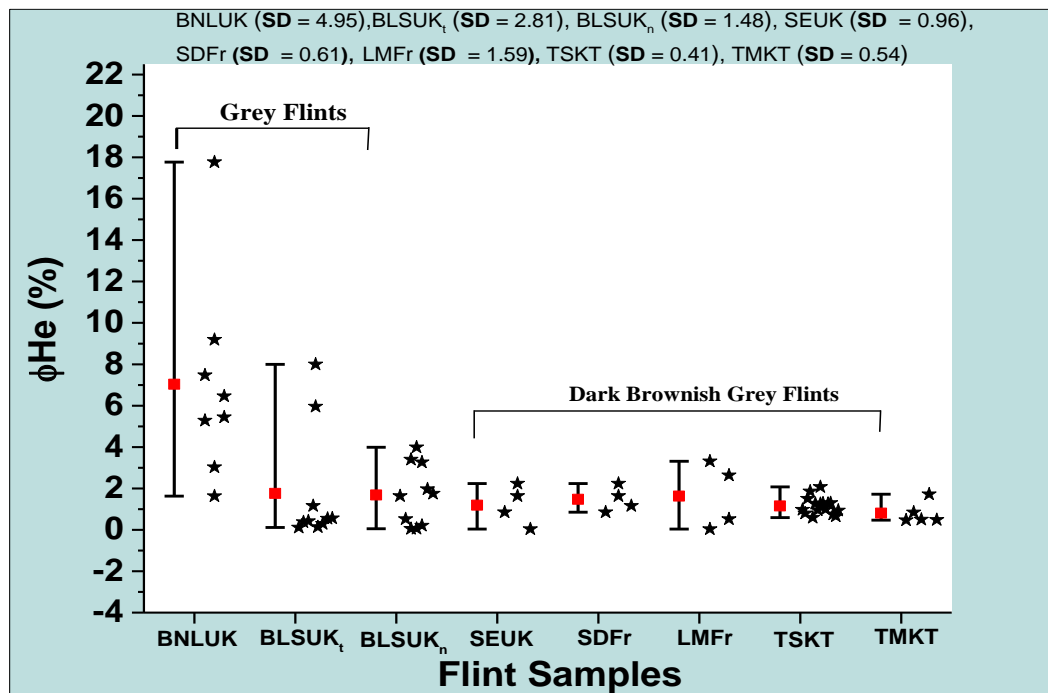


Figure 4.24: Variation of porosity with flint types, location, colour and morphology. Note a decrease in porosity from the grey flints to dark brownish grey flints.

A comparison between  $\phi_{He}$  and  $\phi_{im}$  is presented in Figure 4.25. The Figure indicates the He-Porosimetry provides higher average porosity, which in most cases is about two-fold of the mean  $\phi_{im}$ . By contrast, the difference between the average  $\phi_{He}$  and  $\phi_{im}$  for the SEUK was not clearly identified and this is associated with an outlier in the  $\phi_{He}$  results for SEUK samples, which recorded a least porosity of 0.04 % (Figure 4.25). This low  $\phi_{He}$  significantly reduced the overall mean  $\phi_{He}$  of these samples, this, therefore, explains the slight deviation seen between  $\phi_{He}$  and  $\phi_{im}$  for the (Figure 4.25).

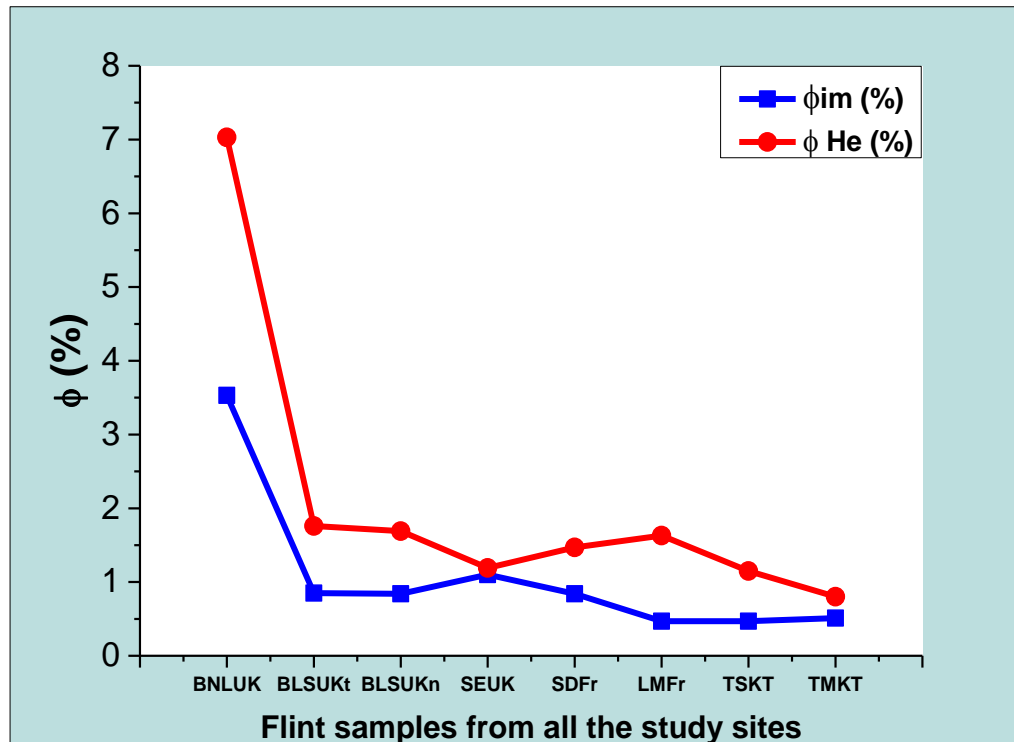


Figure 4.25: Comparison between porosity derived from Helium Porosimetry ( $\phi_{He}$ ) and ImageJ porosimetry ( $\phi_{im}$ ) as a function of flint types/geographical locations. As can be seen the  $\phi_{im}$  is lower than the  $\phi_{He}$  and constitutes about 50% of  $\phi_{He}$ , except in the SEUK this could be related to experimental uncertainties.

#### 4.5 Particle Size Distribution and Shape of Various Flint Colours and Structures

Grain size analysis was carried out on flint samples using image analysis (Image software) on the scanning electron microscopy images. The analysis was achieved by thresholding the image to segregate the quartz grains from the massive cement and pores (backgrounds) within the sample. The segregated particles were determined and the particles were then analysed and the circularity of the particles was noted. The circularity of the particles was needed to determine a suitable method for evaluating the average grain diameter from the average area ( $\mu\text{m}^2$ ). From the mean area ( $\mu\text{m}^2$ ), the minimum, maximum and average particle size ( $\mu\text{m}$ ) of each sample was determined using Equation 3.28. The particles were assumed to be perfect circles as confirmed by the circularity test, which indicates all the samples have circularity greater than 0.8. (Circularity is measured from 0 to 1, where 0 is a straight line and 1 is taken as perfect circle).

The processed SEM images for grain size analysis of different flint materials demonstrated the variation in the microtexture between the analysed flint samples are provided in Figures 4.26 and 4.27 for MKT sample. Figures 4.26 and 4.27 show the DBG flints had fewer aggregates (red spots) but possess more cemented matrix (white portions i.e. the background) when compared with the grey flints.

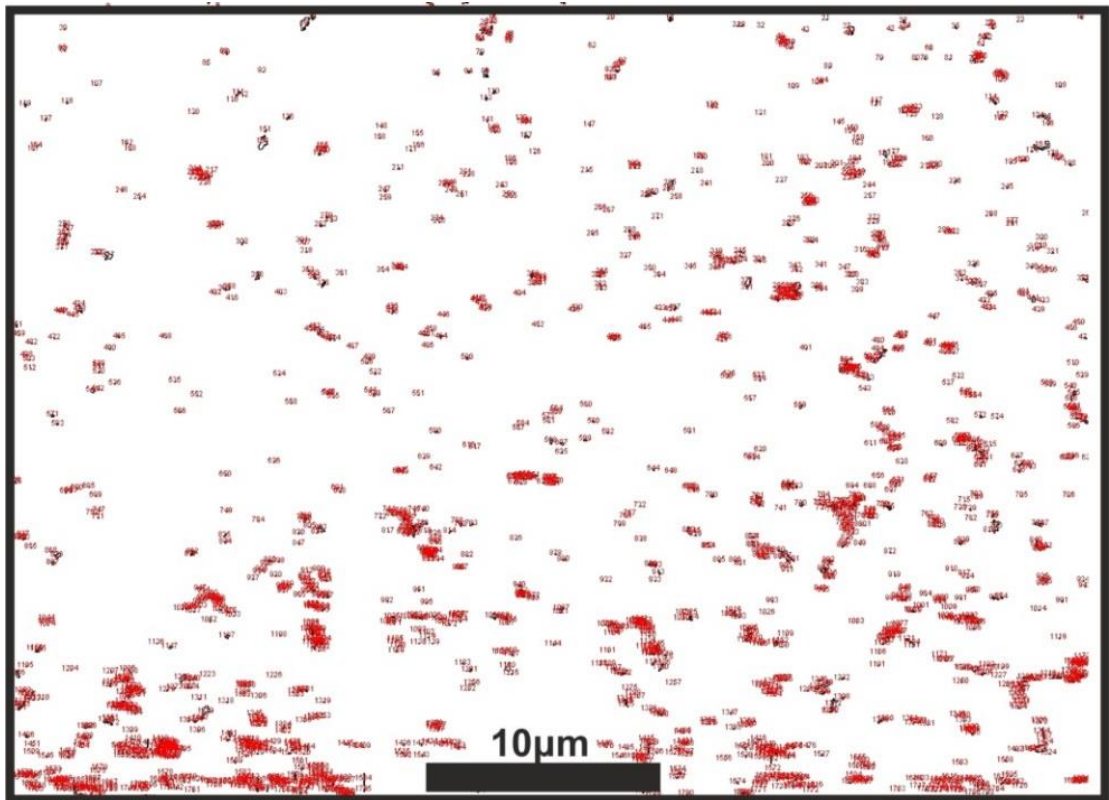


Figure 4.26: Processed SEM of dark brownish grey flints from the Tor Chalk at Møns Klint, Denmark for grain size analysis. Note: the red spots are particles or quartz grains while the white portions are the cemented/recrystallised matrix.

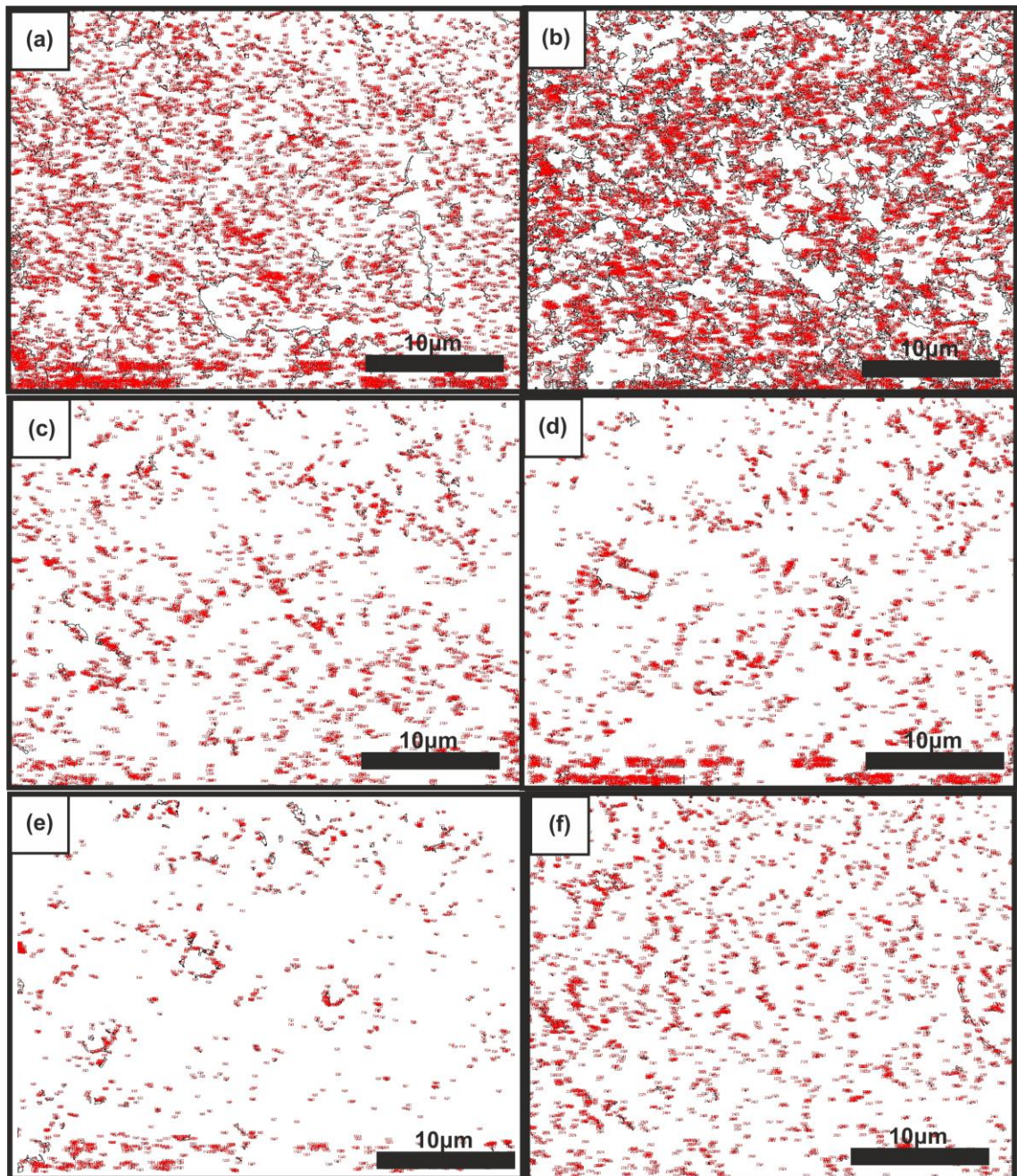


Figure 4.27: Processed SEM images for grain size analysis of flints using ImageJ. (a) Highly fractured, grey flint from the Burnham Chalk at North Landing, UK. (b) Grey flints from the Burnham Chalk at Lincolnshire, UK. (c) Dark brownish grey flints from the Seaford Chalk at East Sussex, UK. (d) Dark brownish grey flints from the Seaford Chalk at Dieppe, France. (e) Dark brownish grey flints from the Lewes Chalk at Mesnil-Val, France. (f) Dark brownish grey flints from the Tor Chalk at Stevns Klint, Denmark. Note the description is same as Figure 4.26.

The particle size of flints determined using image analysis (ImageJ) as described above is shown in Figure 4.28. Figure 4.28 illustrates the average grain size of  $0.77 \pm 0.55 \mu\text{m}$  representing the mean grain sizes for LG, BNLUK samples (carious flints) and this is the largest mean grain size observed in all the flint samples studied.

The average grain size for the BLSUK (Ave.  $0.63 \pm 0.61 \mu\text{m}$ ) is smaller than that of the BNLUK despite being of similar colour.

The DBG flints generally showed lower grain size when compared with the grey flints. The average grain sizes within the DBG flints are very similar and range from  $0.26 \pm 0.05 \mu\text{m}$  to  $0.34 \pm 0.09 \mu\text{m}$ . These similarities in the mean grain sizes are also noticed within the LBG flints. However, a slight variation was seen between the DBG and the LBG flints, with the LBG flints generally having larger mean grain size in most of the study sites. A comparison of the mean grain sizes of the BG and the DBG flints shows no evidence of significant differences between the two flint colours.

The results indicate the weaker, less abrasive grey flints have larger grain sizes and are less compact than the stronger, abrasive, and less porous DBG flints. Among the DBG flints, the larger average grain sizes represent the relatively porous, abrasive LBG materials. Although, as shown above, even between the grey flints, the relatively stronger, more abrasive, less porous and less fractured BLSUK has smaller mean grain size than the weaker, less abrasive, porous and highly fractured BNLUK samples. This, therefore, shows a combination of factors contributing to rock mass properties, grey flint is less abrasive, weaker, more porous, with larger grain size showing factors such as microtexture and mineral composition contribute to the rock mass properties enabling the differentiation between flint types.

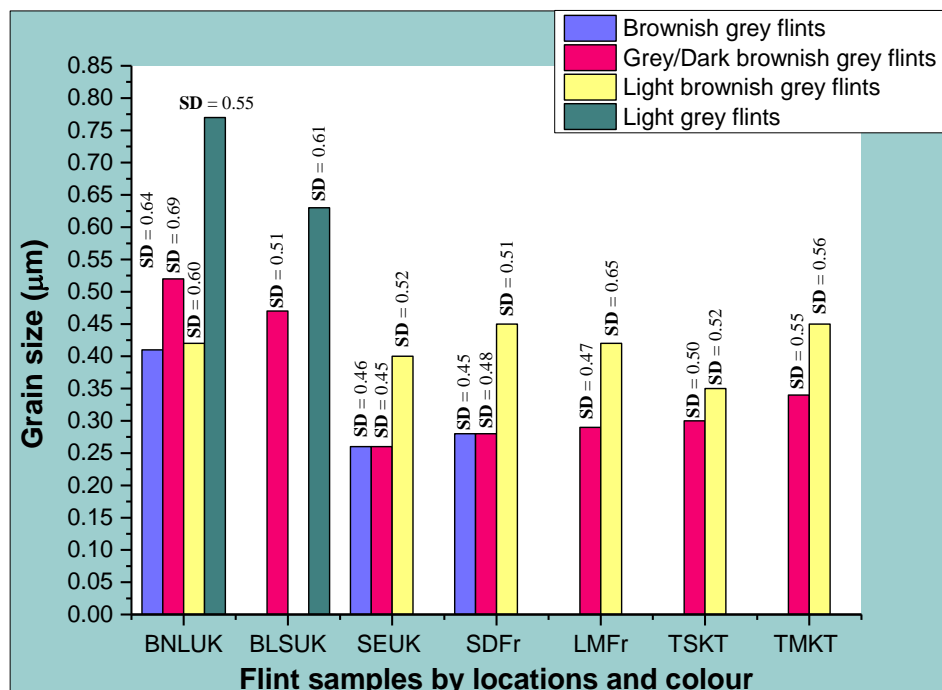


Figure 4.28: Variation of grain size for samples of flints categorised according to colour and geographical locations. Larger grain sizes are consistently observed in the light brownish grey and the light grey flints.

## 4.6 Large Scale Laboratory Drilling Test Results on Flints

Earlier reported tests on intact flints showed the physico-mechanical and petrographic properties of flints vary with colour and structures. Further tests using large scale drilling were used to see if the earlier results could be confirmed. The present section presents a corroboration of the previous observations (results from intact rock tests) using blocks of flints to examine the variation in drillability between different colour of flints. The steps applied to achieve this have already been described in Chapter 3, Section 3.9 (pp. 107-110) and Figure 4.29 (p.151) illustrates the drilling pattern observed in two formations compared.

The physical examination of the drilling pattern in the two tested units can be described by considering two drill hole patterns comprising brittle and ductile bottom hole patterns. The grey flint (Figure 4.29 d to e) indicates brittle chippings with more granular sand-sized drilling chips; where deeper drilled hole was achieved at an axial load of 1 kN under 15 mins drilling, at rotating speed of 740 rpm. By contrast, when the DBG flint was drilled under the same drilling conditions as the grey flint, the drill bit does not record any significant progress, and no drilling chips were observed (Figure 4.29 a to c), instead, dark and shiny appearances similar to that observed in the abrasivity test of this sample were seen.

A closer observation of the dark feature revealed the feature was an impression deposited on the rock as result of wearing of the drill bit. A magnified image of the drilled portion of the same sample (Figure 4.29) showed a drill surface that somewhat resembles ductile behaviour than the more brittle pattern seen in the grey sample. Figure 4.30b indicates the sand-sized drill chips seen in the grey flint, while Figure 4.30c shows the worn tricone bit after drilling through flint. The appearance of the drilled surface showed detachment initiation within the rock matrix, but could not be completed because of the strength, hardness and stronger cohesion between quartz grains in this sample. This, thus, is an indication of more cohesion between quartz grains in this sample, than in the grey flints.

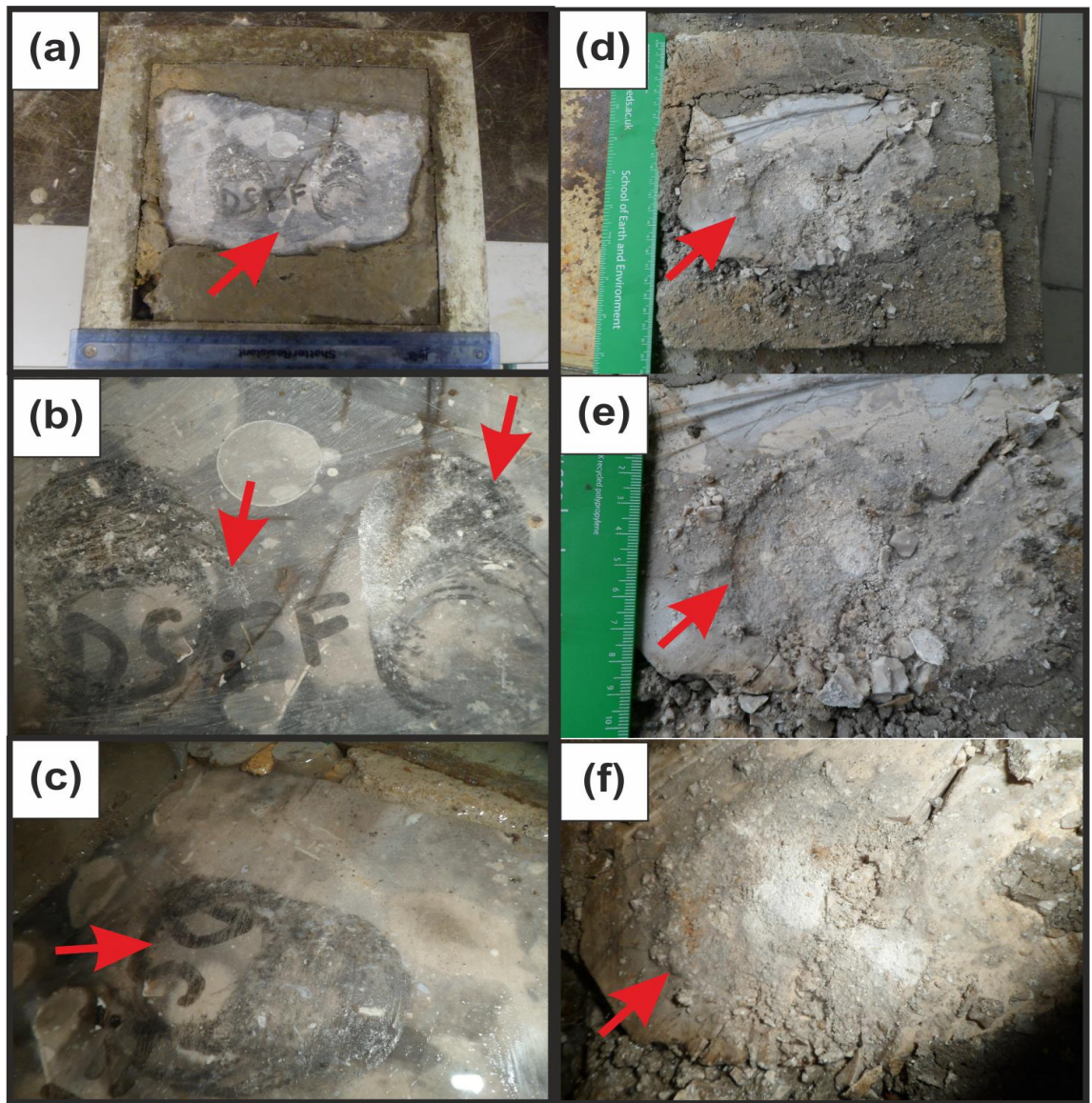


Figure 4.29: Dark brownish grey and grey flints after drilling showing different drilling patterns and grits. (a) Dark brownish grey flint at Dieppe, France showing drilling pattern. (b and c) are larger view of (a). The dark colour on the samples is worn part of the drill. Note the almost absence of drilling grits due to strong cohesion between particles of the sample. (d) Grey flint showing drilling pattern. (e and f) Larger view of the clearly showing coarser drilling grits and fracture widen by drilling.

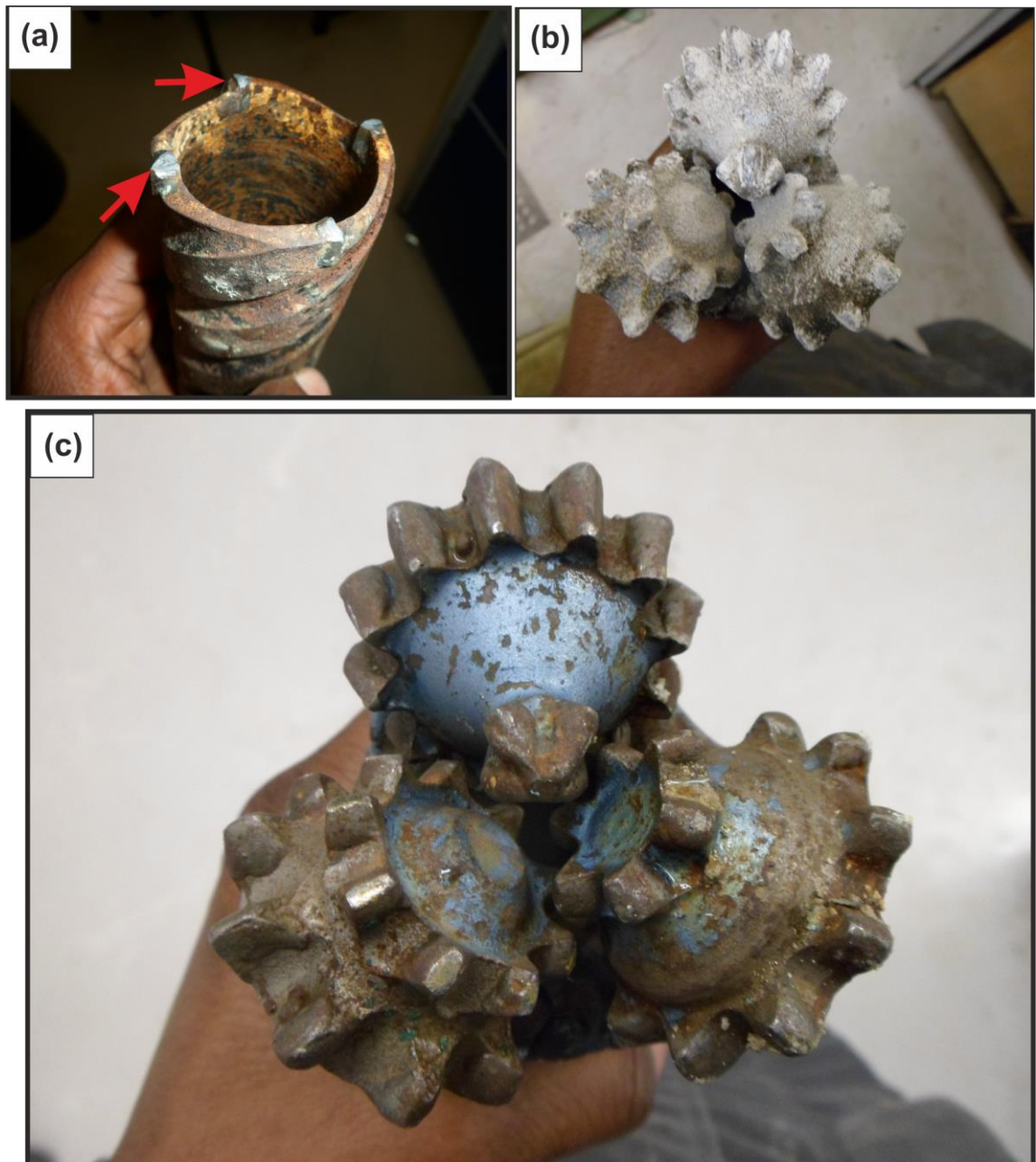


Figure 4.30: Worn drill bits after drilling through flints. (a) Damaged core bit (arrows showing broken Tungsten carbide insert). (b) Tricone bit after drilling test on flints. Note the drilling grits covering the bits. (c) Worn tricone bit after drilling dark brownish grey flints.

#### 4.7 Correlations of different Geotechnical Properties Investigated

The correlations between UCS of flints and corrected point load strength index ( $Is_{(50)}$ ), tensile strength ( $To$ ), compressional wave velocity ( $V_p$ ), and the shear wave velocity ( $V_s$ ) are shown in Figures 4.31 and 4.32. Figure 4.31a shows a trend in correlation between UCS and ( $Is_{50}$ ) defined by three clusters. The cluster enclosed in



dark represents grey tectonically disturbed flints and cluster for dark brownish grey flints shows the highest strength and are widely scattered (enclosed in blue). In between these flints categories are the data points for grey flints sampled away from tectonic disturbance (enclosed in red). The UCS- $I_{s(50)}$  relationship shows a weak linear relationship between the two parameters and suggests the  $I_{s(50)}$  cannot be used to predict UCS for flints. When the UCS- $T_o$ ,  $V_s$ , and  $V_p$  were compared, the relationships (Figures 4.31b, 4.32a, and 4.32b respectively) indicate an increase in UCS does not translate to an increase in  $T_o$  ( $R^2 = 0.12$ ),  $V_p$  (0.07) and  $V_s$  (0.10) as shown by high scattering of the data points. The low correlation coefficients seen in these relationships suggest the estimation of UCS from  $T_o$ ,  $V_s$ , and  $V_p$  is not attainable for flints.

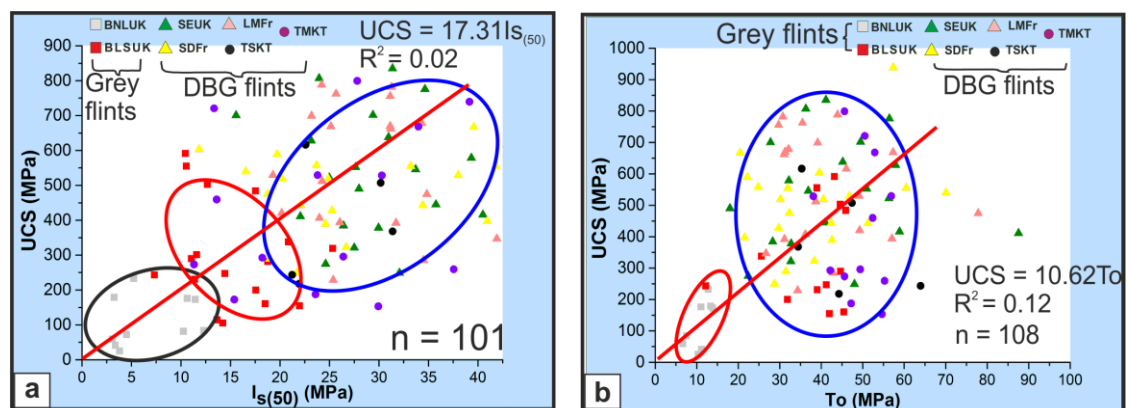


Figure 4.31: (a) Correlation between UCS and  $I_{s(50)}$ . (b) UCS and  $T_o$ .

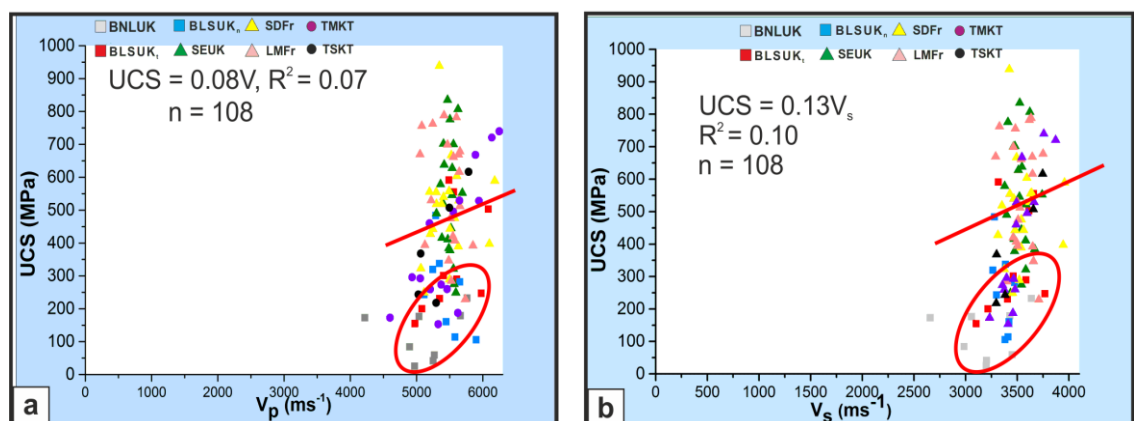


Figure 4.32: Correlation between  $I_{pf}$  and (a) Point load strength index, (b) Tensile strength.

The statistical relationship between the mean longitudinal wave velocity ( $V_p$ ) and transverse wave velocity ( $V_s$ ) is displayed in Figure 4.33. Figure 4.33 shows a clear linear correlation between  $V_p$  and  $V_s$ , with a coefficient of 0.74. As expected the relationship shows an increment of  $V_s$  with an increase in  $V_p$ . The statistical relationship

between  $V_p$  and  $V_s$  indicates a crude prediction of  $V_p$  can be achieved from  $V_s$  using a factor of 1.56.

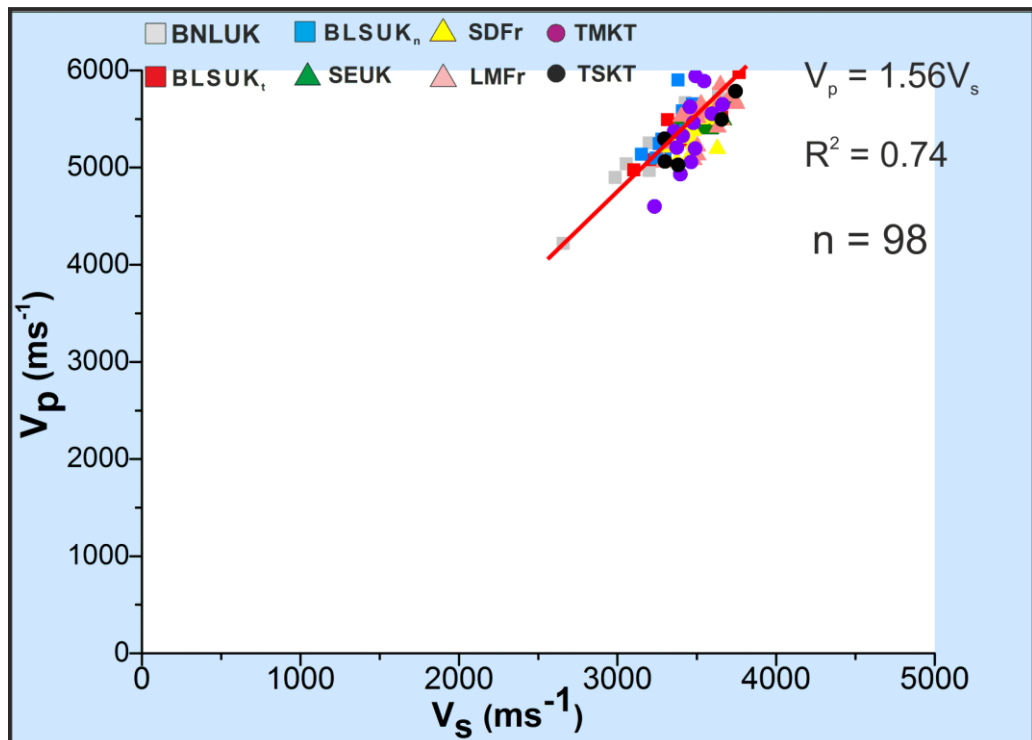


Figure 4.33: Correlation between  $V_p$  and  $V_s$  for flint samples from all the study sites.

The correlation between the mean porosity of flints obtained using He-Porosimetry ( $\phi_{He}$ ) and Image analysis ( $\phi_{im}$ ) depicts a good linear relationship, with a statistical coefficient of 0.94 (Figure 4.34). From Figure 4.34, it can be seen that a data point was specifically higher than any other data points. This data point represents the weakest and most porous sample. Since each data point represents an average porosity of flints from each study site and the comparison covers all the study sites, the specifically higher data point was needed and was used for the analysis. The observed relationship between  $\phi_{He}$  and  $\phi_{im}$  suggests that  $\phi_{He}$  can be estimated from  $\phi_{im}$  for flint samples, especially, where samples preparations for  $\phi_{He}$  proved difficult, or samples size limits the use of  $\phi_{He}$  or where fast and cheap  $\phi_{He}$  of flints is required for preliminary site investigation.

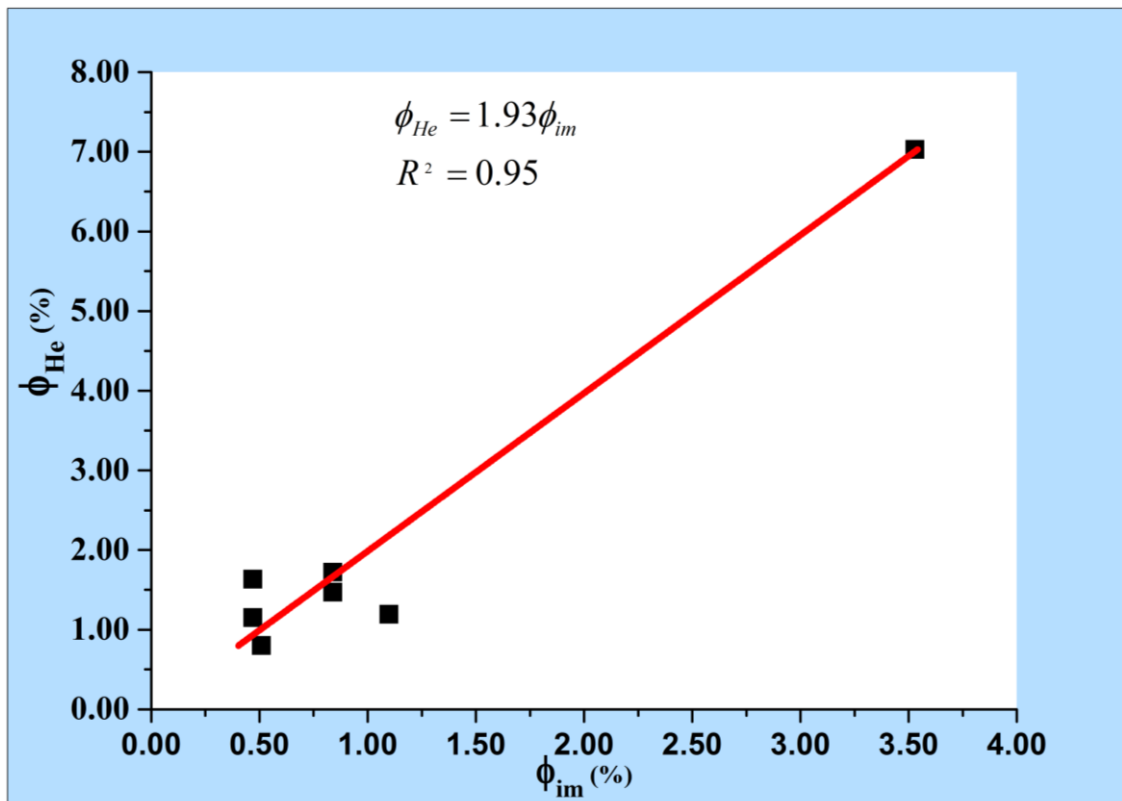


Figure 4.34: Correlation between porosity derived from Helium porosimetry ( $\phi_{He}$ ) and porosity measured using image analysis ( $\phi_{im}$ ).

## 4.8 Chapter Summary

In this chapter the physical characteristics of flints have been presented. This was done in the context of the different structures of flints (WI, WCr, and SSI) and various flint colours. These different structures/features of flints were considered because flints exhibit different colour and structure, which could depend on the location and the geological history (see Sections 2.5 – 2.9) of the flint materials.

The properties of flints examined include the strength (UCS,  $T_o$  and  $I_{S(50)}$ ), deformation ( $E_s$  and  $\nu_s$ ), abrasivity (CAI, EQC, RAI, VHNR, and SH), ultrasonic ( $V_p$ ,  $V_s$ ,  $E_d$ , and  $\nu_s$ ) and Petrophysical ( $\phi_{He}$ ,  $\phi_{im}$ , grain size, and density) for all the study sites. These parameters were compared between different characteristics, depending on the colour of flints, and local geological conditions/history. The comparisons were made using ANOVA and the relationships between parameters explored. The results of these tests and comparisons between different flint classes suggest the following:

- 1) The strength of flints varies depending on structures and colour. This is explained by the lower strength exhibited by the grey flints collected from the Burnham Chalk at Lincolnshire and North Landing. Hence structures and colour can be used to predict the drillability of flints.

- 2) Even within a site, the abrasivity of flints varies, and the chalk, and carbonate-rich samples are less abrasive than the flint materials (flint core). The influence of fracturing is also pronounced on the wear behaviour of flints. The use of CAI or geotechnical wear indices that mainly rely on mineral composition do not properly characterise the abrasivity of flints.
- 3) The ultrasonic properties of flints correlate with the observations from the strength tests.
- 4) Porosimetry derived from image analysis and He porosimetry showed obvious differences between the grey and the dark brownish grey flints, with the BNLUK flints showing the higher porosity. The porosity results by comparison show the measures made by image analysis ( $\phi_{im}$ ) underestimates porosity by 50% by comparison with  $\phi_{He}$ .
- 5) Image analysis from ImageJ shows the grain sizes of flints slightly differ between the grey and the dark brownish grey flints.
- 6) Despite the limitations of some of the testing techniques, One-way ANOVA analysis shows the grey flints at the North Landing are significantly different from the other flints sampled.
- 7) Empirical models derived using linear regression showed variable correlations between engineering properties of flints.

Finally, since variations are observed between flint types, colour, locations and structures, the question on what are the causes of these differences is raised. Are the properties of flints controlled by the geology of the site, mineral composition or microtexture? Why do some testing methods fail to characterise flints properly? These questions will be addressed in Chapter 5.

## **Chapter 5 Microstructural and Mineralogical Characterisation of Flint Materials and the Surrounding Chalk**

### **5.1 Introduction**

In Chapter 4 the material properties of flints were observed to vary between flint colour, structures and flint geographic locations in relation to the strength, abrasivity and drillability of flints. The chapter was then concluded by questioning the causes of these variations. Such questions included the control or differences in microstructures, local geology, mineralogy, geochemistry and/or preservation of fossils/inclusions have had on the test results. The reasons for the inability of some testing techniques to characterise flints properly was also questioned. To answer these questions flint samples from the study sites, representing various colour, structures and origin were examined using petrographic approaches. The petrographic techniques used for this investigation comprised of SEM, XRD, thin section petrography, and SEM-CL. The petrographic data were quantified using micropetrographic index ( $I_{pf}$ ). A correlation between strength, abrasivity and  $I_{pf}$  is presented. This chapter, presents and interprets the data derived from these observation.

#### **5.1.1 Chapter Layout**

This chapter is structured into seven major sections presenting data derived from applying different approaches to characterising flints and the surrounding chalk. Following the introductory section, section 5.2 presents the experimental data for the characterisation of microstructures of flints depicting various degree of silica cementation in different flint types, flint colour, flint structures and the surrounding chalk. There is also a comparison with the microstructural features between chalk surrounding flints, the white crust surrounding grey and the dark brownish grey flints. The data for mineral phase identification and quantification of different colour of flints, flint structures, and the surrounding chalk examined using XRD analysis is presented in section 5.3. The quantified minerals were also compared among different flint types and the associated features in this section. The relationships between flint mineralogy and the trend in the material properties of flints is also presented in this section.

In section 5.4 the microtextural features of flints and the surrounding WCr, the preservation of microfossils, the calcite-silica transition phases, and the presence of inclusions are presented and comparison were made among different flint types and structures. In section 5.5 the microstructural observations of flints, with emphasis on

the presence of impurities, and the types of fabrics/phases identified in the samples is presented. The abundance of preserved fossils and the proportion of inclusions were presented and analysed between flint types, colour and structures. Section 5.6 presents  $I_{pr}$  of flints and the relationships between this property and the abrasivity as well as strength of flints. Section 5.7 provides the overall summary of this chapter and briefly introduces Chapter 6.

## **5.2 Surface Micromorphology and Silica cementation in Flint Materials**

### **5.2.1 Scanning Electron Microscopy of Flints, White Crust and Surrounding Chalk**

To reveal the microstructural features of flints and to compare these microstructures across various locations and flint colour, SEM analysis was used on both rough and polished flint samples, and the chalk surrounding flints. The results of this analysis are presented in Figures 5.1 to 5.13.

#### ***Chalk Surrounding Flint***

Figures 5.1a to d show the SEM photomicrographs of chalk surrounding flints from four different study locations. As expected, these samples predominantly comprised of calcite crystals and well-preserved coccoliths (red arrow) are intermittently scattered in the samples. Texturally, the BNLUK samples (Figure 5.1a) appeared denser, less porous and calcite crystals in the samples are more compacted than the SEUK, SDFr, and LMFr (Figure 5.1 b-d). Thus, the variation in porosity and density observed between these chalk types, could contribute in shaping the material properties of flints through post diagenetic processes associated with rock-water interactions.

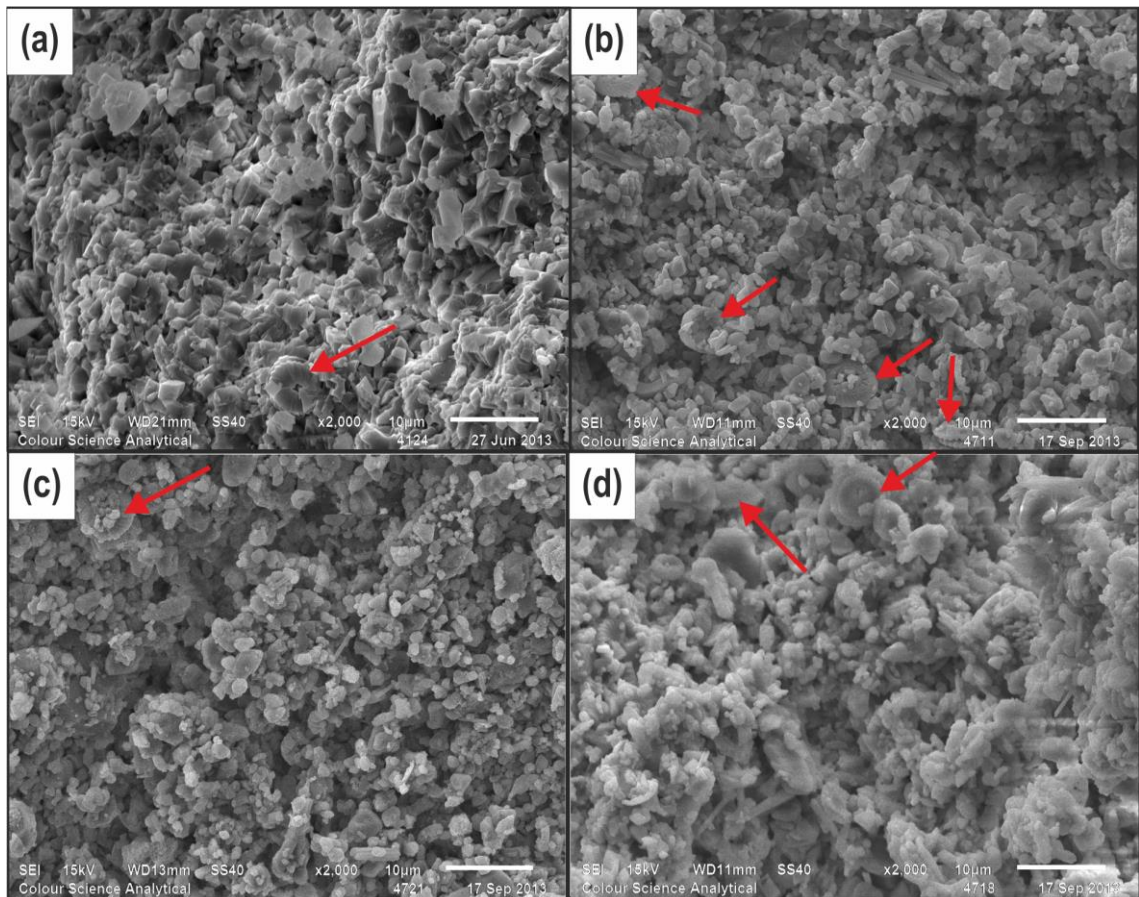


Figure 5.1: SEM secondary images of chalk surrounding flints. (a) Burnham Chalk at North Landing, UK. (b) Seaford Chalk at East Sussex, UK. (c) Seaford Chalk at Dieppe, France. (d) Lewes Chalk at Mesnil-Val, France. The presence of preserved Coccoliths can be seen in all the samples (red arrows). A denser and less porous texture is observed in the Burnham Chalk, North Landing than seen in the remaining samples.

#### *White Inclusions (WI) in the Flint*

The white inclusion (WI) and the silicified white inclusion (SSI) have features, which suggest their genesis from the host (Figure 5.2a-d) chalk. Firstly, the samples indicate the presence of calcite crystals similar to that observed in the surrounding chalk. Secondly, in the white inclusions (Figure 5.2 b and d) preserved coccoliths fragments (red arrows) are noticeable in the samples, thereby showing a likely direct link between these samples and the surrounding chalk (with calcite content from 96-99 %). Comparing the micromorphology between these samples, the WI in the BNLUK ( $\phi_{im} = 3$  %) sample (Figure 5.2a) are more fragmented and possesses smaller spherical calcite grains c.  $1.23 \mu\text{m}$ , than the SWI (Ave. c.  $1.64 \mu\text{m}$ ,  $\phi_{im} = 3$  %), SSI (Ave. c.  $1.64 \mu\text{m}$ ,  $\phi_{im} = 2$  %) and WI (Ave. c.  $1.46 \mu\text{m}$ ,  $\phi_{im} = 9$  %) (Figure 5.2b-d). The silicification of some

calcite grains and the fusion of silica grains in this sample have commenced, as evidenced in Figure 5.2a.

Although, most of the samples have similar microstructures, the preservation of coccoliths fragments are only seen in the SWI (Figure 5.2b) and WI (SEUK, Figure 5.2d), but are absent in the WI (BNLUK, Figure 5.2a). The WI, BNLUK samples appear less porous and compact, with spherical and agglomerated quartz and calcite grains. The differences in microstructures between the WI (BNLUK) and the WI (SEUK) reflect the abrasivity results recorded in this study. Meanwhile, the microstructures of the SSI (Figure 5.2c) have larger quartz crystals, and fewer calcite crystals (with calcite content c. 42.29%) than all the studied inclusions (86.12 – 98.75 %).

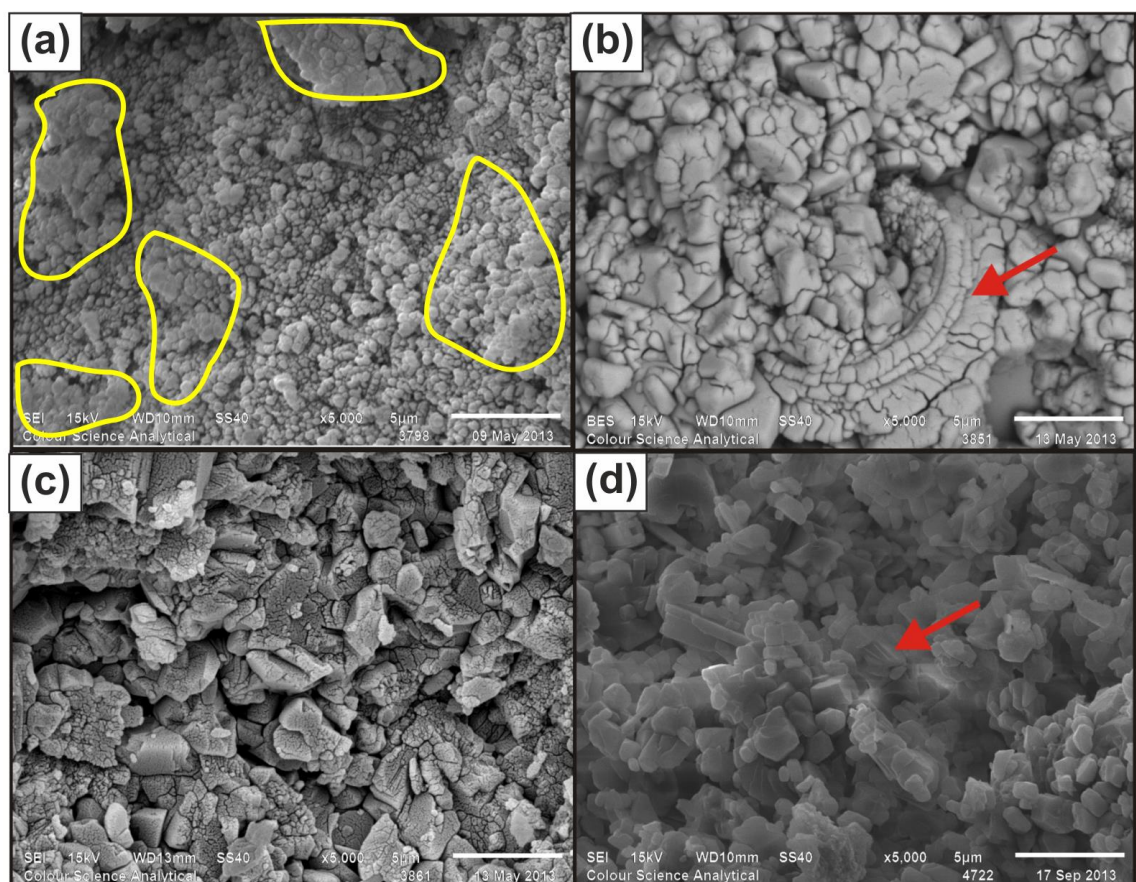


Figure 5.2: SEM secondary images of carbonate inclusions in flints. (a) White Inclusion (WI) in the flints collected from the Burnham Chalk at North Landing, UK. (b) Spotted white inclusion (WI) in the flints from the Burnham Chalk at North Landing, UK. (c) Silicified spotted inclusion (SSI) in the flint samples (this is inclusion with dark spots and have some silica) from the Burnham Chalk at North Landing, UK. (d) White inclusion (WI) in the flint samples from the Seaford Chalk at East Sussex, UK. The red arrows show some preserved Coccoliths fragments.



### *White Crust (WCr)*

The SEM micrographs of white crust (WCr) surrounding flints are presented in Figures 5.3 a-d. Microtextural differences can be seen between the WCr surrounding grey flints (usually softer and thicker c. 20 mm) (Figure 5.3a) and the WCr enclosing the DBG flints (Figure 5.3 c and d) which is mostly harder, thinner, and mostly less 10 mm. The WCr surrounding grey flints have microtextures comprising of calcite crystals, which are gradually replaced by both amorphous and cryptocrystalline quartz. The quartz crystals in this sample is larger (c. 1.28  $\mu\text{m}$ ) and intercrystalline porosity (10.97 %) is noticed in this sample.

While the WCr surrounding the DBG flints (with porosity ranging from 2.24 – 3.55 %) have very fine texture of the cryptocrystalline quartz in most parts of the samples and some quartz crystals, which in some cases have recrystallised and precipitated resulting in the formation of quartz cements (red enclosures). The presence of quartz flakes and quartz grains/crystals (1.15 – 1.17  $\mu\text{m}$ ) are also evident. The quartz grains appear to form clusters of quartz granules, seen intermittently on various spots in the samples. The dense texture and quartz cements characterising the matrix of this WCr explain the higher abrasiveness and hardness seen in these materials as opposed the WCr surrounding the grey flints.

### *White Crust Surrounding Grey Flints*

Figure 5.3b shows the flint-crust boundary from the BNLUK samples. An image of this sample is shown in Figure 5.4 at greater magnification. In Figure 5.4, a sharp boundary can be seen between WCr and flint. At this boundary, the gradual replacement and silicification of calcite crystals are observed. The precipitation of quartz cements from the dissolution of quartz grains are also noticed at this boundary. The various textures of the WCr are also seen, a mixture of amorphous silica, quartz flakes, and recrystallised quartz grains are also observed. The flint portion however, clearly appears more dense, homogenous and less porous than the WCr, with only a few traces of intercrystalline porosity in the flint samples, especially, towards the edges of the WCr-flint boundary.

### *White Crust Surrounding Dark Brownish Grey Flints (DBG)*

Figure 5.3 c and d indicate the WCr from the dark brownish grey (DBG) flints surrounding the flints collected from the Seaford Chalk at the East Sussex and Dieppe respectively. These figures showed the similarity in microstructures between the two

materials. The microstructures of both samples are made up of two components. The first component can be described as very fine, amorphous quartz while the second component comprises of a dense, and cemented silica matrix.

Thus, from the above observations, the larger calcite and quartz grains/crystals ( $1.28 \mu\text{m}$ ,  $\phi_{\text{im}} = 10.97 \%$ ) observed in the WCr surrounding the grey flints (Figure 5.3a) illustrates one of the reasons for the weakness and less abrasiveness of the WCr surrounding grey flints, when compared to the more cemented WCr enclosing the DBG flints. Meanwhile, the finer quartz grains (c.  $1.15 \mu\text{m}$ ) observed in the WCr enclosing the DBG flints explain why the sample is stronger, less porous ( $2.24 - 3.55 \%$ ) more abrasive and harder than the former WCr surrounding grey flints.

### *Flint-Crust Relationship*

The relationship between WCr and the flints can be illustrated by examining Figure 5.5 a to d. In the figures, the boundary between flints and the WCr is clearly displayed (see Figure 5.5a SEI for flint-crust boundary). The growth of flints seems to involve the dissolution and replacement of calcite, by silica which later transformed into dense, homogenous massive quartz cement. Figure 5.5b is the sample analysed, while Figure 5.5c separately shows the flint and Figure 5.5d illustrates the WCr. The figures clearly indicate textural differences between the WCr and flints, where the WCr appears more porous, than the denser and more cemented flints.

Although, these figures clearly show a variation between the different features, the external morphologies were not clearly portrayed because, in Figure 5.5 polished thin section was used for the SEM, while in Figure 5.3, rough samples were used. Therefore, for the characterisation of external micromorphology of flint using SEM, the use of rough sample is recommended. This provides more detail of the fine matrix of flints than the thin section using the polished samples, because the grain profiles must have been ground off.

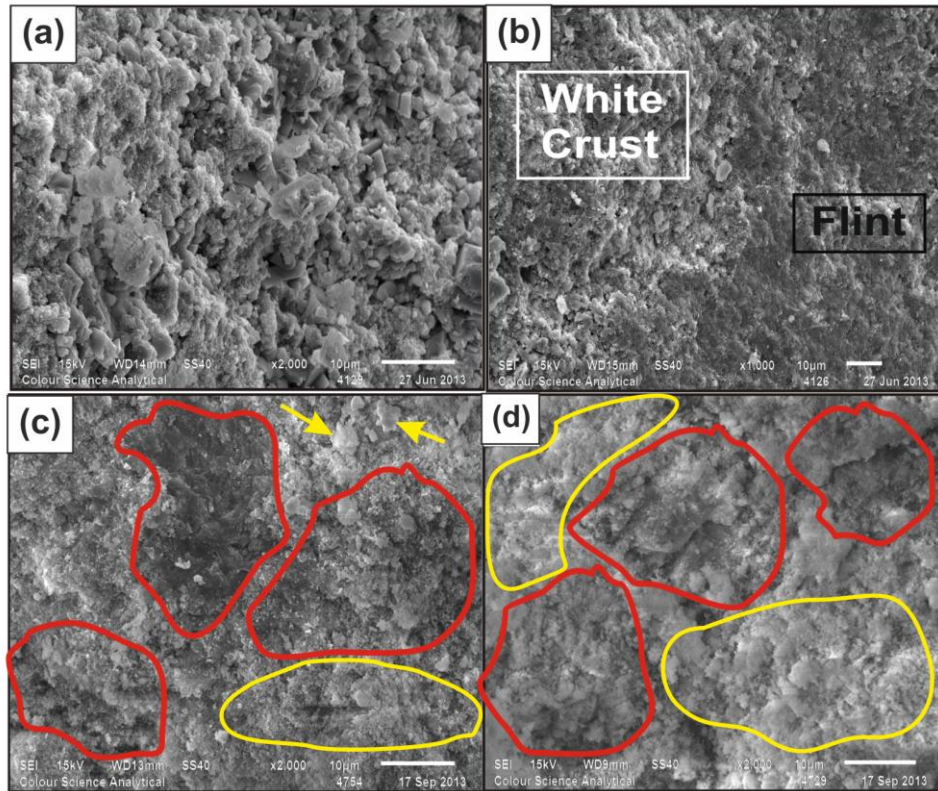


Figure 5.3: SEM secondary images of White crust (WCr) surrounding flints. (a) White crust surrounding BNLUK. (b) Flint-white crust boundary representing BNLUK. (c) White crust surrounding SDFr. (d) White crust surrounding SEUK. Note the gradual gradation between the flint and the WCr. Areas of massive silica cements are also evidenced in the WCr from the SDFr and SEUK( enclosed in red, Figure 5.2 c and d).

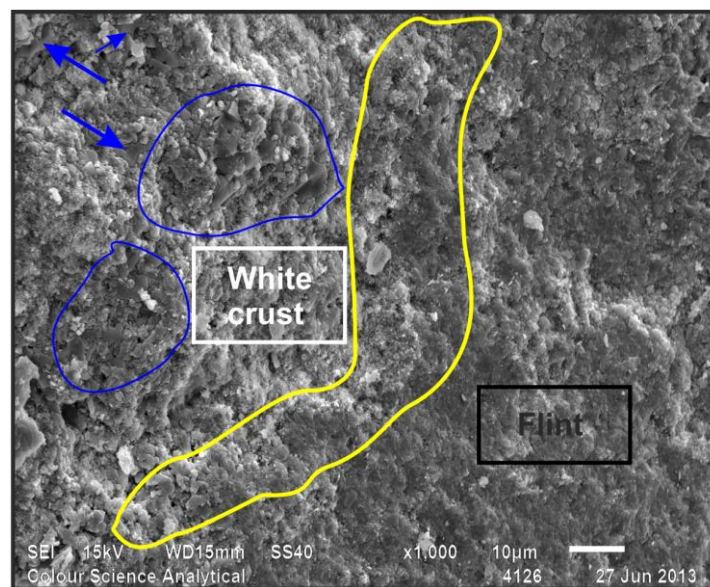


Figure 5.4: Same as 5.3 (b) but magnified version to show the fusing of silica grains/crystals into dense and harder matrix.

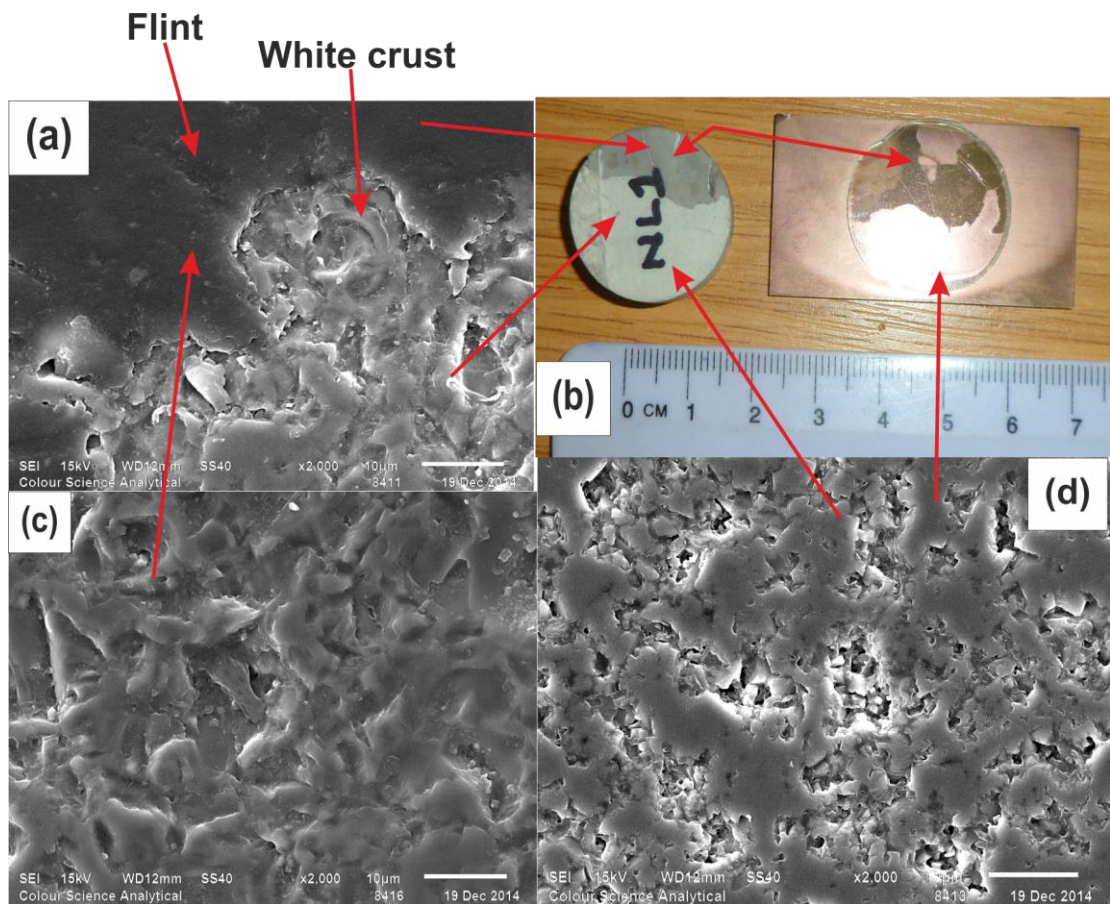


Figure 5.5: (a) Scanning Electron Image (SEI) of flint-crust boundary from the North Landing Flint. (b) Sample used for the SEM analysis with the uncovered polished thin section used for the analysis. (c) SEI of only the flint segment of the samples. (d) SEI of the crust segment of the sample. A textural variation can be seen between the darker flint and the more porous white crust.

#### *Light Grey (LG) and Light Brownish Grey Flints (LBG)*

The microstructural observation of LG and LBG flints using SEM on rough samples are shown in Figures 5.6 a to f and Figure 5.7. The figures illustrate that these samples comprise homogenous cryptocrystalline quartz (Section 5.3, pp. 172-177) as the dominant mineral, with occasional calcite. SEM examination of the LG flints, BNLUK (Figure 5.6a) showed a distinct microtexture characterised with discrete equigranular, spherical quartz grains (ave.  $0.77 \mu\text{m}$ ), also see Figure 5.8. These grains are agglomeration of quartz crystals forming crumbs of larger quartz clots. Intergranular microfractures are also evident (red arrows) and microspherules are seen in this sample (see Figure 5.8 for larger image). Unlike, the light grey flints, BNLUK (Figure 5.6a); the LG flints, BLSUK (Figure 5.6b) shows a different microtexture which is closer to that of the LBG flints, than the BNLUK flints. The micromorphology of the BLSUK shows cemented and remarkably less void in the structure. Spherical quartz grains

(0.63  $\mu\text{m}$ ) were also seen in the samples and have apparently coalesced, thereby forming a dense and flaky matrix.

The more compact and less porous microstructures observed in the LG (BLSUK) explains the higher abrasivity and the hardness results (presented in Chapter 4) recorded by the sample than the LG (BNLUK). Conversely, the LBG flints (Figures 5.6 c to f and Figure 5.7) demonstrated some significant areas of massive quartz cements when compared with LG flints, particularly, the LBG flints, SEUK (0.40  $\mu\text{m}$ ), SDFr (0.45  $\mu\text{m}$ ), and LMFr (0.42  $\mu\text{m}$ ) (Figures 5.6 c, d and e respectively). The microstructures of these samples are very similar, and the traces of previous larger quartz crystals that were not completely melted can be observed, but the samples still have less porous and dense microtextures than the LG flints.

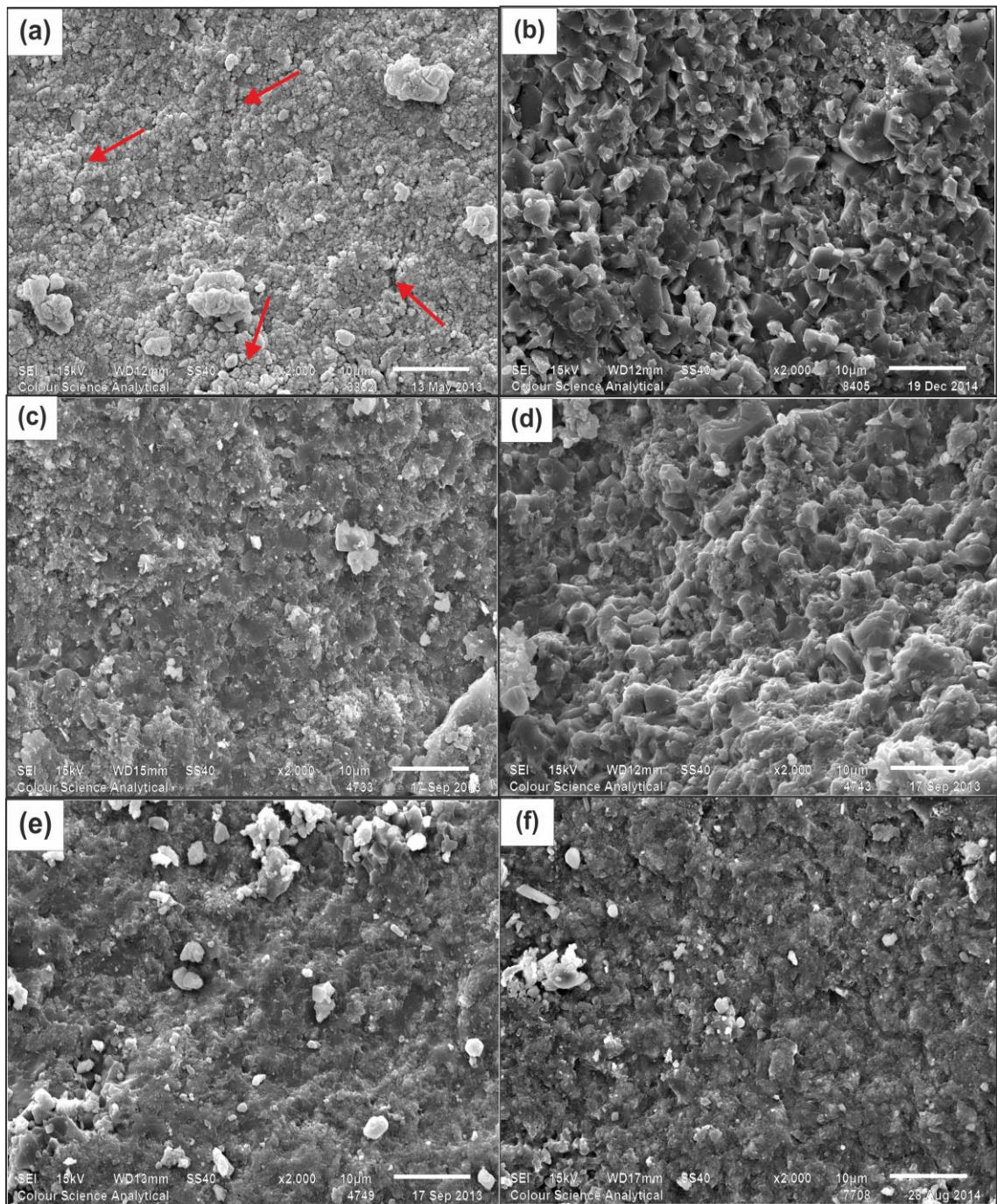


Figure 5.6: SEM secondary images of flints. (a) Light grey flint, BNLUK (larger image of (a) is shown as Figure 5.8). (b) Light grey flint, BLSUK. (c) Light brownish grey (LBG) flint, SEUK. (d) Dark brownish grey (LBG) flint, SDFr. (e) Light brownish grey (LBG) flint, LMFr. (f) Light brownish grey (LBG) flint, TSKT. The red arrows indicate intercrystalline/intergranular microfractures. Note the difference in degree of silica grains/crystals cementation/cohesion between 5.6 a and 5.6 b-f.

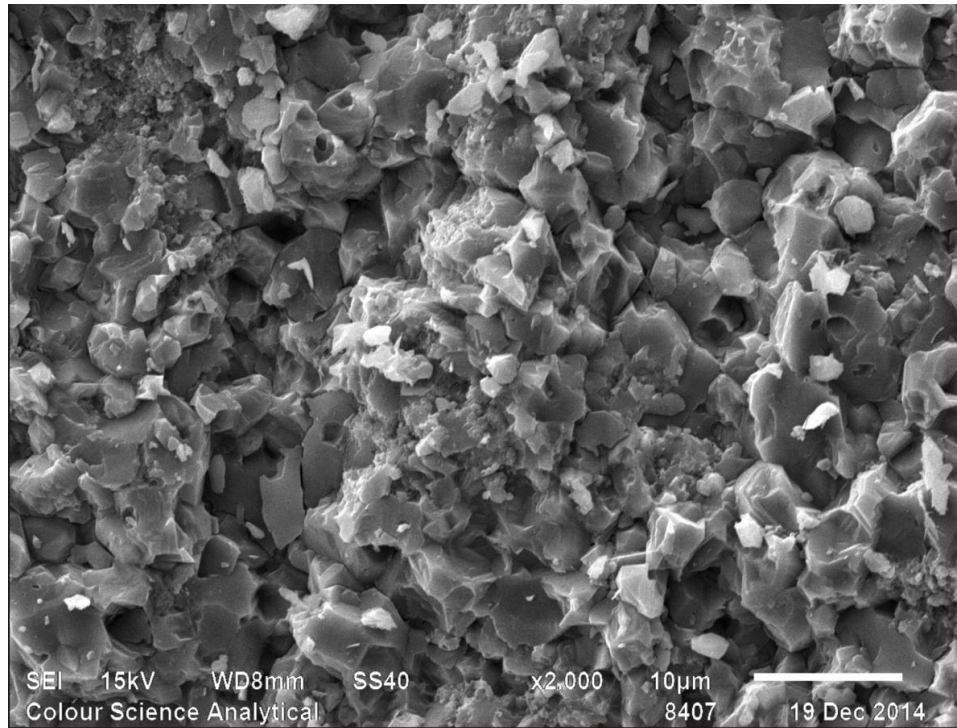


Figure 5.7: Light brownish grey flint from Tor Chalk at Møns Klint, Denmark.

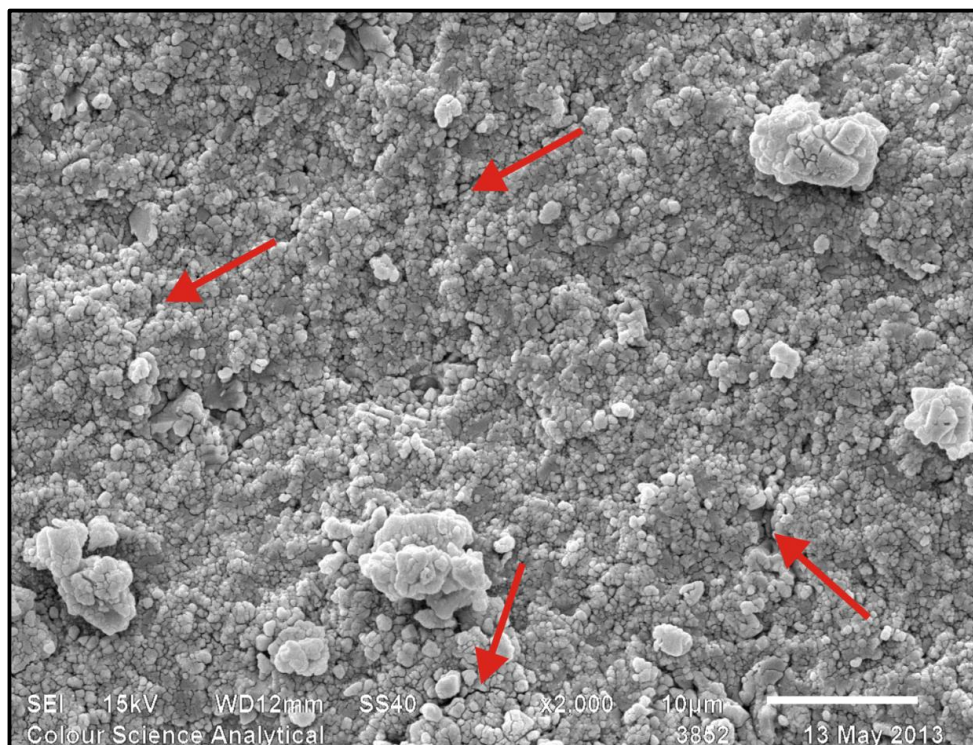


Figure 5.8: Same as Figure 5.6a, but this is an enlarged version to show the intercrystalline and intergranular microfractures/pores. The spherical shapes of the quartz grains and the granular texture are clearly seen in this figure.

### *Brownish Grey Flints (BG)*

The SEM examination of brownish grey flints (BG) is shown in Figures 5.9a to d. All the BG samples are dominated by cryptocrystalline quartz (see Section 5.3, pp. 173-177) as expected, but with different microstructures. Figure 5.9a presents the BNLUK samples, which exhibit an exceptionally, different microtexture from the remaining three samples (Figures 5.9b to d). The BNLUK sample demonstrates a fabric dominated partly by spherical quartz aggregates (enclosed in red) formed by agglomeration of the quartz microspheres. The presence of microfractures are also seen (red arrows) in the sample.

A comparison between the BG flints (Figure 5.9a, 0.41  $\mu\text{m}$ ) from the BNLUK (predominantly grey flints) and the BG flints (c. 0.28  $\mu\text{m}$ ) found within the DBG flints (Figure 5.9b to d) showed the BNLUK samples differed microstructurally. And all the observed features that influence the strength and abrasiveness (microfractures, and quartz grains) of the BG flints (BNLUK) are clearly absent in the BG flints found within the DBG flints (Figures 5.9b to d). These samples displayed uniformly dense masses of cryptocrystalline quartz dominated by more quartz cement when compared with both the BG (BNLUK) and the LBG. The proportion of large quartz crystals previously observed in the LBG flints has clearly reduced in the BG flint samples, with most of the quartz grains/crystals being precipitated out leaving only a few traces at some spots. This results to a clear manifestation of high degree of silica cementation, which dominates the matrix of these samples. Therefore, the possession of more dense masses, and less preserved quartz crystals in these samples explain the abrasiveness, hardness and porosity results for these materials presented in Chapter 4 (Sections 4.3 & 4.4).

A high magnification of BG flints (BNLUK) depicting the peculiar microtextures of the sample can be seen in the Figure 5.10. The figure indicates more silica cementation (enclosed in red) in this sample (with c. 20 % cement and c. 80 % grains) than observed in the LG flints (BNLUK) from the same site and this explains why the BG, BNLUK was noticed to be more abrasive, harder, and less porous (Chapter 4, Sections 4.3 & 4.4). The intercrystalline microfractures (red arrows) and intergranular micropores are also clearly displayed in the sample.



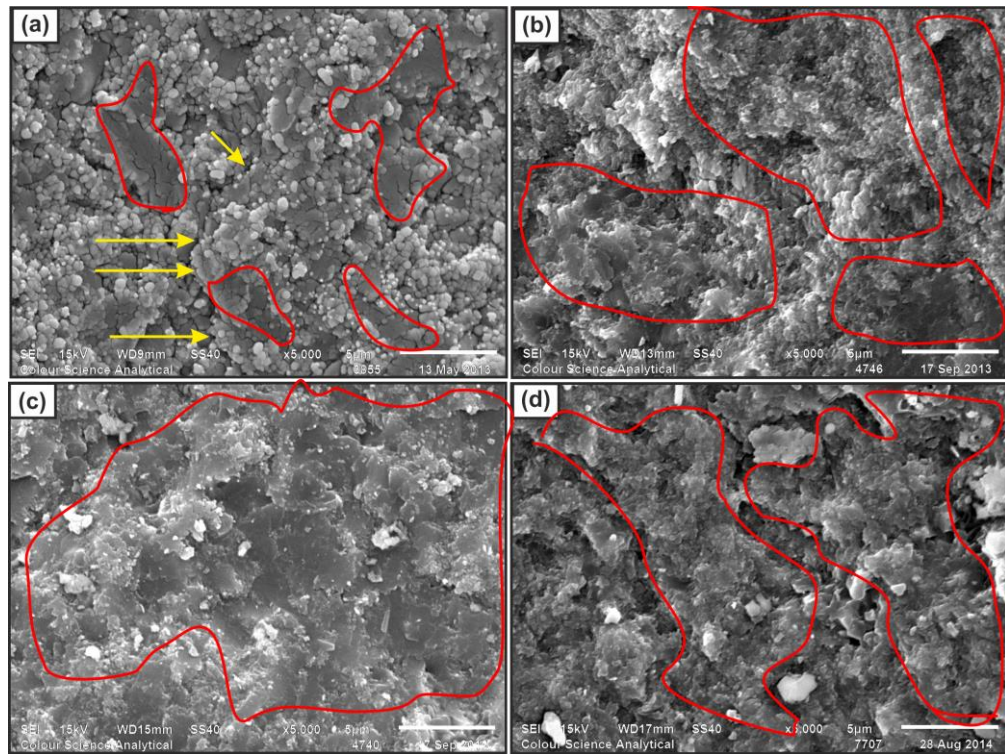


Figure 5.9: SEM secondary images of brownish grey flints. (a) Flint sample representing, BNLUK. (b) Flint sample representing, SEUK. (c) Flint sample representing SDFr. (d) Flint sample representing TSKT. Green arrows show intercrystals microfractures in the North Landing Flint. The massive quartz cement is scattered in sample (a), but massive in samples b-d.

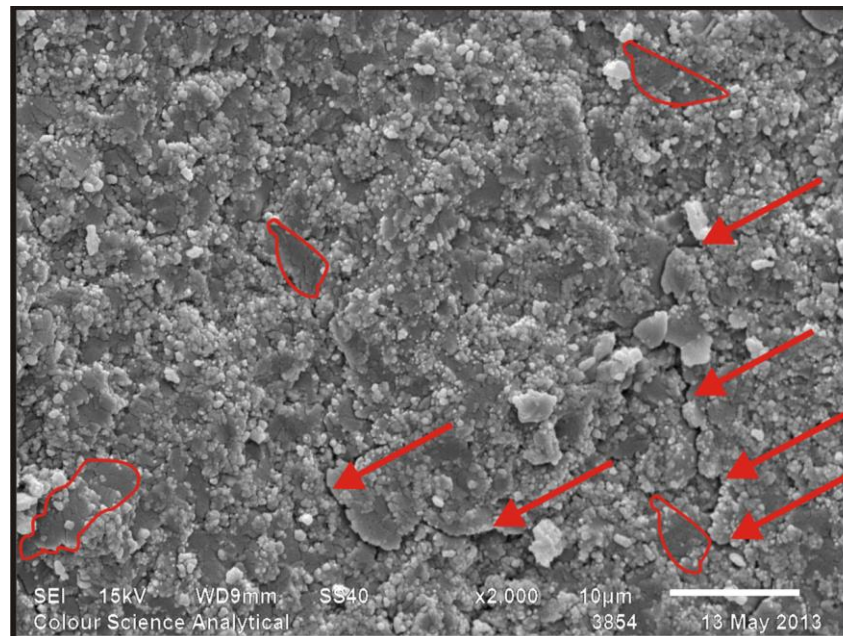


Figure 5.10: Enlarged version of Figure 5.9 (a) depicting the intercrystalline microfractures (red arrows), quartz aggregates and intermittent silica cement (enclosed in red) in the sample.

### *Grey Flints (GF) and Dark Brownish Grey Flints (DBG)*

The SEM micrographs of GF flints (BNLUK and BLSUK) and DBG flints (SEUK, SDFr, LMFr and TSKT) are illustrated in Figures 5.11 a to f. While that of TMKT (DBG) is presented in Figure 5.12. The grey and DBG flints form the dominant flints in the respective sites. In Figures 5.11 a to f and 5.12 a homogeneous matrix dominated by quartz can be seen. The grey flints (Figure 5.11a and b), though, more cemented than LG and BG from the same sites, appeared less cemented than the DBG flints (Figure 5.11 c to f and 5.12). In the grey flints, the previously noted spherical quartz grains (0.47 – 0.52  $\mu\text{m}$ ) associated with samples from the same locations as the grey flints have coalesced and formed a denser microtexture with a high degree of silica cementation than the LG flints. Few micro pores can be seen in these samples, explaining the low porosity of these flints.

In contrast, the DBG flints appear denser and have high degree of silica cementation. The quartz crystals in these samples have significantly recrystallised forming a less porous and more cemented microtexture than any other flint material/colour investigated in this study. The recrystallisation of quartz crystals in the DBG flints is apparently seen in Figure 5.13 where a clear gradation between quartz crystals and massive quartz cement is seen. These observations explain why the DBG flints are stronger, harder, more abrasive, less porous and possess smaller grain sizes (0.26 – 0.34  $\mu\text{m}$ ) than any other colour of flint. The highly cemented microstructures of the DBG flints explain the trends in material properties of flints observed in Chapter 4. The slight microtextural differences observed between the BG (Figure 5.10) and DBG flints (Figures 5.11 and 5.12) translate to the small differences seen in the abrasiveness and hardness of these flints described in Chapter 4.

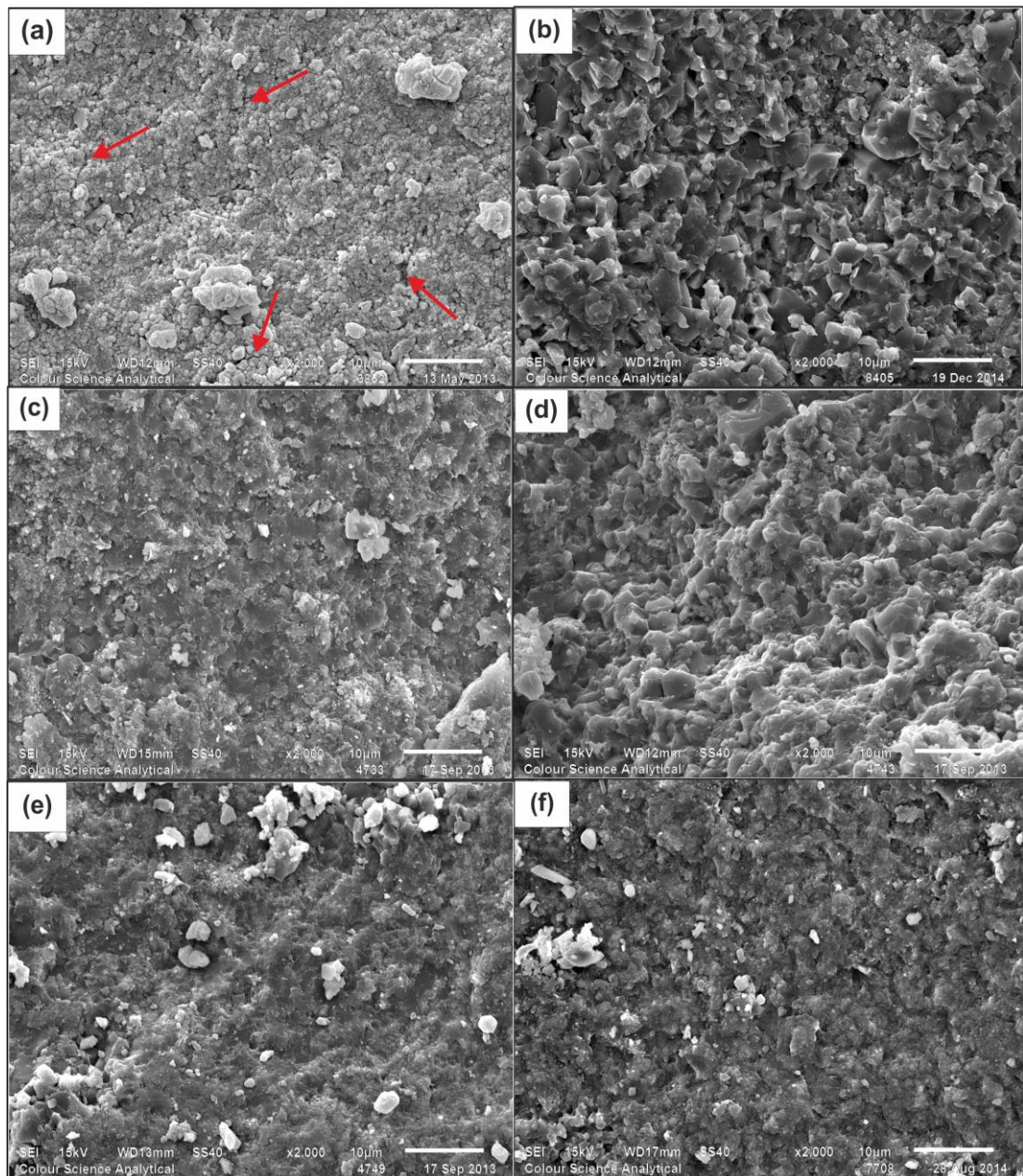


Figure 5.11: SEM secondary images of flints. (a) Grey flint, BNLUK. (b) Grey flint., BLSUK. (c) Dark brownish grey (DBG) flint, SEUK. (d) Dark brownish grey (DBG) flint, SDFr. (e) Dark brownish grey (DBG) flint, LMFr. (f) Dark brownish grey (LBG) flint, TSKT. There is a clear trend in the extent of silica cement between a, b and c-f.

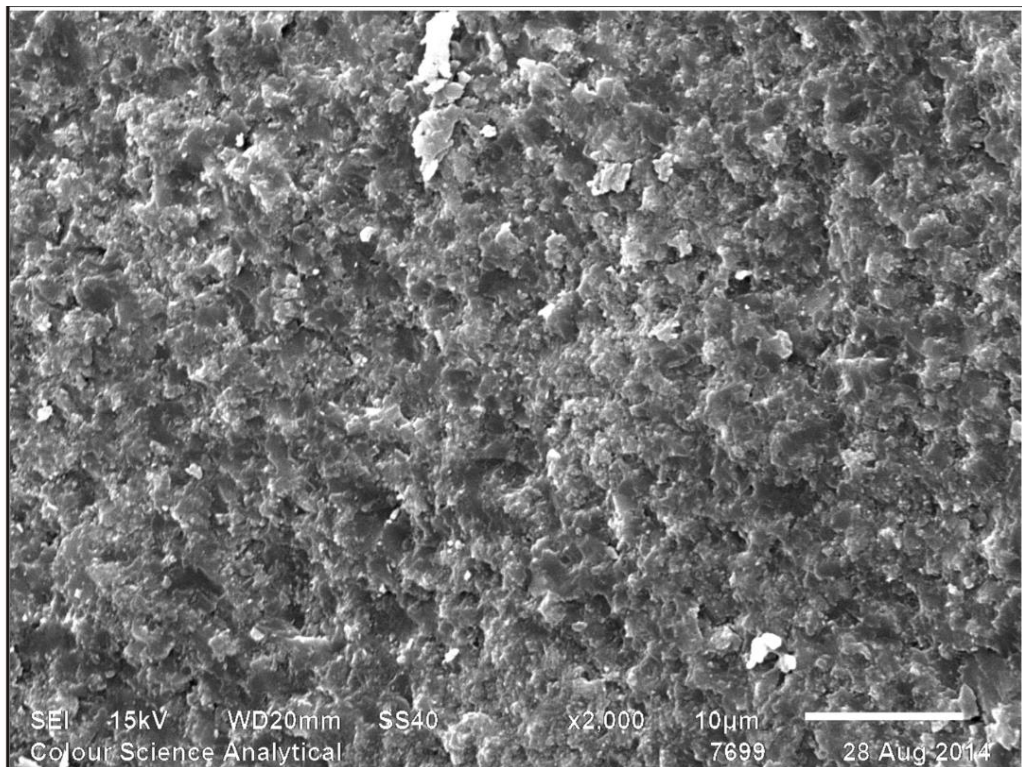


Figure 5.12: Dark brownish grey flint from Tor Chalk at Møns Klint, Denmark.

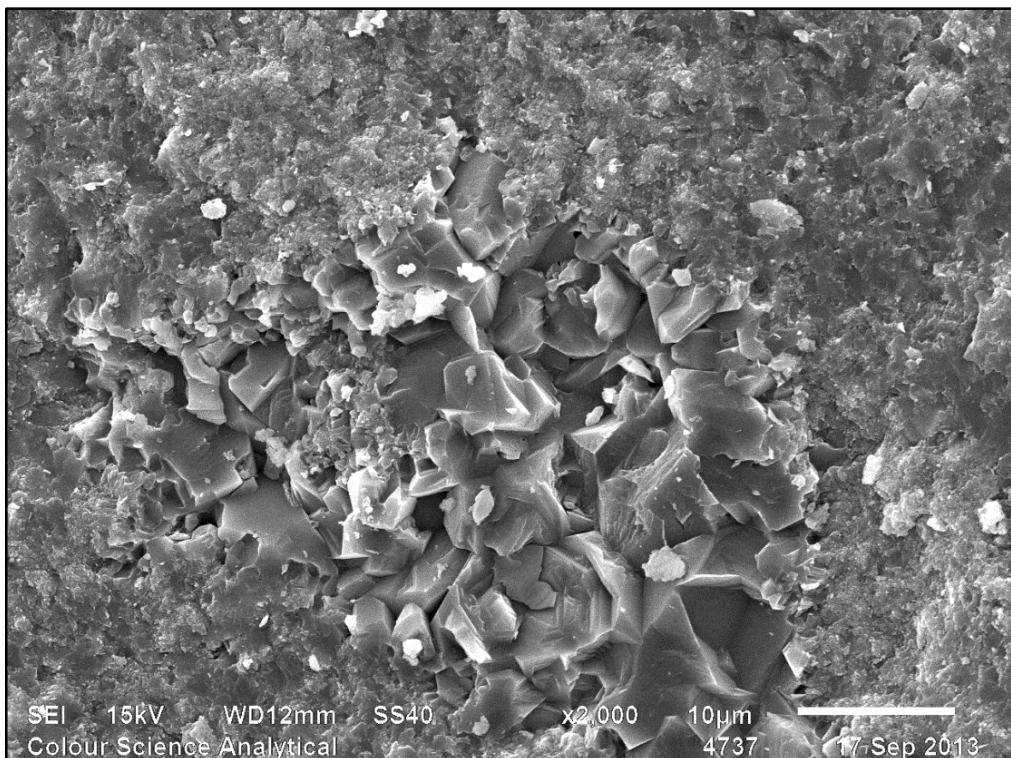


Figure 5.13: Dark brownish grey flint from Lewes Chalk at Mesnil-Val, France. The Figure shows clear recrystallisation of quartz crystals resulting to the formation of massive quartz cement.

### 5.3 Mineral Phase and Composition in Flint Materials

X-ray Diffractometry was used for the qualitative (Section 5.3.1) and quantitative mineral phase analysis (Section 5.3.2) on different colour of flints, WCr and the surrounding chalk. Forty-four samples were examined. The analysis was carried out to: (i) understand the roles of mineral phase and composition on the material behaviours of flints; (ii) how these phase differences vary with colour, structure and origin of flints; and (iii) to establish how the identified and quantified mineral phases and relate these to the trends observed in the material properties of flints described in Chapter 4.

#### *General Mineral Phase Observation*

Mineral phase analysis using XRD identified up to three mineral phases comprising  $\alpha$ -quartz, calcite and halite (although other quartz phases are suspected e.g. see SEM-CL and thin section microscopy photomicrographs (pp. 177-193). All the identified minerals in the investigated samples are represented by the diffractograms shown in Appendices A1 to A7. The mineral composition depended on the structure (flint core or white crust), type (flint or chalk), microstructures (presence of microfractures or micro pores) and the sampling locations (coastal or inland).  $\alpha$ -quartz was identified with typical peaks (101) at d-spacing = 2.34 Å. Calcite was detected with typical peaks (104) at d-spacing = 104 Å. Halite was identified by typical peaks (200) at d-spacing = 2.82 Å.

#### *General mineral composition quantification*

Following the identification of mineral phases in the sample, XRD analysis was also used to quantify the minerals detected in each of the examined samples. Mineral quantification was achieved using Bruker TOPAS profile and structure analysis software. The purpose of this was to establish the relationship between mineral compositions of different types and structures of flint and the surrounding chalk, with the variation in material properties observed in Chapter 4. The detailed composition of these crystalline phases identified in each sample is provided in Section 5.3.1. The mineral composition of the surrounding chalk, white inclusion (WI), silicified white inclusion (SSI), SWI, WCr, LG, GF, LBG and BG flints for each sample (where applicable) are summarised in Tables 5.1 to 5.4. Different flint colours represent sub samples within the flint samples.

The presentation of mineral composition for the investigated samples will be by grouping each flint type or structure from different sites. At the same time comparisons

will be made between flint materials/structures from different locations/origins with different colour in terms of mineral composition.

### 5.3.1 Mineral Phase Identification/quantification of Flints and the Chalk Surrounding Flint

#### *Chalk surrounding flint*

In Table 5.1 the results of XRD analysis on the chalk surrounding flints are illustrated and the XRD diffractograms are given as Appendix A1. As expected calcite (94.64 – 99.38 %) dominates all the samples, with traces of  $\alpha$ -quartz (0.34 – 0.83 %). The percentage of calcite across all the examined samples is uniform. Halite was also seen in the samples collected from the French and the UK coasts, and this originated from the seawater.

Table 5.1: Summary of mineral composition of chalk surrounding flint samples.

	Chalk surrounding flints				
Minerals	BNLUK	SEUK	SDFr	LMFr	TSKT
$\alpha$ -quartz (%)	0.57	0.34	0.77	0.83	0.62
Calcite (%)	99.22	96.66	98.93	94.64	99.38

#### *Carbonate Inclusions (White, Spotted and silicified white inclusions)*

The results of XRD analysis conducted on carbonate inclusions in the flint samples are shown in Table 5.2 and the XRD patterns are presented as Appendix A2. Only the inclusions found in the BNLUK, BLSUK and SEUK are analysed using this method because these samples have significant inclusions. In the grey samples, BNLUK three types of inclusions are noticed and analysed; these are the white inclusion (WI), the spotted white inclusions (SWI) and the silicified white inclusion (SSI), while only the WI are prominent in the grey flint (BLSUK) and the dark brownish grey flint (SEUK). With the exception of SSI with quartz (57.71 %) as the dominant mineral, XRD results (Table 5.2) show the inclusions are dominated by calcite (96.72 – 98.75 %) and traces of quartz (0.87 – 13.88 %). Indicating higher calcite (98.75 %) and lower quartz content (0.87 %) were the grey, less silicified samples (BNLUK), identified with significant calcite inclusions. Halite was seen in the coastal samples (BNLUK and SEUK), but was absent in the Inland sample (BLSUK). This was attributed to the seawater.

Significant quantity of quartz (13.88 %) was seen in the SWI. The SWI samples have some dark spots (possibly siliceous fossils) and usually formed the failure planes in most BNLUK samples during the UCS, To and  $I_{S(50)}$  strength tests. Calcite content (86.12 %) in these samples were compared to that seen in the WI. Unsurprisingly, the stronger samples identified with highly silicified inclusions have slightly higher quartz content (2.55 % for SEUK and 3.28 % for BLSUK). These samples are more abrasive and contain lower calcite content (97.07 % for SEUK and 96.72 % for BLSUK) when compared to the white inclusions in the grey BNLUK (see Table 5.2).

Table 5.2: Summary of mineral composition of the carbonate inclusions in flints

Carbonate Inclusions	BNLUK		BLSUK		SEUK	
	$\alpha$ -quartz	Calcite	$\alpha$ -quartz	Calcite	$\alpha$ -quartz	Calcite
	(%)		(%)		(%)	
<b>SWI</b>	0.87	98.75	-	-	-	-
<b>WI</b>	13.88	86.12	3.28	96.72	2.55	97.07
<b>SSI</b>	57.71	42.29	-	-	-	-

#### *White Crust (WCr)*

Qualitative analysis of WCr shows quartz and calcite as the only mineral in the samples (see Appendix A3). The mineral composition in the WCr derived from the quantitative XRD analysis are illustrated in Table 5.3. Unlike the carbonate inclusions in flints, XRD results for WCr indicated a variation in mineral composition between the WCr (thick and soft) surrounding grey flints and the WCr (thin and hard) surrounding DBG flints (SEUK and SDFr). The XRD patterns of the WCr surrounding the grey flints shows both quartz (35.64 %) and calcite prevailed in the sample, with calcite (64.36 %) being the dominant mineral phase. Distinct patterns were observed in Appendix A3 and c where the diffractograms showed quartz (92.48 - 98.51 %) as the primary mineral phase in the WCr surrounding the DBG flints (SEUK and SDFr), with traces of calcite (1.12 – 5.17 %) in both samples. A comparison between the WCr surrounding the DBG flints (Table 5.3) shows no significant different between these materials in terms of mineral composition. The difference in mineral composition observed between the WCr surrounding the two different flint materials/colour conforms to the trend in abrasivity and hardness results reported in Chapter 4.

Table 5.3: Summary of mineral composition of white crust surrounding flints

Minerals	White Crust		
	BNLUK	SEUK	SDFr
$\alpha$ -quartz (%)	35.64	92.48	98.51
Calcite (%)	64.36	5.17	1.12

#### *Light Grey Flints (LG)*

The light grey (LG) flints that are mainly identified with BNLUK and BLSUK samples have  $\alpha$ -quartz as the major mineral constituent, with minor occurrences of calcite (Appendix A6). The quantitative analysis of LG flints (peculiar to the BNLUK and BLSUK samples) are indicated in Table 5.4. The Table shows the LG flints have quartz content of up to 76.01 % for BNLUK sample, which slightly increased to 92.84 % for BLSUK. The calcite content in these samples reaches 23.99 % for BNLUK and significantly reduced to 7.16 % for BLSUK. The higher calcite and lower quartz contents in the LG flints (BNLUK) explains the patterns observed in the hardness, porosity and abrasiveness between the two flint types, with the LG, BNLUK sample being less abrasive, porous and softer than equivalent material from the BNLUK.

#### *Light Brownish Grey (LBG)*

The mineral phases identified in the light brownish grey (LBG) samples are shown in diffractograms (Appendix A4). The bulk samples consist of  $\alpha$ -quartz as the main phase, with subordinate calcite. Quantitative analysis on these samples revealed slight differences in the mineral composition between the LBG (BNLUK) and the LBG from the stronger flints (Table 5.4). The LBG (BNLUK and BLSUK) contained less quartz content 86.09 % for BNLUK and 92.44 %, BLSUK when compared to the more quartz content (96.53 to 99.11 %) seen in the LBG from the stronger and more silicified DBG flints. Highest calcite content (13.21 %) was found in LBG flints (BNLUK) which reduces to 7.51 % for BLSUK and dips further to the range from 0.89 to 6.26 % for the LBG flints (associated with the DBG flints).



Table 5.4: Summary of mineral composition of different flint categories

Flint category	Flints	Mineral (%)	LG	LBG	BG	GF/DBG
Associated with grey flints	BNLUK	$\alpha$ -quartz	76.01	86.09	97.84	98.09
		Calcite	23.99	13.21	1.96	1.91
	BLSUK	Quartz	92.84		96.81	98.86
		Calcite	7.16		3.2	1.14
Associated with dark brownish grey flints	SEUK	Quartz	-	98.02	99.16	99.23
		Calcite	-	1.98	0.84	0.77
	SDFr	Quartz	-	99.11	99.08	99.5
		Calcite	-	0.89	0.92	0.5
	LMFr	Quartz	-	93.74	-	98.79
		Calcite	-	6.26	-	1.21
	TSKT	Quartz	-	97.78	-	98.54
		Calcite	-	2.22	-	1.46
	TMKT	Quartz	-	96.53	-	98.66
		Calcite	-	3.47	-	1.34

Halite was only traced in the porous LBG, BNLUK. The presence of halite in the porous, less abrasive LBG flints (BNLUK) which was conspicuously absent in the Inland samples (BLSUK), and the more silicified/cemented samples is associated with intergranular microfractures/pores seen in the BNLUK. The trend in mineralogy observed between the two categories of LBG samples is analogous to that seen in the geotechnical wear characteristics of these samples presented in Chapter 4.

#### *Brownish Grey Flints (BG)*

XRD analysis of the brownish grey flints (BG) revealed quartz (c. 99 %, Table 5.4) as the primary mineral with subordinate calcite (Appendix A7). Halite was only detected in the BNLUK samples, Although calcite content is small (0.84 – 0.92%, Table 5.4), the diffractograms indicate more of calcite in the BG flints from the BNLUK than any other sample. The results presented are from samples, where a significant proportion of the BG flints were observed. However, where the BG flint was not detected or not significantly distributed in the samples, XRD analysis was not conducted on the samples (e.g. LMF<sub>r</sub>, TSKT and TMKT).

### *Grey Flints (GF)*

Results from the quantitative XRD analysis of grey flints are listed in Table 5.4. The diffractograms from which the mineral phases in grey flints were identified are provided as Appendix A5. The diffractograms show quartz (98.09 – 98.86) as the main mineral in these samples with subordinate calcite (1.14 – 1.91 %). This mineral composition shows a slight increase in quartz contents when grey flints, BNLUK (98.09%) and BLSUK (98.86 %) were compared with the corresponding LBG flints from the same formations. Although slight, this pattern is reflected in the calcite content, where the calcite content of the grey flints (BNLUK and BLSUK) was lower, ranging from 1.14 to 1.91 %, against higher value of up to 13.21% seen in the LBG flints. There was no evidence of presence of halite in the BNLUK samples (grey flints) as was seen in other colours of flint samples from the North Landing. The absence of halite is due to increase in the degree of silica cementation/silicification noticed in these samples when compared with the LBG flints from the BNLUK sample.

### *Dark Brownish Grey Flints (DBG)*

The XRD analysis of dark brownish grey flints (DBG) are qualitatively presented in Appendix A5 and quantitatively shown in Table 5.4. The DBG flints are dominant in the SEUK, SDFr, LMFr, TSKT and TMKT. XRD analysis results for DBG flints show all the samples have two major minerals comprising:  $\alpha$ -quartz (98.58 - 99.50 %, main mineral) and calcite (0.50 – 1.46 %, minor mineral). The amount of  $\alpha$ -quartz in all the samples is substantial and dominates the matrix of the samples. Traces of calcite were also detected in the samples. The overall results indicate the DBG flints have higher quartz content than any other colour of flint investigated in this study and the higher quartz content in these samples agrees with the mechanical properties of the samples.

## **5.4 Microstructure of Flint Components from Thin Section Microscopy**

Thin section microscopy using the transmitted light was conducted to examine the structure and the composition of flint. The presence and the preservation of microfossils in the samples were also examined. Optical images from the thin section photomicrographs show the variation in the structure, preservation and the distribution of inclusions between the grey and DBG samples. The trends in calcite-silica transition were also observed using this method. SEM analysis shows the calcite-silica transition based on the replacement and cementation but does not reveal the proportion and

distribution of calcite in flints and WCr. SEM does not also clearly show the well-preserved fossils that can be detected using the thin section and this explains the reason for using the thin section microscopy.

#### *The Relationship between Flint Core and White Crust (WCr)*

The relationship between flint core and the WCr was examined using the thin section analysis (Figure 5.14a to c). Note the boundary between flint and the WCr, a gradual gradation through the WCr from the flint core is observed. This gradation illustrates a mixture of both calcite and silica at the flint-core boundary. The mixture of silica and calcite at this boundary explains why when drilling flint the drill bits easily penetrates the first few mm of the flint core, before experiencing higher resistance as drilling progresses through the core. The presence of remarkable calcite at the edge of the flint core and the behaviour of drill bits at this part is suggestive of the role of calcite in affecting the drillability and abrasivity of flints, and variation of these with flint colour.

Foram chambers filled with calcite (dark arrows) are also observed in the WCr, but are conspicuously absent in the flint core and could either be completely replaced at flint formation stage or could have been dissolved and replaced prior to flint formation. Calcite-filled voids are also noticed (lighter or white spots) and partially silicified fossils replacing calcite are also observed (golden spots). The overall microstructures of the flint core are dominated by the  $\alpha$ -quartz as expected and seen in both XRD and SEM, while the WCr is expectedly dominated by the calcite phase. The flint-WCr boundary has the silica-calcite phase as the main phases.

The microstructures of the WCr can be clearly seen in Figures 5.15a and b (CPL). The Foram chambers filled with calcite identified in the above paragraph are seen and silicified fossils evident. The presence of microfractures are also seen (red arrows). The overall microtexture of the sample is dominated by calcite and some traces of siliceous microfossils.

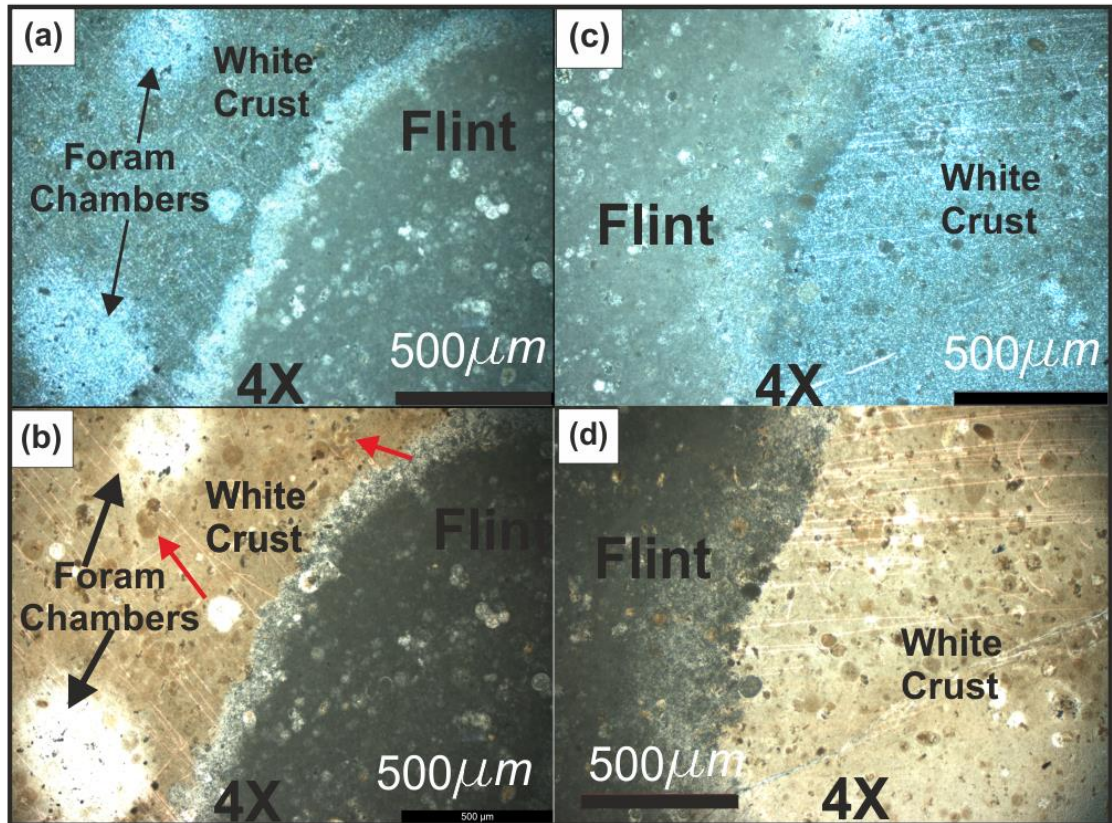


Figure 5.14: Thin Section photomicrographs of crust-flint from samples collected at the North Landing, UK. (b) and (d) are the same as a and c respectively, but are rather illustrated in CPL, to clearly depict the different phases as well as the trace fossils in the samples. Conspicuously foram chambers filled with calcite (indicated by the two arrows in both images) can be seen in Figures 5.24 (a and b) and several foraminifera tests filled with calcite are traceable in all the figures.

The differences in the colour reveal the degree of silicification and possibly the phases of the silica in the sample (opal A, Opal-CT, chalcedony, cristobalite or  $\alpha$ -quartz). Most of these phases have been previously identified in flints (See Jeans, 1983 ; Clayton, 1984). The same traces of completely silicified fossils are also seen appearing as faded brown or dark, while weakly silicified fossils, mostly foraminifera replacing calcite are also noticed. The WCr from the DBG flints were not analysed using thin section because, they are thinner and attempts to prepare suitable thin sections from these samples ended in futility.

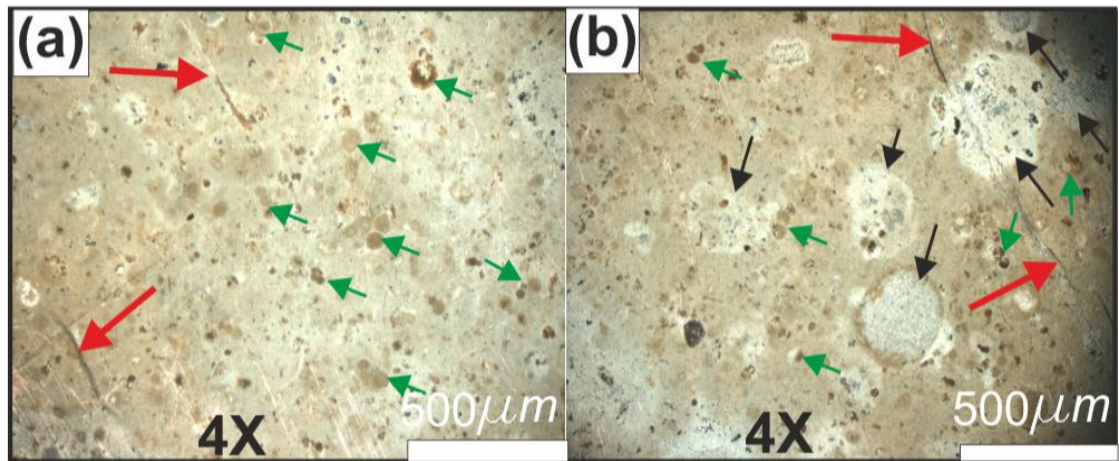


Figure 5.15: (a) Thin Section photomicrographs of white crusts surrounding flints sampled from the North Landing transmitted in CPL.(b) Same as (a) but at higher magnification. The red arrows indicate pre-existing microfractures. Several forams, sponge spicules replacing calcite and foram chambers are clearly seen.

#### *Grey Flints (GF)*

Thin section optical analysis images (Figures 5.16a & b (BNLUK) and 5.17a & b (BLSUK)) discriminate cryptocrystalline quartz phase, from calcite inclusion for grey flints. The analysis shows a significant proportion of calcite/carbonate inclusion (white in both CPL and PPL) and dominant cryptocrystalline quartz (major mineral-grey) in the grey flints. At the same magnification, the transmitted light optical analysis showed the same phases dominated by the fine cryptocrystalline quartz and calcite-filled inclusions (Figures 5.16b, d & f and 5.17b remarkably seen as white spots) using the plane polarised light.

The presence of inclusions probably  $FeO_2$  (dark spots observed in both PPL and CPL) and amorphous silica (opaline mostly from the radiolaria) were also seen in these samples. The radiolaria observed in the BLSUK samples are well preserved and are visible as solid spheres representing solid skeletal elements of the opaline silica. These radiolaria are differentiated from the calcite inclusion by being brighter than the cryptocrystalline quartz, but not as bright (white) as the carbonate inclusion (Figure 5.16f & 5.17b). In some cases the opaline silica from these radiolaria have been transformed to cryptocrystalline  $\alpha$ -quartz (dark, dense spheres, yellow arrows in Figures 5.17a and b).

The presence of opaline silica and opal-CT from other microfossils can also be seen as bright reflection intermittently distributed within sample and these can be differentiated from the calcite inclusions that appear purely as white, filling isolated

pores. Occasionally, the replacement of these calcite inclusions by silica have commenced as identified by the dark spots in the middle of the inclusions. In both crossed-polarised and plane polarised lights, there are widely distributed dark spots especially in these samples. These dark spots are probably inclusions,  $\text{FeO}_2$ .

The major differences between the two grey flints are the presence of open microfractures and higher proportion of calcite inclusions seen in the BNLUK samples (Figures 5.16 c and d) when compared to the few calcite inclusions (white inclusions filling voids) observed in the BLSUK samples. These differences in microstructures between grey flints conforms to the variations in mineral compositions and mechanical properties between the samples.

The distribution of inclusions and the presence of opaline silica (in both samples) and the presence of microfractures in BNLUK samples contribute to the material properties of grey flints.

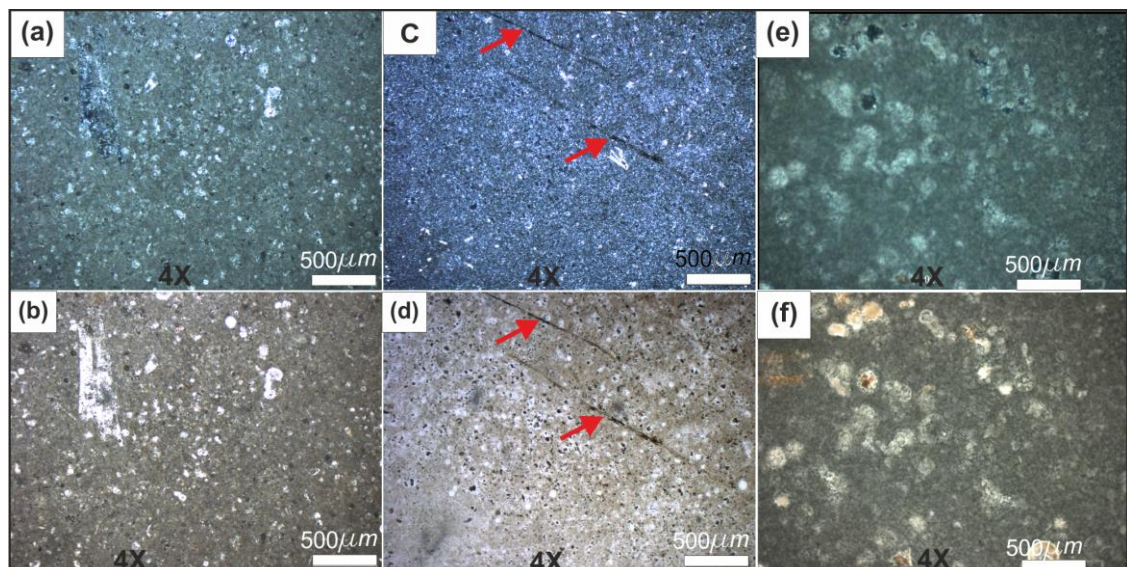


Figure 5.16: Thin Section photomicrographs of flints collected from the Burnham Chalk at North Landing, UK. b,d, and f are a, c and e presented in PPL. The fractres in these samples are mostly perpendicular to the bedding and reflect the general patterns of fractures characterising the host chalk (Figure 3.4 (a-c)), p. 60 and Figure 3.10 (b&d), p. 67 and described in Figure 3.12, p.70). In most block samples related to these flint types about 10-12 fractures are recorded in 200 mm long block of flints (Figure 3.12 a-d).

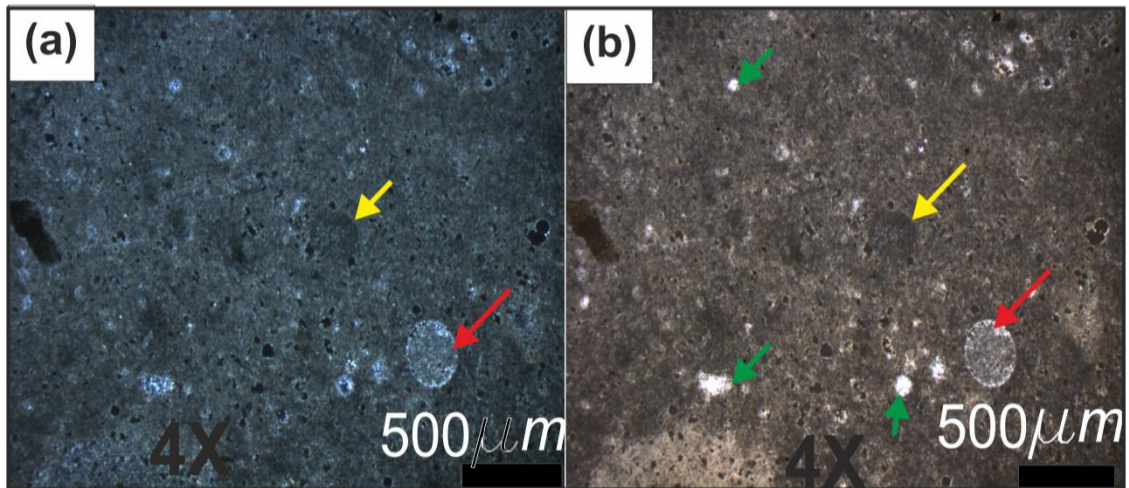


Figure 5.17: Thin Section photomicrographs of flints collected from the Burnham Chalk at Lincolnshire, UK. The presence of pores and carbonate inclusions are prominent. The red arrows show amorphous silica from the radiolarian test. Yellow arrows show former radiolarian solid sphere transformed to cryptocrystalline. The presence of several calcite inclusions (green arrows), pores filled with amorphous silica are also evidenced.

*Microstructural Relationship between Light Brownish Grey (LBG) and Brownish Grey Flints (BG)*

The difference between different colours of flints can be seen in Figure 5.18(a-d). The figure illustrates flint sample with two different colours comprising of brownish grey (BG) and light brownish grey (LBG). Figure 5.18a represents the PPL for both BG (lighter) and LBG (darker) while Figure 5.18b is the LBG part treated separately. The figure shows the presence of well-preserved sponge spicules (dark arrow) and probably iron oxide ( $\text{FeO}_2$ , dark spots in the image) distributed in the sample. Figure 5.18c and d showed more preservation of silicified foraminifera and sponge spicules in the LBG. This sample appeared coarser, darker, and less dense than the BG (red arrows). While the BG appeared dense, lighter and more homogenous in the PPL than the LBG, with relatively fewer preserved fossils (dark arrow). The presence of fewer microfossils in the BG flints than the LBG shows variation in the degree of silicification of fossils between these samples plays a significant role in the microstructure and hence the engineering properties of these materials.

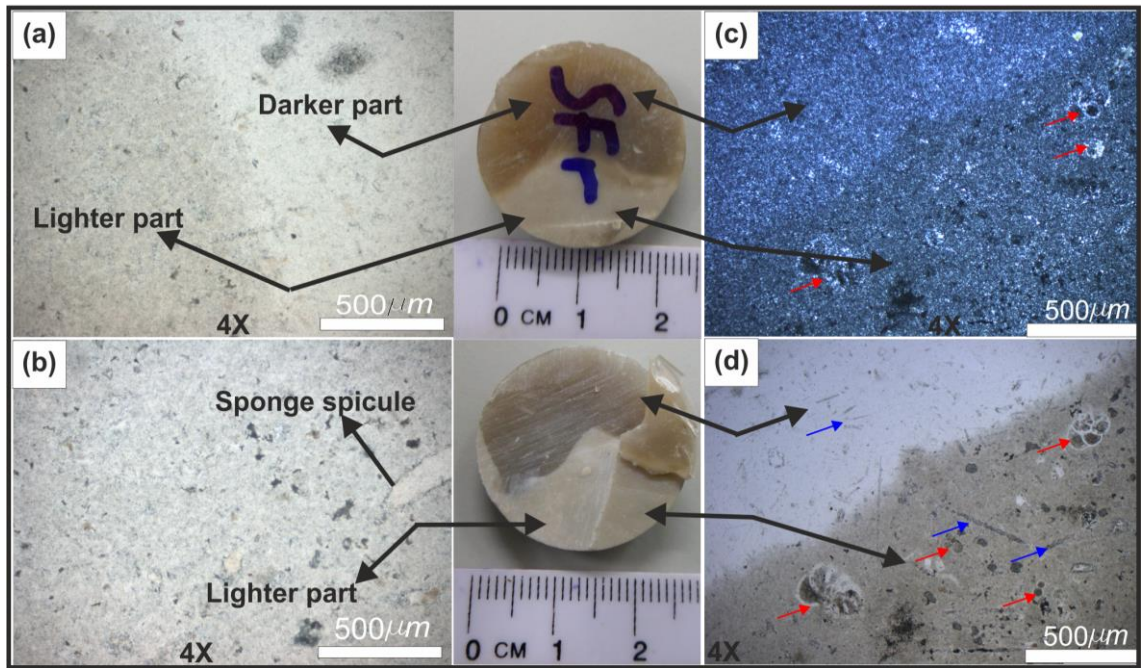


Figure 5.18: Thin Section photomicrographs of flint from the Seaford Chalk at Dieppe, France. (a) shows both light and darker part of the flint sample in CPL. (b) The lighter part of the sample, showing coarser texture, with more preserved fossils. (c) Sample from the same location showing clear variation between the darker part (dense, smooth), and the lighter part. (d) c in CPL, clearly showing more preserved fossils (Forams) in the lighter part.

#### *Dark Brownish Grey Flints (DBG)*

Thin section photomicrographs illustrated in both crossed polarised light (CPL) and plane polarised light (PPL) for dark brownish grey flints (DBG) are shown in Figures 5.18 to 5.26. These photomicrographs show the fabrics of DBG flints (SEUK) is dominated by smooth, dense, homogenous and cryptocrystalline quartz. Partially silicified microfossils, shell fragments, sponge spicules and isolated carbonate inclusions are also seen in these samples (white spots). Brighter reflection suggesting early stage of silicification are also noticed in the samples.

Marked differences in microstructure between DBG flints (with less carbonate inclusions) and grey flints (GF) are seen. In the DBG flints, there is no evidence of well preserved foram chambers or clear grain boundaries or any associated impurities apart from the few scattered distribution of carbonate inclusions in the samples. The reduction of calcite inclusions in these samples when compared to the grey flints suggests most microfossils in these samples are largely silicified. This, therefore, contributes to the high strength and abrasiveness of DBG when compared to the grey flints.



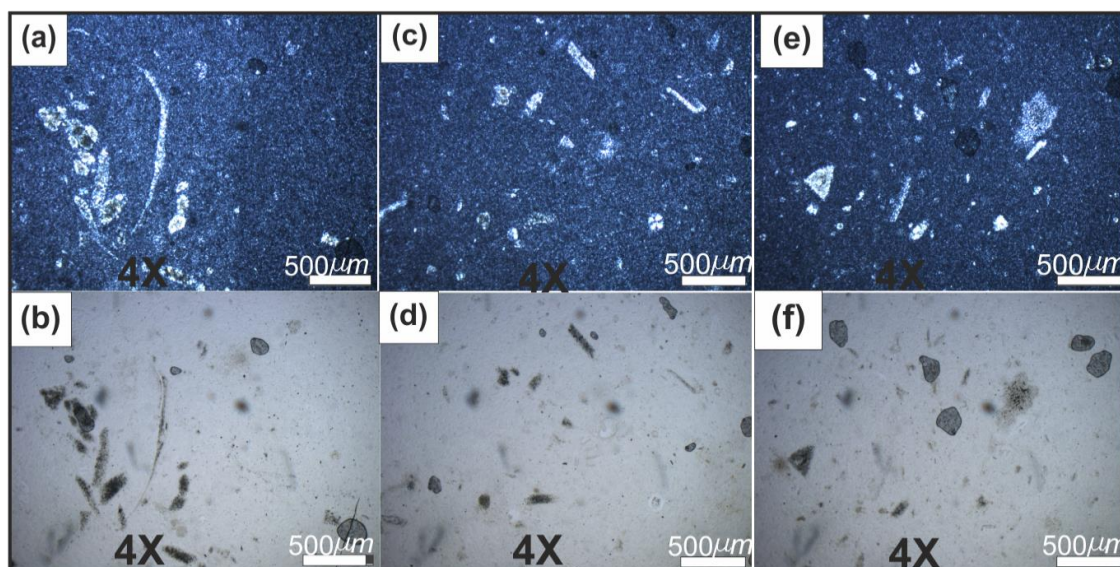


Figure 5.19: Thin Section photomicrographs of flint from the Seaford Chalk at East Sussex, UK. b, d and f are a, c and e in PPL. All the images show the presence of silicified fossil/ fossil fragments, the entire matrices are dense and homogenous.

Additional features of the DBG flints (SDFr, Figure 5.20) are the presence of significant sponge spicules, foraminifera, and other partially silicified microfossils (especially in Figures 5.20 b and d (PPL)). Figure 5.20a also reveals a void-filling phase dominated by euhedral mega quartz crystals surrounded by cryptocrystalline quartz in the SDFr samples.

The LMFr samples (Figure 5.21) contain isolated carbonate inclusions which confirmed the calcite content of the sample detected in the XRD analysis. Also observed in these samples are sponge spicules and siliceous microfossils such as foraminifera (Figure 5.21b and d).

Indicating peculiar microtexture among the DBG flints are the TSKT flints (Figure 5.22 – 5.25). These samples have the most well-preserved varieties of microfossils among the entirely examined flint samples. Unlike the preceding DBG flints, microfossils like bryozoans, and partially silicified microfossil fragments are abundant and well preserved in these samples (Figures 5.22 a to d). Few sponge spicules and silicified forams and other silicified shell fragments are also well preserved in these samples (Figures 5.22 a to f and 5.33a to f).

Deviating slightly from the homogenous matrix of the DBG flints are TMKT samples (Figure 5.26). These samples possessed fewer preserved microfossils. Foraminifera chamber filled with calcite is seen in these samples and partially silicified fossils are also observed in few locations in the sample (Figures 5.26c and d). Calcite inclusions are seen within the matrix of these samples as tiny white spots in the PPL images (Figures 5.26a and c).

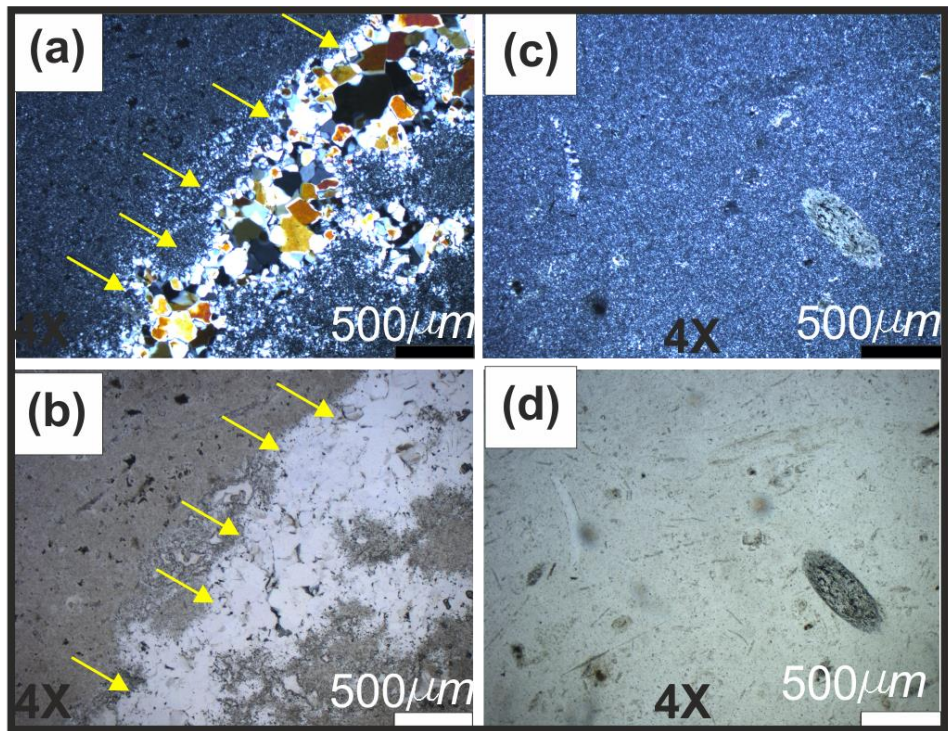


Figure 5.20: Thin Section photomicrographs of flint from the Seaford Chalk at Dieppe, France. (b) and (d) are (a), and (c) presented in PPL. Note the preservation of sponge spicules, and other silicious microfossils (indicated by the red arrows). Euhedral mega quartz crystals surrounded by cryptocrystalline quartz are shown by the yellow arrows.

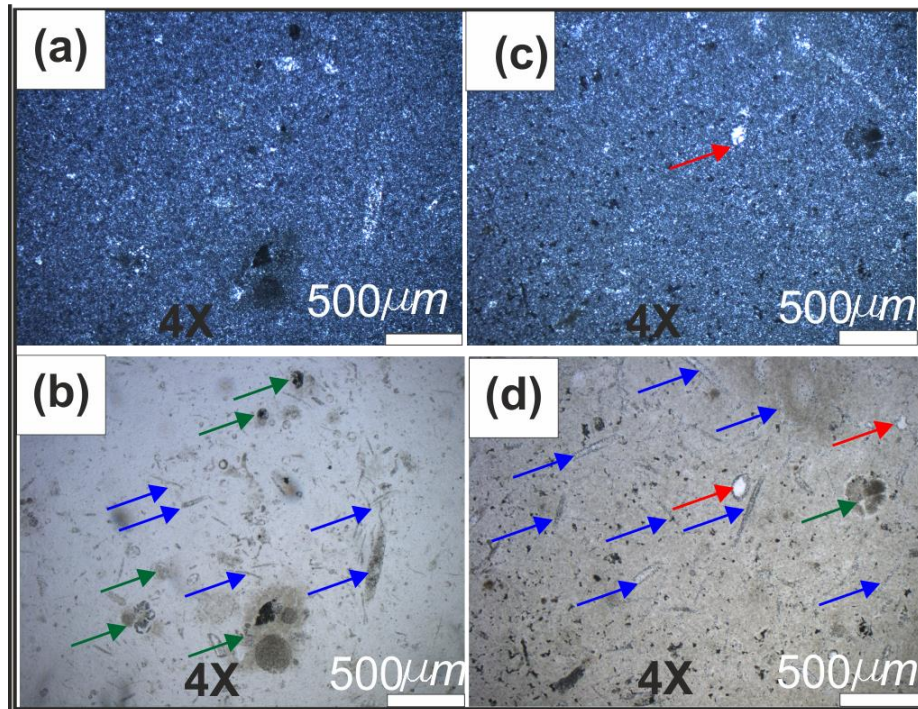


Figure 5.21: Thin Section photomicrographs of flint from the Lewes Chalk at Mesnil-Val, France. (a) and (c) are flint representing different locations. (b) and (d) are (a) and (c) in CPL. Sponge spicules (blue arrows) and forams (green arrows) are well preserved in these samples.

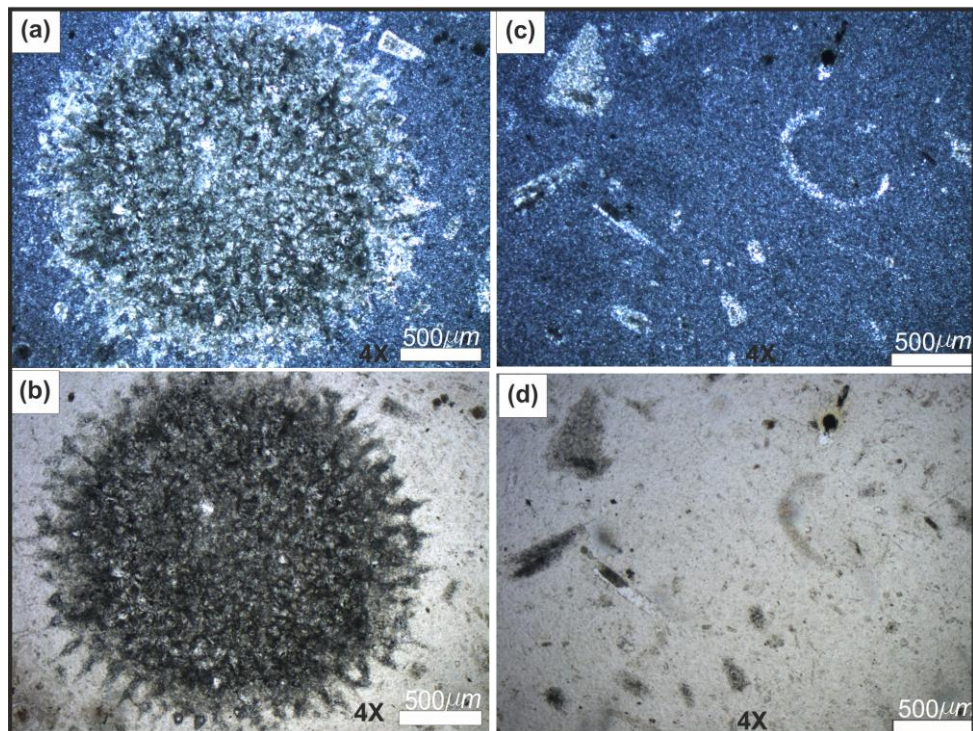


Figure 5.22: Thin Section photomicrographs of flint from the Tor Chalk at Stevns Klint, Denmark. The preservation of fossils can be seen in these samples. (a) and (c) are illustrated in PPL, while (b) and (d) are illustrated in CPL.

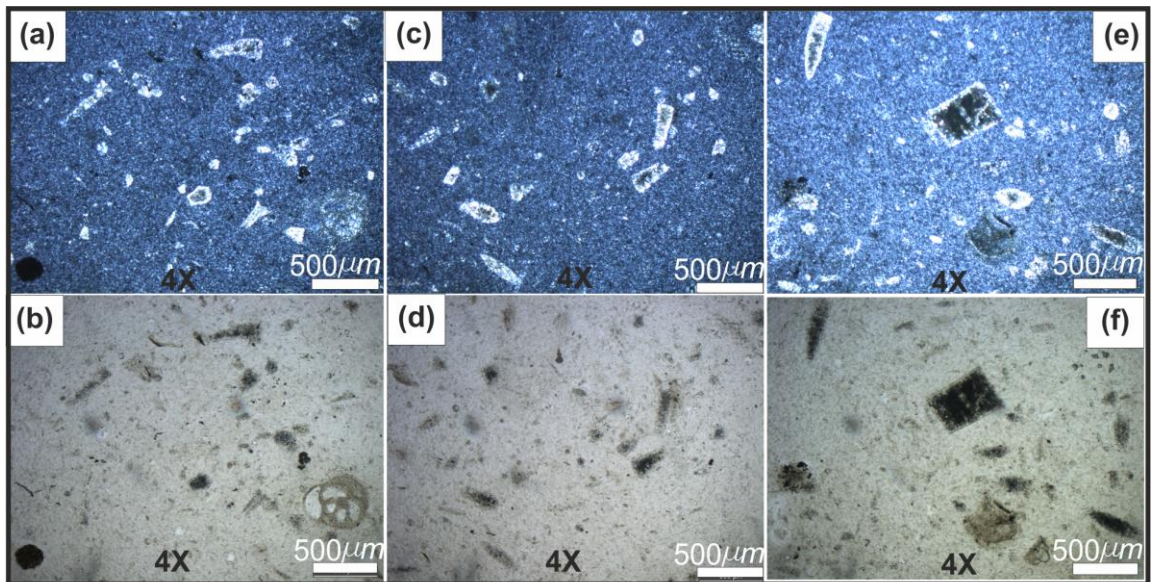


Figure 5.23: Thin Section photomicrographs of flint from the Tor Chalk at Stevns Klint, Denmark. The preservation of shell fragments and silicified fossils are noticed in these Figures. a, c and e are illustrated in PPL, b, d and f in CPL.

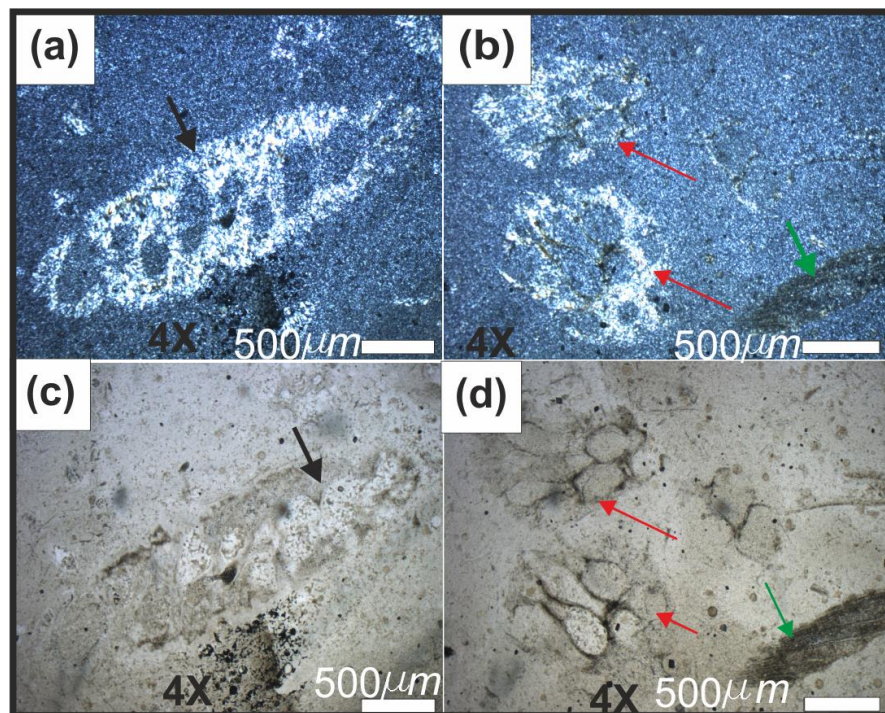


Figure 5.24: Thin Section photomicrographs of different portions of flint from the Tor Chalk at Stevns Klint, Denmark. The figures also show the well preserved forams (red arrows) and Red Algae (black arrows) in the samples. (c) and (d) are illustrated in CPL.

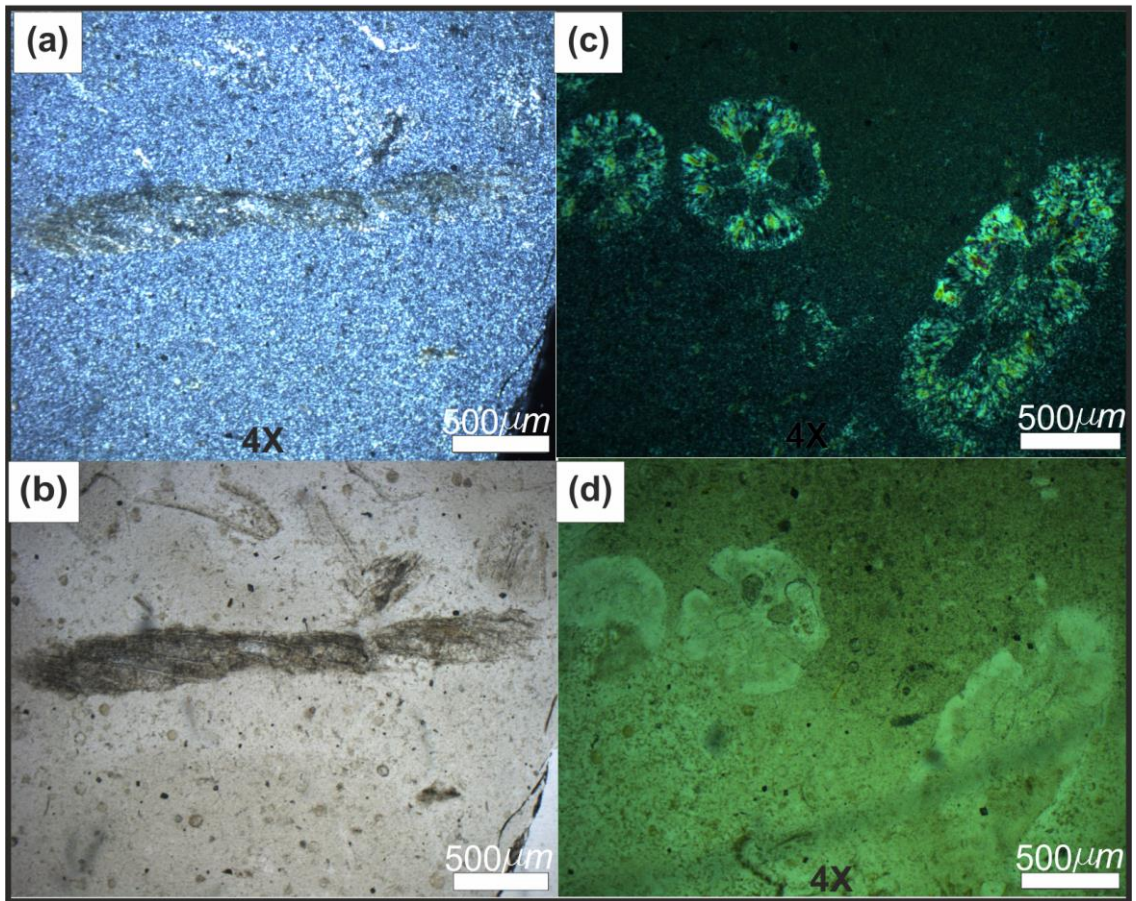


Figure 5.25: Thin Section photomicrographs of flint from the Tor Chalk at Stevns Klint, Denmark showing more preserved fossils.

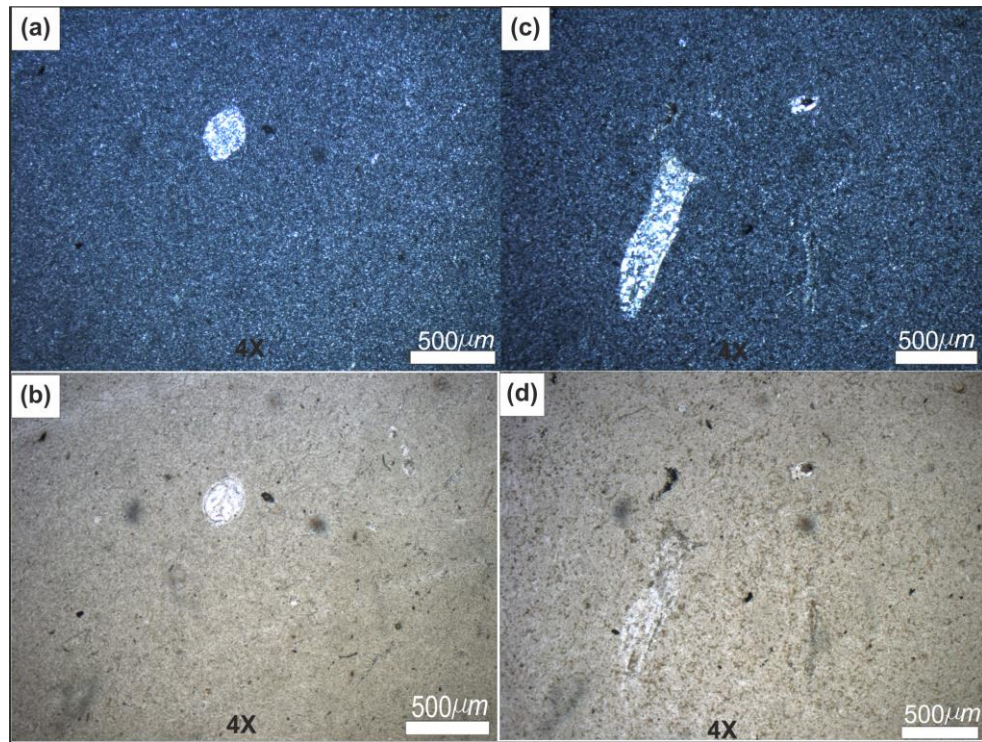


Figure 5.26: Thin Section photomicrographs of flint from the Tor Chalk at Møns Klint, Denmark. The samples appear homogenous with few trace fossils.

The patterns in the microstructural features of the DBG flints (SEUK) reflects the observed material properties of these samples reported in Chapter 4. The dense texture of these samples explain the higher strength and abrasiveness observed in these samples than the GF flints, and by extension the similarity seen between the DBG samples. The different coloured samples investigated represent subsamples within the main flint bands.

## 5.5 Scanning Electron Microscopy-Cathodoluminescence (SEM-CL) of Flint Materials

To differentiate between various quartz phases (opal-A, chalcedony, cristobalite and  $\alpha$ -quartz) and to identify the presence of impurities (possibly fluid Inclusions) not discernible by polarising microscopy and SEM alone, the SEM-CL analysis was conducted on flint samples.

## Grey Flints (GF)

Figures 5.27 and 5.28 show the SEM-CL and backscattered photomicrographs of grey flints (BNLUK and BLSUK). Different sets of CL characteristics indicating various stages of silicification, calcite inclusions and the resultant quartz phases (either opaline silica or  $\alpha$ -quartz) are distinguished in the samples. These CL sets are the CL-grey, CL-white, CL-bright and CL-non luminescence. The initial stage of silicification can be seen at the edge of the silicified microfossils noticeable as the brightest CL-luminescence (probably opal-CT). This forms rims that lined the weakly silicified microfossils (Figures 5.27 a, c & d and 5.28 c & e). The CL-grey luminescence represents the opaline silica (opal-A) thereby confirming the existence of opaline silica previously suspected from the thin section analysis (Figures 5.27 a, c & d and 5.28 a & e).

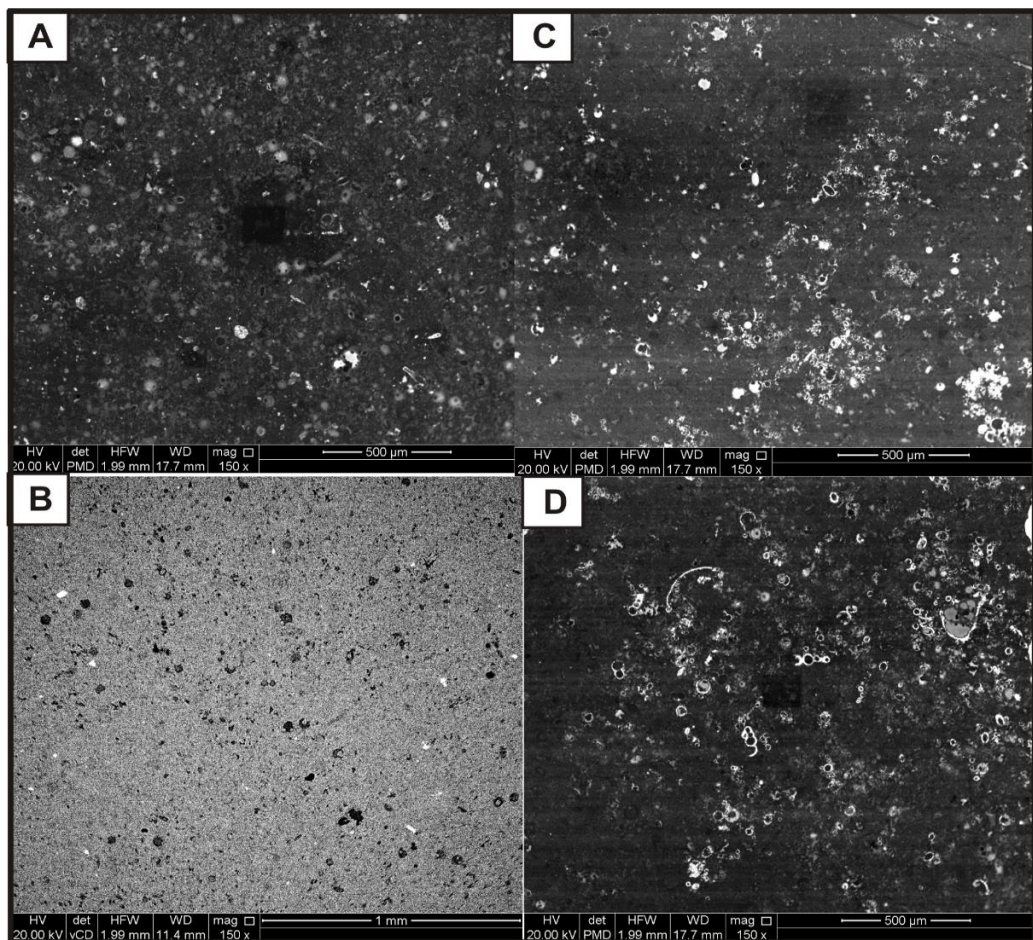


Figure 5.27: a, c and d SEM-CL images of flints from the Burnham Chalk at North Landing, UK. (b) is a Backscattered electron (BSE) image of Figure 5.36a. Note the three different colour in the CL, the dark non-luminescence  $\alpha$ -quartz, CL-grey (amorphous silica/opaline silica), the widely distributed CL-white, calcite (a, c and d) and CL-bright (probably opal-CT forming rim cement around fossils).

The non-luminescence (dark mass) dominate the fabric of the samples and represents low temperature  $\alpha$ -quartz. The low temperature  $\alpha$ -quartz in the samples appear grey in the back scattered images (Figures 5.27b and 5.28b, d & f).

The presence of completely silicified microfossils mostly radiolarians and foraminiferas are also observed the grey flints as dark globules and spheres (Figures 5.28 a - e) which mostly disappear in the backscattered images and formed part of the mass cryptocrystalline phase seen in the samples. The CL-white represents calcite inclusions which appear dark in the backscattered images (Figures 5.28b, d and f) represent calcite inclusions. The concentration of calcite inclusions is higher in the BNLUK than in the BLSUK samples. This observation is inlined with earlier XRD and thin sections results for these samples and is a contributor to the weakness of the sample when compared with any other samples investigated.

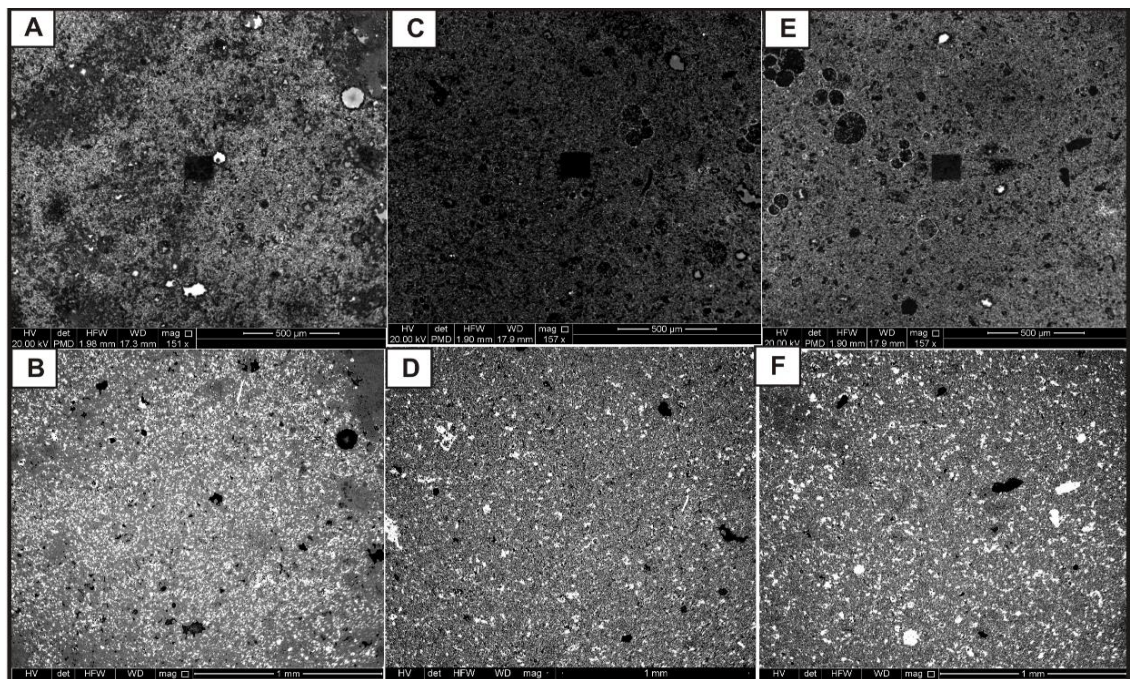


Figure 5.28: a, c and e are SEM-CL of flints from the Burnham Chalk at Lincolnshire, UK. (b, d and f) are Backscattered electron (BSE) images of the same flint samples. Carbonate filled inclusions filling pores are observed in the samples. (b, d and f) are Backscattered electron (BSE) images of the same flint samples. Carbonate filled inclusions filling pores are observed in the samples.



## Dark Brownish Grey Flints (DBG)

The matrices of DBG flints primarily show non-luminescence characteristics dominate, with few distribution of white, grey and bright luminescence. This suggests that the overall microstructure of these samples is dominated by the low temperature cryptocrystalline quartz with few traces of partially silicified fragments of microfossils (grey luminescence) (Figures 5.29 to 5.33).

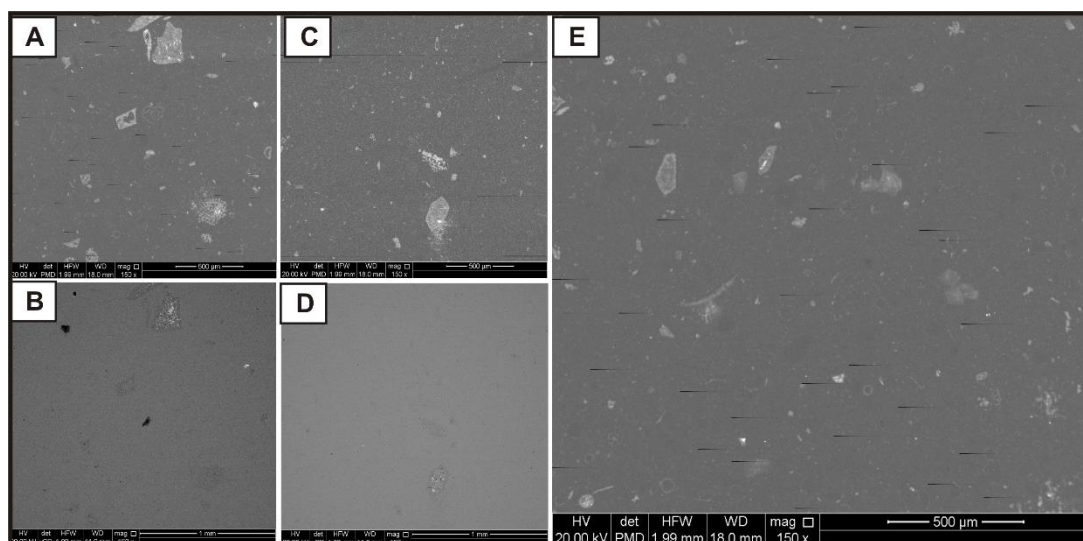


Figure 5.29: (a), (c) and (e) SEM-CL of flint samples from Seaford Chalk, East Sussex, UK. Weakly silicified fossils and shell fragments are observed (CL-grey) in the samples. (b) and (d) backscattered photomicrographs of (a) and (c) respectively. Weakly silicified fossils and shell fragments are observed (CL-grey) in the samples. (b) and (d) backscattered photomicrographs of (a) and (c) respectively.

The concentrations of carbonate inclusions in the matrices of DBG flints seen in both the SEM-CL and the backscattered images are lower when compared to that seen in the grey flints. The SEM-CL photomicrographs of SEUK (Figure 5.29), SDFr (Figure 5.30) and LMFr (Figure 5.31) show the lowest concentrations of calcite filled inclusions among the DBG flints, thereby confirming the results of petrographic analysis presented earlier.

The TSKT flints remain the samples with the most preserved microfossils than any of the investigated DBG flints (Figures 5.3a, c, & e) thereby justifying observation made on these samples in the thin section microscopy. The TMKT flints have the most remarkable significant concentrations of opaline silica (CL-grey scale) and calcite filled inclusions (CL-white) within the rock matrix (Figure 5.33a, b, & c) when compared to the remaining DBG flints. The presence of silica filled fractures (red arrows, Figure

5.42a) is also seen in the TMKT flints. The presence of late stage silicification or calcite inclusions seen in the grey flints, was rarely detected in the DBG flints, this therefore confirms the observation made in the thin section analysis of these samples.

The overall SEM-CL results do not indicate any evidence of fluid inclusions in the samples. The only impurities seen in the samples are the reported calcite inclusions and likely traces of  $\text{FeO}_2$ . The concentrations of calcite inclusions between samples agree with the patterns seen in the mechanical properties of the investigated samples.

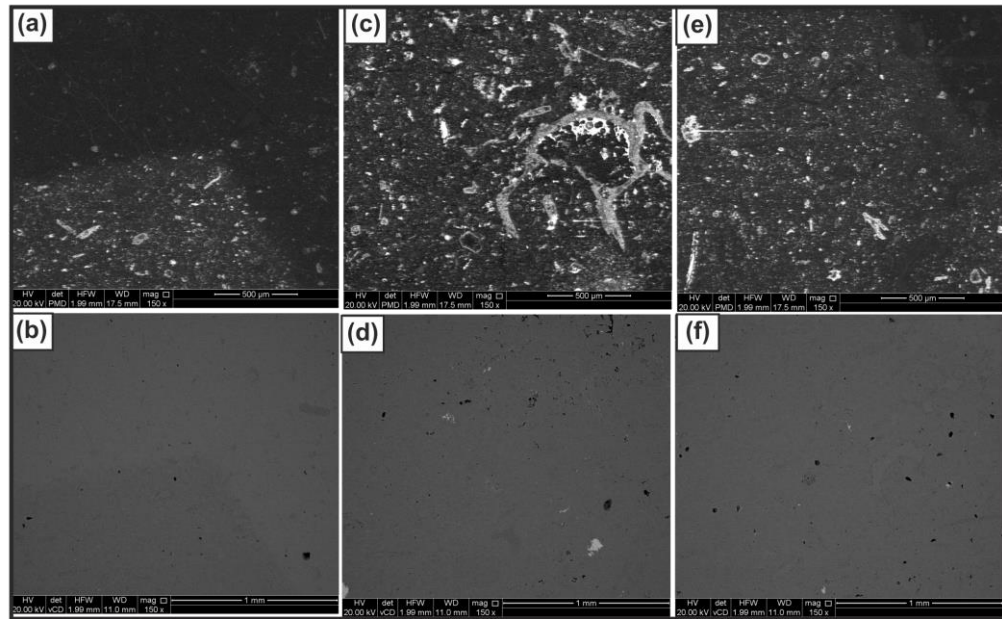


Figure 5.30: (a), (c) and (e) SEM-CL of flint samples from the Seaford Chalk, Dieppe, France. (b), (d) and (f) are backscattered photomicrographs of (a), (d) and (f) respectively. (b), (d) and (f) are backscattered photomicrographs of (a), (d) and (f) respectively.

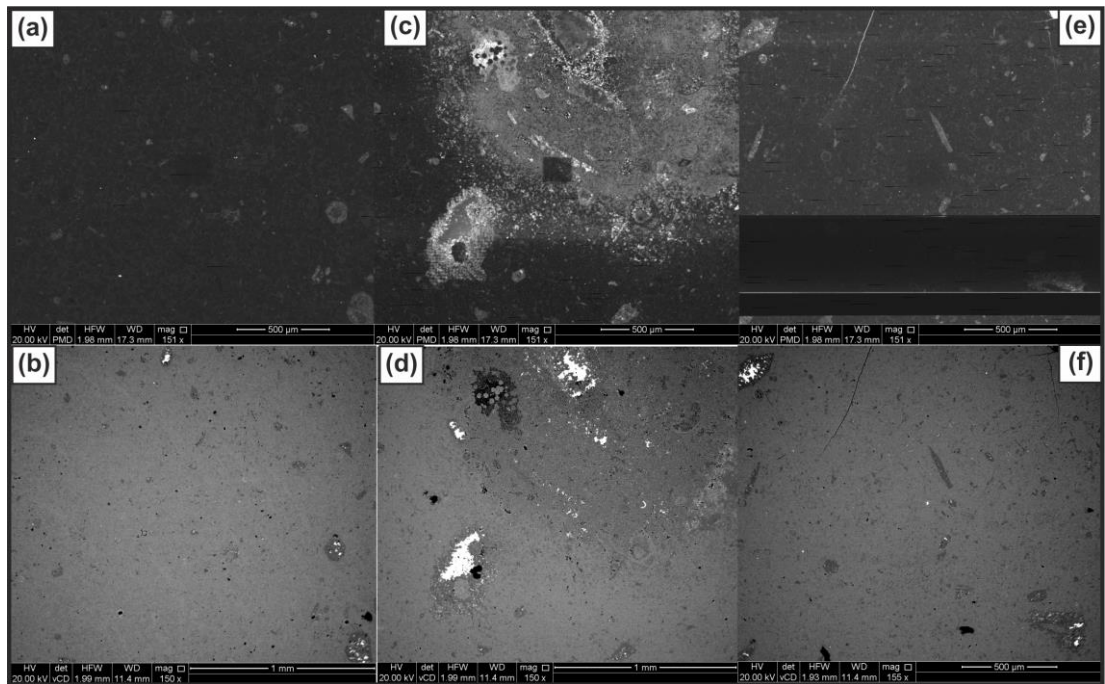


Figure 5.31: (a), (c) and (e) SEM-CL of flint samples from the Lewes Chalk, Mesnil-Val, France. (b), (d) and (f) are backscattered photomicrographs of (a),(d) and (f) respectively. Note the gradual replacement of calcite by silica and the traces of fully silicified forams and sponge spicules.

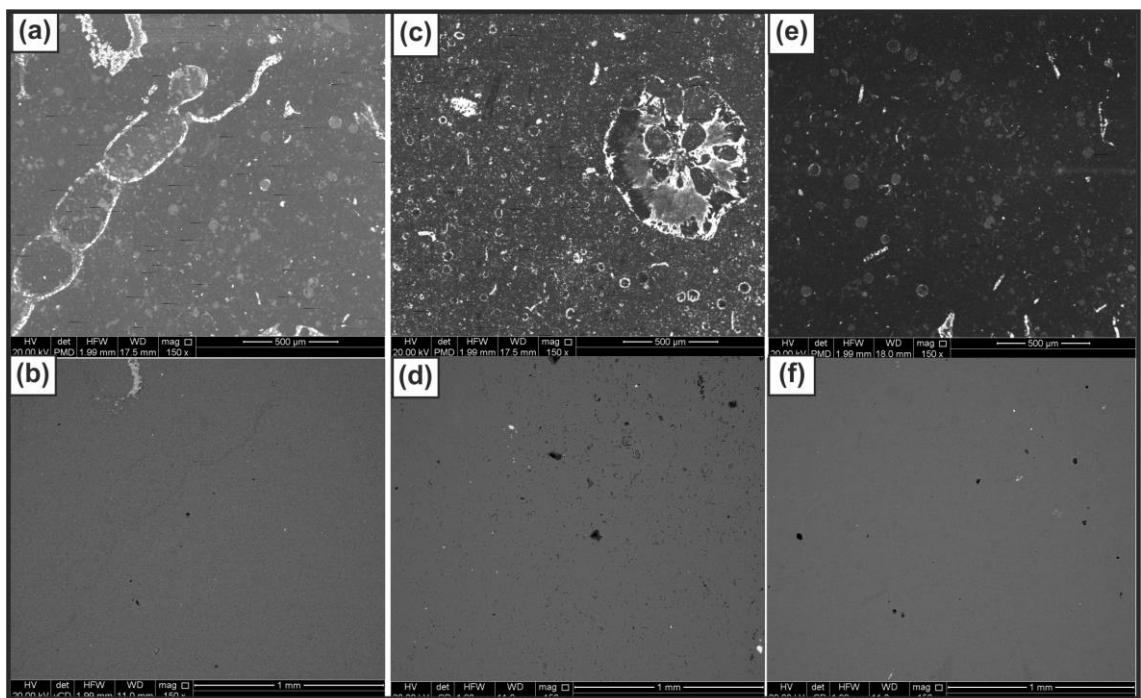


Figure 5.32: (a), (c) and (e) SEM-CL of flint samples from the Tor Chalk, at Stevns Klint Denmark. (b), (d) and (f) are backscattered photomicrographs of (a), (c) and (e) respectively. As observed in the thin section, fossils are well preserved in these samples. The CL images clearly shows the occurrence of three phases of amorphous silica, low temperature quartz and calcite inclusions seen in the remaining samples.

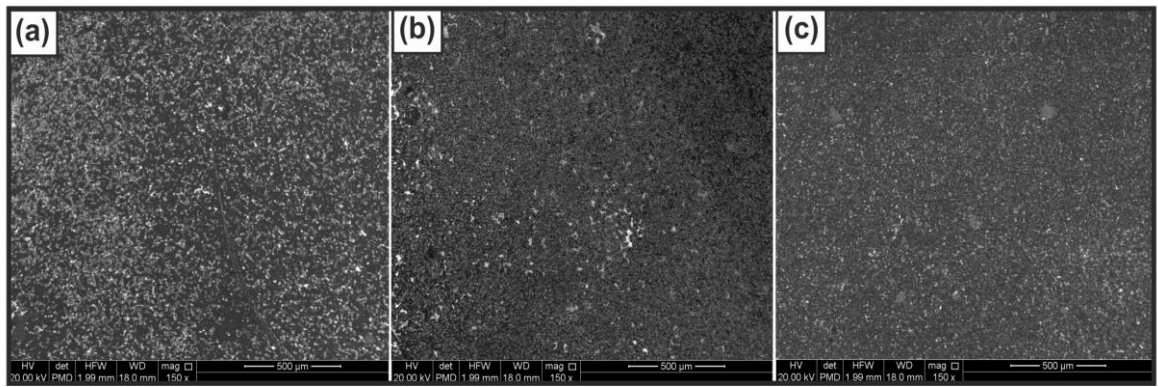


Figure 5.33 : (a), (b) and (c) are SEM-CL photomicrographs of flint samples from the Tor Chalk, at Møns Klint, Denmark. Note the presence of silica filled microfracture, traces carbonate inclusion (white) and amorphous silica.

## 5.6 Micropetrographic Index ( $I_{pf}$ ) and Engineering Properties of Flints

The  $I_{pf}$  was determined as described in Chapter 3, Section 3.8, pp.103-105. Table 5.5 shows the calculated  $I_{pf}$  for flint samples grouped according to tectonic history and mineral composition. The overall data indicates higher  $I_{pf}$  ranging from 9 – 12 for the strongest and the most abrasive dark brownish grey flints, and reduced in the grey flints (4 – 6). The abrasivity (RAI) and strength (UCS,  $I_{s(50)}$ ) properties of flints were correlated with  $I_{pf}$  of flints.

Table 5.5: Micropetrographic index of flints ( $I_{pf}$ , in red fonts)

Flint Colour	Flint types	% Cement	Quartz (%)	Calcite (%)	Voids (%)	Non-cement (%)	$I_{pf}$
Grey	BNLUK	66.02	98.09	1.91	3.53	33.98	4.16
	BLSUK	73.22	98.86	1.14	0.85	26.78	5.98
Dark brownish grey	SEUK	85.46	99.16	0.84	1.10	14.54	11.20
	SDFr	84.02	99.5	0.50	0.46	15.98	10.83
	LMFr	85.76	98.79	1.21	0.47	14.24	11.59
	TSKT	82.64	98.54	1.46	0.47	17.36	9.39
	TMKT	81.64	98.69	1.31	0.51	18.36	8.94

Except for the To, the results of these relationships show that as cementation and quartz content increases, the abrasivity and strength of flints increase with statistical significance (Figures 5.34 – 5.35). As calcite content and microfractures increase, the

strength and abrasivity of flint decrease. The data in Figures 5.34 – 5.35 suggests that  $I_{pf}$  increases as the UCS ( $R^2 = 0.96$ ),  $Is_{(50)}$  ( $R^2 = 0.90$ ) and abrasivity ( $R^2 = 0.94$ ) of flints increase. The high coefficients of determinants identified with  $I_{pf}$ -UCS, RAI, and  $Is_{(50)}$  relationships suggest  $I_{pf}$  is a good predictor of compressive strength and abrasivity of flints. Focusing on To-  $I_{pf}$  relationship, no relationship is observed (Figure 5.35). The poor correlation observed in the To-  $I_{pf}$  relationship is suggested by the high degree of scatter indicated among the data points with low correlation coefficient ( $R^2 = 0.47$ ). This implies that  $I_{pf}$  is not a good predictor of tensile strength of flints.

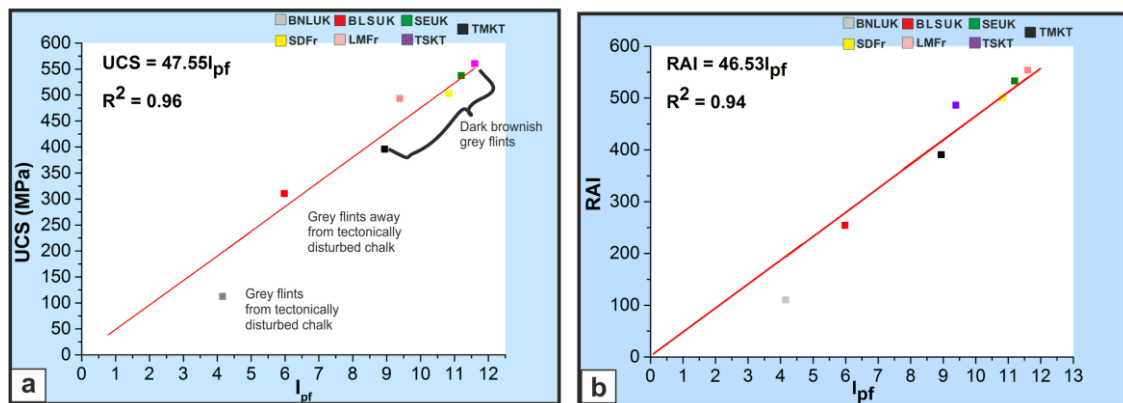


Figure 5.34 : (a) UCS against  $I_{pf}$ , (b) RAI against  $I_{pf}$  (Note the on map description of flint colours in 5.34 (a) applies to 5.34 (b)).

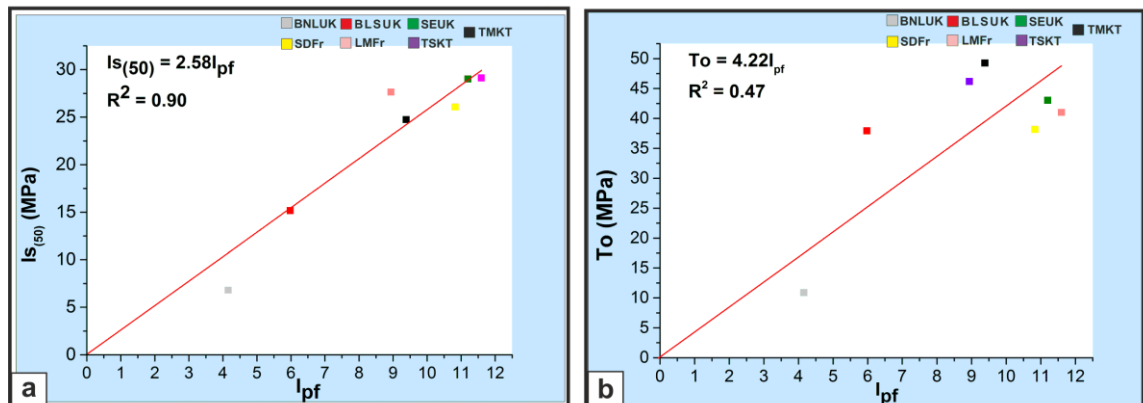


Figure 5.35 : (a)  $Is_{(50)}$  against  $I_{pf}$ , (b) To against  $I_{pf}$  (Note the on map description of flint colours in 5.34 (a) applies here too)

## 5.7 Chapter Summary

Trends in petrographic studies on flints, associated structures and the surrounding chalk show:

1. significant variations between grey flints and the DBG flints in terms of microstructures/microtexture.
2. that the light grey, grey and the brownish grey flints (BNLUK) have less degree of silica cementation, more spherical quartz grains, and remarkable intergranular/intercrystalline micro pores than the dark brownish grey and brownish grey flints.
3. that the DBG flints have less recrystallized quartz crystals/grains, but more massive quartz cements as a results of high degree of silica cementation.
4. that the presence of microfractures in the samples collected from the more tectonically disturbed zones (especially grey flints, BNLUK) than those collected from the less tectonically disturbed zones. The microfractures seen in the grey flints are conspicuously absent in the DBG flints.
5. two major mineral phases in flints, WCr and the surrounding chalk. In flint samples, only  $\alpha$ -quartz and calcite were detected, with  $\alpha$ -quartz being the most dominant mineral phase, while calcite is the minor mineral phase.
6. that the composition and distribution of the  $\alpha$ -quartz and calcite are associated with flint colour, and flint structure. In the white crust (WCr) for example, the dominant phase varies with physical features and the degree of silicification of the WCr. The thick, soft WCr surrounding the grey flints (Figure 5.43), possessed calcite as the main mineral, with lower  $\alpha$ -quartz content. In contrast to the WCr associated with the grey flints, the thin, strong WCr surrounding the DBG flints, has  $\alpha$ -quartz as the main phase, with subordinate calcite phase.
7. that for flints, higher percentage of  $\alpha$ -quartz was found in the DBG flints, while the lowest is recorded by the LG flints. In between this range are the LBG, GF and BG flints presented in increasing order of the  $\alpha$ -quartz content and decreasing order of calcite content. The analysis also indicates the WCr associated with the DBG flints has the highest amount of  $\alpha$ -quartz which is closer to flint, while the WCr related to the grey flints have the least, but is significantly having the higher percentage of calcite more closely to the surrounding chalk.
8. similarity in mineralogy between the chalk surrounding flints across all the investigated study sites.
9. more calcite inclusions in the grey flints, as opposed to fewer in the DBG flints. The DBG have dense homogenous fabrics, with completely silicified

microfossils. Preservation of microfossils varies between flint types. The DBG flints at Stevns Klint have the highest and the most preserved partially silicified calcareous microfossils than any other samples investigated. This can be partly the explanation for the relatively lower strength and abrasiveness of these samples compared with the DBG flints from the Lewes and Seaford Chalk formations.

10. variations in microstructures between WCr and the flint materials. The WCr appears to possess dissolved coccoliths and some silicified fossils that have replaced calcite in the WCr. Contrary to this, coccoliths were not seen in the flint part of the sample. But similar siliceous microfossils seen in the WCr are dominant in the flint samples and have been completely silicified. In between flint and the WCr, thin section analysis also shows a boundary, where calcite-silica relationship reaches equilibrium and this forms the weaker few mm portion of flints that have less resistance to penetration of the drill bits when drilling flints, than the flint core.
11. the relationship between grey flints and the DBG flints observed in other mechanical and physical tests are reflected in the petrographic investigations. SEM-CL displays higher proportion of calcite inclusions in the grey flints, than in the DBG flints. Another striking observation in the SEM-CL analysis is the detection of three sets of CL-luminescence characteristics representing different generations of quartz, especially in the grey flints and DBG flints from the Møns Klint. In the grey flints, the presence of low temperature quartz (CL-non luminescence), amorphous silica (CL-grey) and calcite inclusion (CL-bright/white) were identified and compared with backscattered electron images. The major difference between grey and the DBG flints as identified by the SEM-CL is the fewer calcite inclusions detected in the DBG flints, while several inclusions were observed in the grey flints, and more opaline silica were noticed in the grey flints, than seen in the DBG flints. The analysis also indicated the presence of diatoms and radiolarians in the grey flints, while more sponge spicules and Foraminifera were identified with the DBG flints.
12. A relationship between microstructures, mineral composition, origin, site specific geology, flint colour and the material properties of flints. The cryptocrystalline nature of flint fabric and high degree of silica cementation suggest why Cerchar abrasivity test failed to properly characterised flint as noticed by the sliding of the Cerchar pin over the flint surface.
13. A good relationship between strength, abrasivity and  $I_{pf}$  of flints was found and shows  $I_{pf}$  can be used to estimate the strength and abrasivity of flints.

Finally, in all the petrography techniques employed for this study, Chalcedony was not detected in the samples. The presence of opal-A (amorphous silica) was not also detected by the XRD but was identified by the thin section microscopy and the SEM-CL. Moreover, these are more pronounced in the grey flints and some samples of TMKT. Likewise, in both thin section and the SEM-CL analyses, the presence of fluid inclusions was not also detected, as calcite remains the major impurity identified with the investigated samples. The identification of calcite in the samples was confirmed by all the petrographical approaches used in this study, while the presence of FeO<sub>2</sub> was suspected and inferred using both SEM-CL and thin section examinations.

Figure 5.36 summarises both the physical and petrographic observations made within the different colours, types and structures of flints investigated in this study.

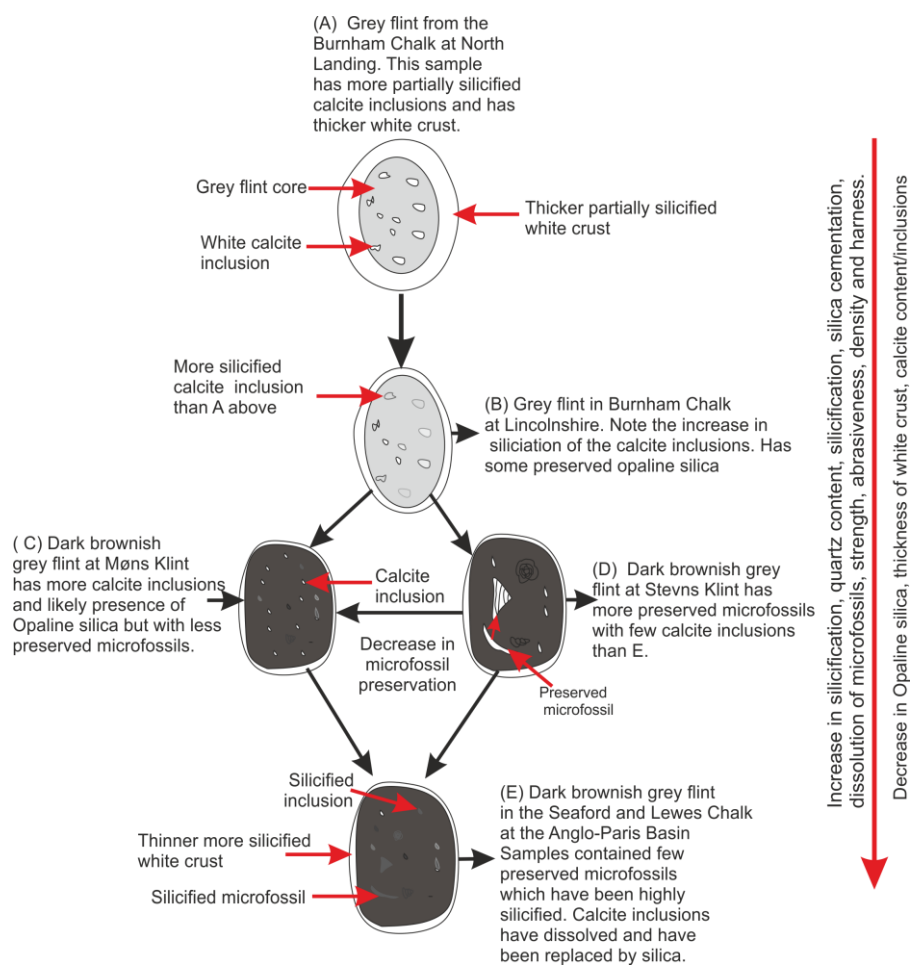


Figure 5.36: Conceptual Model that summarises the evolution of flint as observed in Chapter 5 (not to scale).

Following the identification of controls on material properties of flints, Chapter 6 will discuss the physical, mechanical and petrographic data presented in Chapters 4 and 5.



## **Chapter 6 Discussion of Research Results**

### **6.1 Introduction**

In Chapters 4 and 5, results of physicommechanical and petrographic characterisation of flints were presented. The empirical relationships between selected flint properties were established. The overall results showed variation in material properties of flints with flint type, colour, structure and geographical distribution. The causes of variations derived from petrographic and the SEM-CL approaches were discussed in Chapter 5. In this chapter the overarching geological and geotechnical issues are addressed.

#### **6.1.1 Chapter Structure**

This chapter is divided into twelve sections. Section 6.1 introduces the chapter, while Sections 6.2, 6.3, and 6.4 discuss the mechanical, wear and petrophysical properties of flints respectively. In section 6.5 the correlations between flints from different environments is addressed, while the genesis of flints and geological controls on behaviour of flints are respectively treated in Sections 6.6 and 6.7. These sections are followed by a discussion on the relationships between the engineering properties of flint materials with microtexture, structure (macro and micro), morphology, and mineral composition of flints (Section 6.8). The relationship between the drillability of flints and class of flints are discussed in Section 6.9, while the implications of the study for engineering are discussed in Section 6.10. Correlations between engineering properties of flints are discussed and the chapter is summarised in Section 6.12

### **6.2 Material Mechanical Properties of Flints**

#### **6.2.1 Strength, Density and Static Elastic Properties of Flints**

It has been shown that flint has variable and very high intact strength, stiffness and density which show some variations. The strength, deformability and density of flints from various regions have been examined considering the colour, microtexture, microstructures, mineral composition, spatial constraint and morphology. Different locations were considered to test the link between these mechanical properties of flints and tectonic influence on the embedded flints. To achieve this, grey flints sampled from tectonically disturbed chalk (in fault zone) were compared to the grey flint sampled away from the fault zone. Similarly, the DBG flint from the glacially deformed chalk of

Møns Klint was compared to the dark brownish grey flints (DBG) from the less disturbed chalk. The link between the investigated mechanical properties of flints and factors such as: flint colour; mineral composition; microtexture; and microstructures was investigated by relating the UCS,  $I_{s(50)}$ ,  $T_o$  and  $E_s$  values of grey flints with those of the DBG flints.

Table 6.1 shows that the strength (UCS,  $I_{s(50)}$  and  $T_o$ ), deformation modulus ( $E_s$ ) and density ( $\rho$ ) of flints are related to the microtexture, microstructures, mineral composition, tectonic histories of flints and the lithology of the host chalk. From Table 6.1 it can be established that the DBG flints that were identified as more silicified and had undergone a complete silicification are consistently the strongest, stiffest and densest materials investigated. The extremely high strength, stiffness and high density of these samples are explained by the presence of high intensity of silica cementation (Figure 5.11, p.171), high degree of carbonate silicification, more quartz content (Table 5.4), smaller quartz grains (see Table 6.7), completely silicified inclusions (Figures 5.29 – 5.33, pp.193-196), and relatively lesser calcite content.

Table 6.1: Summary of mechanical properties of flints.

Col-our	Properties Samples	UCS (MPa)	$E_s$ (GPa)	$T_o$ (MPa)	$I_{s50}$ (MPa)	$\rho$ (gcm <sup>-3</sup> )	Remarks
Dark brownish grey flints	SEUK	250-842 <b>537</b>	57-103 <b>80</b>	15-100 <b>43</b>	12-59 <b>29</b>	2.53-2.82 <b>2.69</b>	Sampled from relatively more porous, less dense and less tectonically disturbed chalk
	SDFr	250-943 <b>503</b>	65-133 <b>85</b>	21-70 <b>38</b>	12-42 <b>26</b>	2.48-2.97 <b>2.67</b>	
	LMFr	231-798 <b>560</b>	67-106 <b>85</b>	27-78 <b>41</b>	19-43 <b>29</b>	2.48-2.99 <b>2.66</b>	
	TSKT	155-811 <b>493</b>	38-122 <b>78</b>	38-57 <b>49</b>	10-41 <b>25</b>	2.52-2.59 <b>2.55</b>	
	TMKT	221-625 <b>396</b>	61-90 <b>78</b>	34-64 <b>46</b>	21-37 <b>27</b>	2.56-2.59 <b>2.58</b>	Sampled from glacially deformed chalk
Grey flints	BLSUK	48-609 <b>311</b>	46-100 <b>69</b>	12-46 <b>38</b>	5-26 <b>15</b>	2.38-2.54 <b>2.49</b>	Sampled away from tectonically disturbed zone
	BNLUK	25-232 <b>112</b>	-	7-14 <b>11</b>	3-12 <b>7</b>	2.16-2.55 <b>2.43</b>	Sampled from highly tectonically disturbed zone

Note: The mean values are presented in bold

However, the grey flints, which are generally less dense than any other flint investigated in the present study, have consistently remained the weakest samples. The microstructural and mineralogical variations observed between the grey flints (BNLUK and BLSUK) and the DBG flints explained the reduction in strength, stiffness and density in the grey flints. This was confirmed by the SEM, XRD, and SEM-CL results presented in Chapter 5 (pp.158-195).

However, a relatively high  $E_s$  is seen in the grey flints (BLSUK<sub>n</sub>) and this is questionable, because the mean  $E_s$  is affected by an outlier and only four samples were tested in this flint category. The mean  $E_s$  derived from this group required further study to ascertain the actual stiffness of this flint category. The mean  $E_s$  for grey flint (BLSUK<sub>i</sub>) remained the least of all the flint samples investigated. The low  $E_s$  of this sample is a clear example of how  $E_s$  varied with factors like the silica cementation, carbonate silicification, porosity, mineral composition and microstructures of flint when compared to the DBG flints since the major differences between the flint types are that of mineral content, colour, microfractures and microtexture (Figures 5.11 a-f, p.171 and 5.12, p. 172). For grey flints (BNLUK) collected from the tectonically disturbed chalk  $E_s$  of these samples was not determined because the strain gauges attached to the samples frequently detached from the samples at the early stage of loading due to fracturing associated with the samples.

The variation in UCS,  $T_o$ ,  $I_{s(50)}$ ,  $E_s$  and  $\rho$  of flints with flint colours is explained by comparing grey flints sampled away from the fault zone (BLSUK) with DBG flints which despite being intact; the grey flint still recorded lower strength, stiffness and density than DBG flints. Decreased silicification resulted in slight reduction of strength, density and stiffness of the TSKT in which microfossils were less silicified and TMKT samples when compared with the DBG flints from the Anglo-Paris Basin. Similarly, the presence of minute calcium carbonates filled pores (Figures 5.26, p.190 & 5.33, 196) also lead to a reduction in mechanical properties of the DBG flints (TMKT). These samples, though, more cemented than grey flints, but have more carbonate within the flint matrix with traces of opaline silica as evidenced in both SEM-CL and thin section analyses of the samples than the DBG flints from the Anglo-Paris Basin. Increased in calcium carbonate even as minute  $CaCO_3$  pores reduces flint strength.

A confirmation of the likely role of tectonic deformation, weathering or glacial influence on UCS,  $T_o$ ,  $I_{s(50)}$  and  $\rho$  of flints can be noticed by comparing the mean values of these mechanical properties of the BNLUK samples with that of BLSUK (see Section 2.5, pp.14-15, and Figure 3.4a-c where the fractures in Chalk are seen to persist through the embedded flints). Mechanical characterisation data (Table 6.1) demonstrate the grey flints (BLSUK) are consistently stronger than the tectonically disturbed flints (BNLUK). Most fractures seen in these samples are related to the Flamborough Head Fault Zones as these samples are collected from this crushing zone and are intensified by the microtexture and the significant calcite inclusions in the flint beds. The variation in mechanical properties between the two flint types of the same colour, and from chalk formation at a similar stratigraphic level, but different tectonic history is also because the BLSUK flints are relatively less fractured and at the same time have more silicified matrix and inclusions than the BNLUK. This

observation, therefore, confirmed the suggestion by Cumming (1999) that tectonic activities are among the major factors affecting the strength of flints.

The influence of glaciotectonic history of the Møns Klint Chalk could also contribute to the relative weakness seen in the TMKT sample, as evidenced by the presence of microfractures in the flints. This could be related to the impact of the glaciotectonic processes associated with these flints. This observation cannot be considered robust and a clear conclusion on the effects of tectonics on mechanical properties between the TMKT flints and the rest of the DBG flints cannot be drawn due to the small number of samples tested.

The strength results for DBG flints are within the range of strength results of reported by Cumming (1999). However, the strength results for grey flints (BNLUK) do not fall in the strength range previously reported for flints. The deviation of the strength results for these samples from the previously reported results is suggested to be due to structural defects and the presence of significant calcite inclusions in the samples. Other causes of weakness are ascribed to the: infilled with partially silicified calcite; the extent of carbonate silicification; incomplete silica cementation; the presence of opaline silica and mineral composition (Figures 5.14 (p.180), 5.16 (p.182), & 5.27 (p.191)).

For the deformation modulus ( $E_s$ ), the stiffness of flints found in this study is higher than those reported in the previous study (Cumming, 1999) for flints but is comparable to the  $E_s$  reported for silica polymorphs, low quartz 95.4 GPa, Silica glass 79.3 to 84.40 GPa and Cristobalite 65.2 GPa (Pabst & Gregorová, 2013). The clear discrepancy observed between the  $E_s$  values of flint derived in this study and the previous study is because of the different approaches employed to derive  $E_s$  (earlier highlighted in Chapter 2, Section 2.13.1, 39-44).

Likewise, the mean  $I_{s(50)}$  reported in the present study for the DBG flints contradicts the mean  $I_{s(50)}$  for flint samples from Cray and Brighton reported in Smith et al. (2003). The discrepancy observed between the two studies could be due to the influence of more calcite vugs observed in the flint samples investigated in the earlier study than seen in the DBG flints examined by this study.

The overall density results for the DBG flints investigated in this study are in general agreement with previous studies on density of flints (Iller, 1963; Michelseen, 1971; Hökelek, 2000) and are more like the density of quartz, while that of grey flints differ significantly from the density results reported in previous studies. The reasons for this deviation are due to peculiar mineralogical and microstructural features of the grey flints.

The present findings therefore, imply that the stress required for bit-rock impact in drilling or needed to crush flint in tunnelling can be significantly higher in the DBG flints than in grey flints. This however, depends on the mineralogy, microstructure and

tectonic histories of flints. Therefore, in future projects involving breaking, drilling, cutting or tunnelling flint, an accurate mechanical characterisation of flints that considers the above-mentioned factors affecting the mechanical properties of flints is vital.

### **6.3 Geotechnical Wear Behaviour of Flint**

#### **6.3.1 Abrasivity of Flint (CAI, EQC and VHNR)**

The abrasivity of various flint categories examined and compared as presented in Chapter 4, Section 4.3, pp.126-134. Table 6.2 shows the summary of CAI results of all the flint materials studied using both standard CAI (with 7 kg static load) and the modified CAI using 9 kg static load in this study. The CAI of the two major flint colours comprising the grey and dark brownish grey flints were compared with each other and with their respective lighter counterparts (light grey and light brownish grey). The aim was to characterise the abrasiveness of flint and identify any relationship between the abrasiveness of flint with colour, mineral composition, structures and geographical locations of flints.

The abrasivity results show the flint samples regardless of colour variation and locations fall into two classes of abrasiveness corresponding to very abrasive category (Cerchar, 1986) encompassing most flint samples, and extremely abrasive class that was only identified with the LMFR flints (from Lewes Nodular Flint band). This agrees with most previous CAI investigations on flints (Varley, 1990; Cumming, 1999; Fowell & Abu Bakar, 2007; Ihe, 2011). The reason for the deviation of LMFR flints from other flints is not clear from the result but could be associated with experimental errors or structural variations within the flint samples. Similarly, VHNR values of flints reported this study sites are within the VHNR range reported by Lautridou et al. (1986) for flints.

A slight variation in abrasiveness of flints with colours observed in the data as illustrated by the lower abrasiveness of the light grey flints when compared with grey/dark brownish grey flints is explained by the higher calcite content associated with the lighter samples. However, this variation is not significant and does not reflect any significant engineering implication, since the abrasivity values of both flint colours fall in the same abrasivity class (Table 6.3). A general comparison between abrasivity of grey flints and DBG flints and between tectonically disturbed and undisturbed flints does not show any trend or relationship with geology of the host chalk, microstructures and microtexture of flints. This is explained by the similarity identified in the abrasiveness of most flint materials examined using the EQC and VHNR in this study.

Most notably, this study extends on previous studies by demonstrating that the abrasivity of flints varies with flint structures and with significant differences in mineral composition of flint materials. The wear characterisation data (Table 6.2) demonstrates an increase in abrasivity of flint structures with increase in quartz content and subsequent decrease in calcite content (Tables 6.2 & 6.3).

Table 6.2: Summary of CAI, VHNR and EQC of different classes of flints

Flint colour Flint types	CAI (0.1 mm)		VHNR (kgmm <sup>-2</sup> )	EQC (%)	Remarks
	Grey/dark brownish grey	Light grey/light brownish grey	Grey/dark brownish grey	Grey/dark brownish grey	
<b>BNLUK</b>	2.70 – 4.59 <b>3.47</b>	2.40 – 4.57 <b>3.29</b>	1141.82	98.13	The CAI results categorise these samples in the very abrasive category. Note the slight reduction in CAI between grey and light grey flints.
<b>BLSUK</b>	3.06 – 4.34 <b>3.85</b>	2.75 – 3.30 <b>3.11</b>	1149.55	98.88	
<b>TMKT</b>	3.20 – 3.93 <b>3.46</b>	2.54 – 3.93 <b>3.18</b>	1136.85	98.69	A slight variation (cause by differences in mineral composition) in CAI values can be seen between these these flint types. Except the LMFr flint which belong to the extremely abrasive category, all other flint types in this group fall in the very abrasive category same as the grey flints.
<b>TSKT</b>	3.54 – 4.34 <b>3.87</b>	3.00 – 3.84 <b>3.31</b>	1146.57	98.59	
<b>LMFr</b>	3.26 – 5.27 <b>4.23</b>	2.96 – 4.75 <b>3.57</b>	1148.85	98.81	
<b>SDFr</b>	3.04 – 4.57 <b>3.82</b>	2.77 – 4.30 <b>3.47</b>	1155.98	99.51	
<b>SEUK</b>	2.54 – 4.81 <b>3.59</b>	3.03 – 4.64 <b>3.52</b>	1152.57	99.18	

Increase in calcite content and decrease in quartz content



The differences observed in abrasiveness between the white crust surrounding grey flints and that surrounding DBG flints (Table 6.3 in red font) are associated with their mineral compositions as shown by the higher calcite and lower quartz contents in the WCr surrounding grey flint than in the White crust surrounding the DBG flints (see XRD results in Chapter 5, subsection 5.3.1, pp. 174-177). From Table 6.3 the transition between different abrasivity classes found (highlighted in different colours) purely

reflects the mineralogical variations of the samples, the lower the impurities (calcite) in the samples the higher the abrasivity of the sample and the lower the drill lifetime.

However, the CAI results (Table 6.3) do not indicate significant difference between the CAI results obtained using the standard CAI (7 kg stylus) and the modification (9 kg stylus) by this study. This is due to lack of or very minimal increase in wear flat of the Cerchar pin especially on flints. In most cases the test stylus could not make grooves on the samples; instead the styli slid leaving a minute line with silver appearance. This phenomenon can be attributed to the cryptocrystalline nature and high degree of cementation of the flint particles. These factors rendered the rock particles very difficult to be displaced by the magnitude of the applied static load on the stylus when equilibrium is reached between the applied load and the strength of flint. This, therefore, explain why the additional static load does not significantly affect the abrasivity results of flint materials.

Table 6.3: EQC and VHNR for chalk, the different flint types and structures.

<b>Flint /structures</b>	Chalk	WI	WCr	SSI	WCr	LG	LBG	BG	GF
EQC (%)	2.6	15.6	36.9	58.6	92.6	76.5	86.4	97.88	98.1
VHNR (kgm <sup>-2</sup> )	162.4	296.4	514.8	736.4	1081.8	920.1	1134.7	1139.0	1141.8
CAI (0.1 mm) 7 kg stylus	1.4	1.7	1.7	2.9	-	3.3	2.9	3.5	3.5
CAI (0.1 mm) 9 kg stylus	1.4	2.1	1.7	3.0	-	3.7	3.6	3.5	3.6
Bit life span (mbit <sup>-1</sup> )	Moderate		Very low		Extremely low				

The inability to detect the influence of microstructures on abrasiveness of flints indicates the reliance of EQC and VHNR on only the abrasive mineral in the rock, same techniques do not discriminate wear classification and therefore, are not good indicators of abrasiveness of flint. This observation shows demerits of these wear indices, as some significant wear controlling factors, such as grain size, microfractures; slight variations in mineral composition and silicification are neglected. This also explains the inability of the wear classification methods to detect significant variations in abrasiveness between the different flint categories. Similarly, insensitivity of CAI to detect any variation in abrasiveness between flints with different microstructures reflects the scale effects of the CAI method.

### 6.3.2 Rock Abrasivity Index (RAI)

The investigation of abrasivity of flints using Rock Abrasivity Index (RAI) has not been previously reported. This study is therefore, the first to estimate the abrasiveness of

flint using the RAI method and demonstrates that abrasiveness of flints is a function of microfractures (tectonically controlled), microstructures and mineral composition of flints. Figure 6.1 and Table 6.4 summarise abrasiveness of flints determined using RAI and illustrates how the abrasiveness of flints varies. Figure 6.1 also shows the RAI approach is a promising method of characterising the abrasiveness of flints and provides a better prediction of abrasiveness of flints than previously used methods employed to investigate the abrasiveness of flints (CAI, EQC and VNHR). This is demonstrated by the ability of RAI to clearly show the effects of the rock microfractures on abrasiveness of flints a key factor neglected by the earlier mentioned wear characterisation methods.

The influence of tectonics on the host chalk and silicification of carbonate is suggested by relatively higher RAI values (extremely abrasive material with extremely low drill bit lifetime) seen in the more silicified grey flints sampled away from the tectonically disturbed zone when compared with tectonically deformed and weathered grey flints (BNLUK) with high calcite inclusions. The variation in abrasiveness of flints with factors like colour a function of mineral composition, carbonate silicification, microtexture of flint is explained by the increase in RAI values from grey flints to DBG flints (Figure 6.1).

The DBG flints remain the most abrasive materials investigated and are classified as extremely abrasive materials with drill bit lifetime beyond the most current bit lifetime models. The DBG flints from less disturbed chalk are the most abrasive because they are denser, highly cemented, and stronger, with significantly fewer, highly silicified inclusions than other flint materials. These samples also have higher quartz content, and less calcite. The influence of silicification is demonstrated by the slight reduction of mean RAI among the DBG flints due more preserved microfossils and few calcite inclusions in some DBG flints. Therefore, variations observed in RAI values of flints confirmed the abrasiveness of flints depends on mineral contents, microtexture (grain size), microstructures and fracturing in flints.



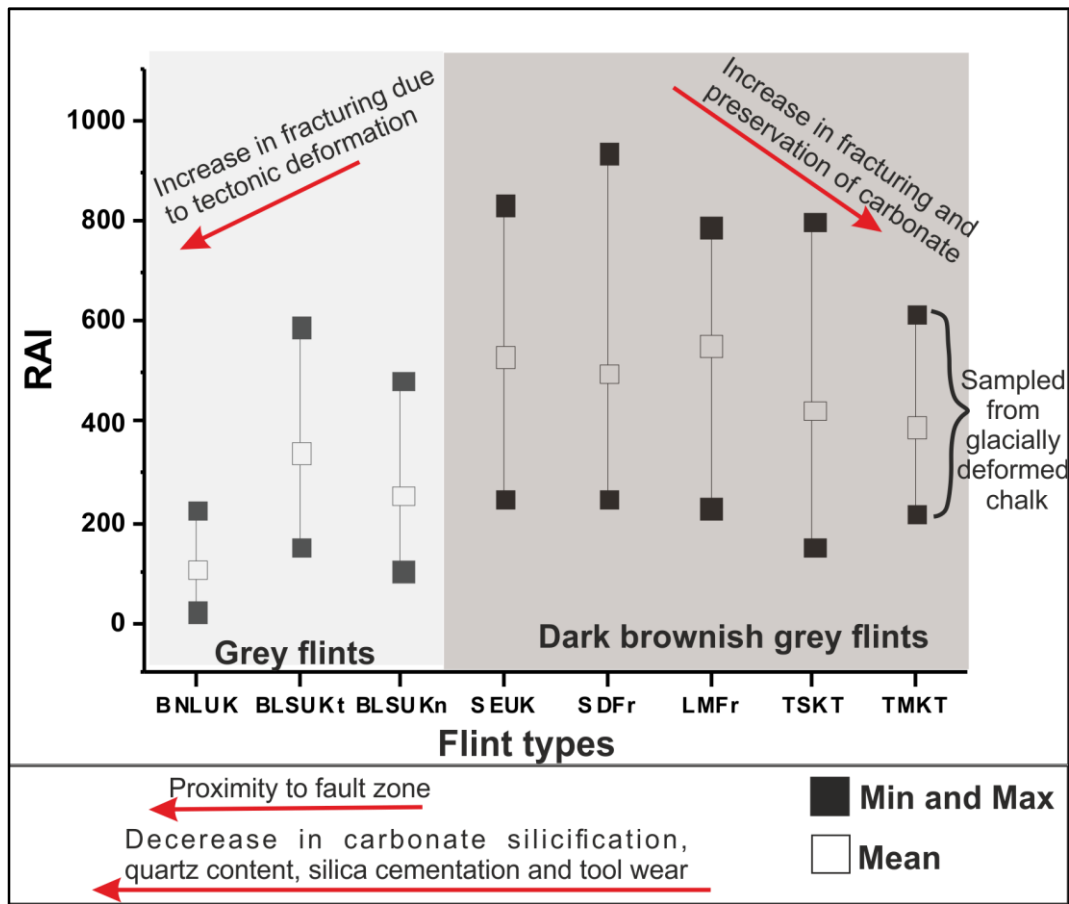


Figure 6.1: Summary of RAI results for different classes of flints.

Table 6.4: Summary of Rock abrasivity index (RAI) results for different flint types/classes

Main Classes	Flint Classes	RAI			Remarks
		MAX	MIN	MEAN	
Grey flints	BNLUK	24.7	236.8	110.1	Carious and highly tectonically deformed flint
	BLSUK <sub>n</sub>	107.5	505.4	261.0	Nodular, less fractured flint
	BLSUK <sub>t</sub>	157.7	616.9	266.9	Tabular, less fractured flint
Dark brownish grey flints	TMKT	217.7	632.9	390.6	Had some calcite inclusions within the matrix
	TSKT	153.0	822.3	486.2	Had more preserved microfossils
	SDFr	249.2	947.9	500.4	Highly cemented, silicified samples with highest quartz content and less calcite content are and structurally competent than grey flints.
	SEUK	230.5	614.9	532.8	
	LMFr	228.7	807.4	553.6	

Increase in silicification, quartz content, abrasivity and decrease in calcite content and fracturing.

The relationship between abrasiveness of flints and the morphologies of flints can be seen by comparing the RAI values of tabular flints, BLSUK<sub>t</sub> with that of nodular flints, BLSUK<sub>n</sub>, tabular flints, BNLUK and nodular flints comprising all the DBG flints (Figure 6.1). For BLSUK<sub>t</sub> and BLSUK<sub>n</sub> relationship the results show the nodular flints have slightly lower RAI values than the tabular flints. The reason for this variation is very difficult to explain because the samples have similar mineral compositions,

microtexture, microstructures and colour. For BNLUK and all nodular DBG flints, the variation in abrasiveness is that of the factors mentioned above, rather than that of morphological differences. Therefore, there is the need for more studies comparing different flint morphologies from different sites as this would help in drawing a reliable conclusion on abrasiveness-flint morphology relationship. The need for testing a wider range of flint types is also important. The variations observed in RAI values of flints confirmed the abrasiveness of flints depends on mineral contents, microtexture (grain size), microstructures and fracturing in flints.

### **6.3.3 Shore Hardness Properties of Flint**

Before the present study, there were probably only two available but unpublished previous studies (Michie, 2010; Ihe, 2011, unpublished dissertations) on testing hardness properties of flint using the Shore Hardness (SH) method. The present study is, therefore, an extension of these studies and further examines the hardness of flints from different origin, and relates the hardness of flint with microtexture, mineral compositions and degree of particle bonding of flints.

SH results in Figure 4.16 (p.135) shows there is a relationship between the microtexture, mineral content and the hardness of flint as observed across all the study sites investigated. The effects of microtexture and mineral contents (which are related to the colour intensity) on hardness of flint is suggested by the lower SH values seen in the light grey/light brownish grey flint (with more granular microtexture and calcite contents), as against the relatively high SH values observed in the grey/dark brownish grey flints (more quartz cement, and the high silica ( $\text{SiO}_2$ ) content).

The present study shows that the hardness of flint is related to the mineral composition, colour of flint, and microstructures of flint. These relationship needs to be considered in modelling flint for prediction of tool wear, cutterbility of flint and on the determination of equipment performance in chalk with flint. However, it is pertinent to note that, suggestion on the role of microfractures on the hardness of flint proposed in this study was based on the relationship between the SH of BLSUK, all DBG flints and the mean SH of a block of flint (BNLUK) and the SH from few samples from previous studies on the North Landing Flint. Thus, further studies that investigate more flint samples from tectonically disturbed chalk elsewhere, considering various flint types should be explored.

## 6.4 Petrophysical Properties of Flints

### 6.4.1 Ultrasonic Properties of Flints: Ultrasonic Velocities $V_p$ , $V_s$ and Dynamic Modulus Young's Modulus ( $E_d$ )

The results from the analysis of ultrasonic velocities ( $V_p$  and  $V_s$ ) dynamic Young's modulus ( $E_d$ ) conducted on flint samples representing different flint colour; morphologies and origin are summarised in Table 6.5. The analysis indicates the ability of the ultrasonic method to detect the influence of fractures/joints identified in the strength test results on the ultrasonic velocities of flint. The results show that the ultrasonic velocities and  $E_d$  of flints are more related to microfractures, carbonate inclusions, microtexture (intensity of silica cementation), carbonate silicification, porosity than to slight changes in mineral composition and colours of flint. This is illustrated by the low ultrasonic velocities and  $E_d$  exhibited by the grey flint (BNLUK) and the DBG (TMKT) samples. These relatively low ultrasonic velocities and  $E_d$  of the grey flint (BNLUK) sample can be simply explained by the high porosity caused by fracturing and high calcite inclusions in the samples.

The low ultrasonic velocities and  $E_d$  of DBG, TMKT samples is attributed to the presence of a wide distribution of calcite within the matrix of the samples (Figures 5.33, p.196). The ultrasonic velocities and  $E_d$  of these samples are slightly higher than those of grey flint (BNLUK) because the TMKT samples are more competent in terms fewer microfractures. The matrix of TMKT flints are also relatively more cemented than BNLUK, and this facilitates the wave travels within the flint matrix as a result of suitable grain contact in the sample.

Further increase in ultrasonic velocities and  $E_d$  of flints is observed in the grey flint (BLSUK<sub>t</sub> and BLSUK<sub>n</sub>) and DBG flint (SEUK, SDFr, LMF<sub>r</sub> and TSKT). These flint samples recorded highest ultrasonic velocities,  $E_d$  and show unexpectedly consistent results across the study sites, with very little variation, regardless of colour variations and geographical locations.

Furthermore, the closer ultrasonic velocities and  $E_d$  values seen between grey flint BLSUK and the DBG flint show the inability of the ultrasonic pulse velocities to detect slight differences in microtexture and mineral composition between different colours of flints. The high ultrasonic velocities and  $E_d$  seen in these samples are related to significantly high degree of silica cementation, high intensity of carbonate silicification, less fracturing, and low porosity characterising these flint samples. These factors are most likely associated with post-depositional diagenetic processes and the physical properties of the host chalk as shall be discussed later.

The high density and quartz (see Table 6.1) of the BLSUK and the DBG flints also contributes to the higher ultrasonic velocities and  $E_d$  seen in these samples as against the slightly weaker BNLUK (with lower density and higher porosity). The effects of density on ultrasonic velocities have been previously identified in several rocks (Soroush et al., 2011) while the roles of porosity, as well as quartz content are also shown in Klimentos & McCann (1990); Jizba (1991); Tutuncu (1994).

Table 6.5: Showing minimum, maximum and average  $V_p$ ,  $V_s$  and  $E_d$  of flints.

		Ultrasonic pulse velocities and dynamic modulus of flints			
Flint colour	Flint type	$V_p$ ( $ms^{-1}$ )	$V_s$ ( $ms^{-1}$ )	$E_d$ (GPa)	Remarks
Dark brownish grey flints	SEUK	5300 - 5690 5494	3379 - 3741 3523	123 - 150 138	Sampled from relatively more porous, less dense and less tectonically disturbed chalk
	SDFr	5064 - 6180 5465	3314 - 3958 3540	120 - 168 138	
	LMFr	5053 - 5852 5479	3291 - 3750 3540	114 - 156 137	
	TSKT	4600 - 6444 5540	3232 - 4166 3547	107 - 183 134	
	TMKT	5027 - 5785 5334	3296 - 3745 3476	114 - 149 128	Sampled from glacially deformed chalk
Grey flints	BLSUK	4975 - 6083 5431	3103 - 3769 3392	104 - 157 127	Sampled away from tectonically disturbed zone
	BNLUK	4131 - 5640 5030	2649 - 3624 3192	68 - 135 104	Sampled from highly tectonically disturbed zone

Due to lack of published data on ultrasonic velocities and  $E_d$  for flints, this study compares the compressional wave velocity ( $V_p$ ) derived in the present study with published  $V_p$  ranging from 5500 to 5900  $ms^{-1}$  for quartz (Ultra Sound Velocity chart, 2015; US Data for solids, 2015), glass quartz, glass silica and fused silica (US Data for solids, 2015), because these materials have very similar properties to flints. The compressional wave velocity ( $V_p$ ) for most of the flint samples tested in this study is within the range reported above, except the  $V_p$  of BNLUK, which is lower. However, for

the shear wave velocity ( $V_s$ ) and  $E_d$  this study does not find any published data to compare with the present results.

#### 6.4.2 Micropetrographic Index and Engineering Properties of Flints

A number of studies (Mendes et al., 1966; Dixon, 1969 & Onodera et al., 1974) have applied the micropetrographic index to assess the extent of weathering of various rocks. Recently, Rigopoulos et al. (2010) introduced micropetrographic strength and replacement indices that determined the extent of alteration on dolerites. The present study introduces new approach by modifying the micropetrographic index presented in Irfan & Dearman (1978). The modification was achieved by considering cemented and un-cemented parts of flint samples as input parameters in addition to the inputs (voids and mineral constituents) proposed in previous studies (Section 3.8, p. 104).

The plots of  $I_{pf}$  versus strength and abrasivity of flints (Figures 5.34-5.35, p.197) represent dark brownish grey flints, grey flints sampled away from tectonic zones and grey flints sampled in the highly tectonic zone. The group with highest  $I_{pf}$  (8 – 12) represent the DBG flints. The explanation to the higher  $I_{pf}$  observed in these flints is due high quartz content, and highly cemented matrix which means less porosity and fracturing. The group with lowest  $I_{pf}$  represent the grey flints (located in tectonic zone, weaker and less abrasive), and the low  $I_{pf}$  seen in this group is due to microfractures, higher calcite content and high non-cemented matrix, implying high porosity. The slightly moderate  $I_{pf}$  (c.6) noted in the third group represent grey flints sampled away from tectonic zone. The moderate  $I_{pf}$  seen in this group is due to slightly higher cementation in the samples, less fractures and consequently less porosity of the samples.

Table 6.6 provides the regression equations and coefficient of determinants derived from the relationships between abrasivity, strength and  $I_{pf}$  of flints. The good linear relationship seen between compressive strength, abrasivity and  $I_{pf}$  as confirmed by the coefficient of determinants shows that these engineering properties of flints can be measured using  $I_{pf}$ .

Table 6.6: Statistical relationships between  $I_{pf}$  and some engineering parameters

Parameters	Equations	$R^2$
$I_{pf}$ vs UCS	$UCS = 47.55I_{pf}$	0.96
$I_{pf}$ vs $Is_{(50)}$	$Is_{(50)} = 2.58I_{pf}$	0.90
$I_{pf}$ vs $To$	$To = 4.22I_{pf}$	0.47
$I_{pf}$ vs RAI	$RAI = 46.53I_{pf}$	0.94

The low coefficient of determinants seen between the tensile strength ( $T_o$ ) and  $I_{pf}$  suggests  $T_o$  is not closely correlated with micropetrographic index of flints (sample set). This is counterintuitive as it is a known fact that, the tensile strength of most rocks is affected by the mineral content and microstructures of rocks. The poor relationship found between  $T_o$  and  $I_{pf}$  is not likely controlled by the material properties of flints, but due to problems with  $T_o$  test method and sample dimensions. This is because the thickness of the samples with higher  $T_o$  but with correspondingly moderate  $I_{pf}$  (6 – 8), is smaller (c. 10 mm) when compared to the thickness of the remaining samples with higher  $I_{pf}$  (10 – 12). Further investigation using flint samples with as similar sizes as possible would help.

#### **6.4.3 What are the Porosity-Flint Colour/Structure and Grain Size-Flint Colour/Structure Trends?**

*Porosity (ImageJ-Porosimetry ( $\phi_{im}$ ) and Helium-Porosimetry ( $\phi_{He}$ ))-Flint Colour/Structures Trends*

The porosity of flint is related to the following factors: microfractures, carbonate inclusions/silicification, and mineral composition of flints. Colour of flints is also related to the porosity of flint. This relationship was established using the He-Porosimetry ( $\phi_{He}$ ) and the ImageJ-Porosimetry ( $\phi_{im}$ ) to determine the porosity of different flint structures, morphologies and various flint colours representing different geographical locations and geological/tectonic histories.


The ImageJ-Porosimetry was used to allow for the determination of porosity of flints with different structures and colours of flints that were too small for He-Porosimetry measurement and to measure the material porosity of flints. The estimated porosity derived from this method was compared with that evaluated from He-Porosimetry with the view of establishing a simple empirical relationship between the two methods so that future prediction of porosity of flint might not need the complex and hard sample preparation usually associated with preparing flint samples for the determination of porosity using other methods.


The porosity of flint derived using the two methods mentioned above as functions of flint samples categorised by colours, morphologies and geographical locations are presented in Table 6.7. It is evident from the results that porosity of flint decreases with increase in silicification of carbonate, the degree of silica cementation, quartz content, and a reduction in calcite content, grain size, as well as microfractures of flint.


However, the influence of microfractures is more pronounced in the results. This can be seen by the two categories of porosity illustrated in the results. The two major classes of porosity results are reflected in both methods used to estimate the porosity of flints (see Table 6.7). The first group comprises of grey flints with relatively higher porosity ( $\phi_{im} = 4.54 \pm 0.34\%$ ) and 5.50% for  $\phi_{He}$  (Table 6.7).

Table 6.7: Summary of porosity of flints measured using Helium prosimetry and image analysis.

		$\phi_{He}$ (%)	$\phi_{image\ analysis}$ (%)			
Flint colour types	Flint colour	Grey/Dark brownish grey	Grey/Dark brownish grey	Brownish grey	Light grey/Light brown grey	Remarks
		BNLUK	1.63 – 7.47 <b>5.50</b>	3.53	3.27	
BLSUK	0.05 - 8.00 <b>1.72</b>	0.85	-	-		
TMKT	0.47-1.72 <b>0.80</b>	0.51	-	0.59	Dark brownish grey flints dominate these samples. These samples have finer microtexture and were from relatively less dense more porous chalk.	
TSKT	0.59 – 2.07 <b>1.15</b>	0.47	-	0.80		
LMFr	0.04 – 3.31 <b>1.63</b>	0.47	-	1.07		
SDFr	0.85 – 2.24 <b>1.47</b>	0.46	0.48	1.35		
SEUK	0.04-2.24 <b>1.19</b>	1.10	1.14	1.65		


 Increase in calcite content

Increase in tectonic disturbance and fracturing 

Increase in silica cementation quartz content and carbonate silicification 

The BNLUK samples exhibit the highest porosity of the entire samples investigated. The porosity of these samples are greater than those of the DBG flint studied in this study and porosity of flint previously reported elsewhere (Weymouth, 1951; Iller, 1963; Jakobsen et al., 2014), apart from the porosity of 16.50 % for white flint from Tyra Field North Sea Central Graben reported in Jakobsen et al. (2014).

The higher porosity characterising the BNLUK flint is mainly due to the massive network of microfractures, higher carbonate inclusions, higher calcite content, poorly silicified microtexture (see Chapter 5), larger and more granular quartz grains (Figures 5.6 (p.166), 5.9 (p.169), 5.10 (p.169), and 5.11 (p.171)) than any other sample investigated. The lower porosity seen in the BNLUK when compared to the higher

porosity (16.50%) reported in Jakobsen et al. (2014) is more or less explained by the variation in silicification of carbonate and mineral composition between the two materials. This is because the samples reported by that study was white flint as mentioned above and contained significantly higher calcite content (6.10%), than the grey flint investigated in this study with relatively lower calcite content (1.91%). Therefore, variation in porosity between these samples further illustrates the relationship between the porosity and the mineral composition of flints.

Table 6.7 also indicates the dark brownish grey flints, DBG (SEUK, SDFr, LMFr, TSKT and TMKT), as the least porous flint of the whole samples studied in this study ( $\phi_{He} = 0.80 - 1.72\%$ , and  $\phi_{im} = 0.47 - 1.10\%$ ). This category of flints represents the second class of porosity. The lowest porosity shown by these samples conforms to the extremely strong (Figure 6.2), abrasive, and stiff categorisation of these samples by the respective strength, abrasiveness and stiffness/rigidity tests previously discussed in this study for this group of flints. The slight range in porosity observed between these samples is attributed to the few defects peculiar to individual sample tested. The mean porosity results for these samples are consistent between sites and with the porosity of flint reported in previous studies (Weymouth, 1951; Iller, 1963; Jakobsen et al., 2014), regardless of the two methods of estimating porosity used in this study.

A statistical relationship between UCS and  $\phi_{He}$  was investigated (Figure 6.2, p.216) to observe the relationship between the strength and porosity of flints. The UCS- $\phi_{He}$  relationship displays an increase in porosity with reduction in strength. This is clearer between grey flints from the tectonically disturbed chalk (enclosed in red). Relatively, higher porosity (2 – 4%) were observed among some data points (enclosed in green) mostly dominated by grey flints. Lowest porosity observed between two clusters of data with strength range between 450 – 800 MPa (enclosed in blue) and (100 – 400 MPa, enclosed in black), shows that the UCS of flints is related to the  $\phi_{He}$  of flints, but this relationship is negative and weak.



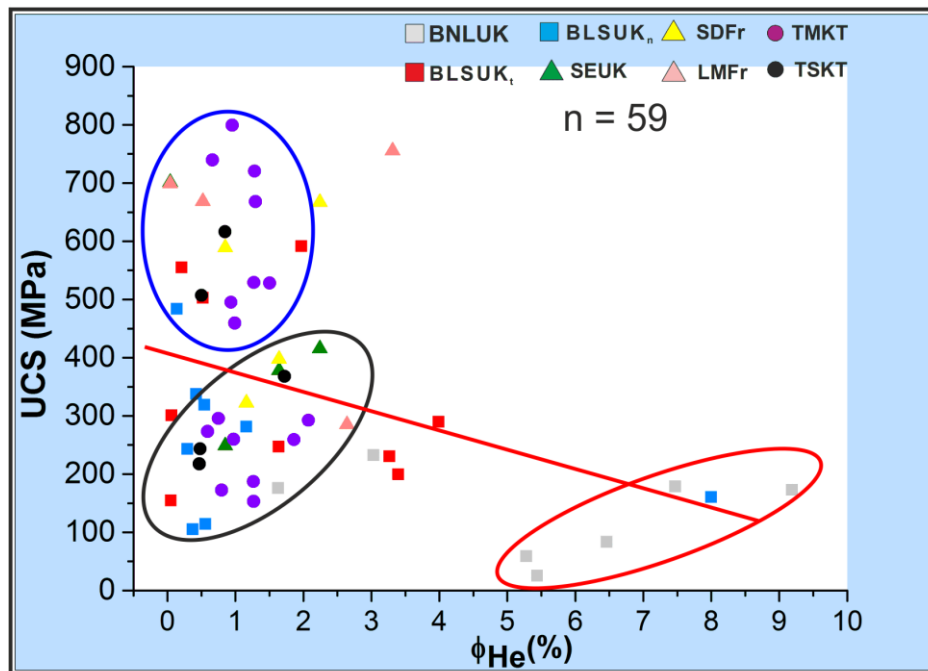


Figure 6.2: UCS versus  $\phi_{He}$ . The grey flints in tectonically disturbed chalk is enclosed in red.

The petrographic approaches employed in this study suggest that the low porosity of DBG flints derived from both methods, is a result well developed quartz cements, and slightly higher quartz content (Figures 5.21 and 5.22, p.187) in the samples. Additionally, the completely silicified/finer matrices, with fewer calcite content and significantly less fracturing seen in the samples than any other flint sample examined in this study also contribute to the low porosity of the samples. These features are mostly comparable between the DBG flints class and explain the consistency seen in the porosity results.

The variation between porosity of flint and classes of flints as well as the physical properties of the host chalk can be compared in Figures 4.23, p.143 and 4.24, p.145. The variation in porosity of flint with physical properties of the host chalk, silicification of carbonates, intensity of silica cementation and mineral composition is clearly explained by the reduction in porosity from the grey flint BNLUK to the DBG flints (Figure 4.24, p.145). In both methods applied for the estimation of porosity, a demonstration of the relationship between flint classes and porosity can be seen even within site (Figure 4.23, p.143), for instance in the BNLUK samples, an increase in porosity with colour can be observed where the porosity of flint increases from the brownish grey to the light brownish grey flint.

The explanation for the change in porosity between these classes of flint is given by the variation in mineral composition, silica cementation and silicification of carbonate. The brownish grey (BG) flint which shows the lowest porosity is characterised by higher quartz content, more silicified matrix, and less calcite content,

than the grey flint (GF), the light grey (LG), up to the most porous sample the BG. Even among the darker flint samples in the remaining sites (Figure 4.24, p.145) variation in the porosity of flint with colour was noted. The variation in porosity between these two colours is those of microtexture and mineral composition. The DBG have finer, better cemented matrices than the LBG. Where a slight deviation from this pattern is observed, as the porosity of SDFr and SEUK where BG and DBG flints have almost the same porosity, this is attributed to the similarity observed in almost every aspect of the two samples.

A drastic reduction in porosity can be noticed when the grey flint BNLUK is compared with the grey flint BLSUK<sub>t</sub> and BLSUK<sub>n</sub> (Figures 4.23, p.143 and 4.24, p.145). The porosity of BNLUK ( $\phi_{He} = 5.50\%$ ,  $\phi_{im} = 3.53\%$ ) is seen to be higher than that of BLSUK ( $\phi_{He} = 1.72\%$ ,  $\phi_{im} = 0.84\%$ ) samples (Figure 4.24, estimated using He-Porosimetry), and 76.20% greater than the porosity of both BLSUK<sub>t</sub> and BLSUK<sub>n</sub> (Figure 4.22, p.143, measured using the ImageJ-Porosimetry). The difference in porosity between these flint samples of the same class is attributed to two major factors: the first factor is the tectonic history; the second factor is the diagenetic geochemical processes leading to silica recrystallisation. These processes explain the microtexture and more silicified inclusions in the BLSUK (BLSUK<sub>t</sub> and BLSUK<sub>n</sub>) samples and the network of microfractures, weak, granular quartz grains suturing, with more carbonate inclusions noticed in the BNLUK flints.

#### *Grain Size - Flint Colour/Structures Trends*

The particle size analysis of different classes of flint sampled from various sites was conducted using image analysis software. The aim was to investigate how grain size of flint relates to the variation in colours, material properties and drillability of flint. Previous studies on grain size of flint (Iller, 1963; Michelseen, 1966; Jeans, 1977; Græstch & Grunberg, 2012; Lindgreen & Jakobsen, 2012) have shown that for most dark flints, the mean grain size is mostly below 1  $\mu\text{m}$ . Image analysis showed that the particle size of flints ranged from 0.25 - 0.77  $\mu\text{m}$  (Table 6.8). Similarly, Iller (1963) illustrated a variation in grain size of flints with colour. Again this study confirmed there is a relationship between grain size of flints and the colours of flint. The present study further extends on previous investigations by illustrating how colour intensity of flint relates with grain sizes, material properties and the drillability of flints.

Table 6.7 shows the grain size of flint varies according to the colour variation of flint across all the study sites. This can be observed by relating the grain sizes of the different colours of flints investigated in this study. The grain sizes of grey/light grey flints (BNLUK and BLSUK) are larger than the grain sizes of DBG/BG flints (SEUK,

SDFr, LMFr, TSKT, and TMKT) across all the study sites. The variation in grain size between different colours of flints from different sites could be associated with the intensity of silicification and re-crystallisation.

Table 6.8: Grain size of the different classes of flints

Flint colour types		Grain Size ( $\mu\text{m}$ )				Remarks
		Grey/Dark brownish grey	Brownish grey	Light brown grey	Light grey	
	BNLUK	0.52	0.41	0.42	0.77	Grey flints dominate these samples. These samples have coarser microtexture and were from denser, less porous chalk.
	BLSUK	0.47	-	-	0.63	
	TMKT	0.34	-	0.45	-	Dark brownish grey flints dominate these samples. These samples have finer microtexture and were from relatively less dense more porous chalk.
	TSKT	0.30	-	0.35	-	
	LMFr	0.29	-	0.42	-	
	SDFr	0.28	0.28	0.45	-	
	SEUK	0.26	0.26	0.40	-	

In samples with larger grain size (BNLUK and BLSUK) the flints are partially silicified and less cemented, and have not undergone significant transformation after recrystallisation than the DBG/BG flint samples with finer/smaller grain sizes (SEUK, SDFr, LMFr, TSKT, and TMKT). These DBG/BG flints are distinguished from grey/light grey flints by being completely silicified and dominated by massive quartz cement. The significant appearance of quartz cement and significantly lower carbonate, as well as silicified inclusions in these samples, suggest these samples are intensely silicified than grey flints.

Although, a slight variation in grain size is observed between different colours of flints, all the investigated flint samples correspond to the cryptocrystalline grain size category. Even though, the grain sizes of all the different colours/varieties of flint investigated in this study correspond to cryptocrystalline materials, a clear, practical difference in drillability and material behaviours between the various colours of flints is observed.

## 6.5 How do Flints from Different Environments Correlate?

In order to investigate how flints from the different environments correlate regarding the material properties of flints, samples were drawn from different geographical locations. A comparison between the material properties of BNLUK samples and that of BLSUK shows the samples are similar in colour, microtexture (Figure 5.11a-b, p.171), and mineral content (Figure 5.21a-b, p.187), but have different physicochemical properties (Figure 6.3). These samples are both from Burnham Chalk Formation at the Northern Province, UK, but have experienced different tectonic disturbance (refer to Chapter 2, Sections 2.5-2.6, pp.14-17). A comparison between grey flints (BLSUK and BNLUK) and the dark brownish grey flints from the Anglo-Paris Basin and from the Danish Chalk (TSKT and TMKT) shows some differences in mineral composition, microtexture and the overall physicochemical properties of flints (Figure 6.3).

When the dark brownish grey flints with similar geological background from the South of England and those sampled from the North-Western France are compared, they show similar material properties (Figure 6.3). However, when the material properties of the dark brownish grey flints from the Danish chalk (TSKT and TMKT) were compared, they exhibited significantly different properties. These samples are both of the same class and from the same region, but have different geological and deformational settings. As such this can be considered as an analogue for the differences in stress history between BNLUK and BLSUK samples. This tends to suggest that stress history exerts a control on the physicochemical properties of flint. The same degree of fracturing observed in BNLUK is not observed in the deformed TMKT samples.

Increase in strength, density, abrasiveness, stiffness, hardness, and silicification

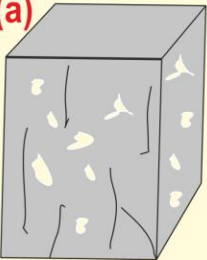
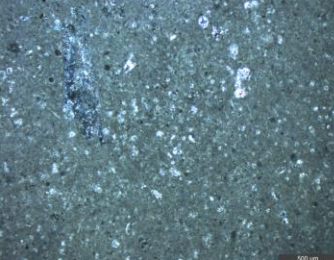
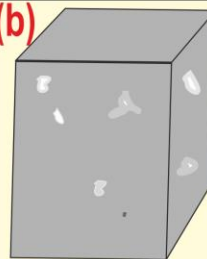
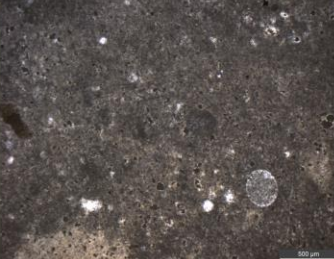


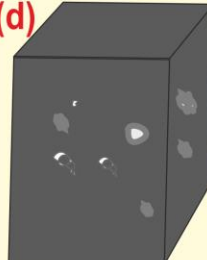
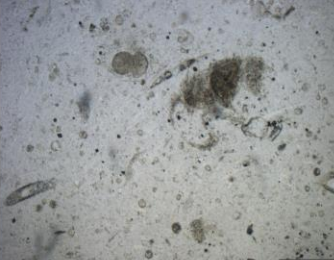
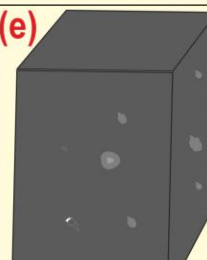

Flint Class	Illustration Image	Physical and petrographic properties
<p><b>(a)</b></p>  <p>Higher calcite inclusions</p> <p>Highly fractured</p> <p>Embedded in denser, tectonically disturbed chalk (in fault zone)</p>		<p>UCS=112 MPa      CAI =3.3</p> <p>RAI = 110      Quartz =98.1%</p> <p><math>I_{(50)}</math> =7 MPa      Calcite=1.9%</p> <p>To =11 MPa      <math>\phi_{H_0}</math> =5.5%</p> <p>EQC =98.1%      Gr. size =0.52<math>\mu</math>m</p> <p>VHNR =1142 kgm<sup>-2</sup>      <math>\rho</math>=2.43 gcm<sup>-3</sup></p>
<p><b>(b)</b></p>  <p>Calcite inclusions slightly silicified</p> <p>More competent</p> <p>Sampled in chalk away from the tectonically disturbed zone</p>		<p>UCS=311 MPa      CAI =3.9</p> <p>RAI = 307      Quartz =98.9%</p> <p><math>I_{(50)}</math> =15 MPa      Calcite=1.1%</p> <p>To =38 MPa      <math>\phi_{H_0}</math> =1.7%</p> <p>EQC =96.9%      Gr. size =0.47 <math>\mu</math>m</p> <p>VHNR =1149 kgm<sup>-2</sup>      <math>E_s</math>=69 GPa</p> <p><math>\rho</math>=2.49 gcm<sup>-3</sup></p>
<p><b>(c)</b></p>  <p>Calcite inclusions well silicified</p> <p>Less preserved fossils/fragments and more competent than A.</p> <p>Embedded in porous and glacially deformed chalk.</p>		<p>UCS=396 MPa      CAI =3.2</p> <p>RAI = 391      Quartz =98.7%</p> <p><math>I_{(50)}</math> =27 MPa      Calcite=1.3%</p> <p>To =46 MPa      <math>\phi_{H_0}</math> =0.8%</p> <p>EQC =98.7%      Gr. size =0.34 <math>\mu</math>m</p> <p>VHNR =1148 kgm<sup>-2</sup>      <math>E_s</math>=78 GPa</p> <p><math>\rho</math>=2.56 gcm<sup>-3</sup></p>
<p><b>(d)</b></p>  <p>Calcite inclusions well silicified</p> <p>More preserved fossils/fragments</p> <p>More competent and embedded in weaker, and porous chalk</p>		<p>UCS=493 MPa      CAI =3.9</p> <p>RAI = 427      Quartz =98.6%</p> <p><math>I_{(50)}</math> =25 MPa      Calcite=1.5%</p> <p>To =49 MPa      <math>\phi_{H_0}</math> =1.15%</p> <p>EQC =98.5%      Gr. size =0.30 <math>\mu</math>m</p> <p>VHNR = 1147 kgm<sup>-2</sup>      <math>\rho</math>=2.55 gcm<sup>-3</sup></p> <p><math>E_s</math>=78 GPa</p>
<p><b>(e)</b></p>  <p>Calcite inclusions mostly silicified</p> <p>Fossils/fragments completely silicified</p> <p>Strongest samples embedded in less dense and porous and chalk</p>		<p>UCS=503-560 MPa      CAI =3.5-3.9</p> <p>RAI = 500-553      Quartz =98.8-99.5%</p> <p><math>I_{(50)}</math> =26-29 MPa      Calcite=0.5-1.2%</p> <p>To =38-43 MPa      <math>\phi_{H_0}</math> =1.2-1.6%</p> <p>EQC =98.5%      Gr. size =0.26-0.29 <math>\mu</math>m</p> <p>VHNR = 1149-1156 kgm<sup>-2</sup></p> <p><math>E_s</math>=80-85 GPa      <math>\rho</math>=2.55-2.66 gcm<sup>-3</sup></p>

Figure 6.3: Conceptual Model illustrating variations in material properties among different flint categories (not to scale).

## 6.6 What is the Origin of Flints?

### 6.6.1 The Formation of Flint

Previous studies that have focused on origin/ formation of flints suggested biogenic origin of flint which is supported by thin section microscopy (Figures 5.14 - 5.26, pp. 180-189) and SEM-CL data (Figures 5.27 - 5.33, pp.191-196) through the calcite-silica replacement relationships. These relationships are strongly influenced by diagenetic processes and other factors such as temperature (Abdel-Wahab et al., 1999), time and depth of the sedimentation (Anselmetti & Eberli, 1993). The biogenic origin of flints suggested in this study is supported by the presence of abundant microfossils consisting of sponge spicules, radiolarians, diatoms, bryozoans and foraminifera in thin sections (Figures 5.14 – 5.26, pp. 180-189) and SEM-CL (Figures 5.27 – 5.33, pp.191-196).

The formation of flints follows evolutionary pattern as indicated by the thin section, SEM, SEM-CL and XRD results presented in Chapter 5. The XRD results indicate a pattern in mineralogy between different flint structures, colours and the surrounding chalk. The trend in mineral composition of flints shows an increment in quartz content in ascending order commencing from the chalk surrounding flint>white inclusion>white crust>light grey flints>light brownish grey flints>grey flints>brown grey flints>dark brownish grey flints, while calcite content decreases in that order (Table 5.4). This pattern in mineralogy is explained by the degree of silicification controlled by the extent diagenetic transformation undergone by the flints or associated structures.

The suggestion of biogenic origin of flints due to silica-calcite replacement and dissolution processes proposed in this study is consistent with the works of Bromley et al., (1975); Clayton (1984:1985); Madsen & Stemmerik (2010) and many others on flint formation and is supported by the petrographic data presented in Chapter 5. The petrographic data shows that the major contributor to the formation of the investigated flints is the dissolution of siliceous microfossils mainly foraminifera, sponge spicules and radiolarians (Figures 5.14 – 5.26, pp. 180-190 and 5.27 – 5.33, pp.191-196). This observation is also consistent with the findings of Von Rad et al. (1978); Abdel-Wahab et al. (1999) on the biogenic origin of flints. The microfossils are mostly seen to replace calcite in the samples and have in some instances filled the dissolved calcite pores in the main carbonate matrix.

Opaline silica filling radiolarian tests are observed in the grey flints (Figures 5.16 e and f & 5.17, 182-183) and have occasionally been transformed or recrystallised to  $\alpha$ -quartz as evidence in the SEM-CL results (pp.191-195), while in some portions precipitated opaline silica is preserved (Figures 5.27 a-d, p.191).The occurrence of

opaline silica in the investigated flint samples suggests that it is unlikely precipitated directly as  $\alpha$ -quartz, but as biogenic Opal-A, which follows the silica transformation pathway from Opal-A  $\rightarrow$  Opal-CT  $\rightarrow$  cryptocrystalline quartz as described in Von Rad et al. (1978); William & Crerar (1985); William et al. (1985). In most dark brownish grey flints, biogenic opaline silica is rarely seen suggesting either this must have been transformed or dissolved due to its unstable nature to cryptocrystalline quartz. This transformation is likely to have been influenced by the porosity/permeability of the chalk hosting the dark brownish grey flints.

In addition to the above sources of silica for flint formation, the precipitation of silica for flint formation was also suggested to occur at oxic-anoxic boundary upon oxidation of the  $H_2S$  at the said boundary (Clayton, 1984; 1985). Clayton (1984; 1985) further provided the detailed chemistry of the entire processes leading to silica-calcite precipitation/dissolution and further described the processes leading to the formation of different flint morphologies. These silica-calcite precipitation/dissolution/replacement relationships are supported in this study as significant part of flint evolution as justified by the presence of preserved calcite in some partially silicified flints; void filling phase dominated by euhedral mega quartz crystals within cryptocrystalline quartz (Figure 5.28 a-b, p.191) and the preservation of siliceous microfossils in the flint samples.

The presence of calcite inclusions (Figure 5.27a-d, p.191) and the evidence of clear/gradual gradation from siliceous phase to calcite phase, with mixture of silica-calcite at the flint-crust boundary (Figures 5.5a, p.164 & 5.14 a-d, p.180) as shown in both thin section results (Figures 5.16-5.26, pp. 182-190) and SEM-CL results (Figures 5.27-5.33, pp.191-196) also support the silica-calcite, precipitation/dissolution or replacement process of flint formation. This mixture illustrates silica gradually replacing calcite, as calcite continues to dissolve.

The dissolution of calcite can be seen in Figures 5.14 a-b, p.179 and Figures 5.15 a-b, p.181 where forams chambers filled with calcite (have started dissolving) are observed in the white crust and even within the white crust some microfossils have already been silicified and have started replacing calcite in the white crust. The gradual replacement of calcite in the white crust explains the quartz content recorded using the XRD in the samples. Significant proportion of calcite content seen in the white crust is indicated by XRD. The presence of siliceous microfossils (mostly foraminifera and sponge spicules) sporadically replacing calcite observed in Figure 5.15, p.181 further justified the calcite-silica replacement theory of flint formation. The present study also provides further details on the genesis of flints by describing the effects of host chalk lithology and pore water geochemistry on diagenesis of flints as detailed in Section 6.7.

## **6.7 What are Geological Controls on Material Properties of Flints?**

### **6.7.1 The roles of physical properties of chalk on physical properties of flints**

There is a link between the physical properties of chalk and the diagenesis of flints (which influences the extent of maturity/degree of silicification in flints). The roles of diagenesis on material behaviour of flints can be understood by comparing different flints structures and locations. Petrographic evidence and comparison between host carbonates with various lithological and the physical properties of flints indicate the importance of porosity/permeability of the host chalk on the formation and mechanical properties of flints. For example, the predominantly grey flints found in the denser, harder and less porous chalk of the Northern Province, UK has coarser microtexture (Figure 5.3a, p.163), significant calcite content (Table 5.4), thicker, softer and weaker white crust, with few silicified microfossils gradually replacing calcite.

The influence of properties of the host chalk on the diagenesis of flints can be understood by studying different flint structures. The white crust associated with the dark brownish grey flints for examples, is thinner, harder, stronger with higher quartz content and less calcite content (Table 5.4) than the WCr in the DBG flints. It is more abrasive than the white crust surrounding grey flints. As outlined earlier in this study, the dark brownish grey flints examined in the present study are formed in weaker, softer, less dense, porous and probably shallower chalk of the Anglo-Paris Basin and Danish Chalk formations (see Chapter 2, pp.18-28) by comparison to the Northern Province Chalk where the light grey and grey flints are formed.

Petrographic results in Chapter 5 show that the predominantly dark brownish grey flints identified with the soft and porous chalk are intensely silicified (Figures 5.11 c-f, p.171), as displayed by the extensive network of massive silica cement, with an increase in density and significantly low calcite content. Silicification in these flints is almost complete as demonstrated by the massive silica cement dominating the samples. Most microfossils and calcite inclusions in these samples have been completely silicified, leaving only very few detectable traces (Figures 5.19 a-f, p.185 and 5.20, p.186) and confirmed by the SEM-CL results (Figures 5.29, p.193, 5.30, p.194 and 5.31, p.195).

Unlike, the light grey and grey flints, the presence of opaline silica are rarely detected in any of the dark brownish grey flints, except in the TMKT samples where it is detected. This, therefore, suggests and further confirms that the two different flint colours were at various stages of silicification, with the dark brownish grey flints being at the advanced phase of silicification. Within the dark brownish grey flints, samples



from stronger chalk at Møns Klint have significant calcite distributions within the fabrics of the samples (Figures 5.26, p.190 and 5.33, p.196).

The light grey and grey flints have experienced an incomplete silicification due to relatively lower level diagenetic alteration partly as a result of low porosity, high density, high strength, and hardness of the host chalk, implying inverse trend was observed in the less porous chalk, where the flint experienced less localised addition and subsequent concentration of dissolved silica following the recrystallisation of the flints. This resulted in higher calcite contents and relatively lower quartz contents in the grey flints, than in the dark brownish grey flints (Table 5.4). Similarly, the partial silicification of these samples also lead to the formation and preservation crystallised aggregates in the light grey (Figure 5.6a, p.166) and grey flints (Figures 5.11a-b, p.171) as evidenced by the random distributions of silica cement and dominant, weakly cemented quartz microspheres, with slightly higher porosity.

In the brownish grey (Figures 5.9b-d, p.169), the light brownish grey (Figures 5.6 c-f, p.166) and dark brownish grey flints (Figures 5.11c-f, p.171), the crystallised aggregates have been transformed to massive silica cement, and some coalesced quartz grains/microspherules/microgranules. The likely explanation to the variation in degrees of the diagenetic transformation of flints as characterised by the difference in physical and engineering properties between grey and the dark brownish grey flints could also be partly due to variations in the physical properties of their host carbonates (chalk) as mentioned above. The roles of the host carbonate properties come into play in the diagenetic changes of flints, because flints that formed in shallower chalk is likely to have experienced pore fluid circulation and intense diagenetic changes. These intense diagenetic changes eventually resulted in likely addition/seeding of silica to the dark brownish grey flints and this resulted into the observed intense silicification of the samples.

The influence of pressure, temperature (Behl & Smith, 1992) and burial depth (Anselmetti & Eberli, 1993) have also been emphasised as significant factors in precipitation processes, and silicification, these have not been investigated in this study. The present observations, therefore, indicate that the depth of burial of host chalk and probably permeability (McBride et al. 1999; Kwiatkowski, 2005; Bustillo 2010) of the host chalk play significant roles in the formation, silicification and cementation of the embedded Chert (flint).

## 6.8 Engineering Properties of Flint

### 6.8.1 Influence of Microtexture/Microstructures in Material Properties of Flint

Petrographic approaches indicated there is a relationship between microtexture/structure of flints and the engineering properties of flints. This is consistent with similar findings reported in Dománski & Webb (2000) see Chapter 1, p. 4. Figure 5.6a, p.164 (clearer in Figure 5.8, p.166) shows the less abrasive (Figures 4.11 (p.129) and 4.14 (p.133)) Light grey flint; BNLUK has a discrete microtexture, with equigranular quartz microspheres sporadically separated by intercrystalline pores and microfractures. These features confirmed the larger grain size and relatively higher porosity (Figure 4.24, p. 145) recorded in this sample. The microtexture of the same colour of flint (BLSUK), but more abrasive than BNLUK has fewer quartz aggregates (microspheres), dense microtexture with clearly less intercrystalline pores (Figure 5.6b, p.166).

In the light brownish grey flints, which are more abrasive, less porous and harder than the light grey flints, the microtexture is denser; more cemented, and does not possess the micro pores seen in the light grey flints. The quartz in these samples have recrystallised and formed a near homogenous flaky matrix. The matrix of the flint samples is more cemented in the denser, harder, less porous, and abrasive in the brown grey flints (Figures 5.9a-d, p.169). Even within this colour the sample from BNLUK still shows the discrete features of quartz microgranules, though more cemented than in the light grey flint of the same sample (Figure 5.9a, p.169, 5.10, p.169). The extent of silica cementation is more in the grey flints, where most of the quartz microspheres have clearly coalesced and silica cement is very clear with only a few traceable micro pores (Figures 5.11a and b, p.171). These features of the grey flints confirm the relatively higher abrasiveness, hardness, and less porosity observed in these samples than the light grey flints.

Silicification is intensified in the dark brownish grey flints as shown by the extensive silica cement in the samples (Figures 5.11c-f, p.171, 5.12, p.172) from the complete fusion of quartz crystals and flakes (Figure 5.13). The intensive suturing of quartz crystals in these samples resulted into a dense, homogenous microtexture devoid of microfractures. These and the intense silicification justify the extreme strength, hardness, stiffness, abrasiveness, finer grain size and less porous nature of these samples. In conclusion, the series of microstructural transformations reflected in the microtexture of various flints investigated with corresponding engineering properties described above indicate a clear relationship between these properties. Therefore,

there is a link between the engineering properties of flints and the microtexture of the flints. This is important when predicting the wear behaviour of flint classes.

### **6.8.2 Influence of Morphology**

The relationship between the material properties of flints and the various morphologies can be understood by observing the differences between the nodular and tabular flints. The tabular flints comprise of grey flints (BNLUK and BLSUK<sub>t</sub>) while the nodular flints were all DBG flints (SEUK, SDFr, LMFr, TSKT and TMKT) and the grey flints, BLSUK<sub>n</sub>. Comparisons between these morphologies in terms of Strength (Figures 4.3; 4.7; & 4.8, pp. p.119, p.124 & p.125 respectively), deformability (Figures 4.4, p.120 and 4.5, p.121), density (Figure 4.6, p.123), abrasiveness (Figures 4.10, p.128, 4.12, p.130, 4.13, p.132, and 4.16, p.135), dynamic properties (Figures 4.17-4.20, pp. 137 -140), and porosity (Figures 4.23-4.24, pp.143-145) do not reveal any clear pattern or reliance on these properties on flints morphology.

The relationship between grey flints comprising the nodular flints (BLSUK<sub>n</sub>) and tabular flints (BLSUK<sub>t</sub>) from Lincolnshire does not indicate any significant relationship or pattern between these morphologies and the material properties of flints. This is unsurprising as both BLSUK<sub>t</sub> and BLSUK<sub>n</sub> have similar microtexture, microstructures, and mineral compositions and are formed in chalk of the same lithology and tectonic history. This observation differs with that between tabular flints from the grey flints (BNLUK and BLSUK<sub>t</sub>) and the nodular flints representing the entire dark brownish grey flints (SEUK, SDFr, LMFr, TSKT and TMKT).

Similarly, the relationship between the porosity of flint and flint morphology can be seen by comparing the porosity results between grey tabular flint, BLSUK<sub>t</sub> and grey, nodular flint, BLSUK<sub>n</sub> (Figures 4.23 and 4.24, pp.143 & 145). In both results, there seems to be no significant relationship between flint morphology and porosity.

However, it should be noted that this comparison was made between samples collected from the same site, which might be biased. Therefore, a further study investigating more flint morphologies from other geographical locations would be significant. These two flint morphologies clearly differ in their material properties, microtexture, microstructures, and mineral compositions and are formed in chalk of different lithology and tectonic histories.

The conclusion that can be drawn is that material properties of flints are not controlled by the morphology of flints. Evidence relating material properties of flints from various regions with flint morphologies indicates the major controls on these properties are the microtexture, microstructures, mineral compositions of flints and the lithology/tectonic histories of the host chalk rather than the structure.

### **6.8.3 Effects of Macrostructures/Tectonic of the Host Chalk on the Properties of Flint**

The tectonic history plays a vital role in influencing the material properties of flints. The relationship between the macro/microstructures and the material properties of flints is illustrated by the significant deviation of the material properties of the highly fractured grey flints, BNLUK from any other investigated flints in this study including the grey flints, BLSUK. A comparison between the strength, abrasivity, sonic, porosity of flints samples (BNLUK) drawn from tectonically disturbed chalk shows a distinct variation regarding these properties. This variation is also seen when grey flints BNLUK were compared with similar flints from same stratigraphic level, but away from the fault zones, Ulceby Vale House Quarry, Lincolnshire, UK (BLSUK).

Although, a slight reduction in mechanical properties is observed in the BLSUK samples when compared to the dark brownish grey flints, the influence of tectonics on the mechanical properties of North Landing flints is significant. This is suggested by the significantly lower strength, stiffness and hardness characterising the North Landing flints, when compared to the BNLUK samples. Additional evidence is the similar behaviour exhibited by the BNLUK flints with both grey flints (BLSUK) and all the DBG flints in CAI, EQC, and VHNR results where the influence of fracturing is less significant (Figure 6.4). This change in mechanical properties of flints, especially in the BNLUK flints is attributed to the presence of a network of both micro and macro fractures in the North Landing flints. This explains the roles of tectonic on the properties of the North Landing flints. The flints from the less tectonically disturbed chalk comprising of both grey flints BLSUK (Inland samples) and the dark brownish grey flints are stronger, harder and the most abrasive flint samples. While the weakest, softer and relatively least abrasive flints are the grey flints from the tectonically disturbed chalk. This observation, therefore, shows that the tectonic histories of the host chalk strongly contribute to the material properties of flints.

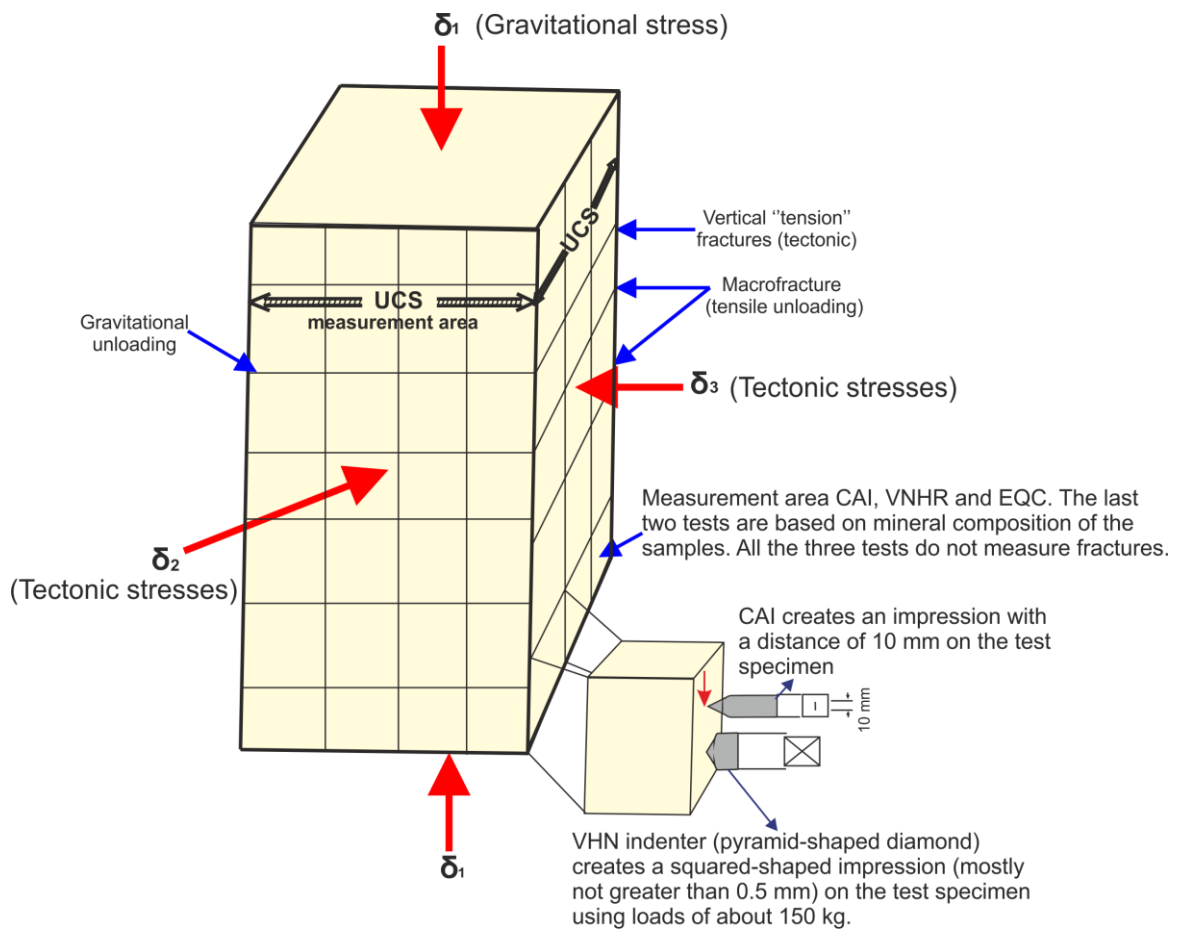


Figure 6.4: Conceptual Model of tectonically disturbed formation showing why other tests are not affected by fracturing.

#### 6.8.4 Influence of Mineral Composition

Several papers have been published on the quantitative mineralogy of flint as shown in Chapter 2, p.44. These papers vary from quantitative X-ray diffraction (Madsen & Stemmerik, 2010; Graetsch & Grunberg, 2012; Lindgreen & Jakobsen, 2012; Jakobsen et al., 2014) to Energy Dispersive X-ray spectroscopy (EDX) (Pawlikowski et al., 2002) and Energy dispersive X-ray fluorescence (EDXRF) analysis (Hughes et al., 2010). All these studies showed flint is dominated by  $\alpha$ -quartz, with few impurities mostly calcite, but the relationship between the mineral composition of flint and the variation in colours of flint, differences in structures of flint as well with engineering properties of flint remain open. The present study therefore, supports these studies (Table 5.4) on the identified mineral phases ( $\alpha$ -quartz (dominant mineral) and calcite (subordinate mineral)) in flints and further extends on the existing literatures by indicating that the mineral composition of flint is associated with colour, structure (white crust, core and white inclusion) and material behaviour of flint (Table 5.4).

The relationship between the mineral composition of flint with colours and structures of flint can be seen in the mineral quantification results of various flint colours and structures shown in Tables 5.2 – 5.4. While the link between the mineral composition of flint and material properties of flint can be understood by comparing the mineral quantification results in Table 5.4 for each colour as well as each structure of flint with corresponding physicochemical properties of flint presented in Chapter 4. In these comparisons, the chalk surrounding flint, which is the least abrasive material investigated (Figures 4.11, 4.12, 4.14 and 4.15, pp.129, 130, 133 & 134 respectively) was observed to have the least quartz, and the most calcite contents, when compared to any other investigated flint colour or structures.

The chalk surrounding flint is succeeded by the white inclusion regarding abrasiveness, but unlike the surrounding chalk, the abrasivity of WI is not consistent, as it varies with mineral content and degree of silicification of carbonates. The WI with smaller grain sizes; more silicified carbonate; more quartz content and less calcite content (BNLUK) is more abrasive than WI with more calcite content and less silicified (BLSUK, SDFr, Figures 4.11, 4.12, 4.14 and 4.15).

Similarly, the mineral compositions of the white crust correspond to the abrasiveness and hardness of this sample and depend on the extent of silicification and the enclosed flint. The white crust surrounding grey flints possess more quartz contents and are harder, more abrasive than the white crust surrounding the grey flints (Figure 5.21, p. 186) with less quartz content. The dark brownish grey flints have more quartz contents, less calcite than grey flints and are stronger, stiffer, and harder than light grey (LG); light brownish grey flints (LBG), grey flints (GF), BG and DBG presented increasing the order of hardness and abrasiveness. Therefore, the above observations clearly demonstrate that there is a link between physicochemical properties of flints and the mineral composition, which is also a function of colours of flints.

## **6.9 Is there any Relationship between Drillability and Colour of Flints?**

Colour of flints reflects the mechanical and physical properties and hence the drillability of flints. This relationship was tested by drilling two blocks of flints comprising grey (GF) and dark brownish grey (DBG) flints as described in Chapter 3, p.107. Figures 4.29 a-f (p.151) show the relationship between the tested variables and revealed the variability in drillability between the GF and the DBG flints in terms of differences in their particles bonding, different bottom-hole patterns and variable drilling grit sizes generated by the different colours of flint. The drilling grits generated by the grey flints (with slightly larger

grain size) is described as brittle chipping. These drilling chips are larger, sand-sized and are seen to be easily detached from each other and from the rock matrix during drilling.

The quartz particles of the dark brownish grey flints on the other hand, proved to be more cohesive, corresponding to the abrasiveness, strength, hardness, intense silicification, high quartz content and fine microtexture of the DBG flints observed in Chapters 4 and 5. These factors confirmed the ductile drilling pattern suggested in this sample. This observation also explained why drilling progress was very slow in this sample and implies that greater force would be required to detach the particles of the DBG sample than those of grey flint and abrasive minerals as well as strong cohesion between highly cemented quartz particles will be the major cause of wear in flints. The strong cohesion of quartz particles in this sample explain why detachment initiation of particles was difficult to progress and this indicates more cohesion exist between quartz crystals in this sample, than in the grey flints. This is significant especially on the need to understand the cutter-flint interaction, prediction of drill bit lifetime, evaluation of tool performance, developing drilling rate models when designing drill bit or excavation tool. The present findings demonstrated that the drillability of flints is significantly affected by variation in colour of flints affirming the observation in other physical and the mechanical properties of the tested flints conducted. However, it is worth noting that only two blocks of flints were tested for the drillability test, therefore, further drillability tests with standard drill bits on other colours of flints on more blocks of flint would help.

## **6.10 What are the Implications of the Study in Practical Concept?**

This section will provide the implications of this study within a practical context.

### **6.10.1 Implications for laboratory/large scale characterisation of flints**

A general observation of the overall wear classification methods employed demonstrates that the RAI method provides the most robust and reliable wear classification of flints. This observation is drawn from the ability of RAI method to classify the investigated flints into extremely abrasive and very abrasive flints as against the remaining wear testing methods employed in this study that classified the entire investigated flints as very abrasive materials. The inability of the CAI to appropriately characterise flints in this study conforms to the observation of Cumming (1999) on measuring the abrasiveness of flints using CAI. Similarly, the failure of VHNR

and EQC to suitably characterise the abrasiveness of flints justifies the views of Plinninger (2002; 2008; 2010) on these methods.

Although, the experimental approaches employed in this thesis were not newly introduced, some of the methods were first tried for flints in this study. For example, experimental methods such as determination of porosity/grain size using ImageJ software on SEM images of flints, ultrasonic pulse methods, Vickers Hardness Number of Rock (VHNR) and Equivalent Quartz Content (EQC) from mineral composition of flints and Rock abrasivity index (RAI) are first applied to examine flints in this thesis. Except the EQC and VHNR, all these testing methods appropriately characterised flints as justified by providing results with patterns and consistency that are similar in trend with other testing methods. The outcomes of these methods are also justified by consistently reflecting the differences in material properties of flints and by yielding similar results obtained using different methods from previous studies. The implication of this is that these methods that are mostly cheap, quick and do not require complex sample preparations can now be applied to characterise flints elsewhere. The UCS, tensile strength, point load strength test, He-Porosimetry, SEM, thin section and SEM-CL were previously employed to test flints as seen in Chapters 2, 3, 4 and 5 and the present study illustrates the suitability of these methods to characterise flints.

Experimental results in this study suggest that one should expect a transition in the behaviour of flint from one structure (White crust, core) to another, and from a flint colour to another. As such, recognising the dominant flint colour is a key and would aid in the design of the type of equipment and mode of excavation or drilling to be employed. The results indicate that the higher the quartz content, the darker the flints, and the higher should be the strength and abrasiveness of the flints. Exception to this is when the flints are highly fractured and have significant quantity of calcite vugs or inclusions. In this case, the strength will strongly rely on these structural flaws. This means that, the darker and finer the microtexture of flints, the stronger, harder, more abrasive and challenging would be to drill through the flints and the more the flint will wear the drilling or cutting tool. This implies that microstructures of flints can be a good predictor of strength and hardness properties of flints.

It is also significant to note that (engineers and project planners involved in tunnelling or drilling projects in chalk with flints ) apart from the tectonic history, the physical, and mechanical properties of the host chalk such as porosity, and permeability are need to be considered in predicting material properties of the embedded flints. Therefore, where the host chalk is highly porous/permeable, extremely strong and abrasive flints are likely to be encountered. This is worth considering when designing for excavation or drilling projects through chalk with flints.



The present study demonstrates how and why material properties of flints vary by examining flints with different colour, morphology and from different regions. The strength results demonstrate variable and extremely high: resistance to penetration; crushing/chipping strength should be expected where flint is darker. However, this theory could be affected by the proximity of the host chalk to tectonic structures, and reduction in intensity of flint colour. More clearly, the outcomes of this study indicate that where the host chalk is formed in fault zone or tectonically disturbed zone, the strength of the embedded flints is likely to be affected by fracturing in the flint samples. These factors need to be considered by tool manufacturers/engineers/policy makers prior to site investigation and when designing for the evaluation of chipping or crushing strength of flints or drillability of flints.

The data on abrasiveness of flints presented in Chapter 4, pp. 126-135 provides important information that addresses one of the major challenges caused by flints in tunnelling and drilling projects in chalk with flints. The data illustrates variable abrasiveness of flint with flint structures, colours, and mineral composition and further identify two categories of flints. These findings, therefore, emphasise the need for careful consideration of the dominant colour of flints encountered in the field as this could provide an important hint on the potential abrasiveness of the material to be drilled. This data is significant given that there are very few comparable studies that looked at the abrasiveness of flints (e.g. Cumming, 1999; Fowell & Abu Bakar, 2007).

## **6.11 Relationships between Some Mechanical Properties of Flints**

### *Relationships between UCS of flints and $I_{s(50)}$ , $T_o$ , $V_p$ , $V_s$*

In support to the previous studies (Cumming, 1999 & Smith et al., 2003) on UCS- $I_{s(50)}$  relationship for flints, the present result shows that the UCS- $I_{s(50)}$  relationship is not statistically significant and revealed that the use of K value to assess UCS of flints is not supported by the present findings. This is because the present result does not show any statistical significant relationship between UCS and  $I_{s(50)}$  for flints. However the observed trend in the UCS- $I_{s(50)}$  plot defined by the three clusters (Figure 4.31a, pp.153) showing an increase in UCS with increase in  $I_{s(50)}$  from weaker flints to the strongest ones. This trend represents a transition from the tectonically disturbed flints to the less disturbed flints, with more silica cements and difference between the microstructures of the flint samples.

The pattern in the data points conform to the variation in respective microstructures (difference in degree of quartz cementation, undetected microfractures)

and mineral compositions of the different flint types. The good  $V_p$ - $V_s$  relationship and  $V_p/V_s$  are consistent with earlier studies on this relationship for several rocks. Poor relationships were observed between  $I_{s(50)}$ ,  $T_o$ ,  $V_p$  and  $V_s$ . The causes of these poor relationships between  $I_{s(50)}$ ,  $T_o$ ,  $V_p$  and  $V_s$  is: firstly attributed to the high degree of heterogeneity among the investigated flints; secondly, lack of duplicate samples to represent all the flints between sites because some specimens were only representatives of sites, not necessarily from the same flint blocks. The present findings, therefore, suggest that  $T_o$ ,  $V_p$ , and  $V_s$  cannot be predictors for UCS of flints.

#### *UCS- $\phi_{He}$ Relationship*

The observed negative relationship between UCS and  $\phi_{He}$  indicates the UCS of flints increases as porosity decreases. Porosity increment in flints occurs because of increased in microfractures and the presence of calcite inclusions in the samples. Very low and similar porosity values (1-2%) between both slightly low strength (100 – 300 MPa) and extremely strong (500 – 800 MPa) flints exist, this implies apart from microfractures, calcite inclusions which have been identified as another major cause of strength reduction in flint affects the porosity of flints. Porosity at these points is similar despite variations in strength due to the likely influence of isolated pores within flint samples that affected the strength of flints, but were not detected by the Helium. The overall UCS- $\phi_{He}$  relationship demonstrates that the UCS of flints cannot be estimated from  $\phi_{He}$ .

## **6.12 Summary of the Chapter**

The objectives of this chapter were achieved by interpreting and discussing the research findings presented in Chapters 4 and 5. The implications of the present study were also discussed.

The key findings drawn from this chapter are the:

1. Identification of variations in strength, density and stiffness between different classes and structures of flints.
2. Establishment of trends in abrasivity of flints with flint types and structures.
3. Identification of suitable methods to characterise the abrasiveness, and stiffness as well as identifying the best sample preparation for microscopic characterisation of flints.
4. Investigation of how the mineral composition/phases relate with the evolution and genesis of flints.

5. Establishment of the links between some properties of the host chalk and the engineering behaviour of flints.
6. Confirmation of the invalidity of predicting UCS of flints from  $I_{s50}$ .
7. Establishment of the relationship between engineering properties of flints and the mineral composition, microstructure and microtexture of flints.
8. Identification of variation in mineral composition of flints with structures and type of flints.
9. Modification of existing micropetrographic index and development of empirical models for predicting engineering properties of flints from the micropetrographic index.
10. Understanding of the porosity and ultrasonic properties of flints and main controls on these properties of flints.
11. Examination of grain size-flint colour relationship and establishing how these relate with the drillability of flints.
12. Support to the biogenic origin of flint through silica-calcite replacement relationships.
13. Application of petrographic techniques to understand the links between microtexture of flints and the engineering properties of flints.

The interpretation and discussions of the present research findings resulted into some conclusions and interesting suggestions for further research which shall be presented in Chapter 7.

## Chapter 7 Conclusions and Recommendations

### 7.1 Conclusions

The aim of this thesis was to develop/determine the suitable methods for characterising flints to better understand this rock type which is frequently the cause of problematic ground conditions so that engineering geologists will better understand flints and best practice can be used to resolve issues with flints. The approaches employed to achieve this aim are listed below:

- Field observation of flints
- Extensive laboratory investigations comprising the following:
  - Physical/mechanical and petrographic classification of flints.

All these approaches were discussed in Chapter 6. In this chapter the success in reaching the study aims is outlined.

Field observation of flints representing different regions resulted into the identification of flints with different features and structures. The main structures identified are the white inclusions and the white crust. The field observation indicates the white crust associated with grey flints is thicker and softer when compared with the white crust surrounding dark brownish grey flints. In grey flints, particularly from the North Landing Chalk significant presence of calcite inclusions have been identified. These inclusions have been significantly silicified in the dark brownish grey flints.

Evidence from mechanical investigations has categorised flints into medium, very strong and extremely strong materials depending on the microstructures, mineral composition and the tectonic history of the flints. The presents findings show that the dark brownish grey flints show the highest strength (UCS,  $T_o$ , and  $I_{s(50)}$ ), stiffness and density. While grey flints located in the proximity of the fault zone at North Landing (BNLUK) have the lowest strength. This suggests that when dealing with flints affected by extensional tectonics, a reduction in mechanical properties of such flints should be expected. This is not the case in glacially disturbed flints (at Møns Klint) which are much stronger and more silicified.

The wear potential of flints and associated structures (white inclusion, and white crust) on cutting tools is significantly affected by the microstructures and mineral composition of flints, which is suggested to be linked to the colour of flints. Wear data suggest that colour differences can be used as indicators for the potential of flint material to cause wear and can be used to predict the abrasivity of flints. The present findings also show that existing tool wear prediction models/graphs do not consider flints. Thus, future research should build on the present findings to develop wear prediction models/graphs that include flints.

Ultrasonic characterisation of flint categories shows higher  $V_p$ ,  $V_s$ , and  $E_d$  within the DBG, which remains similar to the competent grey flints, but apparently reduced in the disturbed grey flints (BNLUK). The present study illustrates that the non-destructive ultrasonic method can be applied to characterise flints, especially where the flints are highly variable in terms of microstructures. However, the surprisingly similar ultrasonic properties of the grey flints (BLSUK<sub>t</sub> and BLSUK<sub>n</sub>) and the dark brownish grey flints, despite the slight differences in their mineral composition reveals the likely insensitivity of the method to slight variation mineral composition.

Porosity investigations on different colours of flints using  $\phi_{He}$ -Porosimetry and Image analysis demonstrate that porosity of flints depends on the presence of microfractures, carbonate inclusions and the microtexture of flints. The grey flints sampled from the disturbed chalk at North Landing are the most porous of the tested samples and the dark brownish grey flints are the less porous flints. The high porosity of these samples is attributed to fracturing, granular quartz grains, micropores and significant calcite inclusions. This is confirmed by the lower porosity seen in the hardly fractured, similar flint colour with silicified calcite inclusions.

The grain size of flints is related to the material properties and drillability of flints. This relationship is a function of re-crystallisation, and structures of flint samples. The extremely strong and abrasive dark brownish grey flints exhibit lower values of grain size, while the weaker, least dense, less abrasive grey flints exhibit higher values of grain size. The light brownish grey and brown grey flints have intermediate grain size. This variation in grain size is reflected in the drillability of flints observed in this study and corresponds to the microstructural details seen in the SEM results and the porosity which, in turn, relate to respective colours of flints.

The present study found the dark brownish grey flints that are formed in soft shallow water chalks are extremely abrasive, strong, and hard, with high density and have significantly very low porosity because of high diagenetic transformation likely associated with the physical properties of the host chalk. The extent of diagenetic change seems to be less where the host chalk is deeper water deposit. Flints in this type of chalk are mostly light grey or grey and are identified with thick, weak, white crust. In most cases, these flints are weaker and less abrasive than the dark brownish grey flints. These observations are important in understanding the behaviour of flints in different chalks across wider geographical locations.

The petrographic studies confirm that the microtexture/microstructures of flints control the engineering properties of flints. The present study has found that the less abrasive, weaker, less hard, more porous light grey flints with larger grain size had more granular microtexture. The microtexture of these flints is dominated by equigranular quartz microspheres, with evidence of some intercrystalline micro pores.

The microtexture became gradually cemented as a result of the partial fusion of some quartz microspheres in the grey flints and this explains the slight change in the physicomechanical properties flints from light grey to grey flints.

There is a significant change in microtexture/microstructures of the extremely: strong; stiff; hard; abrasive and less porous dark brownish grey flints with very fine quartz grains. In these flints, the microtexture is dominated by a massive network of quartz cement as a result of intense silicification and suturing of re-crystallised quartz grains. This microtexture/microstructural-engineering properties relationship of different colours of flints could be used as a vital tool in understanding and predicting the abrasive wear of flints with variable colours.

A comparison between different flint morphologies (tabular and nodular flints) and the engineering properties of flints does not show a relationship. Likewise, comparison of engineering properties between tabular flints in the chalk of north of England and nodular flints (at Lincolnshire), and nodular flints in the chalk of the Anglo-Paris Basin and in the Danish Chalk does not reveal any pattern.

Available evidence from this study demonstrates that the mineral composition and microstructures of flints control its material properties. This is suggested by the increase in the abrasiveness, hardness of flints/structures from the: chalk surrounding flint → white inclusion → white crust surrounding grey flints → white crust surrounding dark brownish grey flints → flint core presented the respective order of increase in quartz content and decrease in calcite contents. Similarly, quartz content increases from light grey → light brownish grey flints → brownish grey flints → grey flints → dark brownish grey flints, while porosity and grain size decrease in that order. The above observations suggest that detail description of flints for engineering purposes would need to consider variation in quartz contents of flints as these significantly influence the overall behaviour of flints in project.

The main factors causing variation in colour of flints, especially the Northern Province flints have been identified as grain size, density, mineral phases, degree of cementation and recrystallisation. The causes of differences in engineering properties of flints have also been identified and found to be related to the causes of colour variation –thus, flint colour an index of the engineering properties of flints.

The relationships between strength, abrasiveness and micropetrographic index ( $I_{pf}$ ) of flints show that  $I_{pf}$  can be used for the assessment of engineering properties of flints. Regression analysis has also shown that the UCS- $I_{s(50)}$  relationship is not valid for flints and the application of  $K$ ,  $T_o$ ,  $V_p$ , and  $V_s$  values to predict UCS of flints is not supported by the present findings.

He porosimetry (on large flint samples), Image analysis (ImageJ), ultrasonic method, Vickers Hardness Number of Rock, Equivalent Quartz Content (EQC) and

Rock Abrasivity Index (RAI) were applied for the first time on flint. While the EQC and VHNR were not successful for characterising flints, the remaining tests were successful; hence they can be used to investigate flints. Similarly, image analysis (ImageJ) gave the porosity and grain size of flints for specific area-hence for better spot characterisation of flints (in terms porosity or grain size determination) image analysis using ImageJ is a better alternative to apply.

Large scale laboratory drilling test on two blocks of grey and dark brownish grey flints using a standard tricone bit has shown that the drillability of flints is related to the microtexture of flints. The observed pattern in drillability between grey and dark brownish grey flints agreed well with the patterns seen in the physico-mechanical and petrographic properties of such flints suggests that the drillability of flint is related to the mineralogy, micro and macrostructures of flints. This observation, implies that significant drill wear or tool damage would be experienced when drilling dark brownish grey flints compared with grey flints. This is, however, subject to further investigation, as only two blocks of flint were tested in the present study.

### *Integration of Present Findings into Engineering Practices*

The following points summarise the implications of the present study:

- The physical and mechanical properties (porosity, permeability, density, strength, etc.), tectonic history of flints and proximity to tectonic structures play significant roles on material properties of the embedded flints. These are significant and worth considering when designing drilling/excavation programmes in chalk with flints.
- Post-formational diagenetic processes have significant influences on mechanical properties of flints, but the diagenetic potential of flints is the key, and this strongly relies on the physical properties of the host chalk and the geochemistry of the pore water. These factors need to be considered when designing of excavation or drilling programmes in chalk with flints.
- The main controls on engineering and geological properties of flints identified in this study are vital inputs for drilling and tunnelling optimisation.
- It is also important to note that, whenever projects involve with flints, besides the properties of the host chalk, the colours (which reflects variation in density, grain size and mineralogy) and structures of flints play vital roles on the mechanical properties of flints. As such flint colour can be used as a guide to their properties or important field observation on the potentials of flints to wear tools or equipment. Ignoring colour variation among flints could lead to significant financial implications on projects in chalk with flints.

- The Rock Abrasivity Index (RAI) provides the best characterisation of abrasivity of flints, than existing methods (CAI, VHNR or EQC) which have traditionally been used to characterise the abrasivity of flints. Therefore, RAI could be employed to predict wear rate or drill bit lifetime of for flints.
- The porosity of flints and associated structures (white crust, white inclusions, and core) can now be accurately measured using image analysis because findings in this study suggest that for flints the  $\phi_{\text{He}} = 2\phi_{\text{im}}$  implying that Helium porosity of flint structures can be estimated using ImageJ.
- When drilling through chalk with variable flints, characterisation should involve detail understanding of dominant colours of flints in that formation. This will help in effective prediction of drillability and optimal drilling performance could be guaranteed. This is because preliminary findings from drilling test demonstrate different colours of flints have specific drillability. The darker the flint the more difficult to be drilled and the more it wears the drill bits, provided both samples have not been damaged by fracturing.

## 7.2 Recommendations for Future Investigation

- Further research comparing dark brownish grey flints with grey flints elsewhere, and from less /tectonically disturbed chalk elsewhere would help.
- Further study should explore flints further away from the North Landing, but within the Flamborough Head Fault Belt and look at the relationship between the diagenesis, depth of deposition, depositional environment of the host chalk and the material properties of the embedded flints.
- All existing drill bit wear prediction graphs/models were developed from rocks that are weaker than flints. Future work should focus on relating the abrasivity of flint with drill bit lifetime. This could provide data that incorporates flints into existing RAI-bit lifetime model which is presently limited to rock samples with maximum RAI of 200.
- The application of etching on flint samples using either HFI or NaOH could provide more details on the presence of preserved opaline silica in both grey and the dark brownish grey flints as well as between other flint classes.
- Further investigations on drillability test on different colours of flints using drill with automatic drill or servo controlled drill (for proper controlled of drilling parameters) and automatic feed with loading capacity of about 2000 kN or more could provide vital drilling parameters like the rate of penetration and weight on bit for use by both engineers and tool manufacturers.



- To investigate the possibility of sourcing silica for flint formation from the host chalk, the mineral composition of chalk immediately surrounding flints and away from flints should be examined. A decrease in quartz content in the chalk towards the flints could suggest the possible migration of silica.
- The identification of calcite at different proportion and concentrations of white inclusions in various flints means difficulties in predicting the material properties of such flints. Further work that would investigate the roles of white inclusions on engineering properties of such flints would help.
- Similarly, better ways of assessing the mechanics of fractured flints would help as the existing studies do not consider this.
- The use of textural analyses to predict other mechanical properties of flints would be useful.
- The use of EDM to map out various mineral phases of different flint structures and classes would be helpful.

## References

- Aber, J. S. (1979). Kineto-stratigraphy at Hvideklint, Møn, Denmark and its regional significance. *Bulletin of the Geological Society of Denmark*, 28(1979), 81-93.
- Abdel-Wahab, A., & El-Younsy, A. R. M. (1999). Origin of spheroidal chert nodules, Drunka Formation (lower Eocene), Egypt. *Sedimentology*, 46(4), 733-755.
- Akbari, B., Butt, S. D., Munaswamy, K., & Arvani, F. (2011). Dynamic Single PDC Cutter Rock Drilling Modeling and Simulations Focusing on Rate of Penetration Using Distinct Element Method. ARMA 11-379, *45th US Rock Mechanics/Geomechanics Symposium*, San Francisco, CA, 11-379.
- Al-Ameen, S. I., & Waller, M. D. (1994). The influence of rock strength and abrasive mineral content on the Cerchar Abrasive Index. *Engineering geology*, 36(3), 293-301.
- Aldiss, D. T., Bloomfield, J. R., Buckley, D. K., Doran, S. K., Evans, D. P., Hopson, P. M., Woods, M. A. (2004). A geological model of the Chalk of East Kent. *British Geological Survey Commissioned Report*, CR/04/092.
- Aliyu, M. M., Murphy, W., Collier, R. & Lawrence, J.A. (2015). Classification of flints for drill wear potential. In: Schubert, W., & Kluckner, A., (eds). Future Development of Rock Mechanics. *EUROCK 2015 and 64th Geomechanics Symposium. Austrian Society for Geomechanics*, 309 – 314.
- Alvarez, L. W., Alvarez, W., Asaro, F., & Michel, H. V. (1980). Extraterrestrial cause for the Cretaceous-Tertiary extinction. *Science*, 208(4448), 1095-1108.
- Andersen M. A. (2013). Core truth in Formation Evaluation. *Oilfield Review*, summer 2013, Schlumberger, 2, 10.
- Anderskov, K., Damholt, T., & Surlyk, F. (2007). Late Maastrichtian chalk mounds, Stevns Klint, Denmark—combined physical and biogenic structures. *Sedimentary Geology*, 200(1), 57-72.
- Anon (2011) <http://www.nuance.northwestern.edu/docs/epic-pdf/Particle%20Analysis%20Using%20ImageJ.pdf> (5th April, 2015).
- Anselmetti, F. S., & Eberli, G. P. (1993). Controls on sonic velocity in carbonates. *Pure and Applied Geophysics*, 141(2-4), 287-323.

- API (1998). *American Petroleum Institute Recommended Practices for Core Analysis Procedure*. API RP 40, American Petroleum Institute, Dallas, Texas.
- ASTM D2845-00. (1995). Standard test method for laboratory determination of pulse velocities and ultrasonic elastic constants of rock. *American Society for Testing Materials*.
- ASTM D7012-07. (2010). Standard test method for Compressive strength and elastic moduli of intact rock core specimens under varying states of stress and temperatures. *American Society for Testing Materials*.
- Behl, R. J., & Smith, B. M. (1992). Silicification of deep-sea sediments and the oxygen isotope composition of diagenetic siliceous rocks from the western pacific, Pigafetta and east Mariana basins. *Proceedings of the Ocean Drilling Program, Scientific Results*, 129, 81-117.
- Bell, F. G., Culshaw, M. G., & Cripps, J. C. (1999). A review of selected engineering geological characteristics of English chalk. *Engineering geology*, 54(3), 237-269.
- Bennett, P. C., Melcer, M. E., Siegel, D. I., & Hassett, J. P. (1988). The dissolution of quartz in dilute aqueous solutions of organic acids at 25 C. *Geochimica et Cosmochimica Acta*, 52(6), 1521-1530.
- Bennett, P. C. (1991). Quartz dissolution in organic-rich aqueous systems. *Geochimica et Cosmochimica Acta*, 55(7), 1781-1797.
- Black, A. D., Green, S. J., & Rogers, L. A. (1977). Full-scale Laboratory Drilling Tests on Sandstone and Dolomite: *Final Report*. United States Department of Energy Technical Information Center. EY-76-C-02-4098.
- Bloomfield, J. P., Brewerton, L. J., & Allen, D. J. (1995). Regional trends in matrix porosity and dry density of the Chalk of England. *Quarterly Journal of Engineering Geology and Hydrogeology*, 28(Supplement 2), S131-S142.
- Bristow, R., Mortimore, R. N., & Wood, C. (1997). Lithostratigraphy for mapping the Chalk of southern England. *Proceedings of the Geologists' Association*, 108(4), 293-315.
- Broch, E., & Franklin, J. A. (1972). *The point-load strength test*. *International Journal of Rock Mechanics and Mining Sciences*, 9, 669-697.

- Bromley, R. G. & Ekdale, A. A. (1986). Flint and fabric in the European chalk. *The Scientific Study of Flint and Chert*, eds G.de Sieveking & M. B. Hart. Cambridge University Press, 71-82.
- Bromley, R. G. (1967). Some observations on burrows of thalassinidean Crustacea in chalk hardgrounds. *Quarterly Journal of the Geological Society*, 123(1-4), 157-177.
- Bromley, R. G., Schultz, M. G. & Peake, N. B. (1975). Paramoudras: giant flints, long burrows and the early diagenesis of chalks. *Det Kongelige Danske Videnskabernes Selskab, Biologiske Skrifter*, 20, 1-130.
- Bromley, R. G. (1979). Chalk and bryozoan limestone: facies, sediments, and depositional environments. *In Cretaceous–Tertiary boundary events Symposium 1. The Maastrichtian and Danian of Denmark* (Eds. Birkelund, T. and Bromley, R. G.), 16–32. Copenhagen.
- Bromley, R. G., & Ekdale, A. A. (1984). Trace fossil preservation in flint in the European chalk. *Journal of Paleontology*, 58, 298-311.
- Brook, N. (1993). The measurement and estimation of basic rock strength. *Comprehensive rock engineering*, Pergamon Press, 3, 41-66.
- Brydone, R. M. (1920). The origin of flint. *Geological magazine*, 57(09), 401-404.
- Busby, J. P., Lawrence, J. A., Senfaute, G., Mortimore, R. N., Pedersen, S. A. A. & Gourry, J. C. (2004). Prediction of the erosion of cliffed terrains: "PROTECT": technical report. *British Geological Survey Internal Report*. IR/04/142, 62.
- Bustillo, M. A., Castañeda, N., Capote, M., Consuegra, S., Criado, C., Díaz-Del-Río, P., Terradas, X. (2009). Is the macroscopic classification of flint useful? a petroarchaeological analysis and characterization of flint raw materials from the iberian neolithic mine of casa montero\*. *Archaeometry*, 51(2), 175-196.
- Bustillo, M. A. (2010). Silicification of continental carbonates. *Developments in Sedimentology*, 62, 153-178.
- Carter, P. G., & Mallard, D. J. (1974). A study of the strength compressibility and density trends within the chalk of South East England. *Quarterly Journal of Engineering Geology*, 7, 43-55.

Cerchar (1986) - Centre d'Études et des Recherches des Charbonages de France. *The Cerchar abrasiveness index*. Verneuil.

Christensen, L., Fregerslev, S., Simonsen, A., & Thiede, J. (1973). Sedimentology and depositional environment of lower Danian fish clay from Stevns Klint, Denmark. *Bulletin of the Geological Society of Denmark*, 22(3), 193-212.

Clayton, C. J. (1983). The influence of diagenesis on some index properties of chalk in England. *Geotechnique*, 33(3), 225-241.

Clayton, C. J. (1984). *The geochemistry of chert formation in Upper Cretaceous chalks*. Unpublished PhD thesis, University of London.

Clayton, C. J. (1986). The chemical environment of flint formation in Upper Cretaceous chalks. In: G. D. G. Sieveking and M. B. Hart (Eds), *The Scientific Study of Flint and Chert*: Cambridge University Press 1, 43-54.

Costa, S., Delahaye, D., Freiré-Díaz, S., Di Nocera, L., Davidson, R., & Plessis, E. (2004). Quantification of the Normandy and Picardy chalk cliff retreat by photogrammetric analysis. *Geological Society, London, Engineering Geology Special Publications*, 20(1), 139-148.

Crabb, G. I., & Hignett, H. J. (1980). A laboratory and pilot-scale study on the cutting of chalk containing flints. *Tunnels & Tunnelling International*, 12, 29-33.

Cumming, F. M. DeF., & Kageson-Loe, N. M. (1995). Shoreham Harbour Tunnel: *Factual Report of Flint Strength, Report prepared for CWC Ltd by the University of Brighton*. Phase 1 investigation.

Cumming, F. C. (1999). *Machine tunnelling in chalk with flint with particular reference to the mechanical properties of flint*. Unpublished PhD thesis, University of Brighton, UK.

Damholt, T., & Surlyk, F. (2012). Nomination of Stevns Klint for inclusion in the World Heritage List. *St Heddinge: østsjællandss Museum*, 160.

Dewez, T. J., Rohmer, J., Regard, V., & Cnudde, C. (2013). Probabilistic coastal cliff collapse hazard from repeated terrestrial laser surveys: case study from Mesnil Val (Normandy, northern France). *Journal of Coastal Research*, 65, 702-707.

- Dixon, H. W. (1969). Decomposition products of rock substances. Proposed engineering geological classification. In *Rock mechanics symposium. Stephen Roberts Theatre, University of Sydney* (39-44).
- Domański, M., & Webb, J. A. (2000). Flaking properties, petrology and use of Polish flint. *Antiquity*, 74(286), 822-832.
- Duperret, A., Mortimore, R. N., Delacourt, B., & De Pomerai, M. R. (2002). Coastal rock cliff erosion by collapse at Puys, France: the role of impervious marl seams within chalk of NW Europe. *Journal of Coastal Research*, 1, 52-61.
- Duperret, A., Genter, A., Martinez, A., & Mortimore, R. N. (2004). Coastal chalk cliff instability in NW France: role of lithology, fracture pattern and rainfall. *Engineering geology special publication*, 33-56.
- Duperret, A., Vandycke, S., Mortimore, R. N., & Genter, A. (2012). How plate tectonics is recorded in chalk deposits along the eastern English Channel in Normandy (France) and Sussex (UK). *Tectonophysics*, 581, 163-181.
- Evans, C. (1859). On some sections of chalk between Croydon and Oxted: With observations on the classification of the chalk. *Proceedings of the Geologists' Association*, 1, 359-387.
- Felder, W. M. (1971). 'Bijdrage tot de kennis der genese van de vuursteenhorizonten'. *Grondboor en Hammer*, 3, 78-89.
- Ferreira, T. & Rasband, W. (2011). ImageJ User Guide IJ 1.45 m. *Image J Softw.* National Institutes of Health, *Bethesda, MD*.
- Forged, N. (1994). Møns Klint: Evaluering af skred og sikringstilag foreløbig vurdering: Lyngby, *Geoteknisk Institut*, Rapport 1, 12.
- Fowell R. J. & Martin J. A. (1997). *Cutterbility Assessment of Paramoudra Flints*. A report for AMEC Civil Engineering Limited/Southern Water Limited. Department of Mining and Mineral Engineering, University of Leeds.
- Fowell, R. J., & Abu Bakar, M.Z. (2007). *A review of the Cerchar and LCPC rock abrasivity measurement methods*. In *11th Congress of the International Society for Rock Mechanics, Second half century for rock mechanics*, Lisbon, 1, 155-160.

- Frykman, P. (1994). Variability in petrophysical properties in Maastrichtian chalk outcrops at Stevns, Denmark. *DGU Service report*, 38.
- Frykman, P. (2001). Spatial variability in petrophysical properties in Upper Maastrichtian chalk outcrops at Stevns Klint, Denmark. *Marine and Petroleum Geology*, 18(10), 1041-1062.
- Gale, I. N., & Rutter, H. K. (2006). *The chalk aquifer of Yorkshire*: British Geological Survey Report. RR/06/004, 68.
- Gerbaud, L., Menand, S., & Sellami, H. (2006). *PDC bits: all comes from the cutter rock interaction*. In: *Proceedings of the IADC/SPE drilling conference*, Miami, FL, USA, 1.
- Gercek, H. (2007). Poisson's ratio values for rocks. *International Journal of Rock Mechanics and Mining Sciences*, 44(1), 1-13.
- Glennie K. W. (ed.). (1998). *Petroleum Geology of the North Sea. Basic Concepts and Recent Advances*. Blackwell Science, London.
- Gokhale, B. V. (2010). *Rotary drilling and blasting in large surface mines*: Boca Raton, FL: CRC Press.
- Graetsch, H. A., & Grünberg, J. M. (2012). Microstructure of flint and other chert raw materials\*. *Archaeometry*, 54(1), 18-36.
- Haarsted, V. (1956). De kvartærgeologiske og geomorfologiske forhold på Møn. *Meddelelser fra Danmarks Geologiske Forening*, 13(2), 124-126.
- Hahn-Pedersen, M. (1999). *AP Møller and the Danish Oil*: Denmark, J.H. Schultz Grafisk.
- Håkansson, E., Bromley, R., & Perch-Nielsen, K. (1974). Maastrichtian Chalk of North-West Europe—a Pelagic Shelf Sediment. *Pelagic Sediments: on Land and under the Sea*, 211-233.
- Hancock, J. M. (1975). The petrology of the Chalk. *Proceedings of the Geologists' Association*, 86(4), 499-535.
- Harding, I.C., Trippier, S., Steele, J., 2004. The provenancing of flint artefacts using palynological techniques. In: Walker, E.A., Wenban-Smith, F., Healy, F. (Eds.), *Lithics*

in Action: Papers from the *Conference Lithic Studies in the Year 2000*. Oxbow Books, Oxford, UK, 8, 78-88.

Harris, C. S. (2007). Chalk facts- <http://www.geologyshop.co.uk/chalk.htm> (Accessed 10th August, 2013).

Hart, M. B., Feist, S. E., Håkansson, E., Heinberg, C., Price, G. D., Leng, M. J., & Watkinson, M. P. (2005). The Cretaceous–Palaeogene boundary succession at Stevns Klint, Denmark: foraminifers and stable isotope stratigraphy. *Palaeogeography, Palaeoclimatology, Palaeoecology*, 224(1), 6-26.

Hart, M. B., Feist, S. E., Price, G. D., & Leng, M. J. (2004). Reappraisal of the K–T boundary succession at Stevns Klint, Denmark. *Journal of the Geological Society*, 161(5), 885-892.

Heiniö, M. (1999). *Rock excavation handbook for civil engineering*: Sandvik, Tamrock.

Henson, D. (1985). The flint resources of Yorkshire and the East Midlands. *Lithics*, 6, 2-9.

Hesse, R. (1989). Silica diagenesis: origin of inorganic and replacement cherts. *Earth-Science Reviews*, 26(1), 253-284.

Hildreth, P. N. (2013). The Vale House Flints Member, a flint-rich unit of the Burnham Chalk Formation of the Northern Province, East Yorkshire and Lincolnshire, UK. *Proceedings of the Yorkshire Geological Society*, 59(3), 177-186.

Hjuler, M. L., & Fabricius, I. L. (2007). *Diagenesis of Upper Cretaceous onshore and offshore chalk from the North Sea area*: Ph.D. thesis, Institute of Environment and Resources. Technical University of Denmark.

Högberg, A., Olausson, D., & Hughes, R. (2012). Many Different Types of Scandinavian Flint—Visual Classification and Energy Dispersive X-ray Fluorescence. *Fornvännen*, 107(4), 225-240.

Hökelek, A. A. & Kayaci, K. (2000). Usage of flint powder in the floor tile body. *Qualicer 2000. VI World Congress on Ceramic Tile Quality*, 3, 157-160.

Hopson, P. (2005). *A stratigraphical framework for the Upper Cretaceous Chalk of England and Scotland with statements on the Chalk of Northern Ireland and the UK Offshore Sector*: British Geological Survey Research Report No. RR/05/01.



Hughes, R., E. Högberg, A., & Olausson, D. (2012). The Chemical Composition of Some Archaeologically Significant Flint from Denmark and Sweden. *Archaeometry*, 54(5), 779-795.

Hughes, R. E., Högberg, A., & Olausson, D. (2010). Sourcing flint from Sweden and Denmark. *Journal of Nordic Archaeological Science*, 17, 15-25.

Hutchinson, J. N. (2002). Chalk flows from the coastal cliffs of northwest Europe. *Reviews in Engineering Geology*, 15, 257-302.

Hutchison, J. E., Woehrlé, G. H., Ozkar, S., & Finke, R. G. (2006). Analysis of nanoparticle transmission electron microscopy data using a public-domain image-processing program, image. *Turkish Journal of Chemistry*, 30(1), 1.

Ihe, H. A. 2011. *Stratigraphic and Microstructural Controls on the Abrasivity of the Flints from the Northern Province Chalk*. Unpublished MSc. Dissertation, School of Earth and Environment, University of Leeds.

Iler, R. K. (1963). Strength and structure of flint. *Nature* 199, 1278-1279.

Illies, H. (1949). Zur Diagenese der südbaltischen Schreibkreide. *GFF*, 71(1), 41-50.

Ineson, J. (1962). A hydrogeological study of the permeability of the Chalk. *Journal of Institute of Water Engineers*, 16, 449-463.

Irfan, T. Y., & Dearman, W. R. (1978). Micropetrographic and engineering characterization of a weathered granite. *Annales de la Société géologique de Belgique*, 101, 71-7.

Jakobsen, F., Lindgreen, H., & Nytoft, H. (2014). Oil-impregnated flint in Danian Chalk in the Tyra Field, North Sea Central Graben. *Journal of Petroleum Geology*, 37(1), 43-53.

Japsen, P. (1998). Regional velocity-depth anomalies, North Sea Chalk: a record of overpressure and Neogene uplift and erosion. *AAPG bulletin*, 82(11), 2031-2074.

Jeanes, C. V. (1978). Silicifications and associated clay assemblages in the Cretaceous marine sediments of southern England. *Clay Minerals*, 13(1), 101-126.

Jelby, M. E., Thibault, N. R., Surlyk, F., Ullmann, C. V., Harlou, R., & Korte, C. (2014). The lower Maastrichtian Hivdskud succession, Møns Klint, Denmark: calcareous nannofossil biostratigraphy, carbon isotope stratigraphy, and bulk and brachiopod oxygen isotopes. *Geological Society of Denmark. Bulletin*, 62, 89-104.

Käsling, H., Thuro, K. (2010). Determining abrasivity of rock and soil in the laboratory. In: Williams, A.L., Pinches, G.M., Chin, C.Y., McMorran, T.J., Massey C.I. (Eds.), *Geologically Active: Proceedings of the 11th IAEG Congress*. CRC Press, London, 1973–1980.

Kazimierz, T., Jacek, T., & Stanisław, R. (2004). Evaluation of rock porosity measurement accuracy with a helium porosimeter. *Acta Montanistica Slovaca*, 9, 316-318.

Kent, P. E. (1975). Review of North Sea basin development. *Journal of the Geological Society*, 131(5), 435-468.

Knauth, L. P. (1979). A model for the origin of chert in limestone. *Geology*, 7(6), 274-277.

Knoll, A. H. (1985). Exceptional preservation of photosynthetic organisms in silicified carbonates and silicified peats. *Philosophical Transactions of the Royal Society B: Biological Sciences*, 311(1148), 111-122.

Knudsen, B. B., & Looten, C. (2013). *Stevns Klint- A candidate for the World Heritage list*. Geography K2 Project-RUC.

Krassakopoulos, G. (2013). *Petrophysical Characterization of Gas Reservoir Rock Samples using High Resolution Micro-CT Images*. PhD thesis, Delft University of Technology, TU Delft.

Kumara, G. H. A. J. J., Hayano, K., & Ogiwara, K. (2011). Fundamental study on particle size distribution of coarse materials by image analysis. *Proceedings of 1st International Conference on GEOMAT*, 399-404.

Kumara, G. H. A., Janaka. J., Hayano, K., & Ogiwara, K. (2012). "Image analysis techniques on evaluation of particle size distribution of gravel". *International Journal of Geomate*, 3(1), 290-297.

Kwiatkowski, S. (2005). Origin of chert nodules from the Polish Muschelkalk, Middle Triassic. *Annales Societatis Geologorum Poloniae*, 75: 287-380.

- Labaš, M., Krepelka, F., & Ivaničová, L. (2012). Assessment of abrasiveness for research of rock cutting. *Acta Montanistica Slovaca*, 17(1), 65-73.
- Lautridou, J. P., Letavernier, G., Lindé, K., Etlicher, B., & Ozouf, J. C. (1986). Porosity and frost susceptibility of flints and chalk: laboratory experiments, comparison of 'glacial' and 'periglacial' surface texture of flint materials, and field investigations. In *The Scientific Study of Flint and Chert*. Cambridge Univ. Press Cambridge, 269-282.
- Lawrence, J. A. (2007). *Engineering properties of chalk in relation to coastal cliff slope instability*. Unpublished PhD thesis, University of Brighton.
- Lawrence, J. A., Mortimore, R. N., Stone, K. J., & Busby, J. P. (2013). Sea saltwater weakening of chalk and the impact on cliff instability. *Geomorphology*, 191, 14-22.
- Lindgreen, H., Driessens, V. A., Salyn, A. L., Jakobsen, F., & Springer, N. (2011). Formation of flint horizons in North Sea chalk through marine sedimentation of nano-quartz. *Clay Minerals*, 46(4), 525-537.
- Lindgreen, H., & Jakobsen, F. (2012a). Marine sedimentation of nano-quartz forming flint in North Sea Danian chalk. *Marine and Petroleum Geology*, 38(1), 73-82.
- Lindgreen, H., & Jakobsen, F. (2012b). Nano-quartz in North Sea Danian chalk. *Geological Survey of Denmark and Greenland Bulletin*, 26, 9-12.
- Lord, J. A., Clayton, C. R. I., & Mortimore, R. N. (2002). CIRIA C574: Engineering in Chalk. Construction Industry Research and Information Association, London, *CIRIA Report C574*.
- MacDonald, M. (2012). River crossings: East of Silvertown crossings supporting technical documentation. *Gallions reach river crossing study (Report J)*.
- Madsen, H. B., Stemmerik, L., & Surlyk, F. (2010). Diagenesis of silica-rich mound-bedded chalk, the Coniacian Arnager Limestone, Denmark. *Sedimentary Geology*, 223(1), 51-60.
- Madsen, H. B., & Stemmerik, L. (2010). Diagenesis of flint and porcellanite in the Maastrichtian chalk at Stevns Klint, Denmark. *Journal of Sedimentary Research*, 80(6), 578-588.

Maliva, R. G., & Siever, R. (1988). Diagenetic replacement controlled by force of crystallization. *Geology*, 16(8), 688-691.

Maliva, R. G., & Siever, R. (1989). Nodular chert formation in carbonate rocks. *The Journal of Geology*, 421-433.

Mansurbeg, H. (2001). *Modelling of reservoir quality in quartz-rich sandstones of the Lower Cretaceous Bentheim sandstones, Lower Saxony Basin, NW Germany*. Dissertation, Lunds Universitet, Lund, Sweden.

Mapstone, N. B. (1975). Diagenetic history of a North Sea chalk. *Sedimentology*, 22(4), 601-614.

Medina C. (2013). *The Use of Image Analysis Software (Image-J) to investigate Porosity in Sandstone*. IGS Spring Seminar, Indiana Univeristy, Bloomington.

Megawati, M., Hiorth, A., & Madland, M. V. (2013). The impact of surface charge on the mechanical behavior of high-porosity chalk. *Rock mechanics and rock engineering*, 46(5), 1073-1090.

Micheelsen H., 1966. The Structure of Dark Flint from Stevns, Denmark. *Meddelelser Fra Dansk Geologisk Forening* 16. Copenhagen.

Michie E. A. H. 2010. Identification of Physical and Chemical Variations in Flint, Unpublished MGeol. Sci. Thesis, University of Leeds.

Minguez, J. M., & Elorza, J. (1994). Diagenetic volume-for-volume replacement: force of crystallization and depression of dissolution. *Mineralogical Magazine*, 58(390), 135-142.

Mitchell, S. F. (1995). Lithostratigraphy and biostratigraphy of the Hunstanton Formation (Red Chalk, Cretaceous) succession at Speeton, North Yorkshire, England. In *Proceedings of the Yorkshire Geological Society*, 50, 285-303.

Moroni, B., & Petrelli, M. (2005). Geochemical characterization of flint artifacts by inductively coupled plasma-mass spectrometry with laser sampling (LA-ICP-MS): results and prospects. *Mediterranean Archaeology and Archaeometry*, 5(2), 49-62.

Mortimore, R. N. 1983. The stratigraphy and sedimentation of the Turonian-Campanian in the Southern Province of England, *Zitteliana*, 10, 515 – 529.

Mortimore, R. N. (1986). Stratigraphy of the Upper Cretaceous White Chalk of Sussex. *Proceedings of the Geologists' Association*, 97(2), 97-139.

Mortimore, R. N. (1987). Upper Cretaceous Chalk in the North and South Downs, England: a correlation. *Proceedings of the Geologists' Association*, 98(1), 77-86.

Mortimore, R. N. (2001). Chalk: a stratigraphy for all reasons. The Scott Simpson Lecture: Proceedings of the Ussher Society, *Geosciences in South West England*, 10(2), 105-122.

Mortimore, R. N. (2010). Fact file: Flint, <https://dl.dropboxusercontent.com/u/81268109/Origin%20of%20flints%20including%20Paramoudra%20flints%20of%20Norfolk%20for%20website%20v4%20compressed.pdf> (Accessed 10th July, 2014).

Mortimore, R. N. (2011a). A chalk revolution: what have we done to the Chalk of England? *Proceedings of the Geologists' Association*, 122(2), 232-297.

Mortimore, R. N. (2011b). Structural geology of the Upper Cretaceous Chalk Central Mass, Isle of Wight, UK. *Proceedings of the Geologists' Association*, 122(2), 298-331.

Mortimore, R. N. (2012). Making sense of Chalk: a total-rock approach to its Engineering Geology. The 11<sup>th</sup> Glossop Lecture. *Quarterly Journal of Engineering Geology and Hydrogeology*, 45(3), 252-334.

Mortimore, R. N., Newman, T., Royse, K., Scholes, H., & Lawrence, U. (2011). Chalk: its stratigraphy, structure and engineering geology in east London and the Thames Gateway. *Quarterly Journal of Engineering Geology and Hydrogeology*, 44(4), 419-444.

Mortimore, R. N., & Pomerol, B. (1987). Correlation of the upper cretaceous white chalk (Turonian to Campanian) in the Anglo-Paris Basin. *Proceedings of the Geologists' Association*, 98(2), 97-143.

Mortimore, R. N., & Pomerol, B. (1997). Upper Cretaceous tectonic phases and end Cretaceous inversion in the Chalk of the Anglo-Paris Basin. *Proceedings of the Geologists' Association*, 108(3), 231-255.

Mortimore, R. N., Pomerol, B., & Foord, R. (1990). Engineering stratigraphy and palaeogeography for the chalk of the Anglo-Paris Basin. *London*. In: *Chalk*, eds J.B.

Burland, R.N. Mortimore, L. D. Roberts, D. L. Jones and B. O. Corbett. London Thomas Telford, 47-62.

Mortimore, R.N. and Pomerol, B. (1996). A revision of Turonian litho- and biostratigraphy in the Anglo-Paris Basin. *Mitteilungen aus dem Geologisch-Paläontologischen Institut der Universität Hamburg*, 77, 423–441.

Mortimore, R. N., & Pomerol, B. (1998). Basin analysis in engineering geology: Chalk of the Anglo-Paris Basin. *8th International Congress International Association for Engineering Geology and the Environment, Vancouver*. Balkema, Rotterdam, 3249-3268.

Mortimore, R. N., Stone, K. J., Lawrence, J. A., & Duperret, A. (2004). Chalk physical properties and cliff instability. *Engineering Geology Special Publication*, London, 20, 75-88.

Mortimore, R. N., & Wood, C. J. (1986). The distribution of flint in the English Chalk, with particular reference to the 'Brandon Flint Series' and the high Turonian flint maximum. *The scientific study of flint and chert*, Eds. G. de G. Sieveking & M. B. Hart. Cambridge University Press, 7-20.

Mortimore, R. N., Wood, C. J., & Gallois, R. W. (2001). *British upper Cretaceous stratigraphy*. Geological Conservation Review Series, No. 23. Joint Nature Conservation Committee, Peterborough, 558.

Mortimore, R. N. (2014). *Logging the Chalk*: Dunbeath, Scotland: Whittles Publishing.

Mortimore, R. N., & Duperret, A. (2004). Coastal Chalk Cliff Instability. Geological Society of London. *Engineering Geology Special Publication*, 20, 57-74.

Nielsen, L. H. (2003). Late Triassic–Jurassic development of the Danish Basin and the Fennoscandian Border Zone, southern Scandinavia. *The Jurassic of Denmark and Greenland. Geological Survey of Denmark and Greenland Bulletin*, 1, 459-526.

Nnemeka, U. (2009). *Creep behaviour and loading rate dependency of chalks*. Unpublished Master's Dissertation, University of Stavanger.

Nygaard, E. (1982). Trace fossils in redeposited chalk. *Mors, Denmark-IAS 3rd Eur. MTG., Copenhagen*, 55-56.

- Olausson, D., Hughes, R. E., & Högberg, A. (2012). Provenance studies on Scandinavian flint. *Acta Archaeologica*, 83(1), 83-86.
- Olivares, M., Larrañaga, A., Irazola, M., Sarmiento, A., Murelaga, X., & Etxebarria, N. (2012). Non-destructive crystal size determination in geological samples of archaeological use by means of infrared spectroscopy. *Talanta*, 98, 172-177.
- Olofsson, A., & Rodushkin, I. (2011). Provenancing flint artefacts with ICP–MS using REE signatures and Pb isotopes as discriminants: preliminary results of a case study from northern Sweden. *Archaeometry*, 53, 1142-1170.
- Owen, H. G. (1995). The upper part of the Carstone and the Hunstanton red chalk (Albian) of the Hunstanton Cliff, Norfolk. *Proceedings of the Geologists' Association*, 106, 171-181.
- Pabst, W., & Gregorová, E. (2013). Elastic properties of silica polymorphs—a review. *Ceramics-Silikaty*, 57, 167.
- Patsoules, M.G., Cripps, J.C. (1982). The application of resin impregnation to the three dimensional study of chalk pore geometry. *Engineering Geology*, 19, 15–27.
- Pawlikowski, M. & Wasilewski, M. (2002). Mineral investigation of Desert patina on flint artifacts: A case study. *Mediterranean Archaeology and Archaeometry*, 2(2), 23-34.
- Pawlikowski, M., Sęk, M., & Sitarz, M. (2014). Research of flint patina from the Eastern Desert of Egypt. *Auxiliary Sciences in Archaeology, Preservation of Relics and Environmental Engineering*, 8, 1-8.
- Pedersen, S. A. S. (2000). Superimposed deformation in glaciotectonics. *Bulletin of the Geological Society of Denmark*, 46, 125-144.
- Pedersen, S. A. S. (2014). Architecture of Glaciotectonic Complexes. *Geosciences*, 4(4), 269-296.
- Pedersen, S. A. S., & Damholt, T. (2012). Cliff collapse at Stevns Klint, south-east Denmark. *Geological Survey of Denmark and Greenland Bulletin*, 26, 33-36.
- Pedersen, S. A. S., & Gravesen, P. (2009). Structural development of Maglevandsfald: a key to understanding the glaciotectonic architecture of Møns Klint, SE Denmark. *Geological Survey of Denmark and Greenland Bulletin*, 17, 29-32.

Peterson M. N. A. (1974). *Deep Sea Drilling Project Technical Report: Core bits* Contract NSF C-482, University of California, San Diego. Retrieved from <http://libguides.unitec.ac.nz/apareferencing/referencingreports>

Pettitt, P., Rockman, M., & Chenery, S. (2012). The British Final Magdalenian: Society, settlement and raw material movements revealed through LA-ICP-MS trace element analysis of diagnostic artefacts. *Quaternary International*, 272, 275-287.

Pitman, J. (1986). Groundwater geochemistry and mass transfer in the East Yorkshire Chalk. *Geological Society, London, Engineering Geology Special Publications*, 3(1), 177-185.

Pittman Jr, J. S. (1959). Silica in Edwards limestone, Travis County, Texas, in *Silica in Sediments*. S. E. P. M. Sp. Publ. No. 7, 121-134.

Plinninger, R. J. (2008). Abrasiveness assessment for hard rock drilling. *Geomechanics and Tunnelling*, 1(1), 38-46.

Plinninger, R. J. (2010). Hardrock abrasivity investigation using the rock abrasivity index (RAI). *Williams, et al.,(Eds.), Geologically Active, Taylor & Francis, London*, 3445-3452.

Plinninger, R. J., & Ralf, J. (2004). Wear prediction in hardrock excavation using the CERCHAR Abrasiveness Index (CAI). *EUROCK 2004 & 53rd Geomechanics Colloquium. Schubert (ed.), VGE*, 1-6.

Plinninger, R. J., Spaun, G., & Thuro, K. (2002). Prediction and Classification of tool wear in drill and blast tunnelling. In *Engineering geology for developing countries. Proceedings of the Ninth IAEG Congress, Durban, South Africa*, 2226-2236.

Pradel, L., & Tourenq, C. (1967). Les matériaux de Fontmaure Choix des Paléolithiques et mesures des caractères physiques. *Bulletin de la Société préhistorique française. Comptes rendus des séances mensuelles*, LXXXI-LXXXV.

Pradel, L., & Tourenq, C. (1972). Choix des matériaux par les Paléolithiques de Fontmaure et essais de fragmentation dynamique. *Bulletin de la Société préhistorique française. Comptes rendus des séances mensuelles*, 69(1), 12-12.

Price, M. (1985). *Introducing groundwater*. Boston Sydney: George Allen & Unwin.



Prudêncio, M. I., Roldán, C., Dias, M. I., Marques, R., Eixea, A., & Villaverde, V. A micro-invasive approach using INAA for new insights into Palaeolithic flint archaeological artefacts. *Journal of Radioanalytical and Nuclear Chemistry*, 1-9.

Rayner, D. H. (1981). *Stratigraphy of the British Isles*: Cambridge University Press, New York, NY: USA.

Rigopoulos, I., Tsikouras, B., Pomonis, P., & Hatzipanagiotou, K. (2010). The influence of alteration on the engineering properties of dolerites: the examples from the Pindos and Vourinos ophiolites (northern Greece). *International Journal of Rock Mechanics and Mining Sciences*, 47(1), 69-80.

Røgen, B., & Fabricius, I. L. (2002). Influence of clay and silica on permeability and capillary entry pressure of chalk reservoirs in the North Sea. *Petroleum Geoscience*, 8(3), 287-293.

Rosenbom, A. E., & Jakobsen, P. R. (2005). Infrared thermography and fracture analysis of preferential flow in chalk. *Vadose Zone Journal*, 4(2), 271-280.

Rowe, A W. (1904). The zones of the White Chalk of the English coast. IV - Yorkshire. *Proceedings of the Geologists' Association*, 18, 193-296.

Rowley, D. S., Howe, R. J., & Deily, F. H. (1961). Laboratory drilling performance of the full-scale rock bit. *Journal of Petroleum Technology*, 13(01), 71-81.

Sass, E., & Kolodny, Y. (1972). Stable isotopes, chemistry and petrology of carbonate concretions (Mishash Formation, Israel). *Chemical Geology*, 10(4), 261-286.

Schmid, F. (2011). Flint stratigraphy and its relationship to archaeology. In *The Scientific Study of Flint and Chert: Proceedings of the Fourth International Flint Symposium Held at Brighton Polytechnic*, 10-15.

Schmidt, P., Léa, V., Sciau, P., & Fröhlich, F. (2013). Detecting and quantifying heat treatment of flint and other silica rocks: a new non-destructive method applied to heat-treated flint from the Neolithic Chassey culture, Southern France. *Archaeometry*, 55(5), 794-805.

Schmidt, P., Masse, S., Laurent, G., Slodczyk, A., Le Bourhis, E., Perrenoud, C., Fröhlich, F. (2012). Crystallographic and structural transformations of sedimentary

chalcedony in flint upon heat treatment. *Journal of Archaeological Science*, 39(1), 135-144.

Scholle, P. A. (1974). Diagenesis of Upper Cretaceous Chalks from England, Northern Ireland and the North Sea: *Special Publication of the International Association of Sedimentologists*, 1, 177-210.

Schumacker, R. E., & Lomax, R. G. (1996). A guide to structural equations modeling. *Hillsdale, NJ: Erlbaum*.

Senfaute, G., Duperret, A., & Lawrence, J. A. (2009). Micro-seismic precursory cracks prior to rock-fall on coastal chalk cliffs: a case study at Mesnil-Val, Normandie, NW France. *Natural Hazards and Earth System Science*, 9(5), 1625-1641.

Sharma, G. D. (1965). Formation of silica cement and its replacement by carbonates. *Journal of Sedimentary Research*, 35, 139-149.

Shepherd, W. (1972). *Flint: Its Origin, Properties and Uses*: Transatlantic Arts.

Sieveking, G. d. G. (1970). "Characterization of prehistoric flint mine products". *Nature*, 228, 251-254.

Sieveking, G. de G., and Hart, M. B. (eds.) (1986). The scientific study of flint and chert, *Cambridge University Press, Cambridge, UK*.

Smith., N A, Hislam, J L., Fowell, R J., A note on the strength of Flint particles  
ISRM Congress, 2003–Technology roadmap for rock mechanics, South African Institute of Mining and Metallurgy, 1105-1108.

Soroush, H., & Qutob, H. (2011). Evaluation of rock properties using ultrasonic pulse technique and correlating static to dynamic elastic constants. In *2nd South Asian geosciences conference and exhibition, New Delhi*, 41-53.

Standard, B. BS 5930: 1999. Code of practice for site investigations. *British Standard Institution*.

Stat Banner (2001). Development of Munroe regional medical centre. *Star Banner 6A*, Ocala, Florida.

Starmer, I. (1995). *Deformation of the Upper Cretaceous Chalk at Selwicks Bay, Flamborough Head, Yorkshire*: its significance in the structural evolution of north-east

England and the North Sea Basin. In Proceedings of the Yorkshire Geological Society, 50, 213-228.

Stemmerik, L., Surlyk, F., Klitten, K., Rasmussen, S. L., & Schovsbo, N. (2006). Shallow core drilling of the Upper Cretaceous chalk at Stevns Klint, Denmark: *Geological Survey of Denmark and Greenland, Bulletin*, 10, 13-16.

Stevens, J. P. (1999). *Intermediate statistics: A modern approach (2nd Ed.)*. Mahwah, NJ: Lawrence Erlbaum Associates.

Strand, S., Standnes, D., & Austad, T. (2006). New wettability test for chalk based on chromatographic separation of  $\text{SCN}^-$  and  $\text{SO}_4^{2-}$ . *Journal of Petroleum Science and Engineering*, 52(1), 187-197.

Suana, M., & Peters, T. (1982). The Cerchar abrasivity index and its relation to rock mineralogy and petrography. *Rock mechanics*, 15(1), 1-8.

Sujaya, J. V. (2014). Mapping and analysis of the steel matrix across the Steel/WC-Composite. Unpublished Masters Dissertation, Royal Institute of Technology, Stockholm.

Sumbler, M. B. (1999). The stratigraphy of the Chalk Group of Yorkshire, and Lincolnshire. *British Geological Survey Technical Report*, WA/96/26C.

Surlyk, F. 1997. A cool-water carbonate ramp with bryozoan mounds: Late Cretaceous–Danian of the Danish Basin. In: James, N.P. & Clarke, J.A.D. (eds) *Cool-Water Carbonates*. SEPM Special Publications, 56, 293–307.

Surlyk, F., & Birkelund, T. (1977). An integrated study of fossil assemblages from the Maastrichtian White Chalk of northwestern Europe. In: Kauffman, E. G., Hazel, J. E. (Eds), *Concepts and Methods in Biostratigraphy*. Stroudsborg, Dowden Hutchinsin and Ross Inc., 257-281.

Surlyk, F., Damholt, T., Bjerager, M., & Forening, D. G. (2006). Stevns Klint, Denmark: Uppermost Maastrichtian chalk, Cretaceous-Tertiary boundary, and lower Danian bryozoan mound complex: *Bulletin of the Geological Society of Denmark*, 54: 1–48.

Surlyk, F., & Håkansson, E. (1999). Maastrichtian and Danian strata in the southeastern part of the Danish Basin. *Field Trip Guidebook, 19th regional European Meeting of Sedimentology*. Contributions to Geology (Copenhagen). Geological Muse-

um of the University of Copenhagen, Copenhagen, Denmark, 29–58.

Symes, C. (2012). Making the connection in Copenhagen. Coping in Copenhagen: The Urban challenges of Denmark's CITYRINGEN Project. *European Foundations, Magazine of the EFFC*, 8.

Tarr, W. A. (1917). Origin of the chert in the Burlington limestone. *American Journal of Science* 44, 409-452.

Thuro, K. (1997). Drillability prediction: geological influences in hard rock drill and blast tunnelling. *Geologische Rundschau*, 86(2), 426-438.

Toft, P. C. (1986). Diagenetic fluorite in chalks from Stevns Klint and Møns Klint, Denmark. *Sedimentary Geology*, 46(3), 311-323.

Tuan, D. A., & Tung, V. T. (2014). Analyzing 2D Structure Images of Piezoelectric Ceramics Using ImageJ. *International Journal of Materials and Chemistry*, 4(4), 88-91.

Ulusay, R., & Hudson, J. A. (2007). *The complete ISRM suggested methods for rock characterization, testing and monitoring: 1974-2006*: International Society for Rock Mechanics, Commission on Testing Methods.

Ultrasonic velocity Table [http://www.advanced-ndt.co.uk/index\\_htm\\_files/Reference%20Chart%20%20Velocity%20Chart.pdf](http://www.advanced-ndt.co.uk/index_htm_files/Reference%20Chart%20%20Velocity%20Chart.pdf) (Accessed 3rd July, 2015).

Umeda, M. (2003). Precipitation of silica and formation of chert–mudstone–peat association in Miocene coastal environments at the opening of the Sea of Japan. *Sedimentary Geology*, 161(3), 249-268.

US data for solids: [http://traktorja.org/files/sonar/passive\\_materials/acoustic\\_impedance\\_of\\_some\\_solids.htm](http://traktorja.org/files/sonar/passive_materials/acoustic_impedance_of_some_solids.htm) (Accessed 4th June, 2015).

Valladas, H. (1992). Thermoluminescence dating of flint. *Quaternary Science Reviews*, 11(1), 1-5.

Van Tuyl, F. M. (1918). The origin of chert. *American Journal of Science*(270), 449-456.

Varley, P.M. (1990). Machine excavation of chalk rock at the first South Killingholme gas cavern, South Humberside. In: Burland, J.B., Mortimore, R.N., Roberts, L.D., Jones, D.L. & Corbett, B.O. (eds) *Chalk. Proceedings of the International Chalk Symposium, Brighton Polytechnic, 1989*. Thomas Telford, London, 485–492.

Von Rad, U., Riech, V., & Rösch, H. (1978). 31. Silica diagenesis in Continental Margin sediments off Northwest Africa. *Initial Report Deep Sea Drilling Project*, 41: 879-905.

Washburn, E. W., & Navias, L. (1922). The relation of chalcedony to the other forms of silica. *Proceedings of the National Academy of Sciences of the United States of America*, 8(1), 1.

Wasilewski, M. (2002). Mineralogical investigation of Desert patina on flint artifacts: a case study. *Mediterranean Archaeology and Archaeometry*, 2(2), 23-34.

Welch, M. J., Souque, C., Davies, R. K., & Knipe, R. J. (2015). Using mechanical models to investigate the controls on fracture geometry and distribution in chalk. *Geological Society, London, Special Publications*, 406(1), 281-309.

West, G. (1986). A relation between abrasiveness and quartz content for some coal measures sediments. *Geotechnical and Geological Engineering*, 4(1), 73-78.

Weymouth, J. H., & Williamson, W. O. (1951). "Some physical properties of raw and calcined flint". *Mineralogical Magazine*, 29(213), 573-593.

Whitehead, E. J., & Lawrence, A. R. (2006). The Chalk aquifer system of Lincolnshire. *British Geological Survey Research Report*, RR/06/03, 70pp.

Whitham, F. (1991). The stratigraphy of the Upper Cretaceous Ferriby, Welton and Burnham formations north of the Humber, north-east England. *Proceedings of the Yorkshire Geological Society*, 48, 247-254.

Whitham, F. (1993). The stratigraphy of the Upper Cretaceous Flamborough Chalk Formation north of the Humber, north-east England. *Proceedings of the Yorkshire Geological Society*, 49, 235-258.

Williams, L. A., & Crerar, D. A. (1985). Silica diagenesis, II. General mechanisms. *Journal of Sedimentary Research*, 55(3).

Williams, L. A., Parks, G. A., & Crerar, D. A. (1985). Silica diagenesis, I. Solubility controls. *Journal of Sedimentary Research*, 55(3).

Woodland, A. W. (ed.). (1975). *Petroleum and the continental shelf of northwestern Europe. I, Geology*. Applied Science Publishers, London.

Wood, C. J. & Smith, E. G. (1978). Lithostratigraphical classification of the chalk in North Yorkshire, Humberside and Lincolnshire. *Proceedings of the Yorkshire Geological Society*, 42, 263-87.

Woods, M. A. (2006). UK Chalk Group stratigraphy (Cenomanian–Santonian) determined from borehole geophysical logs. *Quarterly Journal of Engineering Geology and Hydrogeology*, 39(1), 83-96.

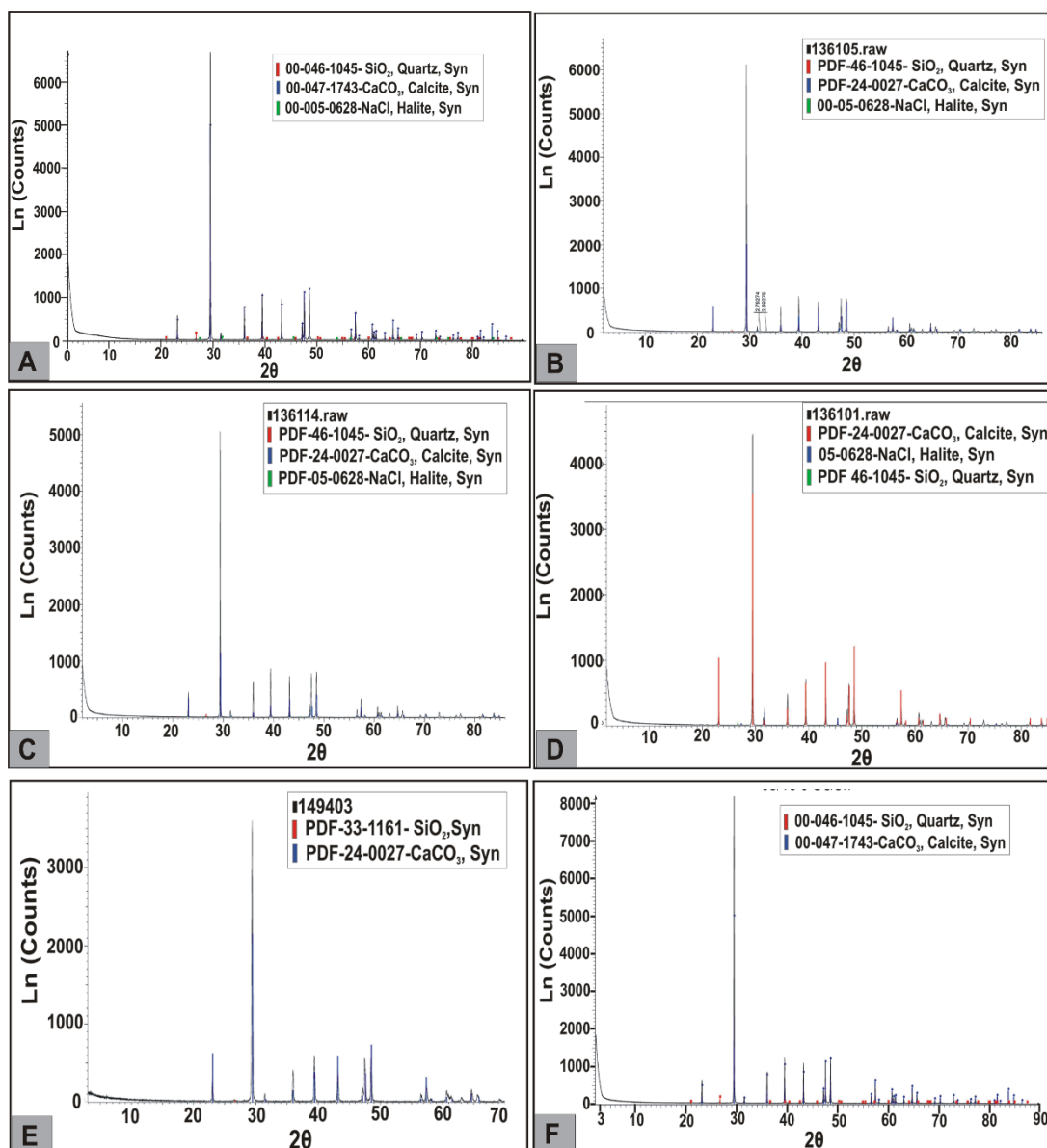
Woods, M. A. & Chacksfield, B. C. (2012). Revealing deep structural influences on the Upper Cretaceous Chalk of East Anglia (UK) through inter-regional geophysical log correlations. *Proceedings of the Geologists' Association*, 123(3), 486-499.

Wroost, V. (1936). *Vorgänge der Kieselung am Beispiel des Feuersteins der Kreide*: Senckenbergische Naturforschende Ges., 432, 1-68.

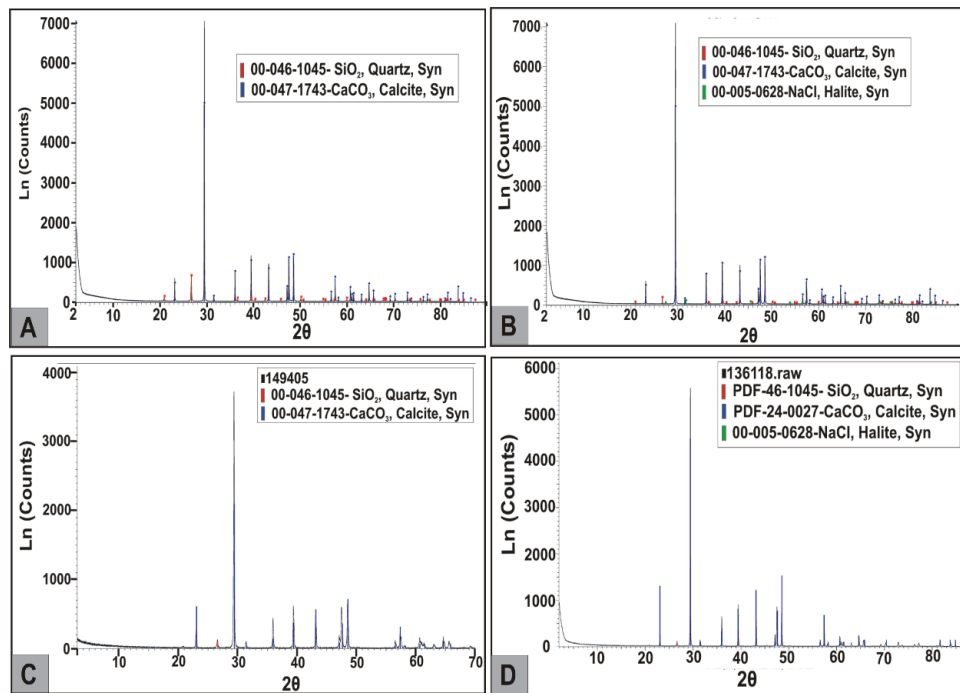
Yahiaoui, M., Gerbaud, L., Paris, J. Y., Delbe, K., Denape, J., & Dourfaye, A. (2011). *Analytical and experimental study on PDC drill bits quality*. 3rd European Conference on Tribology, 475-480.

## Appendices

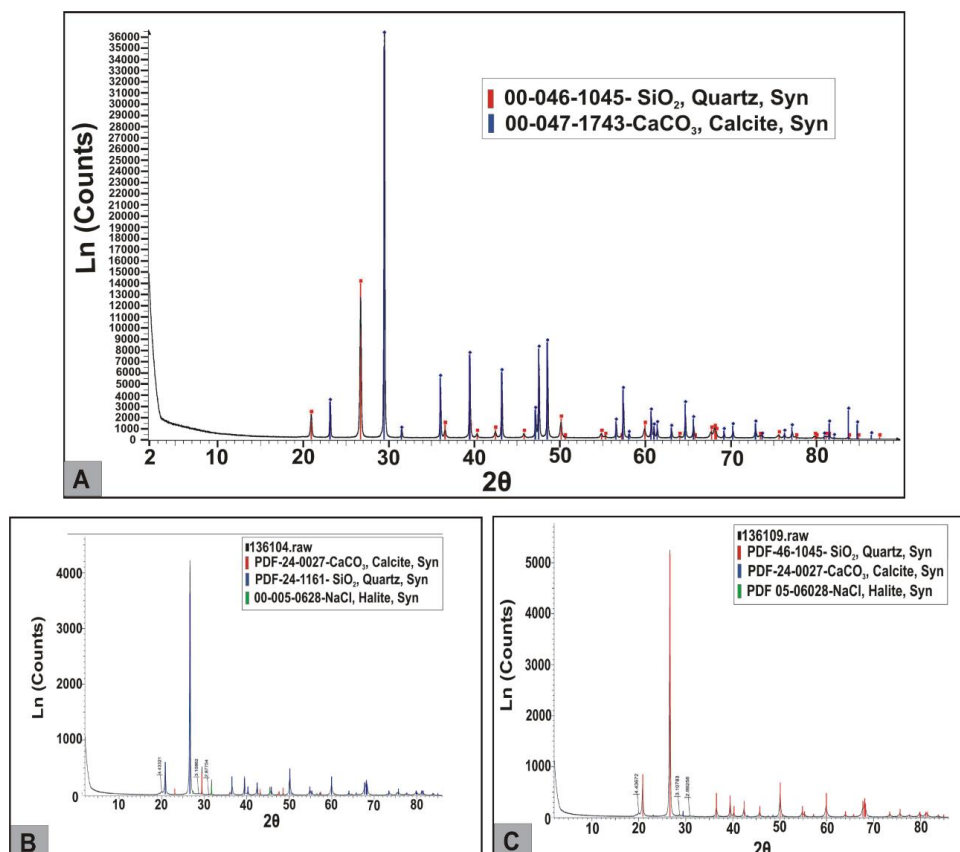
**Appendix 1:** X-ray diffraction patterns for chalk surrounding flints. (A) BNLUK Chalk. (B) SEUK Chalk. (C) SDFr Chalk. (D) LMFr Chalk. (E) TSKT Chalk. (F) BNLUK spotted grey Chalk.



**Appendix 2:** X-ray diffraction patterns for carbonate inclusions in the flint samples. White inclusion in the BNLUK flints. (b) Spotted white inclusion in the BNLUK flints. (c) White inclusion in the BLSUK flints. (d) White inclusion in the SEUK flints.

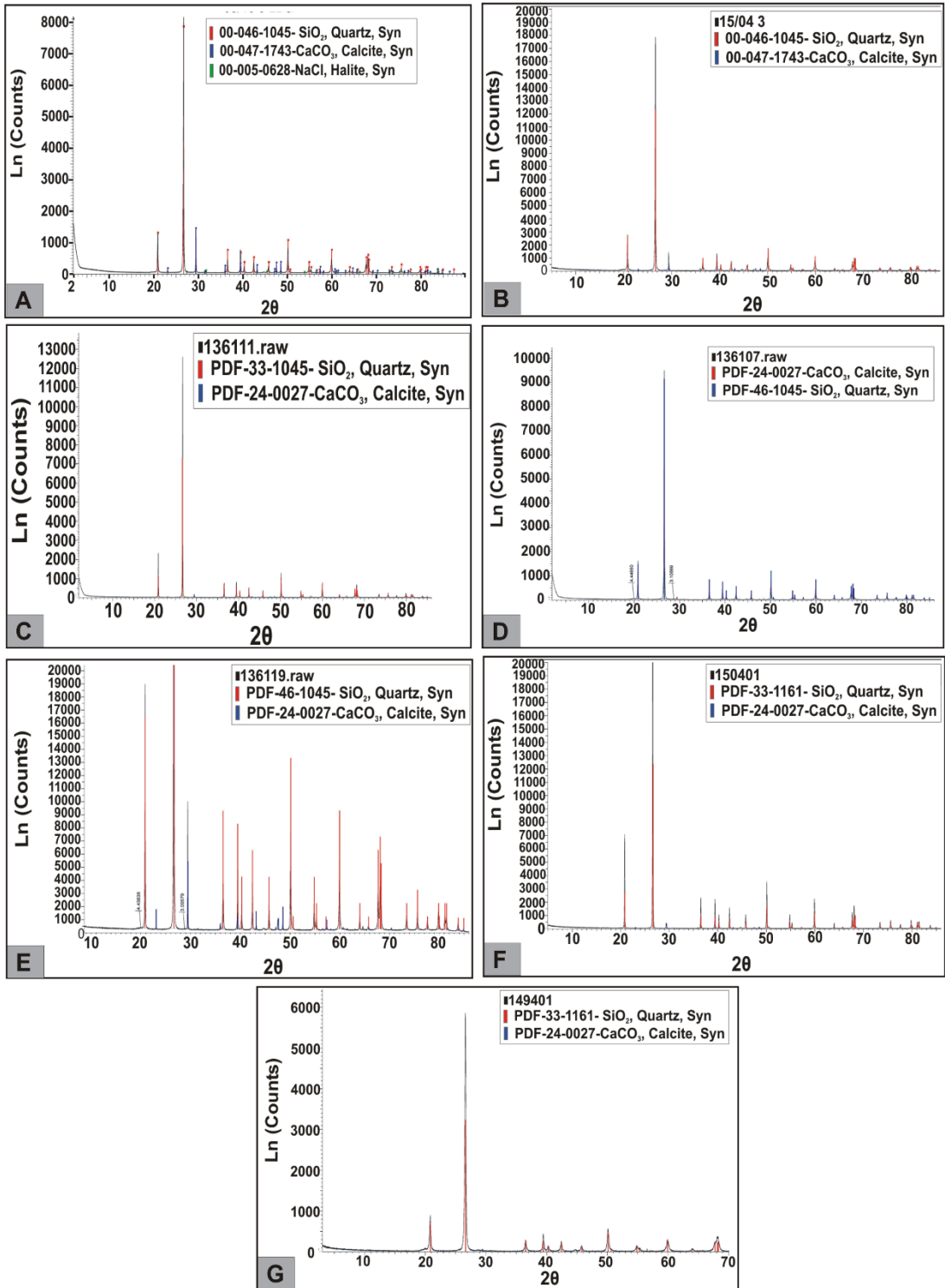


**Appendix 3:** X-ray diffraction patterns for White crust (WCr) surrounding flint. (A) White crust surrounding the BNLUK Flint. (B) White crust surrounding the SEUK Flint. (C) White crust surrounding the SDFr Flint.

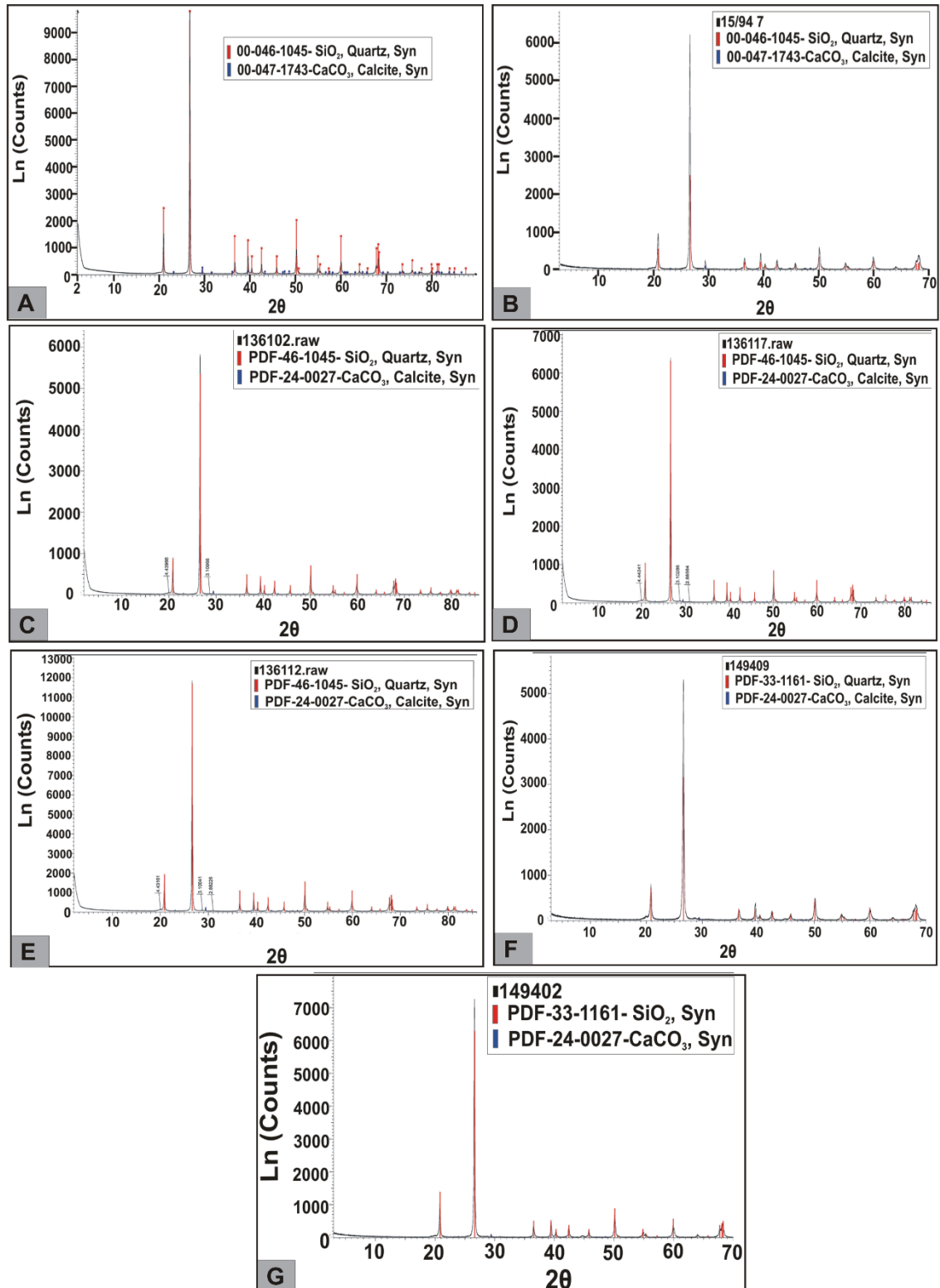




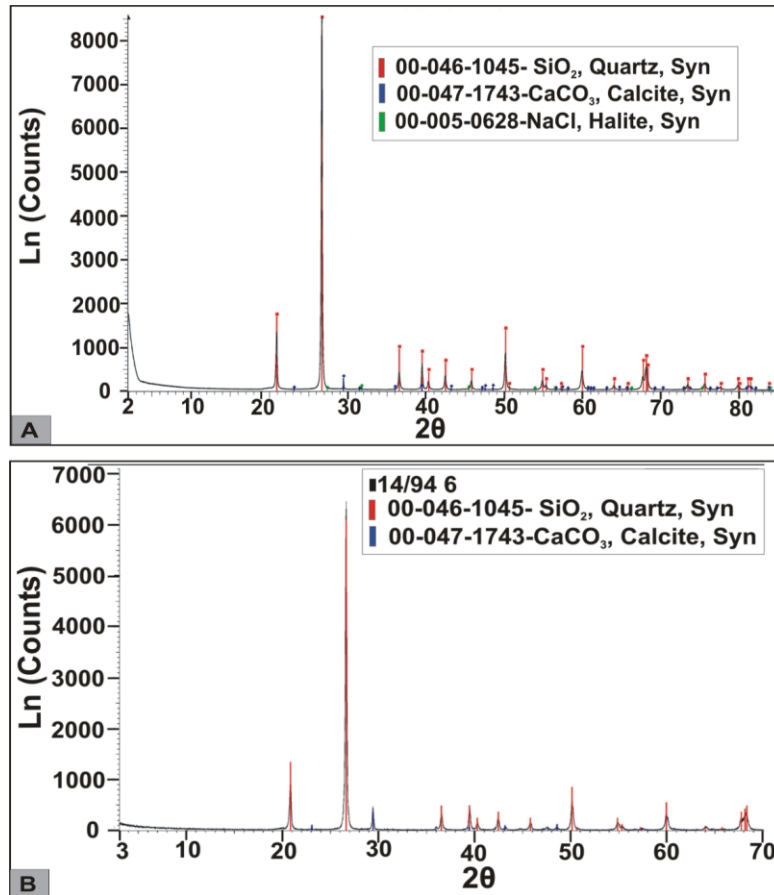
**Appendix 4:** X-ray diffraction patterns for Light brownish grey (LBG) flints. (A) BNLUK Flint. (B) BLSUK. (C) SEUK. (D) SDFr. (E) LMFr. (F) TSKT. (G) TMKT.



**Appendix 5:** X-ray diffraction patterns for Grey flint (GF)/Dark brownish grey (DBG) flints. (A) GF, BNLUK Flint. (B) GF, BLSUK. (C) DBG, SEUK. (D) DBG, SDFr. (E) DBG, LMFr. (F) DBG, TSKT. (G) DBG, TMKT.



**Appendix 6:** X-ray diffraction patterns for Light grey (LG) flints. (A) BNLUK (B) BLSUK Flints.



**Appendix 7:** X-ray diffraction patterns for Brownish grey (BG) flints. (A) BNLUK (B) BLSUK. (C) SEUK. (D) SDFr. (E) LMFr. (F) TSKT. (G) TMKT.

